Pyrolysis of Biomass and Plastics into Renewable Fuel and Value Added Chemicals

Thesis submitted in partial fulfilment of the requirement for the degree of

DOCTOR OF PHILOSPHY

by

Ranjeet Kumar Mishra

(Roll No: 146107003)

Department of Chemical Engineering

Indian Institute of Technology Guwahati

Guwahati-781039, India

May-2019

Department of Chemical Engineering

INDIAN INSTITUTE OF TECHNOLOGY GUWAHATI

CERTIFICATE

This is certify that **Mr. Ranjeet Kumar Mishra** has been working under my supervision since 23 July 2014. I hereby forward his thesis entitled "**Pyrolysis of biomass and plastics into renewable fuel and value added chemicals**" to be submitted for the award of degree of Doctor of Philosophy (Ph.D.) to Indian Institute of Technology Guwahati (IITG). I certify that he has fulfilled all the requirements according to the rules of this institute and the investigations embodied in his thesis have not been submitted elsewhere for a degree or diploma.

Dr. Kaustubha Mohanty

Professor

Department of Chemical Engineering

Indian Institute of Technology Guwahati

Guwahati-781039, India

Date:

IIT Guwahati

ACKNOWLEDGEMENTS

I would like to take this opportunity to express my heartfelt gratitude to them, whose contribution have made this thesis possible.

In particular, the foremost appreciation goes to my supervisor **Prof. Kaustubha Mohanty** for his valuable guidance throughout the research work. I thank him for his encouragement, guidance and moral support throughout, which enabled to pursue my academic skills under his precious guidance and expertise. I would like to acknowledge my sincere gratitude to my doctoral committee members, **Prof.** Vaibhav V. Goud, **Prof.** R. Anandalakshmi and **Prof.** Satyajeet Panda for their insightful advices and suggestions throughout the research.

My sincere thanks to **Prof.** Bishnupada Mandal, Head, Department of Chemical Engineering, for his moral support, inspiration and providing other necessary facilities. I would also like to convey my sincere thanks to the Head of Central Instruments Facility (CIF), IIT Guwahati, for providing me the analytical facilities of CIF. I also would like to thanks Dr. Lepakshi Barbora, Mr. Dhiren Huzuri, and Mr. Debarshi Baruah, Centre for Energy.

I am indebted to the selfless help and cooperation of my research colleagues, Sanjeev Mishra, Barasa Malakar, Sachankar Buragohain, Santosh Kumar Hotta, Sounak Bera, Pranab Jyoti Sarma, Madonna Roy, Bikashbindu Das, Munmi Bhattacharyya and Jayendran Iyer in each and every stage of the work. I would also like to acknowledge the support and encouragement of Dr. Himadri Sahu, Dr. Sanjukta Bhoi, Dr. Anand Bharti, Dr. Saran. S. and Dr. Kulbhushan Samal.

Last but not the least, I express my deepest sense of gratitude to my Parents, for their patience, endless support and inspiration towards the completion of my Ph.D thesis. I extend my sincere thanks to all my dear friends and well-wishers who had consistently supported and encouraged me, without which this work would have never been completed. My sincere apology goes to them whom I forget to mention but helped me at any part of the research work.

Thank you all!!

(Ranjeet Kumar Mishra)

Abstract

The utilization of lignocellulosic biomass and waste plastics as a renewable energy source is becoming progressively essential. The current study emphasizes on some biomass such as *Cascabela thevetia* (SK), *Delonix regia* (SG), *Samanea saman* (SS), *Phyllanthus emblica* (AM), *Azadirachta indica* (NM), *Manilkara zapota* (CK), *Madhuca longifolia* (MH) *Pinus ponderosa* (PW), *Shorea robusta* (SW) and *Areca catechu* (AN) and plastic (waste nitrile gloves) for their potential towards production of fuels and chemicals. The selected biomass and plastic was examined physicochemically to understand their compositional and structural characteristics through proximate (moisture, volatile matter, ash content and fixed carbon), CHNS (carbon-hydrogen–nitrogen–sulphur), FTIR, TGA, XRD, XRF, and EDX analysis. The proximate and ultimate analysis confirmed the higher volatile matter, higher carbon content and lower ash and nitrogen content. Sulphur content is almost negligible for all biomass. FTIR analysis suggested the presence of hemicellulose, cellulose, and lignin while XRD analysis confirmed the amorphous nature of biomass. Thermal analysis of these biomass showed three step degradation and XRF result suggested the presence of various inorganic compounds in ash which had a positive effect during pyrolysis.

The kinetics of the thermal decomposition of PW, SW and AN were estimated using TGA analyzer under the non-isothermal condition at dynamic heating rates (5 ^{o}C min^{-1}, 10 ^{o}C min^{-1}, 15 ^{o}C min^{-1}, 20 ^{o}C min^{-1}, and 25 ^{o}C min^{-1}). The kinetic parameters were evaluated using five model-free methods such as Kissinger-Akahira-Sunose (KAS), Ozawa-Flynn-Wall (OFW), Friedman model (FM), Cots-Redfern model (CR) and Distributed activation energy model (DAEM). The mass loss thermographs showed maximum decomposition in active pyrolytic stage (second stage). However, with an increase in heating rates, TGA curves moved towards higher temperature region. The average activation energy was calculated, and it was observed that activation energy altered with conversion value, due to the diverse composition of biomass. DSC analysis confirmed biomass decomposed under exothermic conditions. TD analysis of these biomass confirmed that change in activation energy and enthalpy showed favorable product formation. Gibbs free energy and higher calorific value of biomass showed its potential for energy and fuel production.

Thermal pyrolysis of selected biomass such as PW, SW, AN, SG, CK, SK, NM, MH, and SS was carried out in a semi-batch reactor under an inert atmosphere at 500 ^{o}C temperature, 80 ^{o}C min^{-1} heating rate, 0.5 mm particle size and 100 mL min^{-1} sweeping gas flow rate. Results revealed that temperature, heating rate, and particle size had a substantial effect on the pyrolytic

products yield. Further, the maximum liquid yield was achieved at the optimized condition. Characterization of thermal oil revealed higher viscosity, oxygen content, lower acidity, and heating value. FTIR analysis confirmed the presence of phenol, aromatics, ether, ester, alkane, alcohol, acid and aldehyde while GC-MS analysis confirmed the presence of higher oxygenated compounds which had a negative effect on pyrolytic oil when the objective is to use as a transportation fuel.

The effect of biomass bed thickness and distance between successive beds on the pyrolytic product yields were investigated in a cylindrical shaped semi-batch reactor under an inert atmosphere. The maximum liquid yield was obtained at optimum condition (500 °C, temperature, 80 °C min^{-1} heating rate, 0.5 mm particle size and 100 mL min^{-1} gas flow rate). Results confirmed that with increasing the number of biomass beds at optimized condition, the liquid yield was higher, however, further increasing biomass beds resulted in reduced liquid yield and increased char formation. At fourth bed arrangement, liquid properties were found to be more effective than in first and sixth beds. Further, GC analysis demonstrated that with increasing temperature, production of hydrogen and hydrocarbons increased significantly. At the same time, increasing pyrolysis temperature reduced the formation of carbon dioxide.

Catalytic pyrolysis of *cascabela thevetia* seeds were carried out at optimized condition. The results confirmed that thermal pyrolysis resulted in higher liquid yield (64.78 %) than catalytic pyrolysis (43.77 %, 53.43 %, 55.55 %, and 58.57 % at 3:1, 6:1, 8:1 and 10:1 B/C ratios). Characterization results confirmed that the introduction of catalysts enhanced the properties of pyrolytic oil by reducing viscosity, density, oxygen content, and increasing heating value. GC-MS analysis confirmed that the introduction of catalysts substantially reduced the oxygenate compounds and increased alcohol, aldehyde, and hydrocarbons.

Co-pyrolysis of NM and WNG were carried out in a cylindrical shaped semi-batch reactor. Physicochemical results of NM and WNG confirmed that a mixture of both substantially altered the pyrolytic liquid yield and enhanced the properties of fuels. The synergistic effect confirmed that the value of ΔW becomes positive when the temperature reached beyond 410 ^{o}C, demonstrated the positive synergistic effect. Among blending ratio NM+WNG(1:1, 3:1, and 5:1), the interaction between NM+WNG(3:1) was positive which indicated effective synergistic effect between NM and WNG. Similarly, NM+WNG(3:1)+CaO(5:1) and NM+WNG(3:1)+Al_2O_3(5:1) also gave the higher synergistic effect. Results confirmed that co-pyrolysis of NM and WNG increased the pyrolytic liquid

yield while with the introduction of catalyst, liquid yield got decreased. Use of catalysts enhanced the properties of oil by reducing viscosity, oxygen content and increasing calorific value of the fuel. NMR analysis confirmed the existence of a maximum amount of paraffin and aromatics. GC-MS analysis of co-pyrolysis and catalytic co-pyrolysis confirmed a reduction in oxygenated compounds, acids, and increase in alcohol and aldehyde which made pyrolytic oil more attractive as a transportation fuel.

Biochar is the solid by-product, generated during biomass pyrolysis in the absence of oxygen, has recently gained interest for both agricultural and environmental management purposes owing to its outstanding unique physicochemical properties. In this study, biochar obtained from pyrolysis of selected biomass at optimized condition are characterized for its physicochemical properties that can signify their relevant environmental applications. Number of parameters were characterized including physical properties (particle size, density, and BET surface area), hydraulic properties (water holding capacity), and chemical and electrochemical properties (organic matter, acidity, oxidation–reduction-potential, zeta potential, and elemental analysis). A wide range of volatile matter (16.69 % - 40.08 %), ash content (7.86 % - 21.50 %) and organic matter (12.74 % - 28.04 %) were observed among all tested biochars. Further BET results confirmed high variability of surface area (1.64 $m^2 g^{-1}$ - 20.26 $m^2 g^{-1}$) and higher heating value (21.78 MJ kg^{-1} - 30.65 MJ kg^{-1}) of all tested biochars. Zeta potential showed high variability from 28.57 mV - 46.87 mV while water holding capacity varied from 39.48 % - 61.60 % for all tested biochars.

Table of Contents

List of Figures

List of Tables

List of Abbreviations and Symbols

PW	Pine sawdust
SW	Sal sawdust
AN	AN sawdust
SK	*Cascabela Thevetia* seeds
SG	*Delonix regia* seeds
SS	*Samanea saman* seeds
CK	*Manilkara zapota* seeds
TGA	Thermogravimetric analysis
DTG	Derivative of thermogravimetric analysis
α_0	Initial mass of biomass material
ϕ	Difference of particular and the reference temperature
T_{max}	Reference temperature
α_f	Final weight of material
α_t	Weight of material at particular temperature
FTIR	Fourier transform infrared spectroscopy
TWCM	Traditional wet chemistry methods
A_n	An initial mass of sample before heating
B	Final mass of the sample after heating
M	Loss of mass
MC	Moisture
VM	Volatile matter
T_S	Total solids
FC	Fixed carbon
A_s	Ash content
R^2	Correlation coefficient

E	Activation Energy
R	Ideal gas constant
T	Temperature
ID	Internal diameter
OD	Outer diameter
DRS	Diffuse Reflectance Spectroscopy
NIST	National Institute of Standards and Technology
PID	Proportional–integral–derivative
GC	Gas chromatography
GC-MS	Gas chromatography–mass spectrometry
WNG	Waste nitrile gloves
NMR	Nuclear magnetic resonance
PID	A proportional–integral–derivative
RPM	Rotation per minute
DRS	Diffuse Reflectance Spectroscopy
$\int(E)$	Distribution curve of activation energy
V	Effective volatile content
V_t	Amount of volatile content
HC	Hemicellulose
C	Cellulose
L_g	Lignin
k	Rate constant
k_o	Arrhenius constant
δ	Heating rate
x	Conversion
KAS	Kissinger-Akahira-Sunose

OFW	Ozawa-Flynn-Wall
DAEM	Distributed activation energy model
CR	Coats-Redfern model
TD	Thermodynamic analysis

Chapter 1

Introduction

1.1. Introduction

The accelerated rate of global energy consumption is fuelled by an on-going triad of population explosion, fast-paced technological developments, and change in lifestyles. This has led to an alarming depletion in the available resources of fossil fuel dependent energy, with a simultaneous and dangerous increase in toxic pollutants [1]. The constant depletion of fossil fuels may be a major reason for the hike in prices of petroleum products, which in turn directly affect the quality of life. The profile of energy consumption in the year 2015 [1], showed that 87 % of energy was supplied by fossil fuels (oil 33.0 %, coal 30 %, and natural gas 24 %), all of which are potent sources of emissions. Further, as per Statistical Review of World Energy (2016) [2], global energy consumption distributed into various power sources such as oil (33 %), coal (30 %), natural gas (24 %), biofuel (10.2 %), nuclear (4.1 %), hydro energy (7.0 %) and other renewable sources such as solar, wind, and geothermal (2 %). In order to mitigate the amount of toxic gases and reduction in consumption of fossil fuel, it is essential to find alternative sustainable, and renewable energy resources [3].

Renewable energy has an advantage over fossil fuel in terms of emissions and sustainability. Among all the renewable energy sources such as solar energy, geothermal energy, wind energy, hydrothermal energy, etc, biomass has gained more attention because it has the potential to be converted into solid, liquid, and gaseous forms of energy. Moreover, biomass fuel is considered as carbon neutral [1, 4]. Biomass had a negligible amount of sulfur, a small amount of nitrogen, and ash which makes biomass more environment-friendly. It is not only a carbon-neutral source but has the potential to fulfill energy deficiency [5]. India is blessed with huge biomass reserve in the form of forest and agricultural residues. According to a survey, about 500 million metric tons of raw biomass are produced annually in India [6]. The cultivated biomass and waste biomass/residue can be used for the generation of energy. Production of energy and value-added chemicals are the best possible routes for the utilization of waste biomass.

Conversion of biomass can be achieved via the biochemical and thermochemical routes. Thermochemical techniques involve breaking of higher molecular weight compounds to smaller molecular weight compounds by supplying continuous heat for a few seconds or minutes. Further, it has an advantage over biochemical techniques in terms of the rate of

degradation and conversion time. Combustion, gasification, pyrolysis, and liquefaction are the major types of thermochemical techniques. Among all the thermochemical technologies, pyrolysis is the most promising technology that converts biomass into fuels as well as other value-added products [7]. Burning of biomass/material in the absence or partial presence of oxygen at moderate temperature (400 ^{o}C - 700 ^{o}C) is known as pyrolysis. Pyrolysis has the potential to convert biomass into solid (biochar), liquid (bio-oil and tar) and gaseous compounds (CO, CO_2, and CH_4). Production of fuels and chemicals from biomass seems a sustainable way to reduce solid waste [8]. A schematic layout of the thermochemical conversion of biomass to energy is presented in Fig. 1.1.

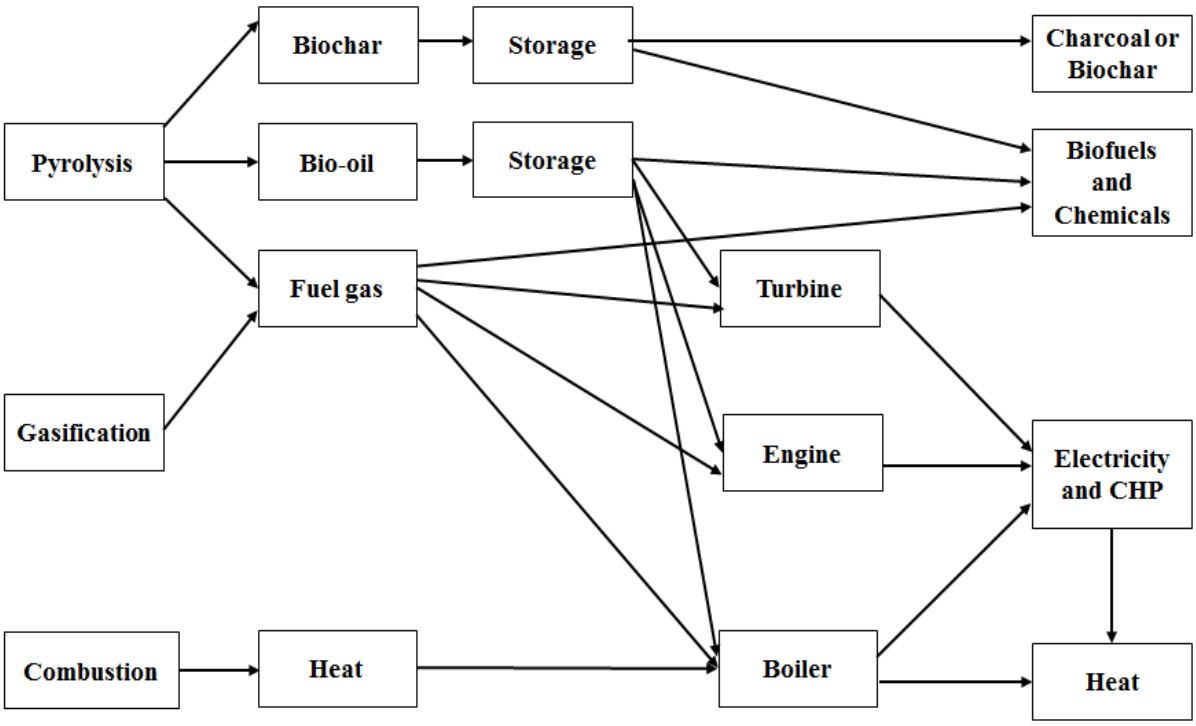

Fig. 1.1. Thermochemical conversion routes of biomass [9]

The liquid product of pyrolysis is known as pyrolytic liquid and is a mixture of the organic phase (oil-rich, known as bio-oil) and the aqueous phase (water, acids, and some amount of hydrocarbons). Since the aqueous phase is enriched with water and other water-soluble hydrocarbon compounds, it has a low standard to meet fuel quality requirements. However, it can be used for extraction of various valuable chemicals such as acids, phenols, etc. The organic phase of the pyrolytic liquid has good fuel properties which can be used directly in boiler operation or can be upgraded to be used as an alternative renewable fuel [10, 11]. However, as compared with diesel fuel, pyrolytic oil has several drawbacks such as lower

calorific value, higher acidity, higher oxygenated compounds, higher viscosity, and higher pour point [10].

The composition of pyrolytic liquid changes with types of biomass and its composition (hemicellulose, cellulose, lignin, and extractive), operating parameters, mode of pyrolysis as well as types of reactor. It was reported that the presence of extractive content significantly increased the yield of pyrolytic liquid during pyrolysis [12]. Therefore, to achieve the higher pyrolytic liquid yield, it is better to select biomass that is rich in extractives. In addition, when biomass has higher extractive content, the separation of the organic and aqueous phase becomes easier [13]. The foremost intent of recent research is to produce high-quality pyrolytic oil with better fuel quality using various waste biomass as feedstocks [12, 14-18]. Research is also being carried out to improve the quality of pyrolytic oil by using various upgradation techniques so that it can be used as a fuel either directly or in blended form.

1.2. Biofuel Options in India

The word biofuel refers to various kinds of fuels such as bio-ethanol, bio-butanol, bio-diesel, bio-hydrogen, and bio-oil (pyrolytic oil). All these alternate options are widely available in India. However, the major impediments include large-scale production with a reasonable price. The current biofuel production technologies result in higher prices than traditional fuels [19]. In this context, the selection of appropriate conversion technology, as well as feedstock, will play a big role in lowering the price of biofuels. Potential feedstocks which are not only waste but also of low-cost and sustainable should be chosen. In the past few years, researchers have focused on non-edible or less edible seeds as feedstock for pyrolysis. Few such seeds which are Indian and were pyrolyzed to produce fuels and chemicals are Mahua, Neem, Jatropha, Karanja, Castor, Kusum, Polanga, Sal, Cotton, Soapnut, etc, [20]. Apart from these seeds, waste biomass such as pine sawdust, sal sawdust, areca nut husk, rice husk, wheat husk, rice straw, wheat straw, and several other biomass that grow in arid or semi-arid tropical regions are also tested for their potential as pyrolysis feedstock [21, 22].

Non-edible seeds have higher extractive content than wood biomass which increases the yield of pyrolytic liquid during pyrolysis. Most of the seeds have approximately 21 % - 58 % oil content [20]. Non-edible seeds do not compete with edible food sources for land, as it can be grown on the marginal lands and can be the source of feedstock throughout the year. Initial studies showed that non-edible seeds can produce good quality of pyrolytic oil with

excellent fuel properties which can go a long way in fulfilling the energy requirement in the near future.

1.3. Biomass Conversion Technologies

Conversion of biomass into renewable fuel and other value-added products can be done via biological, thermochemical, and mechanical processes. Mechanical process is not used predominantly due to lower product yield. The conversion of biomass basically depends on the types of biomass, as well as the type of energy required. During the biochemical conversion of biomass, higher molecular weight compounds break down into smaller molecular weight compounds with the help of bacteria or enzyme. This process requires more time for conversion of biomass into fuel. The other important technology is known as thermochemical conversion. In the thermochemical process, heat is supplied for breaking higher molecular weight compounds into smaller molecular weight compounds within a few minutes or even seconds [23]. During thermochemical conversion, biomass is converted into solid, liquid and gases which are later synthesized into desired products or used directly in engine, furnace, and boilers. The major route of conversion of biomass into renewable fuel and value-added products are summarized in Fig. 1.2.

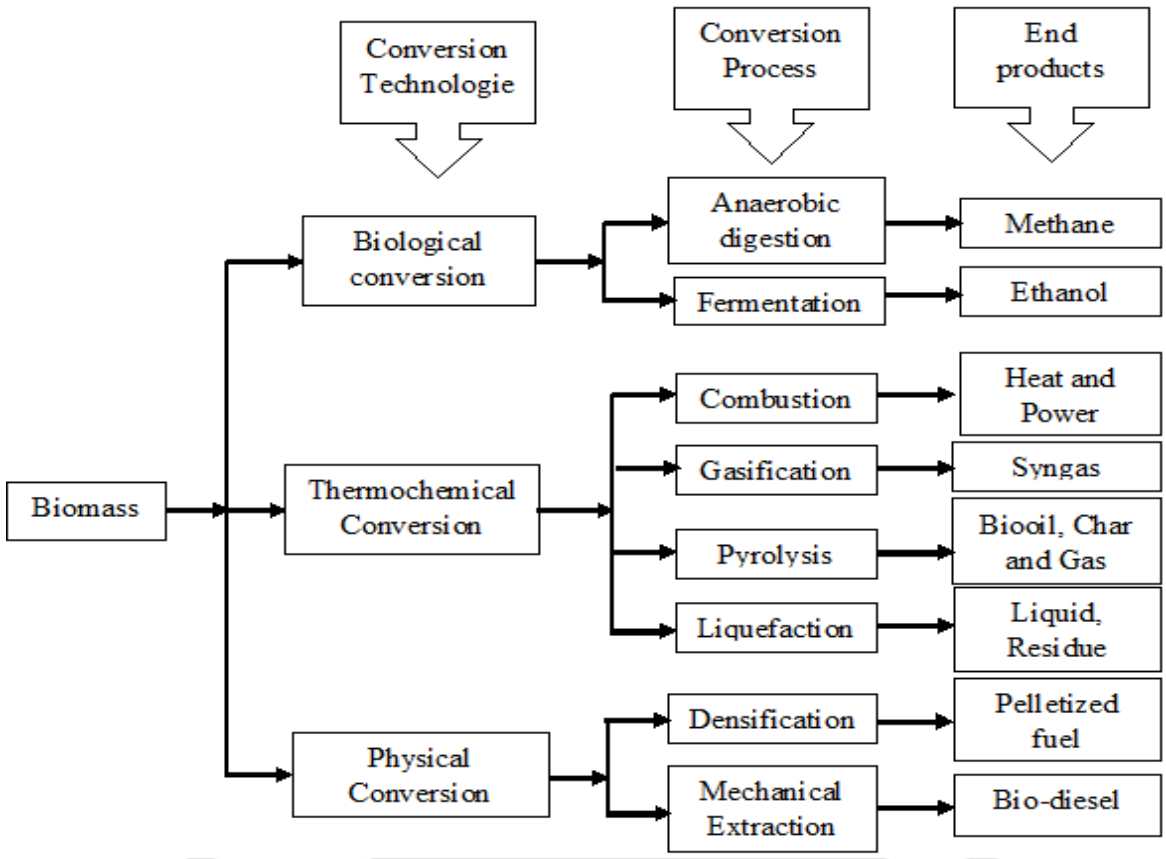

Fig. 1.2. Major process of biomass conversion and possible end products

The thermochemical and biochemical conversion technologies have some merits and demerits. Table 1.1 summarized the merits and demerits of the thermochemical and biological conversion process.

Table 1.1. A brief summary of merit and demerits of the thermochemical and biological process

	Biochemical Conversion	Thermochemical Conversion
1	It involves the use of enzymes, bacteria, microbes for conversion, and can be converted to specific products.	It has the potential for almost all types of biomass but preferably used dry biomass
2	The productivity is lower and it requires large volume reactor which needs higher capital cost	Higher productivity due to complete chemical nature of the reaction

3	Ambient temperature may play an important role in biological conversion	Not dependent on ambient temperature
4	Very limited option for multiple products because the microbial culture is very specific to products	It has the potential to produce different types of end products
5	Biomass sludge is generated due to biological process and poses a problem of secondary waste	No secondary waste generated since complete conversion occurred
6	This process requires a very long period for the conversion of waste into renewable fuel and other value-added products	This process requires only a few seconds or minutes to convert biomass into renewable fuel and other value-added products

1.4. Thermochemical Conversion Technology

The thermochemical conversion process has gained greater attention due to its inherent advantage over other conversion technologies. Thermochemical conversion depends on the process parameters such as temperature, heating rate, residence time, types of feedstocks, etc. Based on the operating condition/process parameters, thermochemical processes are classified into four major forms:

1. Combustion
2. Gasification
3. Pyrolysis
4. Hydrothermal liquefaction

These thermochemical processes have again some merits and demerits. Table 1.2 summarized the advantages and disadvantage of all these processes.

1.4.1. Combustion

Combustion in the simplest and oldest thermochemical technique which involves homogeneous and heterogeneous reactions. Burning of materials in the presence of air or oxygen is known as combustion. By using appropriate devices such as furnaces, stoves, steam turbines, boilers, etc., the chemical energy stored in the biomass is converted into heat energy, power, and electricity during combustion. Biomass having moisture less than 50 % is suitable for combustion process [24].

1.4.2. Gasification

The burning of biomass in the presence of air, steam, or oxygen at a higher temperature (>1000 ^{o}C) is known as gasification. Pyrolysis and gasification are known as an extension of combustion in which gaseous products enhanced as compared to solid (biochar). Production of syngas is the major attraction of gasification which can be used for generation of heat and electricity. Using oxygen gas as the gasifying agent against air improved the heating value of product gas and removed nitrogen. There are many controlling parameters such as heating rate, design of the reactor, and post-processing of gases which produced a clean and high quality of gas through gasification. Gas with lower calorific value can be achieved through direct burning which can be used as a fuel for the gas engine and gas turbine. Production of methanol from these gases is one of the best example [25].

Table 1.2. A brief summary of the advantages and disadvantages of combustion, gasification, pyrolysis and hydrothermal liquefaction

Processes	Advantages	Disadvantages
Combustion	• Produced heat can be used directly for power generation • Industrially mature and commercial technology	• Emission problems • Heat cannot be stored • Larger gas cleaning equipment is required because of the large volume of gaseous products
Gasification	• Lower emission • Less gas cleaning equipment is required due to the comparatively smaller volume of gaseous products • Produced char can be used as activated carbon and/or for soil amendment	• Higher capital cost • Very complex operation as oxygen separation units are required for oxygen • Cost depends on steam and oxygen • Ash content is higher which results in agglomeration
Pyrolysis	• No emission • Lower operating temperature than gasification and combustion • Different types of end products (solid, liquid, and gaseous) • Liquid fuel can be used for boiler operation or various types of chemicals • Bio-oil has higher energy density than syngas • Produced bio-char can be used for different application • Potential integration into bio-refineries	• Not yet fully commercialized • The heating value of bio-oil is lower than heavy fuel such as diesel and petrol • Need separate equipment for engine and boiler application • Immiscible with hydrocarbons • Difficulties in storage due to an unsaturated oxygen content • Corrosive in nature
Hydrothermal Liquefaction	• Lower oxygen content than pyrolytic liquid • Required lower processing of biomass	• More expensive and complex than pyrolysis • Required long residence time and high pressure

1.4.3. Pyrolysis

Pyrolysis has various advantages over other thermochemical technologies. Burning of biomass in the absence of oxygen or partial presence of oxygen at moderate temperature (400 ^{o}C - 700 ^{o}C) is known as pyrolysis. Among all the thermochemical techniques, pyrolysis can produce solid, liquid and gaseous products. Production of liquid fuel is the major consideration through pyrolysis which can be further upgraded to enhance fuel properties. However, recently pyrolysis was used for the production of biochar which can be used for various application such as adsorption of toxic gases, soil abatements, and fertilizers, making of materials and treatment of water and wastewater [26, 27]. The production of liquid fuel from the mixture of biomass and plastic waste can be achieved via pyrolysis. Various process parameters such as heating rate, temperature, particle size, feed composition, types of reactor, sweeping gas flow rate and composition of biomass affected pyrolysis. Further, biomass chemical constituents such as hemicellulose decomposed at a lower temperature (150 ^{o}C - 320 ^{o}C) followed by cellulose (180 ^{o}C - 400 ^{o}C) and finally lignin fragmented at a higher temperature (100 ^{o}C - 900 ^{o}C) due to the occurrence of hydroxyl phenolic groups [28]. Decomposition of these components significantly produces their monomers which further splits into volatiles such as carbon dioxide, carbon monoxide, some condensable vapors, and tars.

1.4.4. Liquefaction

Liquefaction is a thermochemical technique where water acts as catalyst and reactant at a higher temperature which separated all the organic compounds into the individual compound. It has an advantage over pyrolysis and gasification since it does not require dry biomass and reduced the unit operation for the conversion of biomass into renewable fuel [29].

1.5. Biomass as a Source of Renewable Energy

Biomass is a complex matrix of hemicellulose, cellulose, lignin and other compounds which are readily available across the world and considered as a third largest global source of energy [30]. Biomass is used as a direct energy source which accounted for 40 % - 50 % of the energy used for the domestic and industrial sector in many countries that have a large forest and agriculture land [31]. The produced energy from biomass is used for the production of electricity, domestic heating and providing process heat for industrial facilities. Fig. 1.3 showed some important biomass resources. Biomass is considered as an important renewable energy source due to its inherent advantages over other sources. Biomass is known as a clean energy source due to the lower amount of nitrogen and sulphur which limits the formation of SO_x and

NO_x gases. Moreover, lower sulphur and nitrogen percentage made this source more suitable for combustion due to its lower slagging and fouling properties.

Based on the source of biomass, it can be broadly classified as energy crops, forest products, waste aquatic and marine types as shown in Table 1.3.

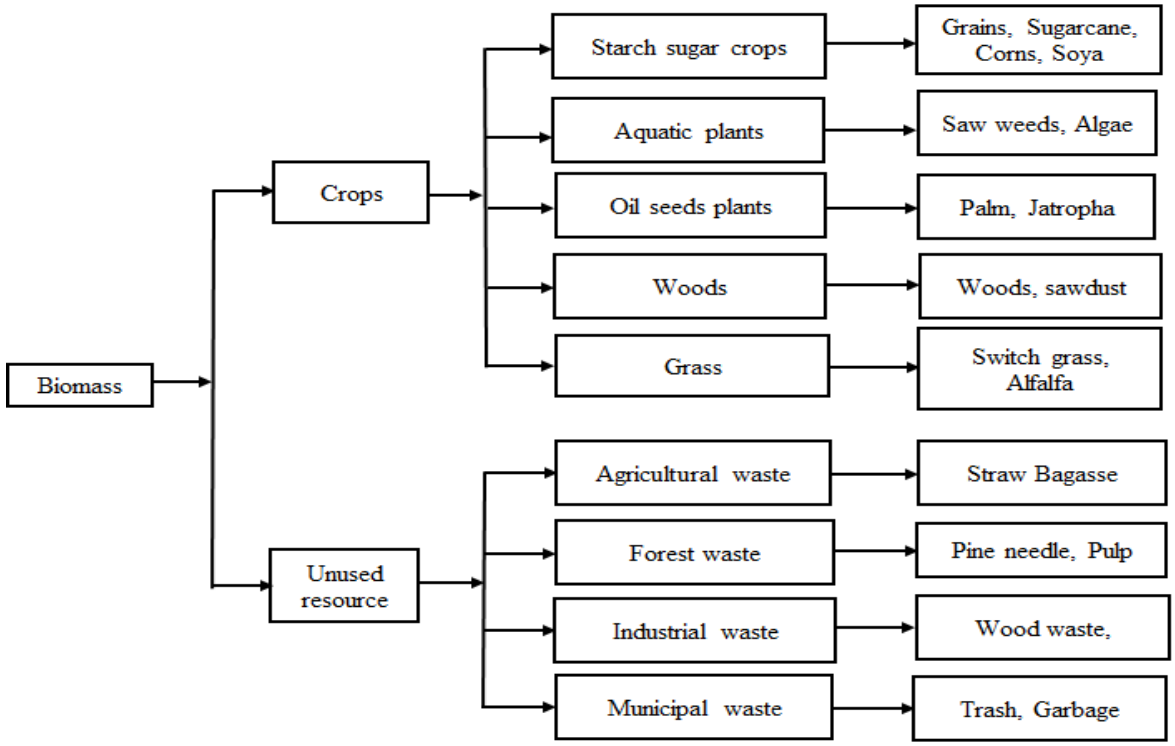

Fig. 1.3. Different types of biomass resources

Table 1.3. Classification of different types of biomass sources

Types of biomass	Examples
Energy crops	Sugar crops, starch crops (corn, barley, and wheat), grasses, herbaceous, oilseed crops (soybean, sunflower, safflower), woody crops (weeds, napier grass), switchgrass, miscanthus
Forest products	Trees, wood, shrubs and wood residues, logging residues, bark, sawdust, etc.,
Waste	Agricultural wastes, urban organic wastes, industrial organic waste, animal waste, crop residues, mill wood wastes
Aquatic plants, marine	Aquatic weeds, Algae, seagrass beds, coral reef, and kelp

1.6. Chemical Composition of Biomass

Biomass is made of a wide range of chemicals and the chemical composition of each biomass varies from source to source and very diverse compared to from fossil fuel. Biomass is mainly composed of macromolecular substances like cellulose, hemicellulose, and lignin together with smaller amounts of low molecular weight extraneous materials and inorganic minerals. Among all the macromolecule substances, the combination of cellulose, hemicellulose, and lignin is known as lignocellulose. The complete summary of common constituents of biomass is presented in Fig. 1.4.

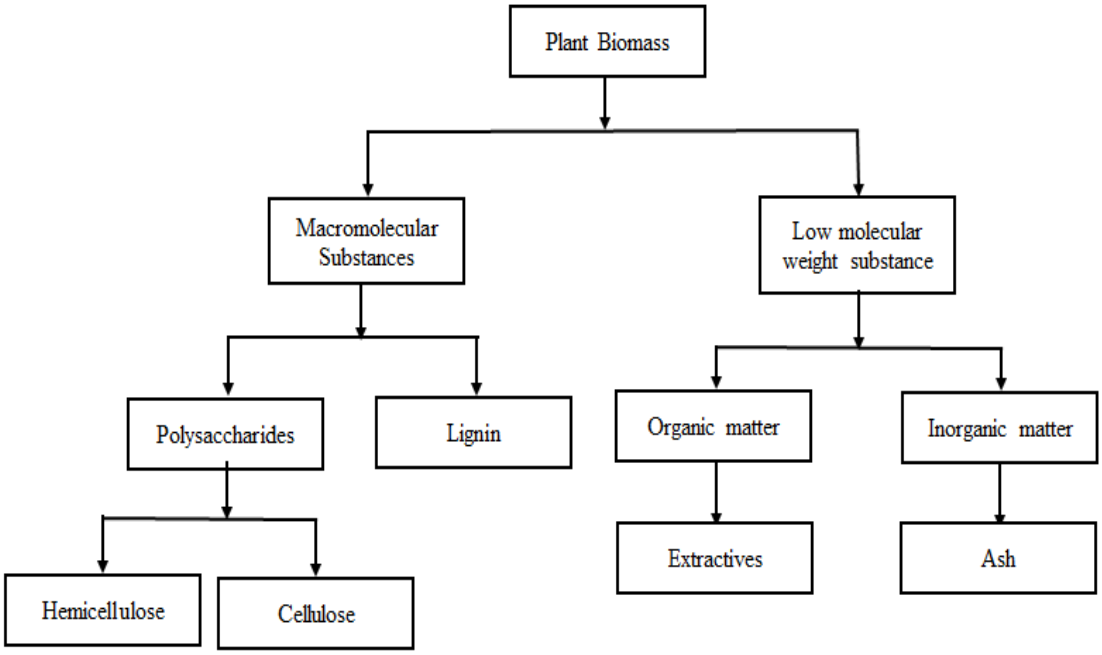

Fig. 1.4. General constituents of plant biomass.

1.6.1. Macromolecular substance

The macromolecular substance is classified as cellulose, hemicellulose and lignin compounds. A brief discussion is given below.

1.6.1.1. Cellulose

Cellulose is the most abundant lignocellulosic constituent in biomass followed by hemicelluloses and lignin. Generally, it includes 40 wt.% - 50 wt.% of dry biomass. It is a linear homopolysaccharide consisting of d-glucose molecule bound together by β-1,4-glycoside linkages. Due to this linkage cellobiose is formed as a repeating unit in cellulose chains, which is basically two units of anhydrous glucose [24]. The cellulose chains are bound together with intermolecular and intramolecular hydrogen bonds between -OH groups and form

a crystalline supermolecular structure. Most of the cellulose chains are highly crystalline, but small parts of the cellulose are amorphous. Fig.1.5 shows the chemical structure of cellulose.

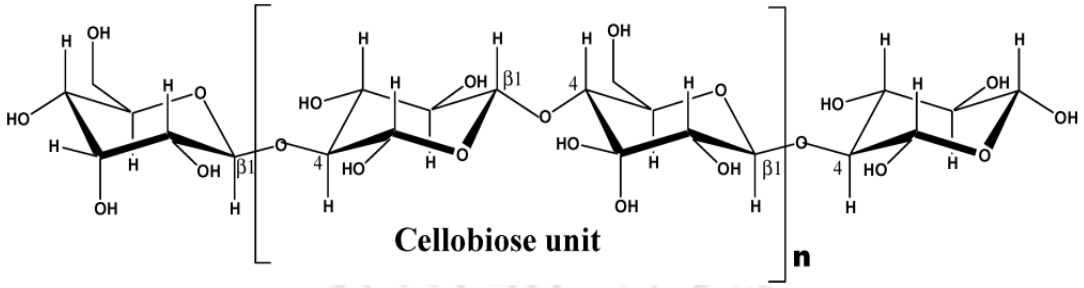

Fig. 1.5. Chemical structure of cellulose [24]

1.6.1.2. Hemicellulose

Hemicellulose is the second major lignocellulosic component in biomass. In contrast to cellulose, hemicellulose is heteropolysaccharide consisting of different monosaccharide units. The composition of hemicellulose usually varies as 25 wt.% - 35 wt.% for dry biomass [24]. The monomeric components of hemicellulose are pentose sugars (xylose and arabinose), hexose sugar (glucose, mannose, and galactose) and sugar acids (methylglucuronic and galacturonic acids). The polymer chains of hemicellulose have short branches and are amorphous in nature. Fig. 1.6 shows the schematic illustration of sugar units of hemicellulose.

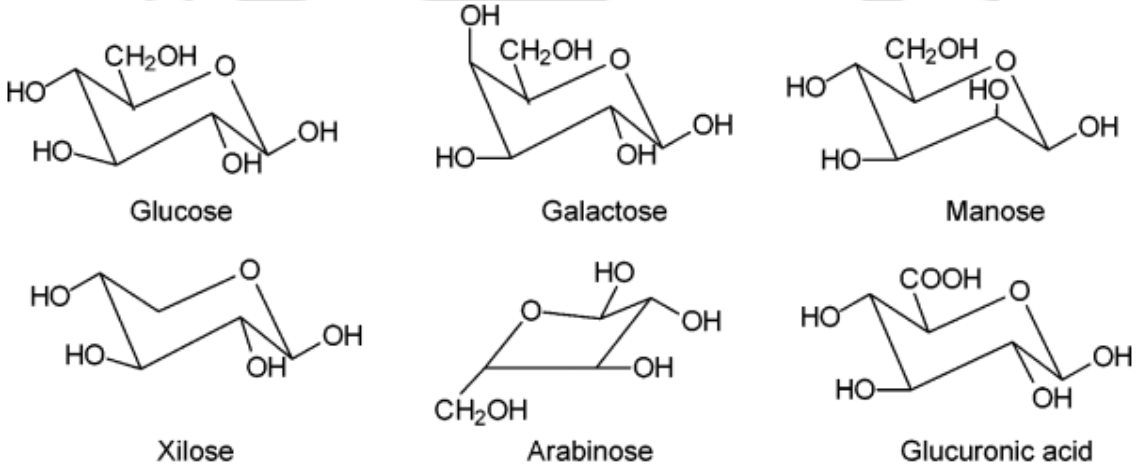

Fig. 1.6. Main components of hemicellulose [24]

1.6.1.3. Lignin

Lignin is the third major lignocellulosic component of biomass. It is a highly branched, substituted, the three-dimensional aromatic polymer of different phenylpropane units which are mainly guaiacyl, syringyl, and p-hydroxy-phenyls bound together by C-O and C-C bonds as shown in Fig. 1.7. Lignin is concentrated between the outer layers of the fibers, it gives the structural rigidity and holds the fibrous cellulosic components. It has a high molecular weight and is amorphous in nature. Lignin content in the biomass is about 20 wt.% - 35 wt.% [24].

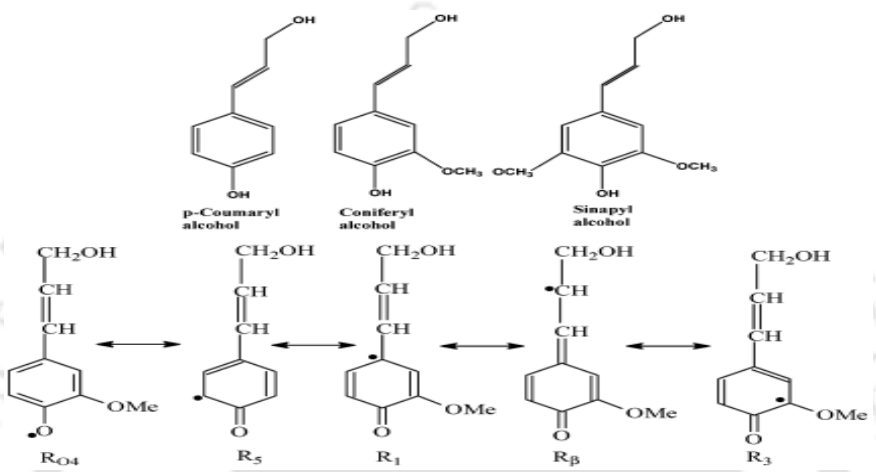

Fig. 1.7. p-Coumaryl, coniferyl, and sinapyl structures and resonance hybrid structures of phenoxy radicals produced by the oxidation of coniferyl [24]

1.6.2. Low molecular weight substance

1.6.2.1. Organic extractive

Biomass includes a small amount of organic extractives, which are lower molecular weight compounds and soluble in neutral solvents. The extractives include fats, proteins, simple sugars, phenolics, waxes, pectins, alkaloids, resins, gums, starches, terpenes, saponins, glycosides, and essential oils. Extractives work as intermediates in metabolism, provide protection against insect attack and microbial destruction [24]. They also contribute to the characteristic properties such as color, odor, and taste of the biomass.

1.6.2.2. Inorganic matter

Biomass contains a small amount of inorganic matters that end up as the ash. Calcium (*Ca*), magnesium (*Mg*), potassium (*K*) and silica (*Si*) are the most common inorganic elements found in biomass. Other inorganics such as sodium (*Na*) and phosphorous (*P*) are found in minor quantities in some biomass [24].

1.7. Major Advantage and Disadvantage of Biomass

It is well established that biomass has several advantages over other renewable energy sources. The various advantages and disadvantages of biomass are listed in Table 1.4.

Table 1.4. Major advantages and disadvantages of biomass

Advantages	Disadvantages
Renewable energy source	Incomplete renewable energy resource for biomass fuel with respect to the complete life cycle assessment
CO_2 neutral conversion and climate change benefits	Miss of accepted terminology, classification systems and standards worldwide
Commonly low contents of ash, C, S, N, and trace elements	Insufficient knowledge and variability of composition, properties, and quality
Normally high concentrations of volatile matter, Ca, H, Mg, O, and P	Commonly high contents of moisture, Cl, K, Na, Mn, and some trace elements
Great reactivity during conversion	Low energy density
Mitigation of hazardous emissions (CH_4, CO_2, NO_X, SO_X, trace elements) and wastes separated	Potential competition with food and feed production if not selected judiciously
Capture of some hazardous components by ash during combustion	Possible soil damage and loss of biodiversity
Huge availability and relatively cheap resource	Odor, potential emission and leaching of hazardous components during disposal
Diversification of fuel supply and energy security	Possible hazardous emissions during heat treatment
Rural revitalization with the creation of new jobs	Potential technological problems during heat treatment
The potential use of oceans and low-quality soils, and restoration of degraded lands	Regional availability
Reduction of biomass-containing wastes	Great collection, transportation, storage, and pre-treatment costs
Cheap resource for the production of sorbents, fertilizers, liming and neutralizing agents, building materials, and for some synthesis or recovery of certain elements and compounds	Unclear utilization of waste products

1.8. Mechanism of Biomass Pyrolysis

Pyrolysis of biomass is a complex process where within a fraction of seconds or few seconds, or minutes many chemical reactions occur in series and parallel including dehydration, depolymerization, isomerization, decarboxylation, and charring [24]. During pyrolysis, biomass involves three major stages of degradation: (i) removal or evaporation of moisture (ii) primary decomposition (formation of char, depolymerization, and fragmentation) and (iii) secondary reaction (cracking of vapors and repolymerization) [32].

1.8.1. Removal of moisture

Moisture removal is an essential part of biomass pyrolysis since pyrolysis is mostly used for conversion of dry biomass. Dehydration reaction involves the removal of water molecules or moisture from the biomass up to 100 ^{o}C. Presence of moisture in biomass during pyrolysis can lead to lower liquid yield, reduced heating value, and formation of a higher quantity of char [33].

1.8.2. Primary decomposition

Biomass is a solid matrix of hemicellulose, cellulose, lignin, extractive and a small amount of inorganic content. At the beginning of pyrolysis, the chemical bonds present in biomass are split into smaller bonds which results in the formation of hot volatiles and rearrangement reactions. These primary reaction involves char formation, depolymerization, and fragmentation.

1.8.3. Char formation

Char formation involves the conversion of biomass into solid residue which results due to the formation and rearrangement of benzene rings into stable polycyclic structures. The release of non-condensable gases occurred during these rearrangement.

1.8.4. Depolymerization

Depolymerization involves fragmentation of polymers into their individual monomers which reduced the degree of polymerization in the chain and produced volatiles. These hot volatiles recovered in the form of liquids. However, depolymerization reaction occurred from temperature range 250 ^{o}C - 500 ^{o}C [24].

1.8.5. Fragmentation

Fragmentation of biomass directed to the destruction of chemical bonds within the monomers unit of the polymer into non-condensable gases. The fragmentation reaction occurred above 600 ^{o}C.

1.8.6. Secondary reaction

The hot volatiles released during depolymerization or fragmentation stages are not stable due to operating conditions such as temperature and further involves in a secondary reaction. These reactions occur in the vapor phase or in between vapor and solid phase. During cracking, higher molecular weight compounds split into smaller molecular weight compounds. Just after in recombination reaction, hot volatiles recombines again to form higher molecular weight compounds such as polycyclic hydrocarbons. Further, when the recombination of volatiles occurs inside the pore of the solid reside, this promotes the formation of char.

1.9. Classification of Pyrolysis

Pyrolysis process is primarily categorized into four types based on their operating conditions such as slow, intermediate, fast and flash pyrolysis.

1.9.1. Slow pyrolysis

Slow or conventional pyrolysis is carried out at lower heating rates, lower temperatures (400 ^{o}C) along with higher residence time (5 min - 30 min or more) [24]. The higher vapor residence time offered formation of secondary reactions which lead to the formation of a higher quantity of char due to partial combustion of biomass (lower heat transfer) and reduced formation of liquid and gaseous product yields. Most preferably, slow pyrolysis is used for the production of solid fuel such as biochar. Slow pyrolysis usually resulted in a 30 % liquid yield and 35 % char yield along with some amount of gas. The condensable vapor consists mostly of water, carboxylic acids, and aldehydes. The slow pyrolysis pyrolytic liquid has low energy content [24, 34].

1.9.2. Intermediate pyrolysis

Intermediate pyrolysis is more suitable than slow pyrolysis for the production of liquid fuel since it is used at moderate temperature (500 ^{o}C - 550 ^{o}C) with higher vapor residence time (10 s - 20 s). In intermediate pyrolysis, quality of end products improved because in this process chemical reaction takes place in a controlled manner which offered a broad range of variation in process parameters optimization. This process yields about 50 % liquid, 30 % gas and 20 %

char [34]. The pyrolytic liquid obtained from intermediate pyrolysis is quite good in terms of energy content, and composition, which may be used as an alternative fuel after suitable upgradation.

1.9.3. Fast pyrolysis

Fast pyrolysis is an advanced process where biomass is heated with the very higher heating rate at a moderate temperature (500 ^{o}C) with a very low residence time (0.5 s - 5 s) [24]. Fast pyrolysis produced about 60 wt.% -70 wt.% liquid, 15 wt.% - 25 wt.% char and 10 wt.% - 20 wt.% gaseous products [24]. It is important to mention that, the production of char and tar is considerably less during this process. Fast pyrolysis is effective with most of the fluidized bed reactors as it deals with high heating rates, rapid de-volatilization, easy control, and easy product collection.

1.9.4. Flash and vacuum pyrolysis

Flash pyrolysis is an effective technique for conversion of biomass into renewable fuel and value-added chemicals. Flash pyrolysis is carried out with a higher temperature (>650 ^{o}C) with very rapid heating rate and lower residence time (<1s) [24]. Flash pyrolysis maximize the yield of tar and bio-oil while producing less bio-char. The important thing is that flash pyrolysis requires a particular kind of reactor. Moreover, it requires a lower particle size of biomass (approximately 105 mm - 250 mm) so as to enable maximum heat and mass transfer. In flash pyrolysis, rapid de-polymerization and cracking of biomass eliminate the side reactions which produced low viscous liquid comparable to diesel oil [24]. Vacuum pyrolysis is another effective technique for conversion of biomass into value-added products and renewable fuels. It reduces the secondary decomposition reactions and prevents further cracking and recondensation reactions which in turn give higher oil yield and lower gas yield. The vacuum facilitates the removal of condensable products from the hot reaction zone [35].

Chapter 2

Literature Review and Research Objectives

2.1. Importance of Pyrolysis

The growing concern about the environmental effect such as global warming has brought pyrolysis in the limelight since few years as it can produce solid (biochar) liquid (bio-oil, tar or pyrolytic oil) and gaseous products such as methane, hydrogen, carbon monoxide, and carbon dioxide simultaneously. Further, pyrolysis is operated at a lower temperature (400 ^{o}C - 700 ^{o}C) than gasification (>1000 ^{o}C) which ultimately reduce the overall energy cost [4]. Pyrolysis offers a wide range of pyrolytic products due to different types of pyrolysis such as slow pyrolysis, fast pyrolysis, and intermediate pyrolysis. Slow pyrolysis offers maximum production of char while fast pyrolysis offers higher production of pyrolytic liquid with improved/better quality. The pyrolytic oil was further upgraded and used as transportation fuel, however; the non-condensable gases can be used for domestic heating since these gases have higher heating value (5 MJ kg^{-1} - 16 MJ kg^{-1}) [36]. Recently, co-pyrolysis was introduced where different types of waste plastics and waste tyres were mixed with biomass in different proportions and converted into renewable fuel and other value-added products [37, 38].

2.2. Biomass

Biomass is a renewable and sustainable fuel that is originated from organic materials such as plants or animals and micro-organisms. This comprises the products, by-products, residues, and wastes from agriculture, forestry, industrial and municipal wastes.

2.2.1. Source of biomass

The common sources of biomass are the agricultural, forest, municipal and biological wastes. Some examples of sources are given below.

1. Agricultural: processed residue, food grain, seed hulls, nut shells, straw, and manure from cattle, poultry, corn stalks, and hogs.
2. Forest: trees, timber slash, wood or bark, sawdust, wood waste, and mill scrap.
3. Municipal: waste paper, sewage sludge, food waste, refuse-derived fuel (RDF), and yard clippings.
4. Biological waste: aquatic species, animal waste, biological waste.

2.3. Available Biomass Resources in India

Biomass is derived from water-based vegetation, a by-product of crop production, forest or organic waste, agro or food industries waste, etc. Different types of biomass resources are available in India. They are classified based on their origins such as grasses, woody and forest plants, fruits, vegetables, manures, and aquatic plants and is represented in Fig. 2.1.

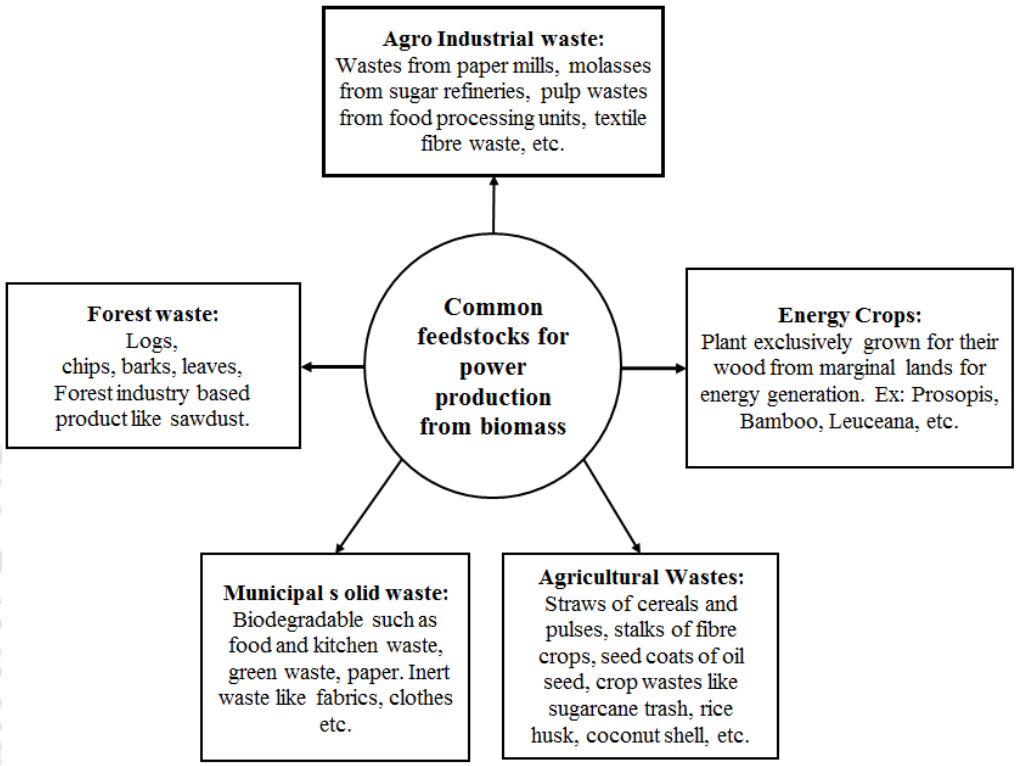

Fig. 2.1. Different types of biomass available in India [21]

2.4. Why Biomass or Waste Biomass?

Biomass energy has rapidly grown during the last few decades and become an essential part of the global renewable energy. Renewable energy satisfies about one-fifth of the total energy consumption worldwide, counting traditional biomass, large hydropower, and renewables sources such as small hydro, solar, geothermal, wind, and biofuels. About 13 % of biomass energy was used for domestic heating and cooking and is growing slowly, however, it is expected to be one-third of the world energy supply in the year 2050 [39]. Renewable energy such as biofuel contributes about 3 % of the world's total fuel for the transportation sector [40]. Waste biomass resources are readily available in rural and urban areas globally. The residue remaining after post-processing of agricultural produce can be used for the generation of

energy. On the other side, biomass-based industries can provide employment opportunities, faster rural development, and endorse biomass re-growth through sustainable land management practices. Biomass wastes include a wide range of materials derived from agricultural, agro-industrial, and timber residues, as well as municipal and industrial wastes. Bioenergy has tremendous potential to replace the use of fossil fuel and reduced greenhouse emissions. Biomass reduces emissions and enhances carbon sequestration as short-rotation crops or forests established on abandoned agricultural land accumulate carbon in the soil.

Biomass can play an essential role in reducing dependency on fuels by making use of thermochemical conversion technologies. In addition, increased utilization of biomass-based fuel will lead to the generation of new job opportunities, sustainable development and health improvements in rural areas. The development of new technologies for the handling and processing of biomass, improvement of agroforestry systems and the establishment of small and large-scale power plants may eventually turn the lifestyle in rural areas. Furthermore, waste biomass such as pine sawdust, sal sawdust, areca nut husk, rice straw, white straw, rice husk, and different types of agricultural residue may be used for generation of fuel and value-added chemicals [41].

2.5. Why Non-edible Biomass?

The non-edible seed is an emerging candidate for the production of fuel and chemical since last decade. Non-edible seeds have an advantage over edible seeds in terms of food versus fuel issue. Moreover, non-edible seeds are usually dumped at the site which further decomposes and releases various toxic gases. Edible and non-edible seeds have a higher amount of extractive content, which lead to the maximum production of liquid fuel. A number of studies are being carried out at various research laboratories on the effective use of non-edible seeds. Conversion of food crops such as palm oil, coconut oil, corn, soybean, and sugarcane to biodiesel could lead to severe food shortage. The higher price of high quality refined edible oil makes them unfeasible as a feedstock to produce biodiesel especially for a developing country like India. Therefore, the non-edible source is the best possible source, which can meet the Indian requirement. Non-edible plants or crops can be cultivated in waste and unproductive lands which lead to effective use of these lands [42]. Free fatty acid is the chemical compounds, which classified seeds into edible and non-edible. Non-edible seeds contain toxic substances such as triterpenoids, furanoflavones, uranodiketones, furanoflavonols, cyanogenic glucoside, chromenoflavones, flavones, curcain, etc., [43, 44]. The composition of these toxic compounds

depends on the type of biomass as well as the quality of the soil where it is grown. Thus, the use of non-edible seeds for the production of fuel and chemical seems more promising.

2.6. Characterization of Biomass

Physicochemical characterization of biomass is the primary step, which involves proximate analysis, ultimate analysis, extractive analysis, and chemical analysis. The physical and chemical analysis confirmed the potential of any biomass towards the production of fuels and value-added chemicals.

Doshi et al. (2014) [45] studied Jatropha curcas (whole seeds, kernel, and hull) and *Pongamia pinnata* (whole seeds, kernel, and hull) and reported presence of higher volatile matter (61 % - 81 %) and lower ash content (4 % - 9 %) along with higher carbon (39.80 % - 44.50 %) and lower nitrogen content (0.90 % - 7.20 %). All biomass has <10 % moisture while hemicellulose (16.34 % - 24.90 %), cellulose (24.6 % - 32.90 %), and lignin (3.50 % - 9.40 %) were found to be significant. The heating value of biomass (17.68 MJ kg^{-1} -19.98 MJ kg^{-1}) was found to be higher.

Nanda et al. (2013) [46] studied *Pinus banksiana* (pinewood), *Phleum pratense* (timothy grass) and *Triticum aestivum* (wheat straw) and reported the presence of higher volatile matter (70.10 % - 78.20 %) and lower ash content (2.30 % - 4.40 %). Further, ultimate analysis confirmed the presence of higher carbon content (43.40 % - 48.90 %) and lower nitrogen (0.10 % - 1.30 %) and sulphur content (0.001 % - 0.01 %). Heating value (15.60 MJ kg^{-1} - 18.10 MJ kg^{-1}) and hemicellulose (23.60 % - 30.10 %), cellulose (34.20 % - 39.10 %) and lignin (16.30 % - 20.40 %) were found to be in appropriate range.

Sasmal et al. (2012) [47] studied areca nut husk (*Areca catches*), moj (*Albizia lucida*) and bonbogori (*Ziziphus rugosa*) and reported presence of higher volatile matter (75 % - 85 %) and lower ash content (2 % - 3%). Ultimate analysis confirmed the presence of higher carbon content (41 % - 54 %) and lower nitrogen (0.22 % - 0.69 %) and negligible sulphur content. The chemical analysis was also found to be higher, 44.46 % - 53.46 % cellulose, 6.37 % - 28.80 % hemicellulose and 11.03 % - 22.97 % lignin.

Kumar et al. (2019) studied wheat straw (WS), rice straw (RS), rice husk (RH), banana trunk (BT), arhar stalk (AS), and sugar cane bagasse (SB) and reported that higher volatile matter and lower ash contents. Further, sugar cane bagasse (SB) showed the highest calorific value (CV) and BT the lowest. The alcoholic and phenolic groups, alkene and alkenes and

some aromatic molecules were present in all biomasses. The RH was highly crystalline and BT was more amorphous in nature [48].

Naik et al. (2010) [49] studied wheat straw, barley straw, flax straw, timothy grass, and pinewood and reported presence of higher volatile matter (77.90 % - 82.40 %) and lower ash content (1.10 % - 9.80 %). Elemental analysis confirmed the presence of higher carbon content (41.40 % - 49.00 %) and lower nitrogen (0.14 % - 1.03 %) and sulphur content (0.01 % - 0.15 %) while heating value of these biomass was higher (16.70 MJ kg^{-1} - 20.30 MJ kg^{-1}).

Raj et al. (2015) [50] studied ten biomass namely rice (*Oryza sativa*) straw (RS), rice husk (RH), cotton (*Gossypium arboreum*) stalk (CS), wheat (*Triticum aestivum*) straw (WS), sugarcane (*Saccharum officinarum*) bagasse (SCB), corn (*Zea mays*) stover (CRS), sorghum (*Sorghum bicolor*) stalk (SS), mustard (*Brassica campestris*) stalk (MS), and corn (*Zea mays*) cob (CC). They reported the presence of higher volatile matter (63 % - 80 %) and lower ash content (3.50 % - 17.40 %). Ultimate analysis confirmed the presence of higher carbon content (38.80 % - 46.80 %) and lower nitrogen (0.20 % - 0.90 %) and sulphur content (0.04 % - 0.9 %). The heating value of biomass was also found to be higher (13.30 MJ kg^{-1} - 19.20 MJ kg^{-1}).

2.7. Pyrolysis Kinetics of Biomass

Kinetics analysis of biomass is essential to understand the decomposition reaction mechanism. The knowledge of pyrolysis kinetic parameters are vital for the design and optimization of pyrolysis reactors [51]. TGA is used to demonstrate the thermal behavior of biomass and generated data are normally used to investigate the kinetics of thermal degradation process. Kinetic analysis can be done via two methods: Isothermal method and non-isothermal method. Isothermal method measures the weight loss at constant temperature and kinetic parameters are calculated using a single mass loss curve [52, 53]. Non-isothermal method is known as dynamic method and usually preferred for kinetic analysis of biomass pyrolysis as in this method mass loss is measured at different temperature regions. More than one mass loss curves are used in this method for calculating the kinetic parameters. Non-isothermal methods produce less error compared to the isothermal methods, therefore, non-isothermal methods are favored over the isothermal methods [52]. Non-isothermal methods are further divided into model free and model fitting methods. In model-fitting methods, TGA data is fitted with different models for acquiring the best statistical model from which various kinetic parameters can be calculated. Model-fitting methods determine the kinetic parameters using a single TGA curve. Model-free methods are simple and avoid the selection of the wrong kinetic model and

consequently estimation of wrong kinetic parameters [52]. Numerous studies have been done on kinetic analysis of biomass using iso-conversional models as discussed below.

Mehmood et al. (2017) [54] studied the thermal decomposition characteristics of camel grass (*Cymbopogon schoenanthus)* by adopting three heating rates of 10 ^{o}C min^{-1}, 30 ^{o}C min$^{-1,}$ and 50 ^{o}C min^{-1}, under an inert atmosphere, in a thermo-gravimetric analyzer using KAS and OFW methods. The kinetic results showed that activation energy for the pyrolysis of camel grass varies with the degree of conversion and the average value of activation energy was found to be 169.01 kJ mol^{-1} and 168.57 kJ mol^{-1} by KAS and OFW methods, respectively.

Ceylan et al. (2014) [55] studied pyrolysis characteristics and kinetics of *Polysiphonia elongata* using a thermogravimetric analyzer using Friedman and Kissenger–Akahira–Sunose method. The main decomposition of samples occurred between 225 ^{o}C and 485 ^{o}C at heating rates of 5 ^{o}C min^{-1} - 40 ^{o}C min^{-1} owing to release of 78 % - 82 % of total volatiles. The average activation energy was calculated by Friedman and Kissenger–Akahira–Sunose methods were 116.23 kJ mol^{-1} and 126.48 kJ mol^{-1}, respectively. A variance in the activation energy with the proceeding conversions was observed for the models applied, which shows that the pyrolysis process was composed of multi-step kinetics. The Coats–Redfern method was used to determine the pre-exponential factor and reaction order.

Huang et al. (2016) [56] performed the pyrolysis experiments of soybean straw in a thermogravimetric analyzer, operated under the non-isothermal condition in order to assess the thermal degradation behaviour of soybean straw. They applied three different kinetic methods such as OFW, KAS, and CR to calculate the kinetic parameters. The average activation energy calculated by KAS and OFW methods were found to be 154.15 kJ mol^{-1} and 156.22 kJ mol^{-1}, respectively.

Varma and Mondal 2016 [57] studied physicochemical properties and pyrolysis kinetics of sugarcane bagasse (SB) in a TGA using Kissinger-Akahira-Sunose (KAS) and Ozawa-Flynn-Wall (OFW) methods. The average activation energy of SB was found as 91.64 kJ mol^{-1} and 104.43 kJ mol^{-1}, respectively.

Chandrasekaran et al. (2017) [58] reported pyrolysis of *Prosopis juliflora* fuel wood using thermogravimetric analysis to determine the kinetic parameters at dynamic heating rates of 2 ^{o}C min^{-1}, 5 ^{o}C min^{-1}, 10 ^{o}C min^{-1}, 15 ^{o}C min^{-1}, 20 ^{o}C min$^{-1,}$ and 25 ^{o}C min^{-1}. The activation energy of pyrolysis was calculated using different methods, namely Kissinger, Kissinger-Akahira-Sunose, Ozawa-Flynn-Wall and Friedman model and corresponding calculated

activation energy were found to be 164.6 kJ mol^{-1}, 204 kJ mol^{-1}, 203.2 kJ mol^{-1}, and 219.3 kJ mol^{-1}, respectively for each method.

Oladokun et al. (2016) [59] studied *Imperata cylindrical* in the temperature range of 40 ^{o}C - 1000 ^{o}C with four heating rates of 5 ^{o}C min^{-1}, 10 ^{o}C min^{-1}, 15 ^{o}C min^{-1} and 20 ^{o}C min^{-1}. The average activation energy was calculated from OFW and KAS methods were 164.93 kJ mol^{-1} and 163.44 kJ mol^{-1} respectively.

Zhang et al. (2016) [60] described the thermo-physical properties of pre-treated agricultural residues (soybean stalk, sorghum stalk, cotton stalk, corn stover, and corncob) in a TGA under dynamic heating rates of 5 ^{o}C min^{-1}, 10 ^{o}C min^{-1}, 20 ^{o}C min^{-1}, 30 ^{o}C min^{-1} and 40 ^{o}C min^{-1} using three different methods as OFW, DAEM, and Kissinger. Results showed that the activation energy varied with the degree of conversion and value of average activation energy for most of the agricultural residues were close to each other and also varied from 189.1 kJ mol^{-1} to 200.0 kJ mol^{-1}, except corncob.

Ma et al. (2015) [61] studied palm kernel shell using thermogravimetric analysis under non-isothermal condition using KAS and OFW methods. Results of pyrolysis showed that the activation energy varied with the degree of conversion. For KAS method, activation energy increased from 231 kJ mol^{-1} to 270 kJ mol^{-1} and for OFW method, it increased from 227 kJ mol^{-1} to 261 kJ mol^{-1} as the degree of conversion increased from 0.09 to 0.3, thereafter, for the increase in degree of conversion from 0.3 to 0.8, activation energy decreased from 282 kJ mol^{-1} - 266 kJ mol^{-1} and 277 kJ mol^{-1} - 262 kJ mol^{-1} for KAS and OFW methods, respectively.

Heydari et al. (2015) [53] studied thermal behavior and kinetic parameters of Canadian lignite coal using thermogravimetric analyzer at 298 K - 1173 K with dynamic heating rates 1 K min^{-1}, 6 K min^{-1}, 9 K min^{-1}, 12 K min^{-1}, 15 K min^{-1} and 18 K min^{-1} in non-isothermal condition using Kissinger, Ozawa-Flynn-Wall, Kissinger-Akahira-Sunose, and Friedman model. Results showed that the activation energy obtained by the iso-conversional methods were in good agreement, but Friedman method was considered to be the best among the model-free methods to evaluate kinetic parameters for solid-state reactions.

Santos et al., (2015) [62] studied thermal behaviour and pyrolysis kinetics of castor beans press cake using KAS, OFW and Kissinger methods to evaluate the pyrolysis kinetic parameters. The activation energy for pyrolysis of castor beans press cake varied with the degree of conversion and suggested a complex reaction mechanism for the process. The

average activation energy calculated by KAS, OFW, and Kissinger was found to be 270.60 kJ mol^{-1}, 263.50 kJ $mol^{-1,}$ and 193.70 kJ mol^{-1} respectively.

Ceylan and Topçu (2014) [63] conducted the pyrolysis experiments of hazelnut husk in a TGA analyzer and calculated the kinetic parameters including activation energy and pre-exponential factor by model-free KAS and OFW methods, and Coats-Redfern method. The average activation energy values for pyrolysis of hazelnut husk were found to be 95 kJ mol^{-1} and 102 kJ mol^{-1} by KAS and OFW methods, respectively.

Damartzis et al. (2011) [51] studied pyrolysis experiments of cardoon stems and leaves in a thermogravimetric analyzer and evaluated the pyrolysis kinetic parameters by KAS and OFW methods. The average activation energy value for cardoon stems was found to be 224 kJ mol^{-1} and 229 kJ $mol^{-1,}$ and for cardoon leaves, it was 350 kJ mol^{-1} and 242 kJ mol^{-1} by KAS and OFW methods, respectively.

Xu et al. (2017) [64] studied the pyrolysis and kinetic analysis of rape straw at a different heating range of 10 ^{o}C min^{-1}, 20 ^{o}C min^{-1}, 30 ^{o}C min^{-1} and 40 ^{o}C min^{-1} in an inert atmosphere of nitrogen using Friedman, KAS, and OFW methods. The activation energies ranged from 191.16 kJ mol^{-1} to 264.31 kJ mol^{-1}.

Rony et al. (2019) studied kinetic and thermodynamic analysis of corn stover (Zea mays) in a TGA under the non-isothermal condition and reported that the average activation energies of CS pyrolysis with FWO and KAS models are 191.57 kJ/mole and 181.66 kJ/mol, respectively. Among tested other kinetics models, 1-D diffusion one well fits the kinetic data with its R2 value being higher than 0.94. The corresponding Gibbs free energies of the pyrolysis process are about 172 kJ/mole [65].

2.8. Effect of Process Parameters on Pyrolysis

Process parameters and reaction conditions or operating conditions play a major role to alter the composition and properties of pyrolysis end products. Biomass is made of hemicellulose, cellulose, lignin, and their fragmentation into lower molecular weight compounds depends only on operating conditions such as temperature, heating rate, residence time etc.

2.8.1. Effect of temperature

Temperature is the most important operating parameter during pyrolysis. At lower temperature (<300 ^{o}C), decomposition of biomass happen, at heteroatom sites within biomass structure which leads to the formation of heavy tars while at higher temperature (>550 ^{o}C), rapid fragmentation of biomass occurred which causes breakdown of higher molecular weight compounds into lower molecular weight compounds and produces numerous types of end products. At such high temperature, the products compositions changed due to various primary and secondary reactions. Numerous studies have discussed the effect of temperature on the liquid oil yield [23, 66-68]. Biomass conversion efficiency increases with increase in temperature, which is mainly due to the extra energy inputs available to break the biomass bonds. Ozbay et al. (2006) [69] studied on cotton seeds cake from temperature 40 ^{o}C - 700 ^{o}C and reported that 17.5 % more decomposition occurred during rapid pyrolysis.

2.8.2. Effect of heating rate

Heating rate is an essential parameter, which broadly influenced the pyrolytic end products. In fast pyrolysis, usually, the heating rate is very fast than conventional pyrolysis. The fast heating rate can cause quick fragmentations, enhances the yield of volatiles and uniform products distribution. It was reported that at fast heating rate hot volatiles increased due to extra tar decompositions [70]. Seebauer et al. (1997) [71] stated that pyrolytic products yield in fast pyrolysis depends on two competing reactions: the tar evaporation and char formation. Fast heating rate reduced the heat and mass transfer limitation and increased the release of hot volatiles by fast endothermic decomposition of biomass, therefore, minimize the time availability for a secondary reaction like tar cracking or repolymerization. Numerous studied has been carried out to elaborate on the effect of heating rate on the yield of pyrolytic liquid. Yorgun et al. (2001) studied pyrolysis of sunflower cake which yielded a maximum of 41 % liquid oil at 550 ^{o}C [72]. Further, Mourant et al. (2013) studied pyrolysis behavior of mallee bark in a fluidized-bed reactor and reported that with increasing temperature from 300 ^{o}C to 450 ^{o}C liquid yield was increased by 43.5 %.

2.8.3. Effect of particle size

Biomass being a poor conductor of heat often poses heat transfer difficulties during pyrolysis. The particle size of biomass is considered an important parameter affecting the yield and properties of liquid oil produced and to minimize the heat transfer problems. During pyrolysis, the smaller particle size of biomass is preferred so as to provide uniform heating.

Larger particle size offers heat transfer limitation (poor heat transfer to the inner surfaces will lead to lower average temperatures and hence expected yield of liquids may decrease). Also, the larger particle size of biomass requires high apparent activation energy to split into a lower size which again attributed to heat transfer limitations [73]. Different reactors need different particle sizes, e.g., 200 mm size required for rotating cone pyrolyzer, <2 mm for fluidized bed system, <1 mm for batch and semi-batch reactors and <6 mm for circulating fluid beds [74]. Nevertheless, there is no literature available to support specific biomass particle size for pyrolysis.

2.8.4. Effect of sweeping gas flow rate

The pyrolytic environment can influence the types and composition of all products. The interaction of escaping pyrolysis vapors with surrounding solid environment provokes secondary exothermic reactions that lead to the formation of char. Pyrolysis conditions that support rapid mass transfer are useful to minimize these reactions such as vacuum pyrolysis, fast purging of pyrolysis vapors, rapid quenching of hot vapors and small feed size [75]. From literature, it is confirmed that sweeping gas flow rate has not much affected the pyrolytic liquid yield. Moreover, sweep gas flow assumed as a secondary parameter for production of liquid yield. Acikgoz et al. (2004) [76] reported that by increasing nitrogen flow rates from 50 cm^3 min^{-1} to 100 cm^3 min^{-1}, observed 3 % more liquid yield. Similarly, Demiral and Şensöz (2006) [77] reported that increasing the sweep gas flow rate from 50 cm^3 min^{-1} - 150 cm^3 min^{-1}, 3.3 % more liquid yield was achieved.

2.8.5. Effect of other process parameters

Vapour residence time is another important parameter which influences pyrolytic products yield. Mostly, shorter residence time offers uniform product distribution which is suitable for the production of liquid fuels. During pyrolysis, vapors are susceptible to secondary cracking or repolymerization. Therefore to minimize the decomposition and coking of tars, lower temperature and lower residence time are preferred [78]. To obtain maximum pyrolytic liquid yield only a few seconds or a few minutes seems to be fine. Types of feedstock is also an important parameter. Biomass is a complex matrix of hemicellulose, cellulose, lignin, extractive and a small amount of inorganics content. The relative mass ratio of the organic and inorganic component may vary with types of feedstocks. Since the composition of biomass changed with types of biomass; the composition of pyrolytic liquid also changed. Presence of mineral matter or metal content also has a wide influence on pyrolytic liquid yield. Biomass

has a trace amount of inorganic compounds (K, Na, P, Ca, and Mg) and extraneous organic materials (4 % - 10 %) which appear in pyrolysis ash [33]. The composition of mineral matter significantly influenced secondary pyrolysis reaction which affects the reactivity of pyrolysis char. Mostly, the presence of mineral matter decreased the pyrolytic liquid yield and increased the formation of char and gas. This is because inorganic materials speed up dehydration and charring reactions during both primary and secondary pyrolysis [33]. Moisture also had a significant effect on pyrolytic products yield. Generally, biomass contains 50 wt.% - 60 wt.% moisture and it is essential to remove it before pyrolysis to increase the yield of liquid fuel or end products. Ambient air solar drying can reduce moisture in the range of 3 % - 12 % [33]. Initial moisture influence both the behavior of biomass during pyrolysis as well as physicochemical properties of pyrolytic oil [33, 74].

2.8.6. Effect of Catalyst on pyrolytic liquid yield

Catalyst is used to boost the reaction rate and increase the targeted products yield. Use of catalysts can increase or decrease the liquid yield and also enhances the properties of the liquid fuel. To understand the effect of a catalyst on pyrolytic products yield many studies were carried out. Shadangi and Mohanty (2014) [79] worked on Niger seed in a semi-batch reactor using Al_2O_3, CaO, and Kaolin at 2:1, 4:1 and 8:1 feed to catalyst ratio and reported that the use of catalysts decreased the liquid yield, however, enhanced the fuel properties of the liquid fuel. Li et al. (2009) [80] studied thermal and catalytic pyrolysis (FCC Equilibrium Catalyst with the composition of Al_2O_3, Na_2O, Fe_2O_3) of cottonseed and reported that catalytic cracking increased the yields of liquefied petroleum gas and gasoline with a lower biodiesel fraction compared to that of thermal cracking. This was attributed to secondary reactions on the catalyst acid site. Almost about 90 % of dry gases were produced by catalytic cracking at 460 °C, while 67 % and 44 % of dry gases were produced by catalytic cracking reaction at 520 °C and 540 °C respectively.

2.8.7. Effect of catalyst on the composition of the pyrolytic liquid

Catalytic cracking of biomass reduced the oxygenated compounds by converting it into carbon dioxide, carbon monoxide, and water. It is evident that pyrolysis of non-edible biomass produced many valuable chemicals such as phenols, acids, and hydrocarbons which have high market value. On the other hand, it also produces some less valuable compounds such as oxygenated and nitrogenated compounds along with acids and carbonyls [80]. The use of appropriate catalysts with the optimized condition may produce more valuable chemicals with

less unwanted fractions. In the presence of oxygen, the calorific value of fuel decreased. Further, reduction in acidity and carbonyl compounds from the liquid fuel is essential for the stability and quality of pyrolytic liquid to be used as transportation fuel.

Onay (2007) [81] studied the composition of *pistacia khinjuk* seed pyrolytic oil in a well-swept fixed bed reactor with and without the presence of catalyst and found that oxygen content was higher (14.2 %) in thermal pyrolytic liquid which was reduced by 10.64 % and 10.46 % by using BP 3189 and Criterion-424 catalysts respectively. On the other hand, the yield of aliphatic and aromatic fractions increased upto 24.6 % and 25.2 % using BP 3189 and 32.6 %, 29.5 % using Criterion-424, while thermal pyrolysis produced 16.9 % aliphatic and 25.6 % aromatic fractions. Further, the use of catalyst also reduced the yield of polar fractions in the pyrolytic liquid. Thermal pyrolytic liquid produced 57.50 % polar fraction while it was reduced upto 42.8 % and 45.3 % by applying BP 3189 and Criterion-424 respectively [81]. Numerous studies have been carried out on thermal and catalytic pyrolysis of biomass using different types of reactors. Some of them are discussed below.

Özbay (2015) [82] studied catalytic and non-catalytic pyrolysis of pine wood sawdust in a fixed bed reactor. The maximum bio-oil yield of 46 wt.% was obtained at a temperature of 550 ^{o}C for non-catalytic pyrolysis. In catalytic pyrolysis, the effect of catalyst types (KOH, $ZnCl_2$, and ZnO) and catalysts dose (5 wt.%, 10 wt.%, 15 wt.%, and 20 wt.%) on the pyrolysis products yield and properties of bio-oil were explored. In catalytic pyrolysis, the yield of gaseous products increase and bio-oil yield decrease as compared to non-catalytic pyrolysis at the same temperature.

Putun (2010) [68] conducted pyrolysis experiment in a tubular fixed bed reactor with a dynamic sweeping gas flow rate and temperature. Thermal pyrolysis provided about 48.3 wt.% bio-oil yield at 500 ^{o}C temperature and 200 mL min^{-1} flow rate of nitrogen gas. At optimized condition, pyrolysis was performed by using MgO catalysts in different proportion (5 wt.%, 10 wt.%, 15 wt.%, and 20 wt.%).

Chen et al. (2017) [83] investigated the role of calcium oxide in the pyrolysis of biomass at various temperatures on the cotton stalk in a fixed bed reactor and reported that the use of CaO catalyst during pyrolysis has resulted in increased furans and hydrocarbons by decreasing the ester and anhydrosugar contents. The pyrolysis of various other biomass are reported in Table 2.1 with their respective major findings.

2.9. Properties of Pyrolytic Oil

The thermal pyrolytic oil has some advantages and some disadvantages. Use of appropriate methods such as catalytic pyrolysis, catalytic vapor upgrading, and hydrothermal treatment along with various physical treatment methods, these drawbacks can be minimized. The important fuel properties are discussed below.

2.9.1. Calorific value

The calorific value is one of the most important fuel properties. The literature revealed that pyrolytic oil has a higher heating value close to diesel fuel [24]. Further, the calorific value of pyrolytic liquid depends on types of feedstocks, operating conditions, and types of process used. Also, it is reported that pyrolytic oil produced from non-edible seeds have a higher heating value than wood pyrolytic oil [84].

Table 2.1. Literature review on various biomass towards production of fuels and chemicals

Biomass	Reactor	Range of operating temperature				Optimum conditions	Optimum products yield (wt. %)	Other findings	References
		Temperature (°C)	Heating rate (°C/min)	Biomass particle size (mm)	N_2 flow rate (mL/min)				
Soursop seed cake	Batch	400	15	-	-	Temperature: 400 °C	Bio-oil: 18.6 Bio-char: 32.2 Pyro-gas: 17.7 Aqueous: 31.5	Analysis of bio-oil	[85]
Cashew nut shell	Batch	300-700	22.5	0.25	100	Temperature: 400 °C	Bio-oil: 40.0 Bio-char: 30.0 Pyro-gas: 30.0	Analysis of bio-oil, bio-char and pyro-gas	
Chinese tallow wood	Fixed bed	500-700	-	0.5-1	1000	Temperature: 600 °C	Bio-oil: 38.1	Analysis of bio-oil	
Tegument		450-600	100	<1	1000	Temperature: 650 °C	Bio-oil: 38.8	Analysis of bio-oil	
Almond						Temperature: 450 °C	Bio-oil: 28.1		

Mahua seed	Semi batch	450-600	20	0.55-1	30	Temperature: 525 °C	Bio-oil: 49	Analysis of bio-oil	[86]
Coconut shell	Semi batch	450-600	20	<1 (avg)	-	Temperature: 575 °C	Bio-oil: 49.5	Analysis of bio-oil and bio-char	[87]
Cornelian cherry stone	Fixed bed	300-700	7	<0.5	30	Temperature: 500 °C	Bio-oil: 47.5	Analysis of bio-oil and bio-char	[88]
Grape seeds				<0.45		Temperature: 700 °C	Bio-oil: 41.04		
Liquorice stalks	Fixed bed	350-550	40	0.150-0.224	100	Temperature: 450 °C	Bio-oil: 30	Analysis of bio-oil and bio-char	[89]
Cotton stalk	Fixed bed	500-600	20	-	20-50	Temperature: 600 °C N_2 flow rate: 20	Bio-oil: 17.14 Bio-char: 38 Pyro-gas: 44.86	-	[90]
Jatropha Curcas cake	Fixed bed	350-600	5	0.5-0.8	100	Temperature: 550 °C	Bio-oil: 45	Analysis of bio-oil	[91]
Cotton seed	Batch	350-600	20	<1	5	Temperature: 550 °C	Bio-oil: 58.6	Analysis of bio-oil	[92]
Pongamia glabra deoiled cake	Fixed bed	350-600	10, 20 & 40	0.2-0.4	-	Temperature: 500 °C Heating rate: 40	Bio-oil: 30.6	Analysis of bio-oil and bio-char	[93]

Castor seeds	Semi batch	400-600	20	-	-	Temperature: 550 ºC	Bio-oil: 62.45	Analysis of bio-oil	[94]
Sal seed	Semi batch	400-625	20	-	35	Temperature: 600 ºC	Bio-oil: 52.8	Analysis of bio-oil and bio-char	[95]
Neem seed	Semi-batch	400-500	20			Temperature: 475 ºC	Bio-oil: 38	Analysis of bio-oil and biochar	[16]
Linseed seeds	Semi batch	350-575	20	-	-	Temperature: 550 ºC	Bio-oil: 68	Analysis of bio-oil and bio-char	[96]
Imperata cylindrica	Fixed bed	450-600	22	0.25-1	100	Temperature: 500 ºC Particle size: 0.5-1	Bio-oil: 20.88	Analysis of bio-oil	[97]
Karanja seed	Semi batch	450-550	20	-	-	Temperature: 500	Bio-oil: 57 Bio-char: 27 Pyro-gas: 16	Analysis of bio-oil	[98]
Castor seeds	Semi batch	450-600	20	-	-	Temperature: 550 ºC	Bio-oil: 64.4	Analysis of bio-oil	[15]
Pomegranate seeds	Fixed bed	400-800	30	3.2	5	Temperature: 600 ºC	Bio-oil: 54.20 Bio-char: 29.28 Pyro-gas: 16.52	Analysis of bio-oil, bio-char and pyro-gas	[66]

Rapeseed oil cake	Fixed Bed	400-900	30	2	5	Temperature: 600 °C	Bio-oil: 58.58 Bio-char: 33.23 Pyro-gas: 8.18	Analysis of bio-oil, bio-char and pyro-gas	[99]
Safflower seed	Fixed bed	400-700	100, 300 and 500	0.85-1.25	50-400	Temperature: 600 °C Heating rate: 300 N_2 flow rate: 100	Bio-oil: 54.0	Analysis of bio-oil and bio-char	[100]
Rapeseed		400-700		0.224-1.8	50-400	Temperature: 600 °C Particle size: 0.224-0.6 N_2 flow rate: 100	Bio-oil: 75	Analysis of bio-oil	[101]
Rapeseed	Fixed bed	400-700	30	0.425-1.8	50-400	Temperature: 550 °C Particle size: 0.6-1.8 N_2 flow rate: 100	Bio-oil: 51.7	Analysis of bio-oil	[102]

Safflower seed	Fixed bed	400-700	5, 40 and 80	0.425-1.8	50-200	Temperature: 500 °C Heating rate: 5 Particle size: 0.425-1.25 N_2 flow rate: 100	Bio-oil: 44.0	Analysis of bio-oil	[103]
Soybean cake	Fixed bed	400-700	5	0.224-1.8	50-400	Temperature: 550 °C Particle size: 0.850-1.25 N_2 flow rate: 200	Bio-oil: 33.78	Analysis of bio-oil	[104]
Cottonseed cake	Fixed bed tubular	300-700	7	-	50-400	Temperature: 550 °C N_2 flow rate: 200	Bio-oil: 29.68	Analysis of bio-oil	[105]
Rapeseed	Fixed reactor	500	40	0.224-1.8	-	Particle size: 0.85-1.8	Bio-oil: 46	Analysis of bio-oil	[106]

2.9.2. Viscosity

High viscosity is one of the principal drawbacks of pyrolytic oil. High viscosity can affect the fluidity and injection spray characteristics in the engine. At low temperature, it may even compromise the mechanical integrity of the injection pump drive systems. The viscosity of the pyrolytic oil is concerned with water content and water-insoluble compounds. The higher water content and less water-insoluble components in the pyrolytic oil reduce the viscosity of the pyrolytic oil. The viscosity of pyrolytic oil is much higher compared to conventional diesel fuel. Thus, the direct use of thermal pyrolytic oil in a combustion engine is not acceptable, and it needs up-gradation to match the fuel properties.

2.9.3. Acidity (pH)

Acidity is an important parameter of pyrolytic oil. The acidity of wood pyrolytic oil varies from 2.0 - 4.0, however, the acidity of seeds pyrolytic liquid varied from 2.0 - 6.0. Also, the acidity of pyrolytic oil depends on the types of feedstocks [24, 34]. The pyrolytic oil has higher acidity due to the presence of carboxylic acid, acetic acid, and formic acid, etc. These acids are formed by the depolymerization of cellulose and hemicellulose [24].

2.9.4. Moisture

The presences of moisture in pyrolytic oil reduced the heating value of fuel and flame temperature. Further, the presence of less moisture in liquid fuel decreases the viscosity of pyrolytic oil which enhances the atomization towards complete combustion and reduces the harmful emissions such as SO_x and NO_x. High moisture is also associated with hydrolysis reaction that is responsible for converting biodiesel to free fatty acids which are also linked to fuel filter blockage and promote corrosion of chromium and zinc parts within the engine and injection systems [34].

2.9.5. Density

The density of pyrolytic oil is an important fuel property, which directly affects the engine performance characteristics. Various performance characteristics such as heating value, cetane number are associated with fuel density [107]. Further, diesel fuel injection systems measure the fuel by volume, thus, changes in the fuel density will influence the engine output power due to a different mass of fuel injected [108].

2.10. Co-pyrolysis of Biomass and Waste Plastic

Co-pyrolysis of biomass and waste plastic is an emerging technology, which has the potential to convert waste plastics into renewable fuel while altering the quality and quantity of pyrolytic oil. Decomposition of plastics takes many years or sometimes they are not degradable which ultimately creates several problems. Various kinds of plastics were used every day to fulfill several unavoidable needs. Polyethylene Terephthalate (PETE or PET), is the most widely used plastic in the world. Polyethylene (PE), Polyvinyl Chloride (PVC), Polypropylene (PP), Polystyrene (PS), Polylactic Acid (PLA), Polycarbonate (PC), and Acrylic (PMMA), are the major types of plastic waste used in daily life. Among these, waste nitrile gloves, polystyrene and waste scrap tire creates huge solid waste which cannot be recycled completely and further the recycling consumes huge energy and also produces a low-quality polymer. Incineration is the promising route of plastic waste management. However, it generates several toxic chlorinated organic compounds, which are injurious to human health and the environment. Literature reported that pyrolytic oil produced from plastic waste is can only be used as fuel [109]. Literature also revealed that co-pyrolysis of polymer and biomass enhanced the quality of biomass pyrolytic oil [109-113]. Biomass is rich in carbon and oxygen compounds whereas polymers are rich in carbon and hydrogen. Plastic has higher hydrogen content compared to biomass [112]. The pyrolysis of biomass and plastic together may balance the C, H and O content, which may result in oxygen lean pyrolytic oil. Also, the addition of polymer to biomass during pyrolysis produces more free radicals and may suppress the formation of long-chain hydrocarbon compounds. Co-pyrolysis of biomass and plastic reduced the viscosity of the pyrolytic oil. Therefore, the co-pyrolysis of waste plastics and biomass seems to be promising. Nitrile gloves are used in the hospitals as well as academic and research institutions. Nitrile gloves cannot be easily recycled back to its monomer and usually produced undesirable and environmentally hazardous products during traditional recycling. Nitrile gloves can be thermally depolymerized at relatively low temperatures to obtain the monomer styrene with high selectivity. Numerous studies have been conducted on thermal and catalytic co-pyrolysis of biomass and waste plastics. Some of them are reported below.

Dewangan et al. (2016) [114] studied co-pyrolysis of biomass (sugarcane bagasse, SCB) with plastic (low-density polyethylene, LDPE), at different ratios in a semi-batch reactor with varying temperature from 350 ^{o}C - 600 ^{o}C at a heating rate of 20 °C min^{-1}. Individual SCB and LDPE yielded 47.15 % and 74.40 % while a mixture of SCB and LDPE at 1:1 yielded 52.75 % oil at 500 °C. Co-pyrolytic oil has a higher heating value than individual pyrolytic

liquid. GC-MS and FTIR analysis confirmed the interaction between SCB and LDPE during co-pyrolysis, which resulted in a decreasing amount of oxygenated compounds, phenol, and acidic compounds, thus, making the co-pyrolysis process more favorable for the production of high calorific value fuel.

Yang et al. (2016) [115] studied cedar wood, sunflower stalk, and *Fallopia Japonica* stem with plastic (polyethylene, LDPE) in a dropdown tube reactor. The synergistic effect was investigated by comparing the experimental relative yield and characteristics of oil with the calculated ones based on the results from the pyrolysis of individual components in the mixture. The results confirmed that co-pyrolysis liquid yield was higher than individual pyrolysis of biomass and plastic at 600 ^{o}C. The synergistic effect was positive during the production of aliphatic compounds. Further, the significant removal of aldehydes, acids, ethers, furans, ketones, phenols and sugars from the final co-pyrolysis oil, in which there was a significant increase in alcohols, was achieved.

Chattopadhyay et al. (2016) [116] studied catalytic co-pyrolysis of biomass and plastics (HDPE, PP, and PET) in a fixed-bed reactor using cobalt-based alumina, ceria, and ceria-alumina catalysts to analyze the product distribution and selectivity. Results confirmed a positive synergistic effect between biomass and plastics whereas the liquid yield increased with the addition of plastics. Gaseous products yield was more during pyrolysis of a blend having biomass/plastics ratio of 5:1 with the presence of 40 % Co, 30 % CeO_2, 30 % Al_2O_3 catalyst with hydrogen gas production touched its peak of 47 vol.%.

Önal et al. (2012) [117] studied co-pyrolysis of high-density polyethylene (HDPE) with potato skin (PS) at optimum process conditions. Thermal decomposition of pure HDPE was performed at a constant heating rate of 5 °C min^{-1} under various pyrolysis temperatures (400 °C, 420 °C, 450 °C, 470 °C, 500 °C and 550 °C) and sweeping gas flow rates (100 cm^3 min^{-1}, 200 cm^3 min^{-1}, 400 cm^3 min^{-1} and 800 cm^3 min^{-1}). About 56 % liquid was produced at temperature 500 ^{o}C and 400 cm^3 min^{-1} sweeping gas flow rate. Co-pyrolysis of pure HDPE-PS and waste HDPE-PS mixtures with different proportions (1:0, 1:1, 1:2, and 2:1 enhanced the liquid yield with increasing the weight ratio of HDPE in mixtures. Characterization of liquid fuel confirmed that oil had higher carbon and hydrogen contents, lower oxygen content with higher heating value than those of pyrolysis.

Xue and Bai (2018) [118] studied co-pyrolysis of acid pre-treated corn stover (CS) and polyethylene (PE) in the presence or absence of zeolite catalyst. During non-catalytic co-

pyrolysis, the use of acid-pre-treated CS was found to synergistically reduce char yield and increase both the yield and quality of CS-derived pyrolysis oil. When acid-pretreated CS was catalytically co-pyrolyzed with PE, the yields of aromatic hydrocarbons and alkene increased whereas the yields of solid residue and carbon oxides decreased to a much greater extent than co-pyrolyzing raw CS and PE.

Wang et al. (2017) [119] studied co-pyrolysis of bamboo residue and waste tire over two catalytic beds of CaO and HZSM-5, and the effect of CaO to HZSM-5 mass ratio on pyrolytic products distribution was investigated and analyzed. The results confirmed that catalytic pyrolytic liquid increased the relative contents of aromatics and olefins. Further, the dual catalytic stage of CaO and HZSM-5 further facilitated the relative contents of aromatics and olefins significantly and inhibited the formation of undesirables like acids.

Lu et al. (2018) [120] studied the synergistic effects of pine wood and plastics (PE and PVC) in a thermogravimetric analyzer and fixed bed reactor. Results confirmed that PW-PE interaction increased the maximum weight loss rate of PW by 8.0 % - 23.7 %. Co-pyrolysis of PW-PE blends produced a lower quantity of char (13.8 % - 22.4 %) and a higher quantity of oil (3.7 % - 4.4 %) as compared to the theoretical results. PW-PVC interaction decreased the temperature corresponding to the maximum weight loss rate of PW by 47 ^{o}C - 51 ^{o}C. Co-pyrolysis of PW-PVC blends yielded more char (15.5 % - 27.9 %) and less oil (7.2 % - 14.4 %) than expected values.

Ding et al. (2018) [121] studied co-pyrolysis of hemicellulose with LLDPE over CaO and HZSM-5 catalysts. Results confirmed that CaO could effectively transform acids into ketones. A minimum yield of acids (2.74 %) and a maximum yield of ketones (42.93 %) were obtained at a catalyst to feedstock ratio of 2:1. The dual-catalyst bed dramatically increased the yield of aromatics. Moreover, hydrogen-rich fragments derived from LLDPE promoted the Diels-Alder reactions of furans and participated in the hydrocarbon pool reactions of non-furanic compounds. As a result, a higher yield of hydrocarbons was achieved.

2.11. Characterization of Biochar

The solid residue left after pyrolysis is known as biochar, charcoal or char. The properties of biochar are diverse and depend to a great extent on the pyrolysis process and the types of biomass. It is majorly characterized by bulk density, mineral matter content, organic matter content, proximate analysis, ultimate analysis, heating values, and surface properties. The thermal treatment removes the moisture and volatile matter from the biomass and the

remaining solid char shows different properties. The remarkable differences are mainly observed in porosity, surface area, pore structures and physicochemical properties such as proximate and ultimate composition [122, 123]. Biochar has a higher heating value of 17 MJ kg^{-1} - 36 MJ kg^{-1}, due to this, it can be used as a source of energy and to internally provide heat for the pyrolysis process. Biochar can be used for various application such as bio-adsorbents, as a fertilizer, making of cosmetic products, making of carbon nanotubes, soil amendment, etc. Numerous studies have been carried out on the characterization of bio-char obtained from different sources. Some of them are discussed below.

Jindo et al. (2014) [124] characterized biochar obtained from rice husk, rice straw, wood chips of the apple tree (*Malus pumila*), and oak tree (*Quercus serrata*) at 400 ^{o}C, 500 ^{o}C, 600 ^{o}C, 700 ^{o}C, and 800 ^{o}C temperature. The results confirmed that at a lower temperature, a higher amount of char was formed compared to a higher temperature. However, at higher temperature pyrolysis led to biochar with high carbon content, large surface area, and high adsorption characteristics. Further, biochar obtained at 600 ^{o}C leads to a high recalcitrant character, whereas that obtained at 400 ^{o}C retains volatile and easily labile compounds. The biochar obtained from rice materials showed a high yield and unique chemical properties because of the incorporation of silica elements into its chemical structure. The biochar obtained from wood materials showed high carbon content and a high absorption character.

Yargicoglu et al. (2015) [123] studied different types biomass (pine wood, coconut shell, 90 % pine; 10 % fir wood, aged oak, hickory wood, and pine wood pellets) at different temperatures (350 ^{o}C - 600 ^{o}C). Physical characterization involve particle size distribution, specific gravity, density, porosity, surface area, hydraulic properties such as hydraulic conductivity, water holding capacity, chemical and electrochemical properties such as organic matter and organic carbon contents, pH, oxidation-reduction potential and electrical conductivity, zeta potential, carbon, nitrogen and hydrogen (CHNS/O) elemental composition, polycyclic aromatic hydrocarbons (PAHs), heavy metals, and leachable PAH. Results showed that these biochars had higher volatile (28 % - 74.1 %), and lower ash contents (1.5 % - 5.7 %). High variability in surface area (0.1 g m^{-2} - 155.1 g m^{-2}) and PAH and heavy metal contents of the biochars was also observed (0.7 mg kg^{-1} - 83 mg kg^{-1}).

Hmid et al. (2014) [125] studied influence of temperature and heating rate on the yield and properties of biochars derived from pyrolysis of solid olive mill waste (pomace) at three pyrolysis temperatures (430 ^{o}C ±10 ^{o}C, 480 ^{o}C ±10 ^{o}C and 530 ^{o}C ±10 ^{o}C) and three heating

rates (25 ^{o}C min^{-1}, 35 ^{o}C min$^{-1,}$ and 45 ^{o}C min^{-1}) in a vertical downdraft gasifier. Results confirmed that with increasing temperature or heating rate, the char yield and surface area decreased while carbon content and biochar aromaticity increased. At lower temperature (430 ^{o}C) and lower heating rate (25 ^{o}C min^{-1}), maximum biochar yield was achieved. Characterization of char confirmed that biochar had higher heating value (31 MJ kg^{-1}) and higher value of carbon content (70.20 % - 84.10 %) while lower electrical conductivity (0.28 dSm^{-1} - 0.47 dSm^{-1}).

Sadaka et al. (2014) [126] studied the characterization of switchgrass biochar produced via carbonization and to explore its potential use as a solid fuel. The biochar was produced in a batch reactor under reactor temperatures of 300 ^{o}C, 350 ^{o}C and 400 ^{o}C for 1 h, 2 h and 3 h residence times. With increasing temperature from 300 ^{o}C to 400 ^{o}C and residence times from 1 h to 3 h, biochar mass yield and volatile solids decreased from 82.6 % to 35.2 % and from 72.1 % to 43.9 %, respectively. Further, the heating value of char and carbon content increased from 17.6 MJ kg^{-1} - 21.9 MJ kg^{-1} and 22.5 % - 44.9 %, respectively, under the same conditions.

Wang et al. (2014) [127] studied the characterization and utilization of biochar derived from rice husk (RH) and elm sawdust (ES) by fast pyrolysis. Results confirmed that volatile and fixed carbon was 2.2 and 1.7 fold respectively higher in elm sawdust biochar (ESB) than those in RHB, but the ash content was 4.2 fold higher in RHB than that in ESB. FTIR results revealed that RHB had more functional groups than ESB. More surface area was found in RHB (78.15 m^2 g^{-1}) than ESB (0.22 m^2 g^{-1}) by BET analysis.

2.12. The Source, Availability, and Production of Non-edible Seeds in India

There are various types of non-edible seeds available in India. These biomass has a higher volatile matter, lower ash content, lower moisture, higher extractive contents, a higher heating value which made these biomass more attractive for pyrolysis. In this study, all the selected biomasses were used for pyrolysis for the production of renewable fuel (bio-crude), however, characterization of pyrolytic oil indicated extraction of various useful compounds form the pyrolytic oil. Some of them are disused here along with their botanical classification and fatty acids composition listed in Table 2.2 and 2.3 respectively.

Cascabela Thevetia (Kanair) belongs to the Apocynaceae family. The plant is toxic because it contains cardiac glycosides and is widely cultivated throughout Torrid Zone. It is found in

the tropics, sub-tropics and monsoon rainforest. Yellow oleander is an evergreen plant which grows upto 2 m - 6 m in height. It starts flowering one and half year after planting and it blooms thrice in a year. Initially, fruits are mostly green in color and once ripen it becomes black. The fruits contain 1 - 4 seed in its kernel as well as milky juice in all organs [128]. The plump angular fruits seeds are more dangerous and about the size of an unshelled walnut. The leaves are hard in texture and narrow to about 16 cm long and 1.0 cm - 1.5 cm wide, and the flower is mostly yellow and usually bell-shaped about 7 cm long [129]. *Cascabela thevetia se*eds have a higher amount of extractive content (40 wt.% - 50 wt.%) which ultimately increased the pyrolytic liquid yield during pyrolysis thus *cascabela thevetia* seeds were selected for the current study for the production of fuel and chemicals [13, 18].

Rubber seed is one of the non-edible oil seed having commercial value. The rubber tree is generally cultivated for the production of latex. Oil from the rubber seed can be used for the production of bio-fuel and bio-chemicals since it contains various fatty acids. The tree is a source of timber and is found in India, and its subcontinent. It requires high humidity atmosphere of around 80 %, with a temperature of 20 °C - 34 °C in the absence of strong wind and a well-drained soil condition. The oil content in rubber seed is about 38.9 % [130].

Delonix regia is a species belong to *Fabaceae* subfamily of *Caesalpinioideae*. In many parts of the world, it is cultivated as an ornamental tree. In India, it is known as Gulmohar or Krishnachura. It is a medium-sized tree (mostly 5 m - 12 m height) widely planted in the garden, bank of rivers to prevent soil erosion and roadside to provide shade. In April to July, it blooms in the bunch of scarlet red flowers (about 8 cm long) when the tree become leafless and the fruits ripening in August to October. The seedpods are long about 40 cm - 70 cm in length and 2.5 cm - 4.0 cm in width. After ripening, it becomes hard, black or brown and can be collected from September to October. Further, one seed pod contains about 20 - 30 seeds (hard, black or brown, with a dark ridge) in size of 1.5 cm - 2.0 cm in length. The wood comprises mostly b-sitosterol, lupeol, quercetin, amino acid [131].

Pongamia pinnata is the species of genus Pongamia, available in India and other parts of the world. The common name of the seed is Karanja in India. Karanja oil is traditionally used for lighting of lamps in the rural areas. Each seed contains about 30 % - 40 % oil. Seedlings attain a height of 25 cm - 30 cm in their first growing season. The suitable propagating time is April to June in India, and the seed yield per tree ranges from about 10 kg to more than 50 kg.

One can plant 200 plants per acre in the formation of 5 m x 4 m and get yield of 25 kg to 40 kg per tree with 30 % - 35 % of oil [13].

Linseed belongs to the genus of Linum. It is a quick grown plant generally harvested after the winter season. It is sown in the month of March or April. Oil is produced from the seed by heating raw Linseed to a temperature of 150 ^{o}C. The seeds contain 30 % to 40 % oil, about 25 % proteins, together with wax, resin, sugar, phosphates, acetic acid, and a small quantity of the glycoside *Linamarin.* The oil enters into veterinary pharmacy as a purgative for sheep and horses, and a jelly formed by boiling the seeds is often given to calves. Mixed with honey, Linseed oil has been used as a cosmetic for removing spots from the face while dried oil is used as ink for printer [132].

Samanea saman (rain tree) belong to the *Fabaceae* (*Legume family*). It is well known due to its characteristic umbrella-shaped canopy. The height of the rain tree is maximum 15 m - 25 m, but in the rare case, it is found upto 50 m which depends on the geographical condition of the place. The crown reaches 30 m in diameter as well as the very large tree reaches upto 50 m - 60 m diameter. The mature pods are usually black-brown, oblong and lumpy (10 cm - 20 cm long, 15 mm - 19 mm wide, 6 mm thick and straight or slightly curved shape. The seeds are plumply oblong-ellipsoid (8.0 mm - 11.5 mm long, 5.0 mm - 7.5 mm wide) and slightly flattened from side to side. After ripening, it's become dark glossy brown with U-shaped yellowish marking on the flattened side. Each pod contains about 15-20 seeds[133].

Phyllanthus emblica (Amla) is an edible tree and found in all states of India. It is a medium-sized tree around 8 m - 10 m in height and contains asymmetrical shaped spreading branches. However, Alma leaves are in 7 cm - 10 cm long and are of oval shape. Further, fruits are found in spherical shape with fleshy sour, and a stringent taste [134]. It is well known that Amla fruits are used in ayurvedic medicines [135]. However, after using the fruits, the kernel is dumped out as a waste.

Azadirachta indica (Neem tree) is a tropical evergreen tree and used in Ayurvedic medicine. The average height of Neem tree is about 25 m - 40 m with straight and semi-straight trunk and about 3 m girth with spreading branches [136]. Neem tree is fast growing tree and starts fruiting after 3-5 year of planting but about 10-12 year later it becomes fully productive with 50 kg - 60 kg seeds annually [137]. After maturation fruit colour becomes yellow and the taste of the fruits are slightly sweeter.

Manilkara zapota tree belongs to *Sapotaceae* family. In India, it is known as Chiku or Sapodilla and found in medium size about 60 ft - 100 ft in height with pyramidal to rounded canopy shape. However, sapodilla fruits are edible in nature, but the kernel part is dumped as waste. The nature of the sapodilla leaves is 5 cm - 20 cm long with a light pinkish color. The fruits are berry with scurfy brown peel and oval shaped or sometime in conical shaped with 5 cm - 100 cm in diameter [138].

Jatropha (*Jatropha curcas*) is being used for the production of bio-diesel since a long time. Around 66 species of Jatropha exist in the earth. It can be grown almost anywhere, even in sandy, saline, or infertile soil. The hot and humid climate is best suited for jatropha cultivation. It lives for more than 50 years and producing seeds all the time. Jatropha curcas is a small, perennial shrub that grows up to 3 m - 5 m in height while the mature seed contains about 35 % - 37 % of oil. The crops need to be initially irrigated for one year and normally yield for 40 years [139].

Madhuca Indica and *Madhuca Longifolia* are two major species of Mahua widely available in India and its subcontinent. Mahua tree is available across the country but extensively found in the north Indian plains forests. The annual production of Mahua flower is ~500000 ton. However, production of Mahua seed is about 180000 ton [140]. The average height of Mahua tree is about 20 m - 30 m, and found semi-evergreen or evergreen foliage and spread over the West Bengal, Uttar Pradesh, Jharkhand, Chhattisgarh, Bihar, Maharashtra, Telangana, Madhya Pradesh, Kerala, Odisha, Gujarat and Tamil Nadu [141]. Mahua seed contains about 35.0 % oil and 16 % protein.

Polanga (*Calophyllum inophyllum*) is a large evergreen tree. It grows along with coastal areas and adjacent lowland forests. It grows in areas up to 98 ft tall and has small, delicate white flowers with yellow centers. In the northern hemisphere, the tree flowers twice a year, in the late fall and spring [142]. Polanga tree can grow in annual rainfall ranging from about 1000 mm to 5000 mm and maximum temperatures ranging from 30 °C to 35 °C. The oil content in the seed is 50 % - 73 % [142] whereas about 60 % of oil can be extracted by the cold pressing process (expelling) [143].

Ricinus communis or castor seeds belong to *Euphorbiaceae* family. Castor is indigenous to the southeastern Mediterranean Basin, Eastern Africa, and India, but is widespread throughout tropical regions (and widely grown elsewhere as an ornamental plant). The castor seeds contain about 35 % - 60 % oil that is rich in triglycerides, mainly *ricinolein*.

It is a fast-growing, suckering shrub that can reach the size of a small tree, around 12 m, but it is not cold hardy. Castor seeds have a warty appendage called the caruncle, which is a type of elaiosome. The caruncle promotes the dispersal of the seed by ants (myrmecochory) [144].

Pinus ponderosa belongs to the *genus Pinus* family, and in India, it is known as the Pine tree. Pine trees are evergreen, coniferous resinous trees growing 3 m - 80 m tall, with the majority of species reaching 15 m - 45 m height. Bud colour is in reddish brown and bud size is in oblong cylindrical and ¾ inch long. The mature trees have yellow to orange-red bark with black crevices while younger trees have blackish-brown bark [145].

Shorea robusta belongs to the *Dipterocarpaceae* family, and in India, it is known as sal tree. This tree is native to the Indian subcontinent like; Myanmar, Nepal, India, and Bangladesh. It is moderate to slow growing and can attain maximum heights of 30 m - 35 m and a trunk diameter about 2.0 m - 2.5 m. The leaves are 10 cm - 25 cm long and 5 cm - 15 cm broad [146].

Areca catechu tree belongs to the *Arecaceae* family. It is widely cultivated in Taiwan, India, Bangladesh, Maldives, Sri Lanka, Cambodia, Laos, Thailand, Vietnam, Malaysia, Indonesia, and New Guinea. Areca catechu is a medium-sized tree usually growing straight, and the height of the tree is about 20 m - 30 m with a trunk 10 cm - 15 cm in diameter along with 1.5 m - 2.0 m long leaves [147]. Details nomenclature about all the biomasses and composition of fatty acids is listed in the Table. 2.2 and 2.3.

2.13. Knowledge Gaps

Conversion of biomass into renewable fuel and other value-added products can be done using different routes. This study is focused on the thermal and catalytic conversion of biomass and waste plastic using different types of catalyst to enhance the properties of liquid fuel. Based on the literature, the main knowledge gaps are:

1. Complete physicochemical characterization of *Cascabela thevetia* (SK), *Delonix regia* (SG), *Samanea saman* (SS), *Phyllanthus emblica* (AM), *Azadirachta indica* (NM), *Manilkara zapota* (CK), *Madhuca longifolia* (MH) is not studied while very few studies are reported for *Pinus ponderosa* (PW), *Shorea robusta* (SW) and *Areca catechu* (AN) wood dust.
2. Kinetic analysis of these selected biomass using iso-conversional method is not reported so far.

3. Effect of biomass bed thickness and distance between successive beds on pyrolytic products yield and properties are not yet reported.
4. Catalytic conversion of these biomass was not studied extensively.
5. Co-pyrolysis of neem seed and waste nitrile gloves is yet to be explored.
6. Physicochemical characterization of biochar of these biomass was not studied extensively.

Table 2.2. Botanical nomenclature of different types of non-edibles seeds biomass.

Common name	Order	Family	Genus	Scientific Name	Reference
Kanair	*Gentianales*	*Apocynaceae*	*Cascabela*	*Cascabela thevetia*	[129]
Gulmohar	*Fabales*	*Fabaceae*	*Caesalpinioideae*	*Delonix regia*	[131]
Rain tree	*Fabales*	*Fabaceae*	*Albizia*	*Albizia saman*	[133]
Amla	*Malpighiales*	*Phyllanthaceae*	*Phyllanthus*	*Phyllanthus emblica*	[134]
Neem	*Sapindales*	*Meliaceae*	*Azadirachta*	*Meliaceae*	[136]
Sapodilla	*Ericales*	*Sapotaceae*	*Manilkara*	*Manilkara zapota*	[138]
Mahua	*Ericales*	*Madhuca*	*Sapotaceae*	*Madhuca longifolia*	[141, 148]
Pine wood	*Pinales*	*Pinaceae*	*Pinus*	*Pinus ponderosa*	[145]
Sal Wood	*Areca*	*Areca*	*Areca*	*Shorea robusta*	[146]
Areca Nut	*Arecales*	*Arecaceae*	*Areca*	*Areca catechu*	[147]
Karanja	*Fabales*	*Leguminaceae*	*Pongamia*	*Pinnata*	[149]
Niger	*Solanales*	*Solanales*	*Hyoscyamus L.*	*Niger*	[150]
Linseed	*Malpighiales*	*Linaceae*	*Linum*	*usitatissimum*	[132]
Rubber	*Malpighiales*	*Euphorbiaceae*	*Hevea*	*H. brasiliensis*	[130]
Jatropha	*Malpighiales*	*Euphorbiaceae*	*Jatropha*	*Curcas*	[139]
Polanga	*Malpighiales*	*Calophyllaceae*	*Calophyllum*	*C. inophyllum*	[142]

Table 2.3. Fatty acid composition of some non-edible oil seed biomass

Formula	Acid name	Mahua	Karanja	Niger	Neem	Jatropha	Rubber	Kusum	Pilu	Polanga	Castor	*cascabela thevetia*	*Samanea saman*
$C_{16}H_{32}O_2$	Palmitic	17.8	11.65	13.0	16-34	11.5	8.7	7.59	18.9-19.5	14.8-18.5	2.0	2.28	6.70
$C_{18}H_{36}O_2$	Stearic	14.0	7.5	7.5	6-24	8.0	6.17	-	-	6.1-19.2	1.0	10.17	4.97
$C_{20}H_{40}O_2$	Arachidic	3.3	-	-	-	-	0.66	-	-	-	0.66	2.41	4.82
$C_{18}H_{34}O_2$	Oleic	46	51.59	39.3	25-58	43.5	38.96	2.83	5.5-12	36.2-53.1	7.0	43.72	-
$C_{18}H_{38}O_2$	Linoleic	17.9	16.64	45.5	6-17	33.5	42.13	49.69	0.0-1.2	15.8-28.5	5.0	19.85	24.63
$C_{12}H_{28}O_2$	Myristic	-	-	3.4	1.7-3.4	-	-	0.01	28.4-54.5	-	-	-	-
$C_{20}H_{32}O_2$	Eicosanoic	-	1.35	-	-	-	-	-	-	-	-	-	-
$C_{22}H_{44}O_2$	Dosocasnoic	-	4.45	-	-	-	-	-	-	-	-	-	-
$C_{24}H_{48}O_2$	Tetracosanoic	-	1.09	-	-	-	-	-	-	-	-	-	-
--	Hexadeconic	-	-	-	25.54	-	-	-	-	-	-	-	-
$C_{20}H_{40}O_2$	Lignoceric	-	-	-	-	1.1-3.5	-	-	-	-		-	
$C_{18}H_{30}O_2$	Linolenic	-	-	-	-	-	2.38	-	-	21.26	-	-	-
$C_{16}H_{32}O_2$	Palmititoleic	-	-	-	-	-	-	1.8	-	-	-	-	-
--	Eicosenoic	-	-	-	-	-	-	29.54	-	-	-	-	-
Reference	-	[148]	[151]	[152]	[153]	[154]	[155]	[156]	[143]	[143]	[143]	[128]	[157]

2.14. Aim and Objectives

Based on the literature gaps, the following research objectives are identified,

1. Physicochemical characterization of selected biomass towards the production of renewable fuel and value-added chemicals.
2. Kinetic analysis (model-free) and thermodynamic analysis of biomass using non-isothermal techniques.
3. Thermal pyrolysis of selected biomass and it's fuel properties evaluation.
4. To study the effect of biomass bed height and biomass bed thickness on the pyrolytic products yields (liquid, char, and gases).
5. To study the influence of catalysts on pyrolytic end products and it's characterization.
6. Thermal and catalytic co-pyrolysis of neem seeds with waste nitrile gloves towards the production of renewable liquid fuel and chemicals.
7. Physicochemical characterization of biochars obtained from the pyrolysis of selected biomass.

Chapter 3

Materials and Experimental Methods

3.1. Samples Collection and Preparations

Cascabela thevetia (SK), *Delonix regia* (SG), *Samanea saman* (SS), were collected from Indian Institute of Technology Guwahati (*IITG*) campus (26 °11′14″N 91°41′30″E) India. However, *Phyllanthus emblica* (AM), *Azadirachta indica* (NM), *Manilkara zapota* (CK), and *Madhuca longifolia* (MH) seeds were collected from Basti district, Uttar Pradesh, India. Further, waste woody dusts biomass *Pinus ponderosa* (PW), *Shorea robusta* (SW) and *Areca catechu* (AN) dust) were collected from Shillong district (25.5667 °N 91.8833 °E), Meghalaya, India. The collected biomass were sun-dried for 2-3 days (depending on the climatic conditions) and stored in airtight plastic bags to prevent moisture absorption. Further, all samples were pulverized into the desired size (0.5 mm - 1.5 mm) as smaller particle size offer higher heat and mass transfer rate. The waste nitrile gloves (WNG) used in this study were collected from the Chemical Engineering Department Laboratories, IIT Guwahati. WNG was washed with hot water and hexane to remove adhered materials as well as bacteria. The photograph of all the selected biomass are presented in Fig. 3.1.

Fig. 3.1. Photographs of all selected biomass and waste nitrile gloves

3.2. Characterization of Raw Materials

Feasibility study is one of the essential parameters to evaluate the potential of feedstocks to produces fuels. The characterization scheme is presented in Fig. 3.2, and the detail processes are discussed below.

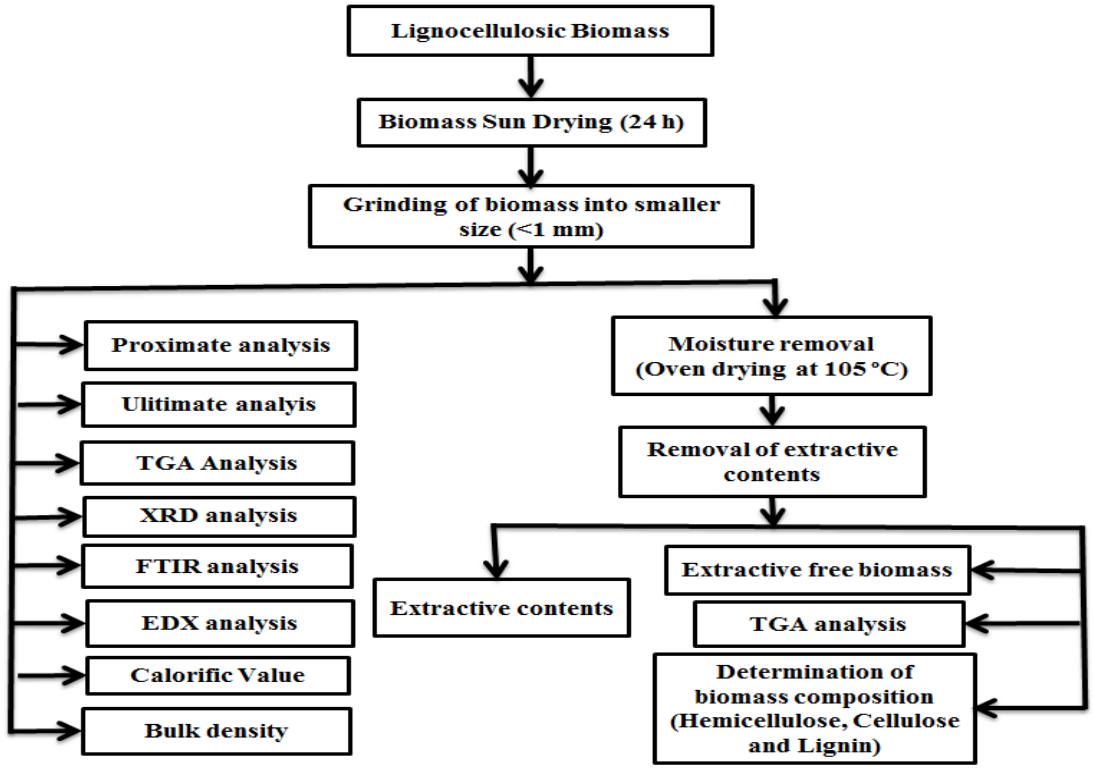

Fig. 3.2. Details characterization schemes of selected biomass

3.2.1. *Extractive content analysis*

The extractive content of all the biomass was determined via Soxhlet apparatus using hexane and ethanol as solvents. About 5.0 g of oven dried (105 ºC for 1.0 h) biomass was taken in a thimble (single thickness, cellulose thimble 24 mm x 100 mm and placed in the soxhlet tube. The solvent was transferred to a round bottom flask (250 mL) which was connected to Soxhlet apparatus. Moderate heating was initiated and continued for 5 h by using a heating mantle. Once hexane extraction finished, extractive free biomass sample was collected and then dried in a hot air oven for 3.0 h at 60 ºC. Extractive free oven-dried biomass was again transferred to the same apparatus, and the same procedure was repeated using ethanol as solvent. It was observed that during hexane extraction, all soluble compounds such as non-polar lipids, hydrocarbons, and terpenoids, etc. were removed whereas the remaining polar wax, chlorophylls, sterol, and other minor compounds were removed during the ethanol

extraction [49]. Both the solvents were recovered by removing the extractives in a rota-evaporator at 45 ^{o}C under reduced pressure. At the end of extraction, extractive free biomass was used for the estimation of chemical analysis (hemicellulose, cellulose, and lignin) based on their degradation temperature profiles. The percentage of the extractive present in the biomass sample was calculated by using the following equation:

$$Extractives\ (\%) = \left[\frac{Weight\ of\ extractives}{Weight\ of\ oven\ dried\ biomass}\right] \times 100 \tag{3.1}$$

3.2.2. Proximate analysis

Proximate analysis is the initial stage of characterization technique which provides an idea about the percentage of moisture (*MC*), volatile matter (*VM*), ash content (*A*) and the amount of fixed carbon (*FC*) in biomass. Biomass is generally hydrophilic in nature; hence, removal of moisture becomes essential as it has a negative impact on the yield of pyrolytic end products. Amount of moisture can be determined by using the following formula.

$$Moisture\ (\%) = \left[\frac{Weight\ of\ wet\ sample - Weight\ of\ oven\ dried\ sample}{Weight\ of\ oven\ dried\ sample}\right] \times 100 \tag{3.2}$$

Amount of fractions other than moisture evaporated under a specific condition is known as volatile matter. ASTM 3175 and EN 15148 standards were used for calculation of volatile matter. Approximately1.0 g of oven dried biomass was taken in a crucible, covered with a lid and kept in a muffle furnace for 7.0 min at specified temperature 925 ^{o}C ±10 ^{o}C. After reaching the required temperature, the crucible was removed and placed in a desiccator for cooling. The difference of weight of the biomass sample gives the amount of volatile matter as per the following calculation,

$$M\ (\%) = \left[\frac{A - B}{A}\right] \times 100 \tag{3.3}$$

where, *A* = initial mass of the sample before heating, *B* = final mass of the sample after heating, *M* = loss of mass.

$$VM\ (\%) = \left[M\ (\%) - M_c\ (\%)\right] \tag{3.4}$$

Amount of ash was determined by using a programmable muffle furnace (Optics Technology, Delhi) as per ASTM 3173 - 87 standard. 1.0 g of oven dried (105 ^{o}C for 1.0 h) sample was taken in a crucible and placed in the muffle furnace at 575 ^{o}C ± 10 ^{o}C for 3 h. Once the temperature reached the desired conditions, the crucible was removed and kept in a desiccator for cooling. This process was repeated until a constant weight was achieved. The weight difference form the initial and final mass provided the amount of ash. Further, the amount of fixed carbon was calculated by an empirical equation given below.

$$FC\ (\%) = 100 - \{MC\ (\%) + VM\ (\%) + A_s\ (\%)\} \tag{3.5}$$

where *FC* represents the amount of fixed carbon, *MC* represents moisture content, *VM* represents the amount of volatile matter and A_s represents the amount of ash present in biomass.

3.2.3. Ultimate analysis

Ultimate or elemental analysis of biomass were done by using CHNSO elemental analyser (Variael CUBE, Germany). The analyser was calibrated using 5 tin capsules packed with a 5L-cystine test. 5.0 mg of biomass was taken in a tin capsule and heated at 980 ^{o}C with a continuous and constant flow of helium enriched oxygen gas. Obtained data were analysed by using Callidus® software for calculation of elemental composition of biomass on a dry basis.

3.2.4. Calorific value and bulk density

The calorific value of biomass play a very important role in identifying the feasibility of biomass towards value-added products. Calorific value was calculated by using an oxygen bomb calorimeter (Model 1341 Plain Jacket Calorimeter, Parr instrument). The following equation was used for calculation of calorific value.

$$\text{Calorific value} = \left(\frac{\Delta T \times w - e_1 - e_2 - e_3}{m} \right) \tag{3.6}$$

where ΔT represents temperature difference (^{o}C), w energy equivalent of the calorimeter, m represent mass of the fuel (g), e_1 represent correction in calories for heat of formation of nitric acid, e_2 represent correction in calories for heat of formation of sulphuric acid, e_3 represent correction in calories for heat of combustion of fused wire. The experiment was repeated three times for results accuracy and the average value is reported in the present study.

The bulk density of biomass is defined as the ratio of the mass of biomass particles to the total volume of the biomass particle along with pore space volume between and within biomass particles. The bulk density of biomass depends on the size and shape of particles, the density of particles, moisture, surface characteristics and degree of fill tightness. The bulk density of biomass is an essential property as it is directly related to biomass transportation and storage cost. The density of biomass impact on the sizing of material, fuel storage requirements, handling of material and most importantly behavior of biomass during thermo-chemical or biological processes [158]. The bulk density of biomass was measured using a digital balance and graduated cylinder. The weight and the volume of biomass were measured in a digital laboratory balance. The volume of biomass was determined by using a graduated cylinder. The experiment was repeated thrice for reproducibility of accurate data, and average data is reported in the present study.

3.2.5. Biofuel reactivity

Biofuel reactivity provides the reactive nature of particular biomass based on their elemental ratio (*C*, *H*, *VM*, and *FC*) for the best possible utilization of the materials. Reactivity of biomass was calculated by the ratio of volatile matter to fixed carbon along with the atomic ratio of oxygen to carbon and hydrogen to carbon ratio based on the proximate and ultimate analysis [159].

3.2.6. Van Krevelen plot

Van Krevelen plot indicates the amount of carbon-hydrogen and oxygen composition of organic matter. Also, it tells the depth at which particular type of biomass (organic matter) was formed; hence tracking of hydrocarbons becomes easy. In the present study two parameters, the atomic ratio of hydrogen to carbon (*H:C*) and oxygen to carbon (*O:C*) was used for plotting the Van Krevelen plot.

3.2.7. Thermogravimetric and compositional analysis of biomass

Thermogravimetric analysis was performed using a thermogravimetric analyser (STA7200, Hitachi). Approximately 8.0 mg of biomass was taken in a crucible (Al_2O_3) and kept inside the furnace and was heated from 30 ^oC - 900 ^oC at a heating rate of 10 $^oC\ min^{-1}$. Nitrogen gas was used as a purge gas for maintaining an inert atmosphere with a constant flow rate of 40 mL min^{-1}. Nitrogen gas was purged before 15 min prior to each experiment for

cleaning the reaction chamber. The profile of weight loss versus temperature was obtained for each biomass and the data thus generated were analyzed using STAR software. Compositional analysis of each biomass sample was also found out from the weight loss data.

3.2.8. Change in activation energy over raw and extractive free biomass

Kinetic study of biomass plays an essential role during process parameter optimization, designing, and development of new pyrolyzer. Also, knowledge of kinetics helps choosing the appropriate temperature range during pyrolysis. Many researchers have studied the kinetic parameters of biomass by using the dynamic decomposition of solid materials [160, 161]. In the present study, the Horowitz and Metzger model [162] for the determination of kinetic parameters of all biomass was adopted. According to Horowitz and Metzger, two-fold logarithmic plots of reciprocal of reactant against temperature provides activation energy while assuming that order of the reaction is first order. The proposed mathematical model by Horowitz and Metzger is given in the following equation.

$$\ln\left[\ln\left\{\left(\frac{\alpha_0-\alpha_f}{\alpha_t-\alpha_f}\right)\right\}\right]=\frac{E\phi}{RT_{\max}^2} \tag{3.7}$$

where α_0 is an initial mass of biomass material, α_f is the final weight of the material and α_t represent the weight of material at a particular temperature, R is ideal gas constant, (J mol^{-1}. K^{-1}.), ϕ is a difference of particular and reference temperature. T_{max} is reference temperature effective when,

$$\left(\frac{\alpha_t-\alpha_f}{\alpha_0-\alpha_f}\right)=\frac{1}{2.718} \tag{3.8}$$

The activation energy was calculated from the slope of the straight line.

3.2.9. XRD analysis

XRD pattern of biomass samples was obtained by using Rigaku TT Rax diffractometer in conjugation with a Cu-Kα radiation source and X-ray generated at 9.0 kW and 250 mA. Scanning angle (2θ) was taken 5^o - 50^o for all biomass at a speed of 0.03 min^{-1}. The crystallinity index of biomass samples was calculated by the following equation,

$$CrI\,(\%) = \left[\frac{I_{Crystalline} - I_{amorphous}}{I_{amorphous}} \right] \quad (3.9)$$

where, the intensity of the crystalline peak at about 2θ = 22.25 for the crystalline portion of biomass sample (i.e., cellulose) and intensity of amorphous peak was 2θ = 16.12 for an amorphous portion (i.e., cellulose, hemicellulose, and lignin).

3.2.10. EDX analysis

Minerals are present in raw biomass as well as in ash. Amount of minerals affects the products yield during pyrolysis. EDX analysis was carried out by using ZEISS, Sigma FESEM/EDX analyser by placing a small amount of oven dried sample on carbon tape.

3.2.11. FTIR Analysis

Fourier transform infrared spectroscopy (FTS 3500 GX attached with DRS) was utilized to obtain functional groups present on biomass material. A small amount of biomass was mixed with oven dried potassium bromide (KBr) powder in 1:100 ratio and loaded in a sample holder with a scanning rate of 40 with a step size of 4.0 cm^{-1} within the range of 400 cm^{-1} - 4000 cm^{-1} wave number.

3.2.12. X-ray fluorescence (XRF) analysis of residual

Ash comprises lots of inorganic elements such as, SiO_2, K_2O, Al_2O_3, CaO, TiO_2, P_2O_5, Na_2O, Fe_2O_3, MnO, SO_3, and MgO which behaves as catalysts during pyrolysis [163]. To identify the existence of inorganic materials in residual biomass, X-ray fluorescence spectroscopy (AMETEF SPECTRO XEPOS) analysis was carried out. Ash deposition tendency was represented by a slagging and fouling factor. Slagging is defined as, the formation of molten or partially fused deposits on furnace wall exposed to radiant heat, while fouling is defined as, the formation of fussed deposits on convection surface. Further, the tendency of ash deposition was also calculated [164] by the following equation.

$$Base\ to\ Acid\ \ Ratio\left(\frac{B}{A}\right) = \frac{\%\left[Fe_2O_3 + CaO + MgO + K_2O + Na_2O\right]}{\%\left[SiO_2 + TiO_2 + Al_2O_3\right]} \quad (3.10)$$

$$\text{Slica to Alumina Ratio}\left(\frac{S}{A}\right) = \frac{\%\left[SiO_2\right]}{\%\left[Al_2O_3\right]} \quad (3.11)$$

$$Iron\ \ Calcium\ \ Ratio\left(\frac{I}{C}\right) = \frac{\%\left[Fe_2O_3\right]}{\%\left[CaO\right]} \quad (3.12)$$

$$Total\ alkalis\ \ (TA) = \%\ Na_2O + \%\ K_2O \tag{3.13}$$

3.2.13. Differential scanning calorimetry (DSC) analysis

Differential scanning calorimetry (*DSC*) analysis was carried out in the METTLER TOLEDO DSC STAR for three different waste biomass at 10 °C min^{-1} heating rate. Heat flow was the main property measured during DSC analysis. During the analysis, energy flow was expressed as a function of time or temperature and represented in the unit of mW on the y-axis.

3.3. Synergistic Effect on NM and WNG

The synergistic effect of neem seed (*NM*), waste nitrile gloves (*WNG*) along with catalyst was calculated by using the experimental and theoretical mass loss of *NM* and *WNG* along with catalysts based on the equation given as;

$$\Delta W = W_{\text{exp.}} - W_{calc.} \tag{3.14}$$

where ΔW = theoretical weight loss of samples, $W_{\text{exp.}}$ = experimental moss loss of the sample, $W_{calc.}$ = theoretical moss loss of the sample based on the weight averaged sum of the isolated samples, which is calculated as;

$$W_{calc.} = x_p W_P + x_C W_C \tag{3.15}$$

where, x_p and x_C represents the mass ratio of the NM, WNG, and catalysts respectively. W_P and W_C represents the mass loss of NM, WNG, and catalysts at the same experimental conditions. It was reported that the positive value of ΔW accelerated formation of volatiles, while negative value of ΔW inhibiting the formation of volatile.

3.4. Kinetic Theory

Pyrolysis of lignocellulosic biomass is a very complex phenomenon because of variations in chemical composition within the biomass. Hundreds of reactions occur simultaneously within a fraction of second during the reaction. Therefore, it is not easy and possible to predict the exact reaction mechanism. However, the overall reaction mechanism can be written as;

$$\text{Biomass (Solid)} \xrightarrow{k(t)} \text{Volatile (Gases + Tar)} + \text{Char (Solid residue)} \tag{3.16}$$

It is assumed that the conversion of raw material into the product is only single step process [165]. Hence, according to Arrhenius, the rate constant of a reaction (k) is represented by the following equation:

$$k = k_o \, e^{-\left(\frac{E}{RT}\right)} \tag{3.17}$$

where k= reaction rate constant, k_o = pre-exponential factor, (min^{-1}), E = activation energy (kJ mol^{-1}), R = Gas constant (8.314 J mol^{-1} K^{-1}), and T = Absolute temperature (K). For conversion of biomass from solid state to a volatile state, the rate equation can be written as:

$$\frac{dx}{dt} = k \;\; f(x) \tag{3.18}$$

where x = rate of conversion within sample and t = time. The conversion of biomass into fuel is a function of temperature. Thus, the conversion factor is defined as:

$$x = \left(\frac{\alpha_O - \alpha_t}{\alpha_O - \alpha_f} \right) \tag{3.19}$$

where α_o is initial weight of biomass, α_t is mass of biomass sample at a particular time while α_f is mass of biomass at the end of pyrolysis reaction. By combining equation (3.18) and (3.19) the following equation is obtained,

$$\frac{dx}{dt} = A e^{-(E/RT)} \, f(x) \tag{3.20}$$

According to the uniform kinetic reaction of samples, *f(x)* can be represented as:

$$f(x) = (1 - x)^n \tag{3.21}$$

From equations (3.20) and (3.21), it can be written as,

$$\frac{dx}{dt} = k_o \, e^{-\left(\frac{E}{RT}\right)} (1 - x)^n \tag{3.22}$$

where δ is heating rate. Heating rate (δ) can be defined as:

$$\delta = \frac{dT}{dt} = \frac{dT}{dx} \times \frac{dx}{dt} \tag{3.23}$$

Combining equations (3.22) and (3.23),

$$\frac{dx}{dT}=\frac{k_o}{\delta}e^{-\left(\frac{E}{RT}\right)}(1-x)^n \tag{3.24}$$

After simplifying equation (3.24), the following equation is obtained,

$$\frac{dx}{(1-x)^n}=\frac{k_o}{\delta}e^{-\left(\frac{E}{RT}\right)}dT \tag{3.25}$$

Equation (3.25) expressed conversion of biomass with respect to temperature. Integrating equation (3.25),

$$g(\kappa)=\int_0^x\frac{dx}{f(x)}=\int_0^T\frac{A}{\delta}e^{-(E/RT)}\,dT \tag{3.26}$$

$$g(\kappa)=\frac{AE}{\delta R}\int_0^x u^{-2}e^{-u}du=\frac{AE}{\delta R}p(x) \tag{3.27}$$

where $g(\kappa)$ represents integral conversion and $x=\frac{E}{RT}$. However, $p(x)$ has no exact solution; therefore, it can be solved by the numerical approximation method. $p(x)$ is varied with respect to the type of approximation selected for simplifying the integral part [166].

3.4.1. Kissinger–Akahira–Sunose (KAS) method

Kissinger–Akahira–Sunose (*KAS*) is a model-free (iso-conversional) method used to calculate the kinetic energy of the material. Applying approximation of $p(x)=x^{-2}e^{-x}$ in equation (3.27) and simplifying the following equation is obtained,

$$\ln\left(\frac{\delta}{T^2}\right)=\ln\left[\frac{AE}{Rg(x)}\right]-\frac{E}{RT} \tag{3.28}$$

Equation (3.28) is known as Kissinger-Akahira-Sunose (KAS) model. The kinetic plot between $\ln\left(\frac{\delta}{T^2}\right)$ versus $\frac{1}{T}$ will give slope and intercepts used for calculation of activation energy and frequency factor.

3.4.2. Ozawa–Flynn–Wall (OFW) method

Ozawa–Flynn–Wall (OFW) method is used to calculate kinetic parameter (activation energy) of material by using Doyle's approximation [167], which is:

$$p(x) = -2.315 + 0.457x \tag{3.29}$$

By putting Doyle's approximation in equation (3.27) and rearranging,

$$Ln(\delta) = Ln\left[\frac{AE}{Rg(x)}\right] - 2.315 - 0.457\frac{E}{RT} \tag{3.30}$$

The plot between $Ln(\delta)$ versus $\frac{1}{T}$ at different heating rates provide parallel lines for conversion values of 0-1, and each and every conversion yield corresponds to E from slope -$0.457\frac{E}{R}$.

3.4.3. Friedman method

The first and more general iso-conversional method is the Friedman method, which is used for kinetic analysis of samples. By applying natural log on both sides of equation (3.20),

$$\ln\left(\frac{dx}{dt}\right) = -\frac{E}{RT} + \ln\left(Af(x)^n\right) \tag{3.31}$$

The kinetic plot between $\ln\left(\frac{dx}{dt}\right)$ versus 1/T provides slope $-\frac{E}{RT}$ and intercept of $\ln\left(A\,f(\alpha)^n\right)$.

In this method, it is considered that conversion functions $f(x)$ remain constant, which indicates that biomass decomposition is independent of temperature and depends only on the loss of mass rate.

Friedman considered that there was a single (*n)* order of reaction which indicates that value of *E/R* is same for all levels of conversion and plot $\ln\left(A\,f(\alpha)^n\right)$ versus $\ln(x)$ may be liner with an n^{th} slope with an intercept $\ln(A)$. However, the actual value of $\frac{E}{R}$ is not the same for all levels that cause the conversion of complex materials.

3.4.4. Coats-Redfern method

Coats-Redfern model is a model-free method broadly used for calculation of order of reaction and pre-exponential factor [51]. Coats-Redfern method has been derived from KAS and OFW methods. Coats-Redfern model was used to calculate the pre-exponential factor in this study at a heating rate of 10 °C min^{-1}. When selecting the order of reaction (n), the rate of reaction can be written as,

$$\frac{dx}{dT} = \frac{A}{\delta} e^{\left(\frac{-E}{RT}\right)} (1-x)^n \tag{3.32}$$

On arranging the above equation, it becomes

$$\frac{dx}{(1-x)^n} = \frac{A}{\delta} e^{\left(\frac{-E}{RT}\right)} dt \tag{3.33}$$

Integrating equation (3.33) gives,

$$\frac{1-(1-x)^{1-n}}{1-n} = \frac{A}{\delta}\int_0^T e^{\left(\frac{-E}{RT}\right)} dT \tag{3.34}$$

An integral part of equation (3.34) has no exact solution. Therefore, by applying asymptotic series and neglecting higher order terms, solution will become as,

$$\ln\left\{\frac{1-(1-x)^{1-n}}{T^2(1-n)}\right\} = \ln\left\{\frac{AR}{\delta E}\left(1-\frac{2RT}{E}\right)\right\} - \frac{E}{RT} \qquad (for\ n \neq 1) \tag{3.35}$$

$$\ln\left\{\frac{-\ln(1-x)}{T^2}\right\} = \ln\left\{\frac{AR}{\delta E}\left(1-\frac{2RT}{E}\right)\right\} - \frac{E}{RT} \qquad (for\ n = 1) \tag{3.36}$$

However, the term $\frac{2RT}{E}$ <<1; hence, it can be excluded. With this assumption simplifying equation (3.35) and (3.36) becomes,

$$\ln\left\{\frac{1-(1-x)^{1-n}}{T^2(1-n)}\right\} = \ln\left\{\frac{AR}{\delta E}\right\} - \frac{E}{RT} \qquad (for\ n \neq 1) \tag{3.37}$$

$$\ln\left\{\frac{-\ln(1-x)}{T^2}\right\}=\ln\left\{\frac{AR}{\delta E}\right\}-\frac{E}{RT} \qquad (for\ n=1) \qquad (3.38)$$

where *n, T, β, R, A,* and *E* referred as the order of reaction, absolute temperature (K), heating rate (°C/min), Gas constant ($J\ mol^{-1}K^{-1}$), pre-exponential factor (min^{-1}), and activation energy (KJ mol^{-1}), respectively. The kinetic plot between $\ln\left\{\frac{1-(1-\alpha)^{1-n}}{T^2(1-n)}\right\}$ versus $\frac{1}{T}$ for $n\neq1$ and $\ln\left\{\frac{-\ln(1-\alpha)}{T^2}\right\}$ verses $\frac{1}{T}$ for (n=1) provides slope $-\frac{E}{R}$ and intercept $\ln\left\{\frac{AR}{\delta E}\left(1-\frac{2RT}{E}\right)\right\}$. It is assumed that $\frac{2RT}{E}$ <<1, intercepts will become $\ln\left\{\frac{AR}{\delta E}\right\}$. Thus, using this intercept, calculation of pre-exponential factor and order of reaction can be done.

3.4.5. Distributed Activation Energy Model (DAEM)

Distributed activation energy model (DAEM) model was developed by Vand [168] for analysis of very complex reactions taking place during pyrolysis and combustion of fossil fuels. Later on, it was used to calculate the kinetic parameters of different types of biomass fuels to understand complex reaction mechanism [169, 170]. DAEM model assumes that during pyrolysis, the first order of reaction and several irreversible parallel reactions are associated with different activation energy varying with different bond strength species [171]. DAEM model is a powerful tool for understanding and expanding pyrolysis kinetics of several materials. Moreover, it is in good agreement with experimental data, especially at low heating rates [170]. According to Vand, at a given temperature, change in total volatiles can be written as:

$$1-\frac{V}{V_t}=\int_0^{\infty}\exp\left(-A\int_0^{t}e^{-\left(\frac{E}{RT}\right)}dt\right)\int E\ dE \qquad (3.39)$$

where *V* represents effective volatile content and V_t represents the amount of volatile content at time *t*, *A* is the pre-exponential factor, and $\int(E)$ represents the distribution curve of activation energy. In equation (3.39), the integral part has been proposed by Miura [172]. A simplified method of DAEM model is as follows:

$$\frac{V}{V_t} \cong 1 - \int_{E_s}^{\infty} (E)dE \; = \int_{0}^{E_s} (E)\, dE \tag{3.40}$$

Furthermore, the simplified DAEM model regarding the Arrhenius equation is given as:

$$Ln\left(\frac{\delta}{T^2}\right) = \ln\left(\frac{AR}{E}\right) + 0.6075 - \frac{E}{RT} \tag{3.41}$$

From equation (3.41), the plot between $Ln\left(\frac{\delta}{T^2}\right)$ versus 1/T gives a straight line equation. $\frac{E}{R}$ provides a slope of the equation; however, $\ln\left(\frac{AR}{E}\right)$ provides intercept value while value 0.6075 was kept constant for simplicity.

3.5. *Thermodynamic Analysis (TD)*

The thermodynamic parameter of biomass correlated with the thermal stability of biomass, such as the change in enthalpy indicated the nature of reaction process (endothermic or exothermic) and the change in entropy indicated by the reactivity of the reaction system; however, change in Gibbs free energy indicates how far the system was from thermodynamic equilibrium. Thermodynamic parameters such as pre-exponential factor (A), Enthalpy (ΔH), Gibbs energy (ΔG) and change in Entropy (ΔS) were calculated by the equations given below.

$$A = \frac{\delta \times E \times e^{\left(\frac{E}{RT_m}\right)}}{RT_m^2} \tag{3.42}$$

$$\Delta H = E - RT_m \tag{3.43}$$

$$\Delta G = E + R \times T_m \times \ln\left(\frac{K_B T_m}{h\, A}\right) \tag{3.44}$$

$$\Delta S = \frac{\Delta H - \Delta G}{T_m} \tag{3.45}$$

where A is the pre-exponential factor or frequency factor (s^{-1}), T_m is peak decomposition temperature in (K), K_B is Boltzmann constant, and h is Plank constant 6.626 $X10^{-34}$ Js.

3.6. Experimental Procedure for Thermal Pyrolysis

Thermal pyrolysis of all biomass was carried out in a semi-batch SS. reactor under an inert atmosphere. A cylindrical shaped reactor (made of SS-304, 4.0 cm ID × 4.6 cm OD × 30 cm length) was used. The pyrolysis experiment was performed between 450 ^{o}C - 600 ^{o}C, 80 ^{o}C min^{-1} heating rate, 0.5 mm - 2.0 mm particle size and 50 mL min^{-1} - 100 mL min^{-1} sweeping gas flow rate. The desired amount of biomass (50 g) was kept inside the reactor and placed vertically in the furnace. A PID controller was installed which is connected to the furnace with a K-type thermocouple. The temperature and heating rate was controlled by PID controller. The top of the reactor was connected to the condenser which was used to condense the hot volatile gases. At the bottom of the reactor, nitrogen gas inlet was connected to the reactor. Nitrogen gas was used as a carrier gas during the pyrolysis experiment. The flow rate of nitrogen was controlled by using rotameter which was installed before the reactor inlet. The residue (biochar) was removed from the reactor after the end of the experiment (cooled to room temperature). The detail configuration of the experimental setup is presented in Fig. 3.3.

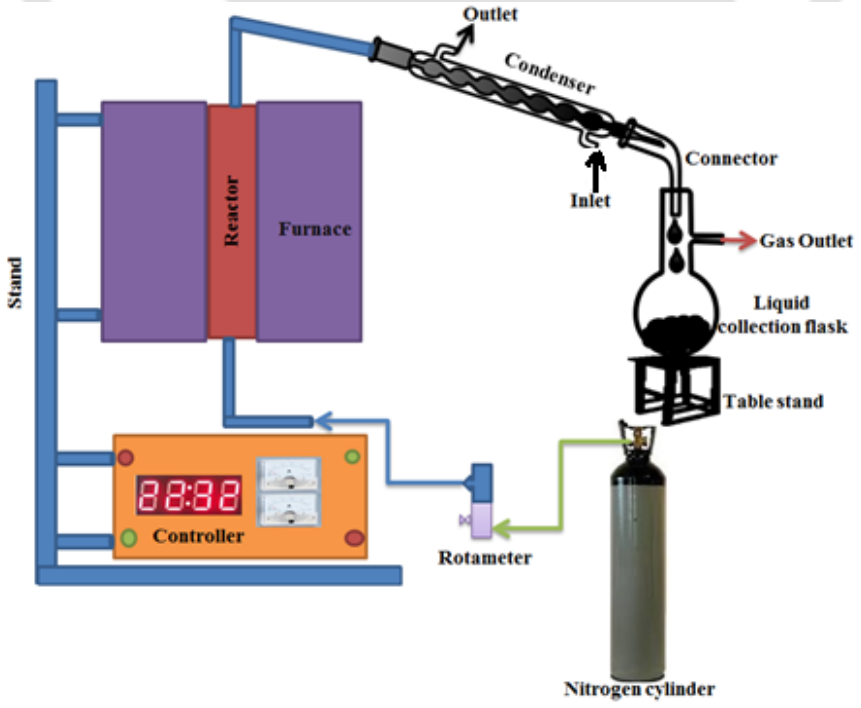

Fig. 3.3. A systematic layout of the pyrolysis experimental setup

Calculation of liquid, char and non-condensable gases yield was done using the following equation.

$$\%\ Liquid\ yield = \left[\frac{Liquid\ fuel\ weight}{Weight\ of\ total\ feed}\right]\times 100 \tag{3.46}$$

$$\%\ Char\ yield = \left[\frac{Mass\ of\ char}{Weight\ of\ total\ feed}\right]\times 100 \tag{3.47}$$

$$\%\ Gas\ yield = 100 - (\%\ Liquid\ yield + \%\ char\ yield) \tag{3.48}$$

3.7. Experimental Procedure for Catalytic Pyrolysis

Catalytic pyrolysis was also performed in the same reactor as mentioned in section 3.6 where various biomass to catalyst (B/C) ratio was fed to the reactor at optimized conditions (450 ^{o}C - 600 ^{o}C, 80 ^{o}C min^{-1} heating rate, 0.5 mm - 2.0 mm particle size and 50 mL min^{-1} - 120 mL min^{-1} sweeping gas flow rate. Zeolite (ZSM-5, 23:1 molar ratio) was used as a catalyst in this study which was purchased from Alfa Aesar (Thermo Fisher Scientific India Private Limited, India). The average grain diameter of ZSM-5 is 19 µm, and the surface area is 425 m^2 g^{-1}. The catalyst was placed in the hot air oven at 110 ^{o}C for 2.0 h for the removal of moisture before the experiment. Biomass to catalyst loading is one of the important parameters, which influences the pyrolytic liquid yield. Therefore, optimization of B/C ratio becomes essential. In this study, ZSM-5 was mixed with biomass with different proportions (3:1, 6:1, 8:1 and 10:1).

3.8. Experimental Procedure for Co-pyrolysis

Co-pyrolysis of biomass and waste plastic was carried out in the same reactor as discussed in section 3.6. The mixture of biomass and waste plastics were optimized and fed to the reactor. In this study, neem seeds (NM) and waste nitrile gloves (WNG) were used at different ratios (1:1, 3:1, and 5:1). The aim of this study was to convert WNG into renewable fuel which has the potential to alter the quality and quantity of pyrolytic liquid. Two catalysts such as CaO and Al_2O_3 were purchased from the Sigma-Aldrich, India. The particle size of the catalyst varied from 0.05 mm - 0.07 mm. The catalysts were placed in the hot air oven at 110 ^{o}C for 2.0 h for removal of the moisture before the experiments. Further, biomass to catalyst loading (B/C) is one of the important parameters, which enhanced pyrolytic liquid yield. CaO and Al_2O_3 were used to improve the pyrolytic liquid yield and their properties by using different

biomass to catalyst (B/C) ratios (3:1, 5:1, and 8:1). The pyrolysis parameters were kept the same as discussed in thermal and catalytic pyrolysis of biomass.

3.9. Characterization of Pyrolytic Oil

Characterization of pyrolytic oil was done by calculating their physical properties, functional groups, and composition. The physical properties such as viscosity, density, heating value, moisture, acidity were determined. However, chemical properties were analysed by using Fourier-transform infrared spectroscopy (FTIR), Gas chromatography-mass spectrometry (GC-MS) and Nuclear magnetic resonance (NMR) techniques. Further, gas composition was analysed by using Gas-chromatography (GC) analysis.

3.9.1. Elemental analysis of pyrolytic oil

Elemental analysis of thermal and catalytic pyrolytic liquid was carried out by using CHNS analyser. The details process of CHNS analyzer is already discussed in section 3.2.3.

3.9.2. Viscosity

The viscosity of pyrolytic oil was determined by using rheometer (Cone and Plate) (HAKEE Rheostress 1) at 40 ^{o}C at 50 RPM where temperature was controlled accurately ±0.05 ^{o}C by HAAKE DC-50 temperature controller. The series of data obtained from the analysis and average data is reported in this study.

3.9.2. Heating value

The calorific value of pyrolytic oil was measured using oxygen bomb calorimeter (1341 Plain Jacket Bomb Calorimeter, Parr Instrument). The detail process is discussed in section 3.2.4.

3.9.3. Acidity, density, and moisture of pyrolytic oil

The acidity of pyrolytic oil was checked by Eutech waterproof (pH Spear) pH meter, and moisture was estimated by Karl Fischer water analyzer (Metrohm 787 KF Titrino). ASTM E-203 and E-1064 standards were used with an error of ±3.5 % of the standard used. The density of pyrolytic oil was measured using a density meter (Anton Paar, DMA4500M).

3.9.4. FTIR analysis

FTIR analysis was carried out using the model FTS 3500 GX attached with DRS. The pyrolytic oil was analyzed by using Attenuated Total Reflectance (ATR) method. A small drop of pyrolytic oil was placed on the ATR crystal with the scanning rate of 40 with a step size of 4 cm^{-1} within the range of 400 cm^{-1} - 4000 cm^{-1} wave number.

3.9.5. Gas chromatography-mass spectrometry (GC-MS) analysis

Gas chromatography and Mass spectroscopy (GC-MS) was used to identify the qualitative and quantitative analysis of unknown samples while the separation of compounds is the major focus, concurrently the compounds groups were also separated by their mass percentages. In this study, GC-MS was used to identify the pyrolytic oil composition. Perkin Elmer (*Clarus* 600/680) GC–MS analyzer was set at 40 ^{o}C for 30 s then increased from 10 ^{o}C min^{-1} to 300 ^{o}C. Total GC run time was set for 30 min. Elite 5 ms column (30 mm × 0.250 µm) was used. 1.0 µL pyrolytic oil was injected, and the carrier gas flow rate was set at 0.6 mL min^{-1}. The chromatograph was collected with the individual retention time and mass spectra of the compounds. NIST library was used to identify the compounds and their composition.

3.9.6. ^{1}H NMR analysis

^{1}H NMR spectra were performed for pyrolytic liquid in a Bruker Advance 600 MHz NMR spectrometer (Bruker BioSpin, Canada) equipped with a 5 mm inverse triple resonance (TXI) probe for ^{1}H. The sample was prepared with approximately 40 mg of the pyrolytic liquid (oil), which was first filtered using 0.2 µm sterilized filter discs (cellulose nitrate) and then dissolved in 0.6 mL of Deuterated chloroform ($CDCl_3$). All the acquired NMR spectra were processed through Topspin version 2.1 software with a Gaussian function. Further, NMR is an analytical tool which is used to estimate the various functional groups such as paraffins, olefins, and aromatics. Myers et al. (1975a) [173], Myers et al. (1975b) [174] and Sınağ et al. (2006) [175] developed a correlation which is used for the determination of the composition of co-pyrolytic oil. These correlation involves equation (3.49) - (3.53). However, *A, B, C, D, E,* and *F* represent an integrated area of NMR spectra (ppm) as referenced with TMS and the chemical shift is listed in Table 3.1. These correlations have been recognized based on the known standards (with an error of ±1.20 %).

$$Aromatics, vol.(\%) = \frac{\left(\frac{A+C}{3}\right)\times 0.97\times 10^2}{\left(\frac{A+C}{3}\right)\times 0.97+\left(D-2B+\frac{E}{2}+\frac{F}{3}\right)\times 1.02+3.33B} \quad (3.49)$$

$$Paraffins, vol.\% = \frac{\left(D-2B+\frac{E}{2}+\frac{F}{3}\right)\times 1.02\times 10^2}{\left(\frac{A+C}{3}\right)\times 0.97+\left(D-2B+\frac{E}{2}+\frac{F}{3}\right)\times 1.02+3.33B} \quad (3.50)$$

$$Olefins, vol.\% = \frac{3.33B\times 10^2}{\left(\frac{A+C}{3}\right)\times 0.97+\left(D-2B+\frac{E}{2}+\frac{F}{3}\right)\times 1.02+3.33B} \quad (3.51)$$

$$\frac{H}{C} = \frac{(A+B+C+D+E+F)}{\left(\frac{A+C}{3}\right)\times 1.28+\left(D-2B+\frac{E}{2}+\frac{F}{3}\right)\times 1.02+3.42B} \quad (3.52)$$

Albahri (2003) [176] reported that branch structure of paraffinic hydrocarbons has close relation in petroleum sectors. The ratio of CH_3:CH_2 for an unknown or mixture of paraffins can be estimated by using NMR techniques.

$$Isoparaffin\ index = \frac{CH_3}{CH_2} = \frac{\left(\frac{F}{3}\right)}{\left(\frac{E}{2}\right)} \quad (3.53)$$

Table 3.1. NMR spectra region [173, 174]

Presentation	Proton types	Chemical shift region
A	Aromatic rings	6.6-8.0
B	Olefins	4.5-6.0
C	α - methyl	2.0-3.0
D	Methane (paraffins)	1.5-2.0
E	Methylene (paraffins)	1.0-1.5
F	Methyl (paraffins)	0.6-1.0

3.9.7. Gas chromatography (GC) analysis

Pyrolysis gas was collected in Tedlar gas sampling bags and further analyzed by multiple gas chromatography (SRI GC, Torrance, CA). Helium ionization detector (HID) and thermal conductivity detector (TCD) were used in this study. Silica gel column (6' Molecular Sieve 13X and 6' Silica Gel) was used, and helium gas was used as a carrier gas for the present study. The column temperature was initially set at 65 ^{o}C for 10 min at a rate of 15 ^{o}C min^{-1} to 250 ^{o}C as a final temperature.

3.10. Biochar Characterization

Pine sawdust char (*PWC*), Sal sawdust char (*SWC*), Areca nut husk char (*ANC*), *Cascabela thevetia* seeds char *(SKC), Delonix regia* seeds char (*SGC*), *Manilkara zapota* seeds char (*CKC*), *Azadirachta indica* kernel char *(NMC), and Madhuca Indica* seeds char *(MHC)* were obtained from the pyrolysis (500 ^{o}C temperature, 80 ^{o}C min^{-1} heating rate, 0.5 mm - 2.0 mm particle size and 100 mL min^{-1} sweep nitrogen gas flow rate). Further, activated charcoal with acid treated *(ACWA)* (LOBA Chemie, India) was selected as the standard to compare.

3.10.1. Acidity, oxidation-reduction potential (ORP) and electrical conductivity (EC)

Dried biochar sample (10 g) was soaked in 1:1 slurry of 0.01 M $CaCl_2$ solution for 2 h prior to measurement of pH, ORP and EC (Orion720A Model pH meter) as per ASTM D4972. The pH meter was calibrated with standard pH buffers at pH 4, 7 and 10 prior to analysis. All analyses were performed in triplicate, and the results were averaged.

3.10.2. Particle size distribution, and Zeta potential measurement

The particle size of biochar samples were measured by a particle size analyzer (Delsa Nano C, Beckman Coulter, Nyon, Switzerland). A volume of 5 cm^3 of the sample was filled in the cuvette. A HeNe laser (632.8 nm wavelength) was used to irradiate the sample, which produced intensity fluctuations of the scattered light. The fluctuation was absorbed faster for smaller and faster-moving particles while slowly for the larger particles. The non-negative least square method which is inbuilt in the software was used to obtain overall size distribution. A particle size analyzer (Delsa Nano C, Beckman Coulter, Nyon, Switzerland) was used to measure the Zeta-potential of biochars. The solution of biochar and water (centrifuged) injected (about 1 cm^3) in the flow cell of the analyzer. All the experiments were repeated thrice and the mean value is reported.

3.10.3. Water holding capacity (WHC)

Oven dried biochar sample (60 ^{o}C for 12 h) was used to determine the water holding capacity (*WHC*). A known amount of dried biochar sample was loaded in the ceramic Buchner funnel lined with filter paper (size P8; Fisher brand), and a known amount of deionized water was added to the biochar slowly until the biochar was saturated and the water was allowed to drain by gravity for the biochar approximately for 3 h. The WHC was determined by calculating moisture of saturated biochar and the relative proportion of water passing through the biochar sample after correcting for the water absorbed by the filter paper.

3.10.4. Surface area analyzer (BET)

Surface areas were determined on dry biochar samples via N_2 adsorption at 77 K on a Surface Area Analyzer (Micromeritics ASAP-2020 BET). BET and Langmuir adsorption isotherms were generated to determine the single-point surface area. The degasified temperature was kept 300 ^{o}C for 6 h.

3.10.5. Biochar morphology (FESEM)

The morphology study of biochar was carried out by using Field Emission Scanning Electron Microscope (FESEM, Zeiss Supra 40) equipped with an Energy Dispersive X-ray Spectrometer (EDS, Oxford Inca Energy 350). The oven-dried biochar was placed on the carbon tape, and the gold coating was done to prevent sample charging. FESEM was used under high vacuum with acceleration voltage between 5kV-15 kV.

Results and Discussion

Chapter 4

Characterization and Kinetic Analysis of Biomass

4.1. Characterization of Raw Biomass

4.1.1. Physicochemical characterization of biomass

Physicochemical characterization of selected biomass is listed in Table 4.1. From results, it was confirmed that selected biomass have higher volatile matter (75.05 % - 78.05 %) and a lower amount of ash (1.14 % - 3.26 %). Higher volatile matter and lower ash content indicate that ignition of fuel will be easy. Further, ash content acts as a heat sink which reduced the heating value of fuel which means lower the ash content, higher the heating value of the fuel. Also, the presence of a higher amount of ash leads to the formation of fouling and slagging problems which reduced the efficiency of operation and equipment [45, 163]. Moisture was also found to be <10 % which makes these biomass more suitable for pyrolysis and combustion [33]. Amount of fixed carbon was also found to be lower. The obtained results have good agreements with other reported biomass such as castor seed [62], cotton stalk, mustard stalk [50], *Pongamia pinnata* seed [45], and pomegranate seeds [66]. The elemental analysis involves finding out of the amount of carbon, hydrogen, oxygen, nitrogen, and sulpher present in the biomass. From results (Table 4.1), it was confirmed that all biomass contained higher amount of carbon (48.46 % - 61.48 %) along with lower amounts of nitrogen (0.59 % - 7.3 %) and sulpher (0.34 % - 0.70 %) which made these biomass more suitable for pyrolysis. The lower value of nitrogen and sulpher indicates that the formation of SO_x and NO_x will be lower during combustion. The heating value of biomass was found to be higher (17.10 MJ kg^{-1} - 26.88 MJ kg^{-1}). The bulk density of biomass is an indication of ease of handling the biomass during transportation and storage. From results (Table 4.1), it was noticed that the bulk density of seed biomass was higher (454.26 kg m^{-3} - 635.62 kg m^{-3}) than wood biomass (297.27 kg m^{-3} - 396.91 kg m^{-3}). Further extractive content of biomass significantly effects of pyrolysis and thermal stability. From results (Table 4.1), it was found that extractive content varied from 7.69 % - 57.40 % while chemical analysis of biomass varied from 67.95 % - 89.38 %. Chemical analysis of biomass depends on the composition of biomass, therefore, varied from biomass to biomass. The calculated results are in good agreement with other reported biomass as presented in Table 4.1.

Table 4.1. Physicochemical characterization of selected biomass along with other reported biomass

Analysis	SK	SG	SS	AM	NM	CK	MH	PW	SW	AN
Proximate analysis (wt. %)										
M_C	4.97 ± 0.10	6.85 ± 0.15	6.19 ± 0.16	6.56 ± 0.08	7.32±0.2	8.07 ± 0.16	6.88±0.5	6.09±0.3	8.88±0.2	7.43±0.10
VM	78.05 ±0.71	76.27 ±0.65	76.00 ±0.67	75.20 ±0.92	76.20±0.1	77.02 ±0.73	78.05±0.2	79.03±0.2	78.03±0.1	75.05±0.20
A_s	2.19 ± 0.14	2.78 ± 0.12	3.06 ± 0.14	2.69 ± 0.16	3.26±0.02	1.19 ± 0.11	3.08±0.05	2.07±0.03	1.14±0.01	2.48±0.05
FC	14.78±0.11	14.10±0.13	14.74±0.13	15.55±0.12	13.32±0.2	13.73±0.13	11.63±0.3	11.16±0.1	12.09±0.2	14.55±0.3
VM/FC	5.28±0.13	5.40±0.12	5.15±0.12	4.83±0.13	5.72±0.13	5.60±0.11	6.71±0.12	7.08±0.11	6.45±0.09	5.15±0.13
Ultimate analysis (wt. %)										
C	54.93	53.5	48.46	48.76	54.36	52.67	61.48	50.3	49.83	48.8
H	9.99	6.93	6.75	5.91	7.36	6.74	8.69	6.00	6.01	5.79
O	31.07	32.55	37.47	43.31	33.68	38.78	26.86	42.99	43.56	43.45
N	3.33	6.99	7.3	2.01	3.89	1.46	2.62	0.69	0.58	1.95
S	0.66	-	-	-	0.7	0.34	0.34	-	-	-
O/C	0.42	0.45	0.58	0.67	0.46	0.55	0.33	0.64	0.65	0.66

H/C	2.18	1.55	1.67	1.46	1.62	1.54	1.69	1.43	1.44	1.42
Heating value (MJ/kg)	24.50 ±0.10	19.75 ±0.11	17.68 ±0.20	17.10 ±0.33	22.19±0.12	20.05 ±0.19	26.88±0.18	18.44±	18.2±0.16	18.21±0.20
Bulk density (kg/m^3)	496.96 ± 02	635.62 ± 06	657.41 ± 04	396.91 ± 07	563.05±1.5	454.26 ± 06	462.27±1.8	297.27±1.8	325.91±2.1	249.56±2.0
Extractive analysis (wt. %)	57.40±0.60	30.12 ±0.40	30.66 ±0.39	25.86 ±0.30	29.24±0.60	29.84±0.48	62.52 ±0.40	10.54 ±0.39	7.69 ±0.30	10.17±0.48
Hexane	48.44±0.15	13.87 ±0.19	9.86 ± 0.10	10.60 ±0.14	25.80±0.15	25.44±0.25	54.49 ±0.19	10.33 ±0.10	7.23 ±0.14	9.94±0.25
Ethanol	8.96 ± 0.45	16.25 ±0.21	20.80 ±0.29	15.26 ±0.16	3.44 ± 0.45	4.40 ± 0.23	8.03 ±0.21	0.21 ±0.29	0.41 ±0.16	0.23± 0.23
Hemicellulose (%)	21.01±0.16	27.22±0.13	26.55±0.17	21.98±0.16	21.94±0.16	26.55±0.15	27.33±0.13	18.35±0.17	16.59±0.16	16.81±0.15
Cellulose (%)	36.00±0.16	48.16±0.13	30.81±0.17	48.11±0.15	38.04±0.16	34.03±0.18	37.92±0.13	50.92±0.17	49.36±0.15	48.98±0.18
Lignin (%)	15.23±0.13	14.06±0.11	10.59±0.16	5.48±0.13	13.58±0.13	7.61±0.17	15.20±0.11	12.55±0.16	11.18±0.13	13.27±0.17

4.1.2. Thermogravimetric Analysis (TGA)

From Fig. 4.1, it was confirmed that all biomass underwent three major stages of degradation (drying, active pyrolytic stage and char formation stage or passive stage) during the thermal process. Ceylan and Topçu (2014) [63] studied hazelnut husk, Chandrasekaran et al. (2017) [58] studied *Prosopis juliflora* and Damartzis et al. (2011) [51] studied cardoon (*Cynara cardunculus*) biomass and reported that these biomass undergone three major stages of degradation during thermal analysis. All the above literature reported that maximum decomposition occurred within 200 ^{o}C - 500 ^{o}C which is considered as the active pyrolytic stage. At the initial stage, moisture and light volatile matters (lower molecular weight compounds) evaporated up to 150 ^{o}C. However, maximum volatilization occurred in the temperature range of 200 ^{o}C - 500 ^{o}C. Further, at the higher temperature (>500 ^{o}C), slower weight loss was observed due to the decomposition of lignin which substantially contributed towards the generation of char. Maximum volatilization took place in the second stage which is known as the active pyrolytic stage. In this stage, higher molecular weight compound broke and fragmented into smaller molecular weight compounds by the continuous supply of heat. Further, aliphatic chains were broken into small gaseous compounds due to the continuous supply of heat/temperature which helped escaping of molecules from their shells by providing enough energy. Further, at the final stage, lignin decomposed at a higher temperature at a slower rate due to the presence of hydroxyl phenolic groups and resulted in the maximum formation of char. The char can be utilized as solid fuel, bio-adsorbent, fertilizer, catalyst, fuel cell, and activated carbon.

Generally, biomass contains moisture, hemicellulose, cellulose, lignin, non-polar lipid compounds, hydrocarbons, chlorophylls, polar wax, sterol, and some other (organic and inorganic) compounds. DTG profile (Fig. 4.1) of biomass showed that the first peak was observed due to the removal of moisture and very light volatile compounds up to 150 ^{o}C. Degradation peak of hemicellulose and cellulose were observed in the temperature range 200 ^{o}C - 500 ^{o}C. Literature reported that hemicellulose degrades at lower temperature (220 ^{o}C - 315 ^{o}C) followed by cellulose (315 ^{o}C - 400 ^{o}C) and lignin (160 ^{o}C - 900 ^{o}C) [177]. Lignin degrades at a higher temperature greater than 500 ^{o}C due to higher thermal stability. Phenolic hydroxyl group which represents the presence of lignin increase the thermal stability which promotes lignin degradation at the higher temperature (>500 ^{o}C). During thermal depolymerization,

lignin provides more aromatic compounds along with small chains of organic molecules as well as gaseous products such as CO and CH_4.

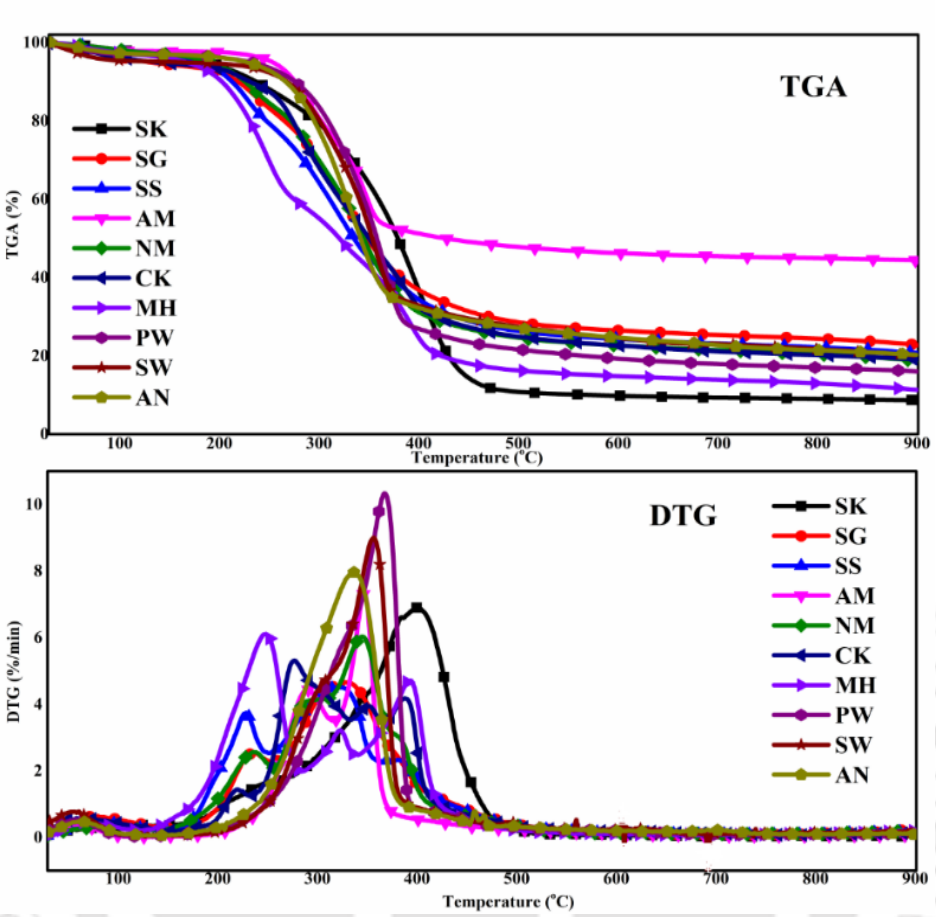

Fig. 4.1. TGA and DTG profiles of raw biomass at heating rate 10 $^{o}C\ min^{-1}$

Apart from the degradation profile of hemicellulose, cellulose, and lignin, separation of extractives and other component becomes essential. After soxhlet extraction, the entire component gets withdrawn except hemicellulose, cellulose, and lignin [178]. Hence, the exact composition of hemicellulose, cellulose, and lignin can be calculated from TGA and DTG profile of extractive-free biomass (Table 4.1). From Fig. 4.1 and 4.2, it was confirmed that the presence of extractives influences thermal degradation profiles of the biomass. From Fig. 4.1, it was confirmed that the first peak (hemicellulose) was found at 216 ^{o}C, 230 ^{o}C, 226 ^{o}C, 218 ^{o}C, 290 ^{o}C, 218 ^{o}C, 247 ^{o}C, 303 ^{o}C, 298 ^{o}C, and 270 ^{o}C while second peak (cellulose) was found at 401 ^{o}C, 331 ^{o}C, 325 ^{o}C, 390 ^{o}C, 344 ^{o}C, 345 ^{o}C, 350 ^{o}C, 392 ^{o}C, 369 ^{o}C, 357 ^{o}C, and 337 ^{o}C for *Cascabela thevetia*, *Delonix regia*, *Samanea saman*, *Sapodilla* and *phyllanthus emblica*, *Azadirachta indica*, *Manilkara zapota*, *Madhuca longifolia*, *Pinus ponderosa*, *Shorea robusta* and *Areca catechu* . Further, from Fig. 4.2 (extractive free biomass), it was noticed that

first peak (hemicellulose) was found at 252 ^{o}C, 232 ^{o}C, 229 ^{o}C, 285 ^{o}C, 286 ^{o}C, 272 ^{o}C, 287 ^{o}C, 257 ^{o}C, 321 ^{o}C, 296 ^{o}C, and 279 ^{o}C while second peak (cellulose) was found at 352 ^{o}C, 326 ^{o}C, 317 ^{o}C, 353 ^{o}C, 354 ^{o}C, 350 ^{o}C, 355 ^{o}C, 290 ^{o}C, 367 ^{o}C, 359 ^{o}C and 336 ^{o}C for *Cascabela thevetia, Delonix regia, Samanea saman, Manilkara zapota* and *Phyllanthus emblica, Azadirachta indica, Sapodilla , Madhuca longifolia, Pinus ponderosa, Shorea robusta* and *Areca catechu*. Also, DTG thermograph (Fig. 4.1) showed that raw biomass does not contain any sharper peaks in the hemicellulose and cellulose region. However, DTG thermograph of extractive-free biomass (Fig. 4.2) has shaper peaks in the same region which represents a higher rate of degradation of hemicellulose, cellulose, and lignin. Further, from Fig. 4.2, it was noticed that the decomposition temperature of all biomass at the second peak (cellulose) decreased which indicated a reduction in the crystallinity of cellulose. It was reported that cellulose crystallinity increased due to the presence of extractives [140]. Also, it may affect the pyrolytic products composition, increase the heating value of fuel, and reduce the amount of acids, alkanes, and water [140]. Hence, it can be concluded that the presence of extractives affected the thermal degradation temperature of all these biomass. On the other side, the presence of extractive reduces the formation of CO_2, CO, and H_2O. Also, it improves the deterioration of lignin at lower temperature and produces phenolic homologues, more organic compounds such as methanol, methane, and aldehyde [179].

4.1.3. Variation in activation energy fresh and extractive free biomass

Kinetic study of biomass used to determine the kinetics parameters such as activation energy, the order of reaction and frequency factor. The results obtained from the Horowitz and Metzger model is listed in Table 4.2. From this table, it was confirmed that the presence of extractive content in biomass significantly lowered the thermal decomposition temperature as well as activation energy. However, fresh biomass required higher activation energy to start the reaction. Moreover, the use of these extractives depends on the desired products or requirements. It was reported that biomass having significant extractive content creates several problems during industrial application [180]. Extractives contain lower molecular weight compounds which encourage the decomposition of biomass at a lower temperature [181, 182].

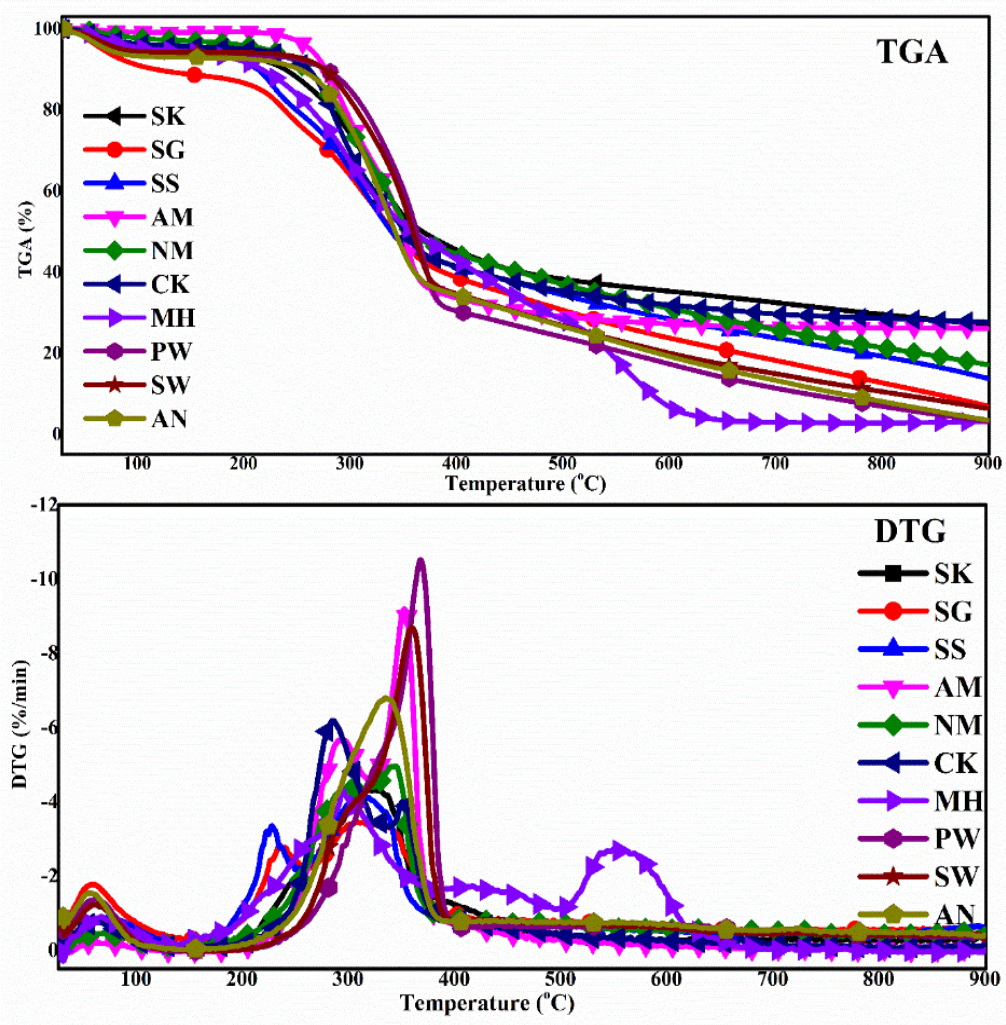

Fig. 4.2. TGA and DTG profiles of extractive-free biomass at a heating rate 10 ^{o}C min^{-1}

Generally, woods extractives associated with triglycerides free long chain fatty acids, resin acids, waxes, sterols, and steryl esters [183]. The presence of the higher amount of extractives may be directed to undesirable complex properties such as browning, which decrease the mechanical strength of the materials and moreover extrusion process is affected by wood thermal degradation property [184]. Sheshmani (2013) [185] reported that extractives are generally hydrophilic in nature. In the pulp and paper industries, extractives can deposit in the paper machine which encourages the cracking of the paper sheets [186].

Table 4.2. Kinetic parameters determined by *Horowitz and Metzger* model

Biomass	With Extractive contents		Without Extractive contents	
	E, (kJ/mol)	R^2	*E*,(kJ/mol)	*R2*
SK	12.96	0.9355	22.95	0.9789
SG	14.07	0.9993	16.57	0.9828
SS	17.53	0.9872	38.94	0.9782
AM	52.41	0.9787	59.62	0.9708
NM	16.19	0.9978	23.33	0.9910
CK	15.97	0.9857	22.12	0.9742
MH	10.63	0.9739	54.64	0.9803
PW	76.86	0.9969	80.52	0.9982
SW	24.42	0.999	55.04	0.9988
AN	22.58	0.9904	27.05	0.9950

4.1.4. Van Krevelen diagram

Van Krevelen diagram is presented in Fig. 4.3. The atomic ratio of all the biomass varied in the order: SK>MH>SS>NM>CK>SG>AM>SW>PW>AN. The alteration in the atomic ratio indicated ignition order of these biomass. From results (Fig. 4.3), it was noticed that biomass *SK* will be easy to ignite as compared to other biomass. Biomass having higher calorific value indicated that the burning of fuel will be easier compared to the biomass having lower calorific value. The present results are in good agreement with other studies [45, 163].

4.1.5. Biofuel reactivity

Biofuel reactivity obtained from the molar ratio of the O/C, H/C and VM/FC for each biomass sample is presented in Fig. 4.4. It was observed that the VM/FC ratio varied widely for each biomass in the decreasing order of PW>MH>CK>SW>NM>SG>SK>AN>SS>AM. From Fig. 4.4, it was confirmed that biomass having a higher volatile matter to fixed carbon ratio was more reactive than those having a lower volatile matter to fixed carbon ratio. Also, these biomass shows a better advantage over other biomass for utilization as solid biofuel. The present results are in good agreements with other studies [45, 163].

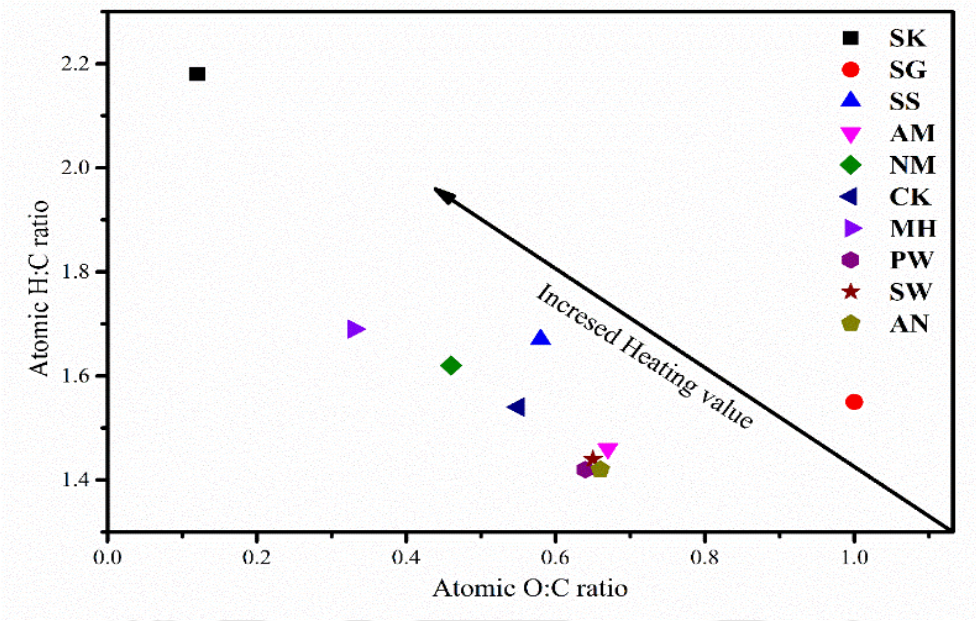

Fig. 4.3. Van Krevelen plot of selected biomass

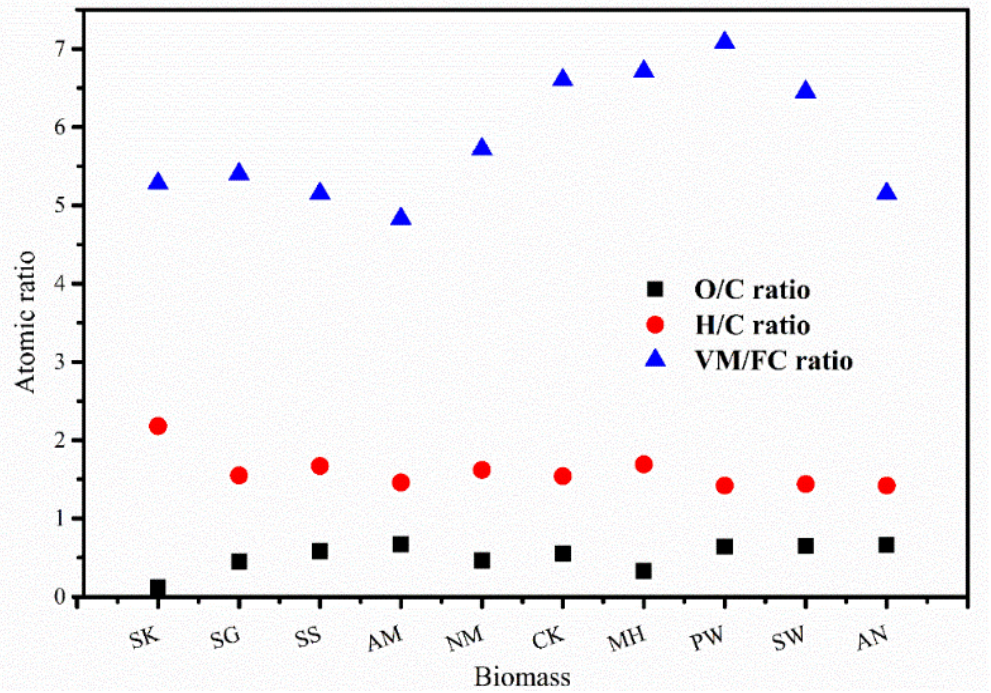

Fig. 4.4. Biofuel reactivity of selected of biomass

4.1.6. Energy Dispersive X-ray analysis

Presence of minerals in biomass provides a positive effect during pyrolysis or combustion [163]. The presences of mineral increase the catalytic effects by enhancing the rate of conversion during pyrolysis. According to Sjöström (1993), the presence of calcium acted as a catalyst at the beginning of gasification or pyrolysis [187]. Potassium had a foaming effect during pyrolysis and increased the conversion rate because of the movement of potassium catalyst to the active site due to possible by the fragmentation of carbon structure [188]. Solid biomass fuel contains the maximum amount of B, Al, Si, Mg, Mn, Ca and K along with the other minerals such as Cu, Co, Zn, Cl, and Na [163]. The presence of useful compounds in biomass was presented in Table 4.3.

4.1.7. XRD analysis

XRD analysis of all biomass is presented in Fig. 4.5. From literature, it was found that biomass crystallinity depends on the presence of wax, which is mainly high molecular mass hydrocarbons and some fatty acid components. Usually, crystallinity is associated with complex bonding between cellulose and waxes present in biomass [49]. From Fig. 4.5, it was noticed that SK, SG, and SS do not have sharper peaks hence; these biomass may be amorphous in nature. However, AM, NM, CK, MH, PW, SW, AN have crystalline peaks. The crystallinity index was calculated and listed in Table 4.4. From a result, it was confirmed that AN, AM and PW have higher crystallinity than other biomass.

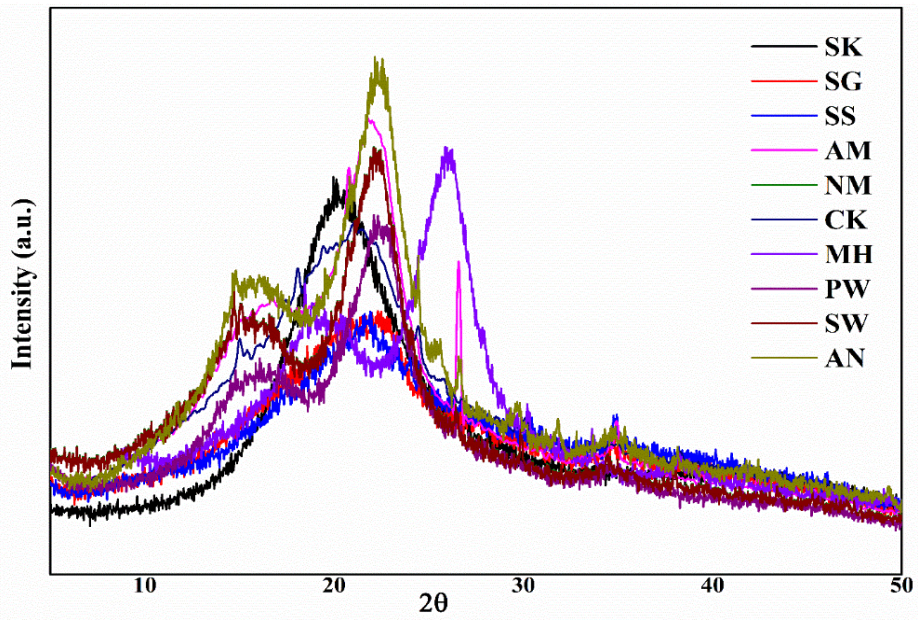

Fig. 4.5. XRD analysis of selected biomass

Table 4.3. EDX analysis of the selected biomass

Minerals	SG	SK	SS	AM	NM	CK	MH	PW	SW	AN
B	√	√	√	-	√	√	-	-	-	-
K	√	√	√	√	√	√	√	√	√	√
P	√	√	√	√	√	√	√	√	√	√
Ca	√	√	√	√	√	√	√	√	√	√
Zn	√	√	√	√	-	-	√	√	√	√
Mg	√	√	√	√	√	√	√	√	√	√
Ti	√	-	√	-	-	√	-	-	√	√
Cu	√	-	√	√	-	-	-	√	√	√
Ni	√	√	√	√	√	-	-	-	√	√
Co	√	√	-	-	√	-	√	√	√	√
Al	√	√	√	-	-	-	-	√	-	√
Mn	-	√	√	√	-	√	-	√	√	√
Si	-	√	-	√	-	√	√	√	√	√
Zr	-	-	-	√	√	√	√	√	√	√
Fe	-	-	-	√	√	√	√	√	√	-
Cl	-	-	-	√	√	√	√	√	√	√
Cr	-	-	-	√	√	√	√	√	-	√
Ar	√		-	-		-	√	-	-	-
Na	-	-	-	√	√	-	√	-	-	-

Table 4.4. Crystallinity Index of different types of selected biomass

Biomass	I_{002}	$I_{amorphous}$	Crystallinity Index *CrI* (%)
AM	4028	2428	65.00
NM	3742	2560	46.17
CK	3096	2018	48.77
MH	3734	2504	49.00
PW	3175.65	1901.85	66.97
SW	3770.85	2534	48.77
AN	4526.81	2667	69.70

4.1.8. FTIR analysis

The wave number vs. transmittance spectra for selected biomass are presented in Fig. 4.6, and their functional groups are listed in Table 4.5. The adsorption band 3313 cm^{-1} - 3455 cm^{-1} attributed to the axial deformation of -OH which indicated the presence of phenols, water, aromatics, protein and alcohol [45]. The peak 2927 cm^{-1} attributed with the C-H_2 asymmetric alkanes [45]. Peak 2852 cm^{-1} - 2856 cm^{-1} was due to the axial deformation of the C-H group. The presence of carbonyl group like ester (C=O) was observed at peak 1750 cm^{-1} - 1783 cm^{-1}, which signified the presence of hemicellulose in the biomass [189]. The peak 1458 cm^{-1} was the symmetric deformation of CH_2 group of cellulose and the peak 1158 cm^{-1} referred C-O-C of the cellulose and hemicellulose [47, 189]. The peak 1369 cm^{-1} - 1374 cm^{-1} signified the presence of C-H and aliphatic C-H stretching in methyl and phenol. The peak 1636 cm^{-1} referred to C=C aromatic ring that indicated the presence of lignin and protein [49, 190].

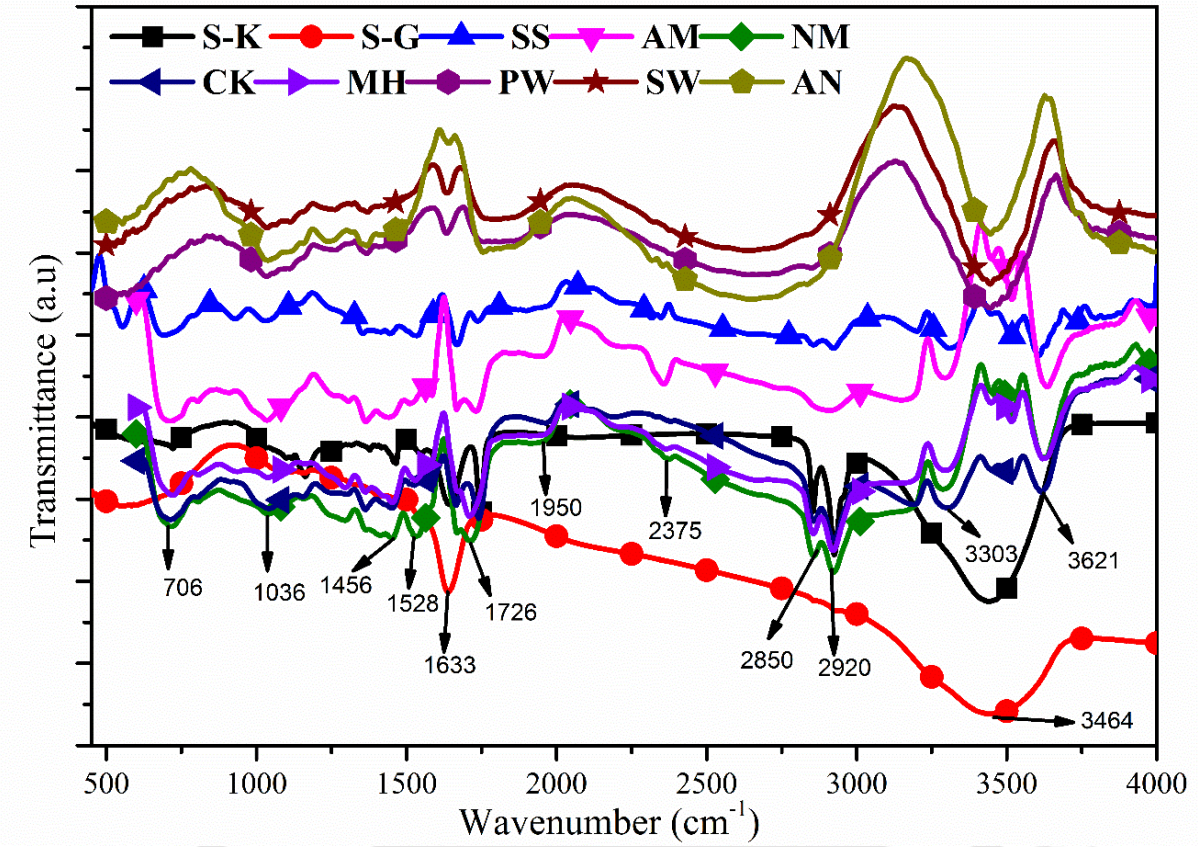

Fig. 4.6. FTIR analysis of selected biomass

4.1.9. Slagging and fouling indices and ash deposition tendencies of residual biomass

Ash encloses inorganic elements, which result in positive effect during pyrolysis. Presence of ash either increase the yield of pyrolytic liquid or improve the properties of fuels. There are several criteria for deposition tendencies such as when B/A <0.5, deposition tendency is low when 0.5 < B/A < 1 deposition tendency is medium and when B/A > 1 deposition tendency is usually high. Further, when values < 0.31 or > 3 of silica-alumina and iron-calcium ratios deposition tendency is low, while for values between 0.3 and 3 deposition tendency is high. When S < 0.6, deposition tendency is low, when 0.6 < S < 2 deposition tendency is medium and when S > 2 deposition tendency is high. Finally, when TA < 0.3, fouling tendency is low, when 0.3 < TA < 0.4 fouling tendency is medium and when TA > 0.4, this tendency is higher. X-ray fluorescence analysis is presented in Table 4.6 and results were very similar to other reported biomass such as, rice straw, rice husk, cotton stalk, wheat straw, bagasse, corn stover, sorghum stalk, mustard stalk, corn cob, *jatropha pruning, Jatropha (Jatropha curcas)*, Karanja, coal, oak wood and wheat straw [45, 50, 163].

Table 4.5. FTIR analysis of selected biomass

Wavenumber (cm^{-1})	Type of vibration and functional group
3313-3455	O-H, stretching vibration, (alcohol, aromatics, water, protein, and Phenols)
3008	=C-H, stretch alkenes
2927	C-H_2 asymmetric alkanes
2856	C-H stretch alkanes
2852-2860	Axial deformation of C-H group
2632-2637	C-H and =C-H stretching vibration (alkanes and alkenes)
1757-1783	C=O stretching in unconjugated ketone carbonyl and aliphatic group
1631-1657	C=O stretching unconjugated to the aromatic ring
1636-1545	-C=C- stretch alkenes and C-C stretch (in the ring) aromatic
1458	CH_2 symmetric deformation
1238-1269	C-C plus, C-O plus, C=O stretching
1158	C-O-C and C-OH, asymmetric deformation, stretching vibrations
1031-1033	C-O stretching vibration (cellulose, hemicellulose, and lignin)
779- 902	C-H deformation in cellulose and C-H stretching, aromatic ring
551-724	-CH bending, monoaromatic ring

Results obtained from the empirical equation of slagging and fouling indices are presented in Table 4.7. Slagging and fouling indices were calculated based on the results obtained by XRF analysis. Deposition tendencies were calculated by the method described by Carpenter (1998) [164]. However, deposition tendency depends on various parameters and different conditions. Based on these, it is predicted that use of these biomass in the boiler will create ash-related problems due to the higher amount of alkali which produces molten salts via vaporization, condensation, secondary reactions, and high acid to base ratio [191]. Use of herbaceous biomass for the combustion process, having a higher amount of alkaline may lead to fouling and corrosion problems [192]. However, these problems can be solved by proper monitoring and control of the blowing system. Such systems are commercially available and significantly help to optimize blower operation and ash deposition control [193]. Additionally, these biomass and their ash are less corrosive and abrasive compared to conventional fuels because of lower quartz and pyrite level. Co-combustion of biomass with fossil fuel is the more

prominent way to overcome these disadvantage which will help in the growth of the economy and the best possible way of the utilization of biomass [194]. Furthermore, alkali metal present in biomass helps during the thermal process especially Na, K, Mg, P, and Ca. The reaction between silica and alkali metal, present in ash helps the formation of the sticky liquid mobile phase, which further leads to blockage of the airway of boiler and furnace [195].

4.2. Kinetic and Thermodynamic Analysis of Biomass

In this section, three biomass PW, SW and AN were selected as these biomass are not studied extensively while their characterization results showed enough potential to produce liquid fuel. Also, these sawdust biomass are available abundantly across the country almost throughout the year.

4.2.1. Burnout temperature

Burnout temperature is extensively used by various researchers [196, 197] for the characterization of pyrolysis and combustion property of biomass. The temperature at which less than 1 % decomposition occurs is known as burnout temperature. It was observed that PW and SW had lower burnout temperature (552 ºC, 560 °C) than AN (570 °C) at 10 °C min^{-1} heating rate. Lignin decomposed at higher temperature due to the presence of phenolic compounds. Therefore, it can be concluded that PW and SW biomass are relatively more combustible compared to AN biomass. The effect of heating rate on burnout temperature is presented in Fig. 4.7.

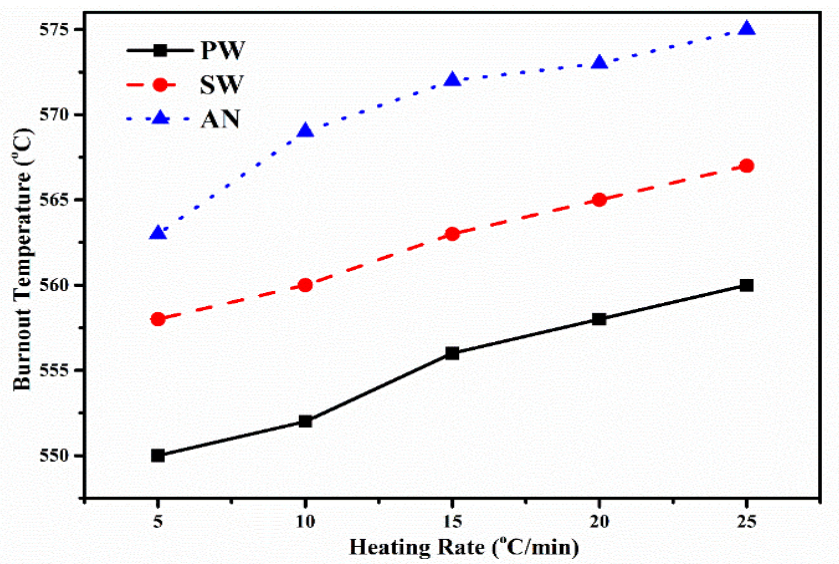

Fig. 4.7. Effect of heating rates on burnout temperature of PW, SW, and AN biomass

Table 4.6. Elemental compositions of residual biomass ashes (%)

Element	Present as	SK	SG	SS	AM	NM	CK	MH	PW	SW	AN
Silicon	SiO_2	<0.001	<0.0016	<0.0020	<0.0011	<0.0016	<0.0020	<0.0024	37.16	51.83	48.63
Aluminium	Al_2O_3	<0.003	<0.0018	<0.0016	<0.0039	<0.0028	<0.0041	<0.0031	10.36	10.62	11.36
Calcium	CaO	18.68	17.25	20.13	19.7	16.86	18.86	17.56	26.21	11.52	13.2
Titanium	TiO_2	0.0154	0.066	0.0032	0.0028	0.0036	0.0029	0.0028	0.96	0.63	0.52
Phosphorus	P_2O_5	35.6	32.05	33.02	31.8	28.69	27.66	25.36	3.26	1.8	0.93
Sodium	Na_2O	<0.017	<0.05	<0.06	<0.042	<0.032	<0.060	<0.026	3.26	4.02	3.05
Manganese	MnO	0.16	0.34	0.5	0.46	0.83	0.73	0.46	0.025	0.003	0.01
Magnesium	MgO	15.28	16.23	14.64	15.26	18.63	17.93	18.86	0.03	2.3	2.8
Iron	Fe_2O_3	0.62	0.25	0.32	0.72	0.52	0.51	0.34	5.88	4.38	5.92
Chlorine	Cl	1.26	1.15	1.05	0.95	0.73	0.85	1.62	-	4.97	3.73
Potassium	K_2O	28.39	32.56	30.26	31.36	34.25	33.28	35.86	8.36	7.67	8.96
Sulfur trioxide	SO_3	0.03	0.1	0.25	0.09	0.17	0.26	0.14	5.09	0.91	0.92

Table 4.7. Slagging and fouling indices of residual biomass

Biomass	*B/A* ratio	*S/A* ratio	*I/C* ratio	Total Alkalis (*TA*)
SK	3245.20	0.33	0.033	28.377
SG	955.91	0.88	0.014	32.61
SS	9589.70	1.25	0.015	30.22
AM	5887.43	0.28	0.031	31.40
NM	8761.50	0.57	0.030	34.08
CK	7848.88	0.49	0.027	33.34
MH	8740.48	0.77	0.019	35.88
PW	0.91	3.59	0.23	11.62
SW	0.47	4.88	0.38	11.49
AN	0.56	4.28	0.45	12.01

4.2.2. Thermal analysis of biomass

Thermal decomposition behavior of waste biomass was studied by using thermogravimetric analysis under non-isothermal condition. TGA curve (Fig. 4.8) confirmed that PW decomposed at a lower temperature (192 °C) followed by SW (196 °C) and next AN (203 °C). TG profile (Fig. 4.8) ascertained that biomass underwent into three main stages of degradation: drying (up to 150 °C), devolatilization (200 °C - 500 °C), and char formation (>500 °C). Moreover, the study revealed that PW decomposition started at a lower temperature (206 °C) followed by SW (209 °C) and AN (213 °C). It was also noticed that the removal of water molecules and lower molecular weight compounds occurred up to temperature 150 °C (Fig. 4.8). In the second zone, from temperature 200 °C to 500 °C, maximum decomposition was observed, which appeared due to the decomposition of hemicellulose and cellulose. This zone is known as the active pyrolytic zone. In this zone, higher molecular weight compounds fragmented into smaller molecular weight compounds by the continuous supply of heat. The second stage involved two exothermic simultaneous processes where hemicellulose, cellulose, and lignin decomposed, which resulted in the formation of higher volatiles. In the temperature

range of 200 °C - 500 °C (second stage) conversion of PW was found to be the highest (74.48 %) followed by SW (70.03 %) and finally AN (69.09 %) at 5 °C min^{-1} heating rate. Hemicellulose decomposed at a lower temperature (180 °C - 340 °C) than cellulose (230 °C - 450 °C) and lignin (> 500 °C). According to White et al. (2011) [52] decomposition of cellulose occurred in two ways. First, the bonds split into polymers at a lower temperature (up to 300 °C in this study) and form CO, CO_2, and carbonaceous gases. In the second stage, at higher temperature (240 °C in this study) integration of bonds lead to the formation of liquid. The third stage is known as the endothermic decomposition of lignin, where lignin was decomposed at a higher temperature (>500 °C) and at a slower rate because lignin is associated with the phenolic hydroxyl groups.

DTG thermograph (Fig. 4.8) confirmed that the first peak was observed due to the removal of moisture and light volatile matter when heated up to 150 °C. The second and third peaks appeared due to the decomposition of hemicellulose and cellulose compounds. Finally, at the end, lignin decomposed at a slower rate and yielded maximum char. By comparing DTG thermographs of these three biomass, it was observed that they differ in peak position and height which directly indicated the presence of organic and inorganic components whose distribution affected broadly due to the influence of thermal decomposition.

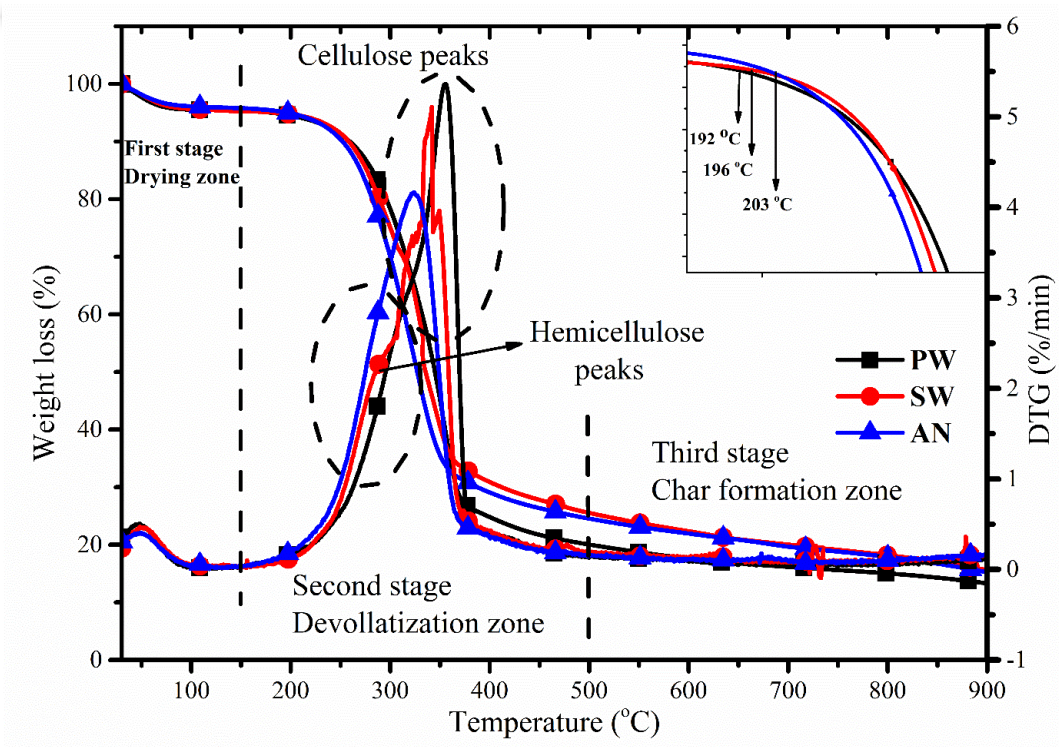

Fig. 4.8. TG profiles of PW, SW and AN at a heating rate of 5 °C min^{-1}

4.2.3. Effect of heating rates on biomass decomposition

Thermal degradation profile of PW, SW, and AN at dynamic heating rates of 5 °C min^{-1} - 25 °C min^{-1} in an inert atmosphere is shown in Fig. 4.9. It can be seen from TGA curve that with an increase in heating rate thermal decomposition shifted towards higher temperature zone without affecting decomposition. One possible reason for alteration in TGA curve could be the fact that biomass is a poor conductor of heat which might have formed a thermal lag (temperature gradient) throughout the cross-section of biomass. At the lower heating rate, the temperature profile along the cross-section of biomass assumed to be linear as the outer surface, and the inner core of the biomass achieve the same temperature at a specific time as enough time is given for heating. On the other hand, at the higher heating rate, the temperature profile has a substantial difference from the inner core to the outer core along the cross-section of biomass [198]. The effect of the heating rate of the secondary reactions of the primary pyrolysis products such as tar and high molecular weight compound may be the other possible reason [199]. A recent study indicated that a lower heating rate provides better heat transfer inside the particle surface [200]. Kim et al. (2013) [201] reported that increasing the heating rate resulted in a maximum rate of decomposition because of the increase in thermal energy. The results of this work demonstrated that the peak temperatures for PW are 353 °C, 370 °C, 375, 382 °C, 386 °C; for SW, these are 341 °C, 356 °C, 360 °C, 370 °C, 374 °C; and for AN, these are 325 °C, 335 °C, 340 °C, 349 °C, 355 °C at heating rates of 5 °C min^{-1}, 10 °C min^{-1}, 15 °C min^{-1}, 20 °C min^{-1}, and 25 °C min^{-1} respectively. Similar studies were also conducted by Chandrasekaran et al. (2017) [58] and Samuelsson et al. (2015) [202]. Chandrasekaran et al. studied *Prosopis juliflora* biomass under non-isothermal condition with dynamic heating rates of 2 °C min^{-1}, 5 °C min^{-1}, 10 °C min^{-1}, 15 °C min^{-1}, 20 °C min^{-1}, and 25 °C min^{-1} and demonstrated that with increase in heating rate, TGA curve shifted to higher temperature zone of 315 °C, 328 °C, 339 °C, 345 °C, 348 °C, and 356 °C, respectively. Samuelsson et al. worked Norway spruce under a non-isothermal condition at dynamic heating rates of 2 °C min^{-1}, 5 °C min^{-1}, 10 °C min^{-1}, 15 °C min^{-1} and 20 °C min^{-1} and concluded that with increasing heating rate, TGA curve shifted to a higher temperature zone of 340 °C, 355 °C, 368 °C, 376 °C, and 381 °C respectively. The present study suggested that when heating rate increases, initial and final temperatures of hemicellulose, cellulose, and lignin also increases. Moreover, an increasing rate of the overall volatile conversion in the active zone (second stage) was found (74.48 %, 74.62 %, 74.70 %, 75.42 %, and 75.70 %) at heating rates of 5 °C min^{-1} - 25 °C min^{-1}. Similar pattern was also found for SW (69.11 %, 69.19 %, 69.71 %, 70.17 %, and 70.35 %) and AN (69.12 %, 69.68

%, 69.95 %, 70.08 %, 70.18 %). From the results, it was confirmed that with increasing the rate of heating, total volatile products increased while at the lower rate of heating, volatiles stay for longer time in reactor due to longer residence time, which favored the formation of secondary reaction such as cracking, re-polymerization and re-condensation which again lead to the formation of char [198]. Biomass has a complex matrix of reaction kinetics which may create resistance at lower heating rates while at higher heating rates, it may overcome this resistance due to the higher heat and mass transfer between the particles, which eventually lead to higher conversion. However, the TGA curve suggested that with sequential increase in heating rate from 5 °C min^{-1} - 25 °C min^{-1}, solid residue also increased sequentially (12.78 %, 13.46 %, 13.68 %, 14.57 %, and 16.51 %, respectively) for the PW at a constant weight for each experiment; a similar pattern was also noticed for SW (15.52 %, 17.21%, 18.71 %, 20.09 %, and 21.99 %, respectively) as well as for AN (15.15 %, 20.24 %, 20.42 %, 20.54 %, and 21.73 %, respectively). At a lower heating rate, heat transfer between biomass particles is higher (complete combustion, due to higher residence time), which results in higher decomposition and lower ash content. At a higher heating rate, combustion occurred partially due to the thermal lag between biomass particles which resulted in the formation of higher char formation.

4.2.4. Differential scanning calorimetric analysis of biomass

In this study, DSC analysis was performed at a heating rate of 10 °C min^{-1} under an inert atmosphere with a flow rate of 50 mL min^{-1} of nitrogen gas (Fig. 4.10). DSC curves indicate the reaction pathway of biomass. DSC analysis provides results on a qualitative and quantitative basis. DSC curve established that the curve went from endothermic to the exothermic region. The first peak appeared (below 100 °C) was due to the evaporation of water molecules, which signified the endothermic process. At temperature zone of 150 °C - 500 °C, the peak was observed due to the degradation of cellulose and hemicellulose compounds. Since DSC has temperature limitation, finding the effect of heat on biomass beyond 500 °C was difficult; however, the TGA analysis confirmed that all biomass went into the endothermic stage.

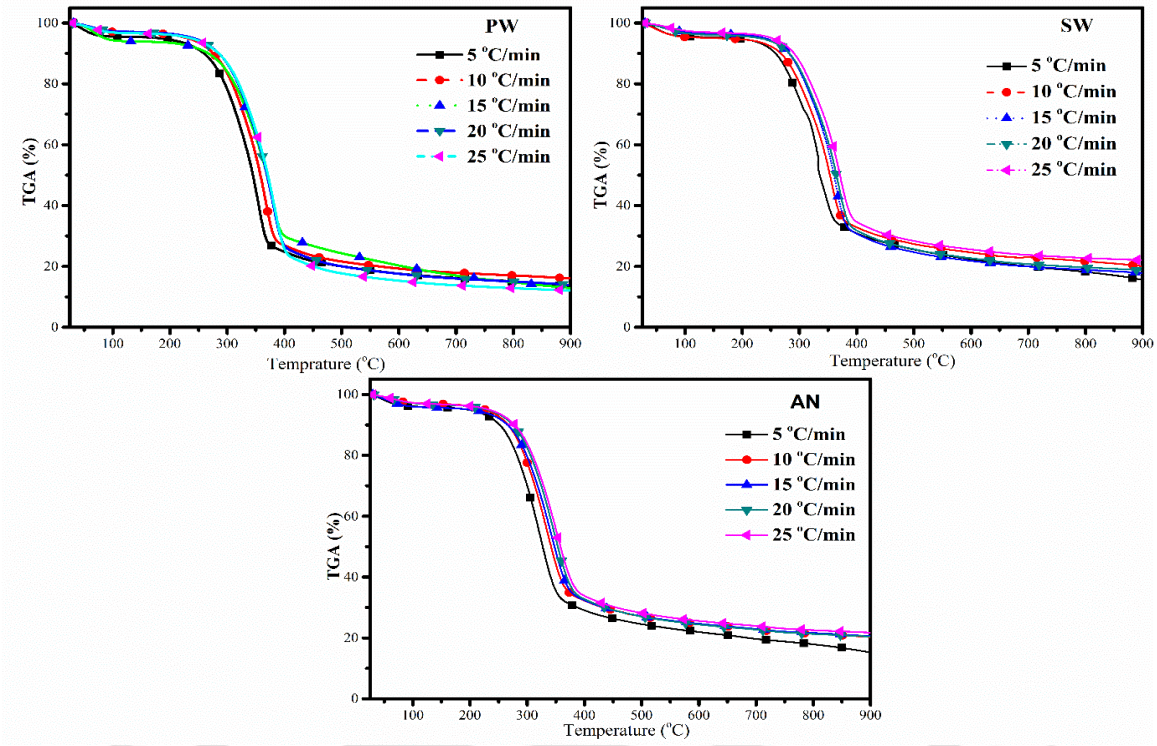

(a)

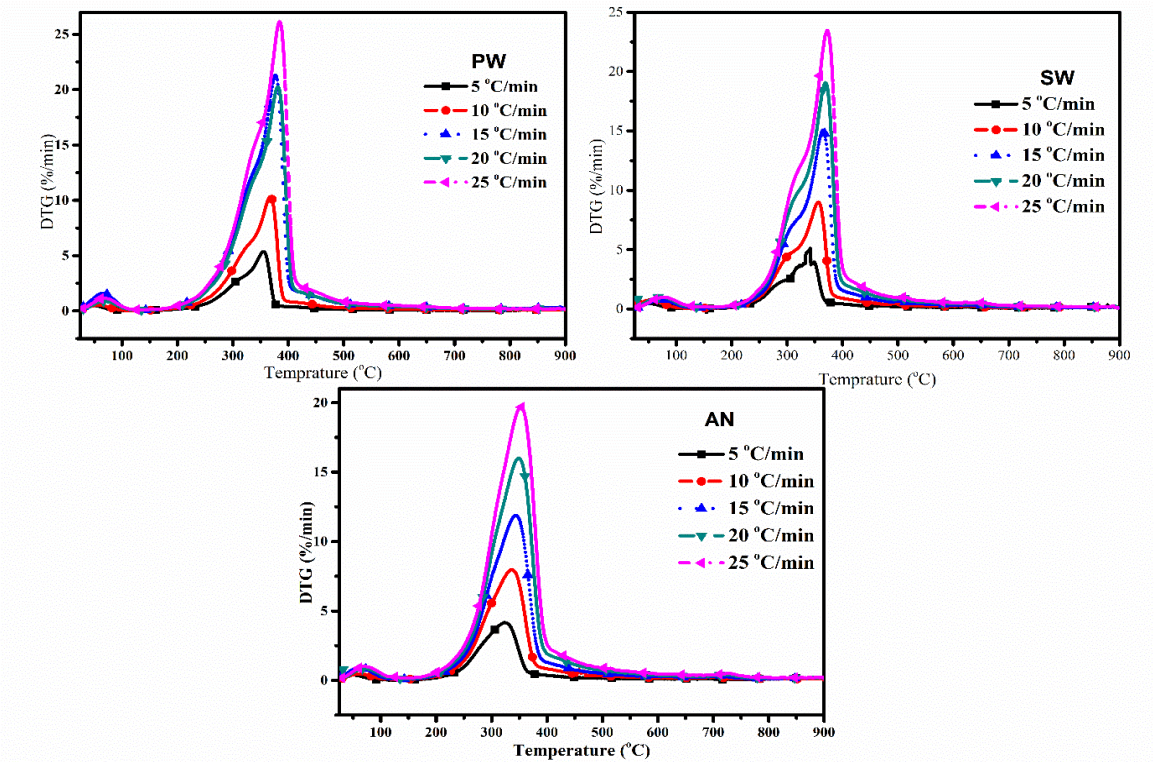

(b)

Fig. 4.9. TG profile of PW, SW and AN (a) TGA and (b) DTG thermograph at different heating rates

4.2.5. Kinetic analysis

Model-free methods (KAS, OFW, FM, CR, and DAEM model) were used for the determination of kinetic parameters such as activation energy, pre-exponential factor, and order of the reaction. During the fitting of data in models, conversion value higher than 0.7 did not fit because of low correlation values [51]. The average values of kinetic energy calculated from KAS, OFW, and Friedman were 171.66 kJ mol^{-1}, 179.29 kJ mol^{-1}, 168.58 kJ mol^{-1}, respectively for PW; 148.44 kJ mol^{-1}, 156.58 kJ mol^{-1}, 181.53 kJ mol^{-1}, respectively for SW; and 171.24 kJ mol^{-1}, 179.47 kJ mol^{-1}, 184.61 kJ mol^{-1}, respectively for AN. The correlation coefficient was higher than 0.9 for each model which signified best-fitted value with experimental data (Tables 4.8 - 4.10). It was also observed that activation energy barely changes with the rate of conversion (Tables 4.8 - 4.10), indicating a high degree of probability of a single step reaction [203].

The activation energy calculated from the Friedman method was slightly higher than the other two methods. Friedman method is an efficient way to calculate activation energy [53, 204] as it is related to the simple differential form of kinetic rate law which is only applicable for integral data (TGA) and comprises of no oversimplified approximation. This is one of the drawbacks of this model. The conversion and temperature curves yield noisy rate data which results in very scattered data of activation energy. The average activation energy calculated from the Friedman model for PW was slightly lower than that obtained from KAS and OFW model. The data obtained from the TGA experiment was used for model fitting. The curve fitting with KAS, OFW, and Friedman models are presented in Fig. 4.11 - 4.13. It was observed that conversion value higher than 0.7 was not suitable for model fitting due to the lower correlation coefficient. The variation in activation energy values calculated from the KAS, OFW, and Friedman models were: 162.27 kJ mol^{-1} - 158.82 kJ mol^{-1}, 114.30 kJ mol^{-1} - 144.34 kJ mol^{-1}, and 162.02 kJ mol^{-1} - 156.28 kJ mol^{-1} for PW, 171.35 kJ mol^{-1} - 166.28 kJ mol^{-1}, 115.46 kJ mol^{-1} - 154.06 kJ mol^{-1}, 171.48 kJ mol^{-1} - 161.10 kJ mol^{-1}, for SW; and 145.89 kJ mol^{-1} - 167.86 kJ mol^{-1}, 146.65 kJ mol^{-1} - 174.78 kJ mol^{-1} and 172.84 kJ mol^{-1} - 178.85 kJ mol^{-1}, for AN with conversion value of 0.1 - 0.7. Activation energy is dependent on the pyrolysis reaction mechanism Higher value of activation energy indicates a slower reaction. Gai et al. (2013) [205] reported that reactivity of fuel could be calculated from the activation energy. The reactivity of fuel plays an essential role in pyrolysis and gasification. It provides exposure to optimize process parameters, and design and development of new pyrolyzer.

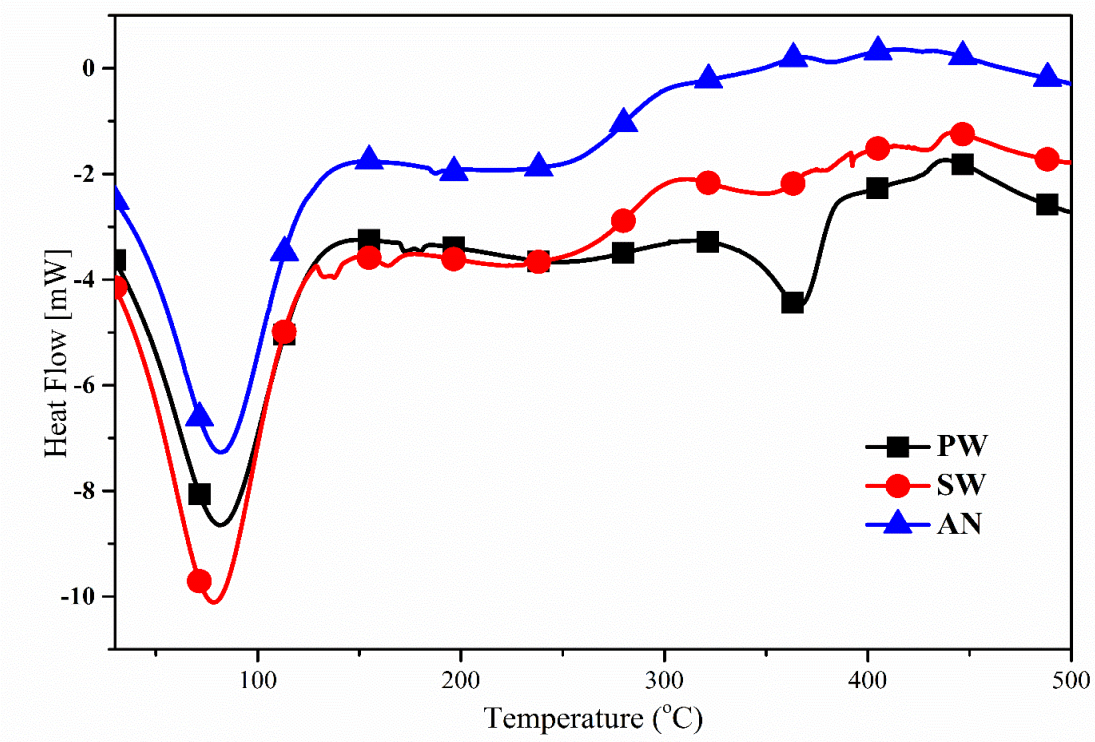

Fig. 4.10. DSC analysis of *PW, SW* and *AN* biomass at a heating rate of 10 °C min^{-1}

The Coats-Redfern model works on a single heating rate. This model has been used widely to determine the order of reaction during pyrolysis. In the present study, Coats-Redfern model was used at a heating rate of 10 °C min^{-1}. It is important to mention that orders of reaction and pre-exponential factor calculated from the iso-conversional methods have no physical significance; it is only considered as fitting parameters [51]. This model was used widely to determine the order of reaction during pyrolysis. The order of reaction was calculated by the CR method using trial and error method by putting the various values of the order of reaction (*n*) such as n = 0.1, 0.2, 0.3, 0.4.....∞. The best-fitted value of the order of reaction was calculated as *n* = 0.2 for the PW, *n* = 0.1 for SW, and *n* = 0.1 for AN, which also corroborated the present experimental data. The activation energy values were found to be 64.13 kJ mol^{-1}, 57.97 kJ mol^{-1}, and 63.41 kJ mol^{-1} for PW, SW, and AN, respectively, whereas the frequency factors were found to be 1.61E+3 min^{-1}, 4.11E+3 min^{-1}, and 1.26E+3 min^{-1} for PW, SW, and AN, respectively, at *n* = 1. On the other hand, at $n \neq 1$, the activation energy values were found to be 50.19 kJ mol^{-1}, 43.89 kJ mol^{-1}, and 52.90 kJ mol^{-1} for PW, SW and AN, respectively while the frequency factors were found to be 2.608 E+3 min^{-1}, 7.10 E+3 min^{-1} and 1.797 E+3 min^{-1} for PW, SW, and AN, respectively. The correlation coefficient was greater than 0.99 which showed the best fitting.

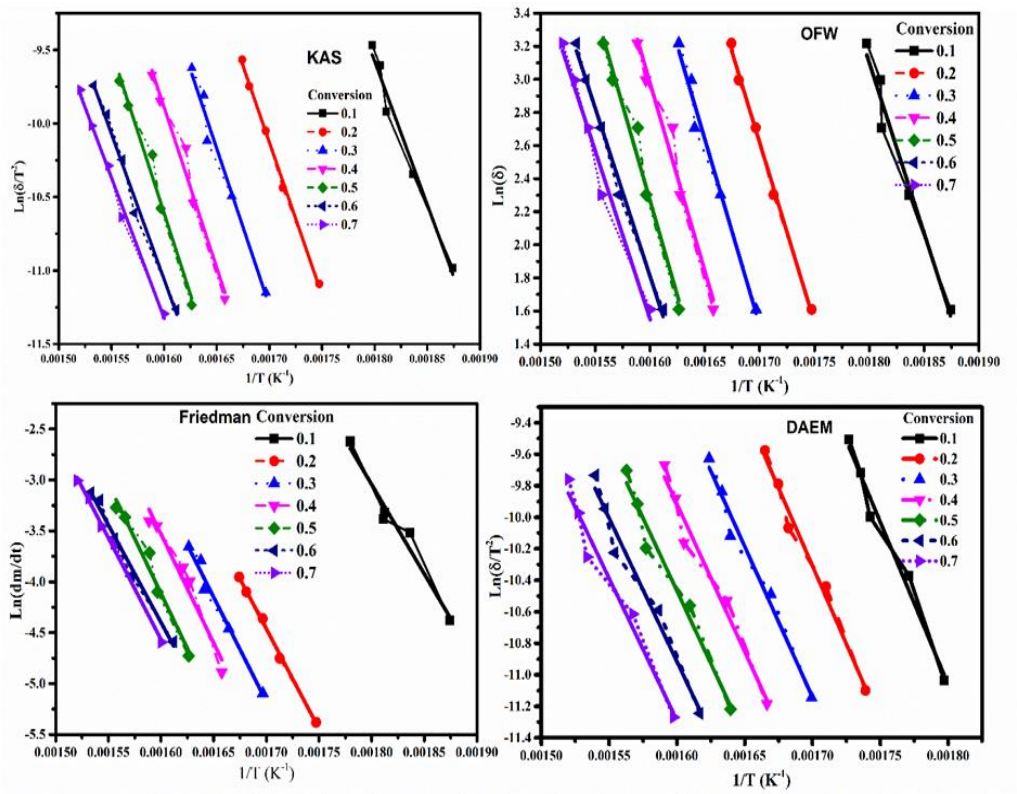

Fig. 4.11. Kinetic plots of KAS, FWO, Friedman and DAEM models of PW

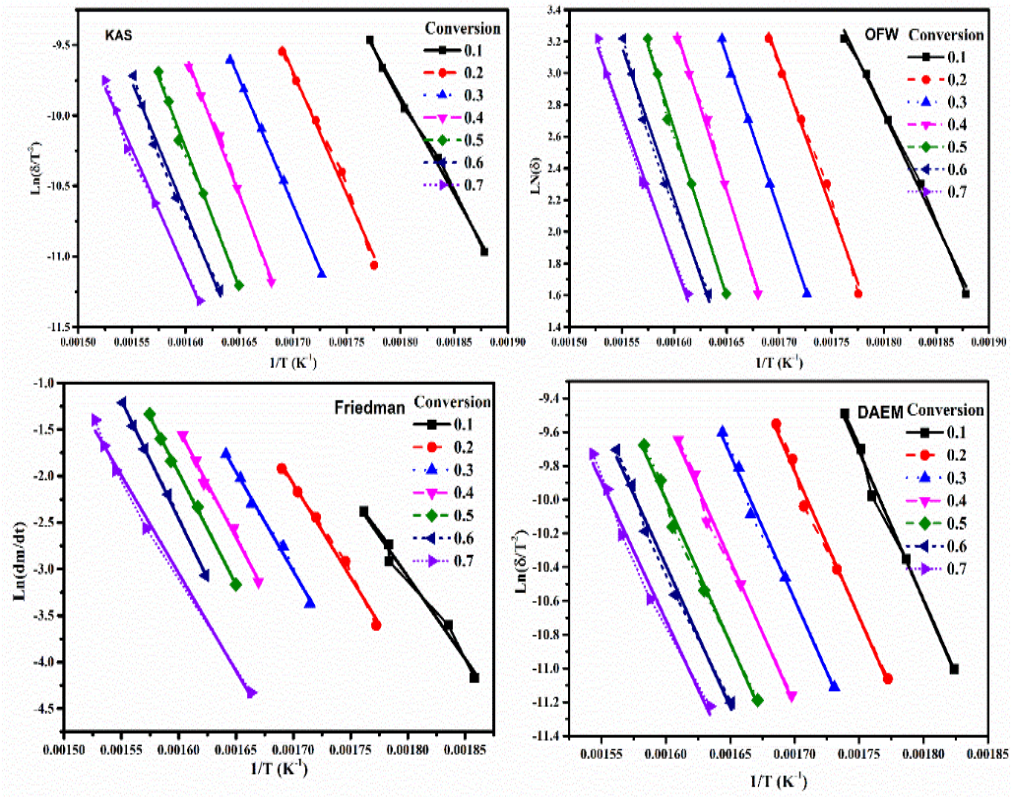

Fig. 4.12. Kinetic plots of KAS, FWO, Friedman and DAEM models of SW

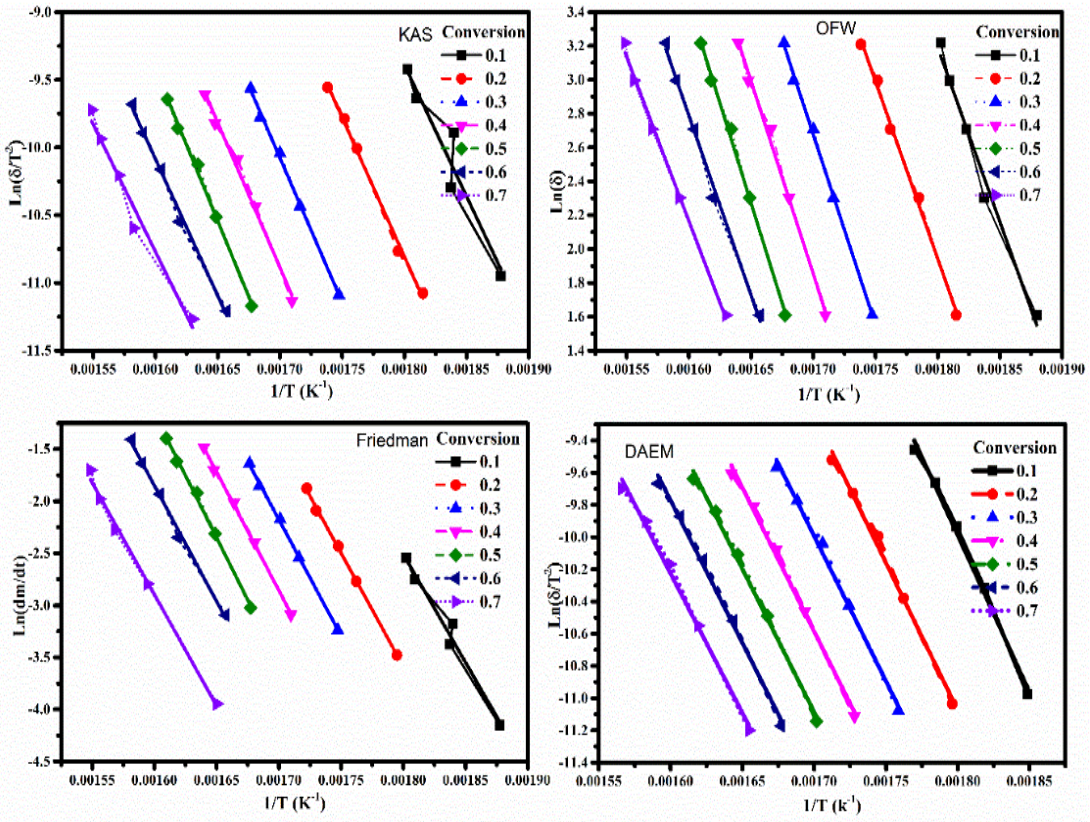

Fig. 4.13. Kinetic plots of KAS, FWO, Friedman and DAEM models of AN

Activation energy is directly proportional to the rate of heating. The pyrolysis process is a continuous procedure which implies that with an increase in temperature, volatilization increases by means of heat transfer between biomass particles. Conversion is a function of temperature which means with an increase in temperature conversion values increase. However, in case of the rate of conversion, with an increase in temperature the rate of conversion increases. Once it reaches the maximum point (0.0023 min^{-1}), it started to decrease. A similar trend was observed in temperatures versus DTG curve. The conversion value, rate of conversion, and DTG thermograph with respect to temperature at a heating rate of 10 °C min^{-1} for PW is shown in Fig. 4.14.

Table 4.8. Kinetic parameters obtained from a model-free method with the fitted equation for *PW* biomass

x	KAS			OFW			Friedman		
	Equation	R^2	*E*, (kJ/mol)	Equation	R^2	*E*, (kJ/mol)	Equation	R^2	*E*, (kJ/mol)
0.1	y = -19518x + 25.555	0.9803	162.27	y = -20610x + 40.198	0.9717	171.35	y = -17548x + 28.541	0.964	145.89
0.2	y = -20771x + 25.181	0.9975	172.69	y = -21728x + 39.555	0.9967	180.64	y = -19628x + 28.905	0.9977	163.18
0.3	y = -21421x + 25.174	0.9973	178.09	y = -22505x + 39.772	0.9821	187.10	y = -20520x + 29.707	0.9805	170.60
0.4	y = -21816x + 25.016	0.9744	181.37	y = -22754x + 39.385	0.9677	189.17	y = -21383x + 30.679	0.961	177.77
0.5	y = -22107x + 24.762	0.9799	183.79	y = -23029x + 39.115	0.9731	191.46	y = -21586x + 30.422	0.9734	179.46
0.6	y = -19799x + 20.618	0.9892	164.60	y = -20336x + 34.349	0.9935	169.07	y = -21086x + 28.449	0.9796	175.30
0.7	y = -19103x + 19.242	0.993	158.82	y = -2000x + 34.095	0.981	166.28	y = -20191x + 26.298	0.9968	167.86

Table 4.9. Kinetic parameters obtained from the model-free method with the fitted equation for *SW* biomass

x	KAS			OFW			Friedman		
	Equation	R^2	*E*, (kJ/mol)	Equation	R^2	*E*, (kJ/mol)	Equation	R^2	*E*, (kJ/mol)
0.1	y = -13748x + 14.876	0.961	114.3	y = -13888x + 27.738	0.9948	115.46	y = -17639x + 28.668	0.9842	146.65
0.2	y = -17354x + 19.81	0.9914	144.28	y = -18484x + 34.488	0.9923	153.67	y = -20094x + 32.076	0.992	167.06
0.3	y = -17884x + 19.767	0.9877	148.68	y = -19571x + 35.4	0.9992	162.71	y = -21352x + 33.278	0.9932	177.52
0.4	y = -19889x + 22.256	0.9961	166.18	y = -20956x + 36.836	0.9958	174.22	y = -23243x + 35.69	0.9946	193.24
0.5	y = -20212x + 22.15	0.994	168.04	y = -21100x + 36.405	0.9951	175.42	y = -24035x + 36.49	0.9987	199.82
0.6	y = -18441x + 18.82	0.9893	153.31	y = -19311x + 33.102	0.9886	160.55	y = -25460x + 38.275	0.999	211.67
0.7	y = -17361x + 16.672	0.9927	144.34	y = -18531x + 31.457	0.9934	154.06	y = -21023x + 30.594	0.9944	174.78

Table 4.10. Kinetic parameters obtained from a model-free method with the fitted equation for *AN* biomass

x	KAS			OFW			Friedman		
	Equation	R^2	*E*, (kJ/mol)	Equation	R^2	*E*, (kJ/mol)	Equation	R^2	*E*, (kJ/mol)
0.1	y = -19488x + 25.691	0.9805	162.02	y = -20626x + 40.318	0.9854	171.48	y = -20790x + 34.913	0.9773	172.84
0.2	y = -20556x + 26.193	0.9961	170.90	y = -20949x + 39.651	0.9962	174.16	y = -21823x + 35.711	0.993	181.53
0.3	y = -21318x + 26.163	0.9923	177.33	y = -22498x + 40.936	0.9931	187.04	y = -22371x + 35.864	0.9962	185.99
0.4	y = -21419x + 25.526	0.9922	178.07	y = -22779x + 40.578	0.9942	189.38	y = -22770x + 35.859	0.9961	189.30
0.5	y = -22412x + 26.436	0.996	186.33	y = -23629x + 41.259	0.9965	196.45	y = -23876x + 37.043	0.9971	198.50
0.6	y = -20181x + 22.202	0.9825	167.78	y = -21256x + 36.799	0.9941	176.72	y = -22275x + 33.789	0.9956	185.19
0.7	y = -18798x + 19.305	0.9762	156.28	y = -19377x + 33.169	0.9965	161.10	y = -21524x + 31.499	0.9986	178.95

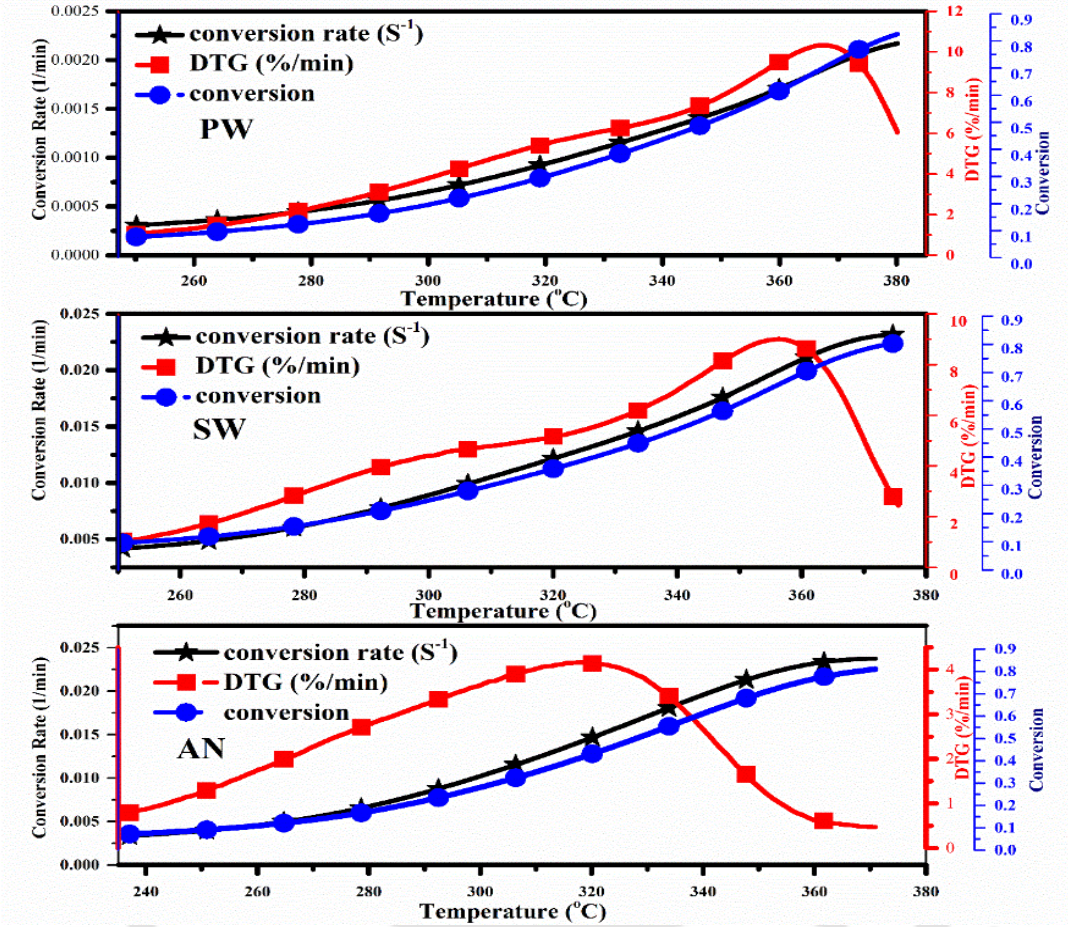

Fig. 4.14. Conversion, rate of conversion, and DTG thermograph with respect of temperature at a heating rate 10 ^{o}C min^{-1} of PW, SW and AN biomass

4.2.6. Kinetic parameter by using DAEM model

DAEM model showed that plots are nonlinear and showing different behavior (Fig. 4.11 - 4.13). The different chemical reactions taking place simultaneously could be one of the probable reasons for this phenomenon. The correlation coefficient (R^2) varied between 0.97 and 0.99 (greater than 0.90) with a conversion value range of 0.1 - 0.7, which implied the best model fitted value. The activation energy calculated from the DEAM model varied from 165.42 kJ mol^{-1} to 200.20 kJ mol^{-1} for PW, 146.44 kJ mol^{-1} to 157.01 kJ mol^{-1} for SW, and 144.73 kJ mol^{-1} to 143.52 kJ mol^{-1} for AN biomass. The activation energy varies with each conversion value throughout pyrolysis. The frequency factor varies from 1.13E+12 min^{-1} to 1.02E+13 min^{-1} for PW, 2.56E+10 min^{-1} to 5.02 E+9 min^{-1} for SW, and 3.323E+10 min^{-1} to 6.15E+9 min^{-1} for AN. The complete kinetic analysis of all biomass obtained from DAEM model is shown in Table 4.11. The kinetic results confirmed that activation energy is dependent on conversion value which indicated that these biomass (PW, SW, AN) conversion were a very intricate

process and related different types of reactions. The variation of activation energy versus conversion value is presented in Fig. 4.15. A comparison table of calculated kinetic parameters is shown with other reported studies [51, 53, 58, 63, 170, 206-208] and summarized in Table 4.12. The calculated activation energy values from iso-conversional models from the present study for all biomass were very similar to other reported biomass. However, kinetic energy is the function of temperature, and each biomass composition has its own degradation temperature; and the composition of biomass depends on soil condition where it is grown. This may be the reason for the slight variation of activation energies of biomass. Furthermore, activation energy depends on fuels, mathematical calculation, and experimental conditions. KAS, OFW, and DAEM models are conversional dependent models, but Friedman model is independent of mathematical assumption; hence, results contained a minimal error. The iso-conversional model or model-free methods predict comparably accurate kinetic data compared with model fitting techniques.

4.2.7. Thermodynamic analysis

Thermodynamic properties such as pre-exponential factor (A), enthalpy (ΔH), Gibbs energy (ΔG) and entropy (ΔS) of PW, SW and AN were calculated and presented in Table 4.13. All thermodynamic calculations were based on activation energy obtained from the Friedman model because it produced a minimum error and had more accuracy than others. The variations in frequency factor were apparently due to conversion rate and structural integrity of biomass. Variation in the pre-exponential factor confirmed that the presence of complex structural composition and existence of very composite reactions during thermal conversion such as pyrolysis and gasification [209].

From Table 4.13, it was confirmed that as conversion value increased the value of enthalpy changed (increased) with all models for all biomass. This type of alteration confirmed that as conversion value increased, a higher amount of energy was required to decompose the biomass. Further, change in enthalpy can be an indicator to understand the pyrolysis and co-pyrolysis behavior of materials. A positive value of enthalpy indicated endothermic decomposition which means energy will be needed for the decomposition of biomass during pyrolysis or combustion. Moreover, DSC analysis (Fig. 4.10) of biomass also confirmed that the nature of the reaction process was endothermic. Change in enthalpy was apparently due to variation in activation energy which is a function of the conversion value. Yuan et al. (2017)

[210] studied cattle manure, and Ahmad et al. (2017) [211] studied *Urochloa mutica* biomass and reported that calculated enthalpy value was very similar to the reported enthalpy.

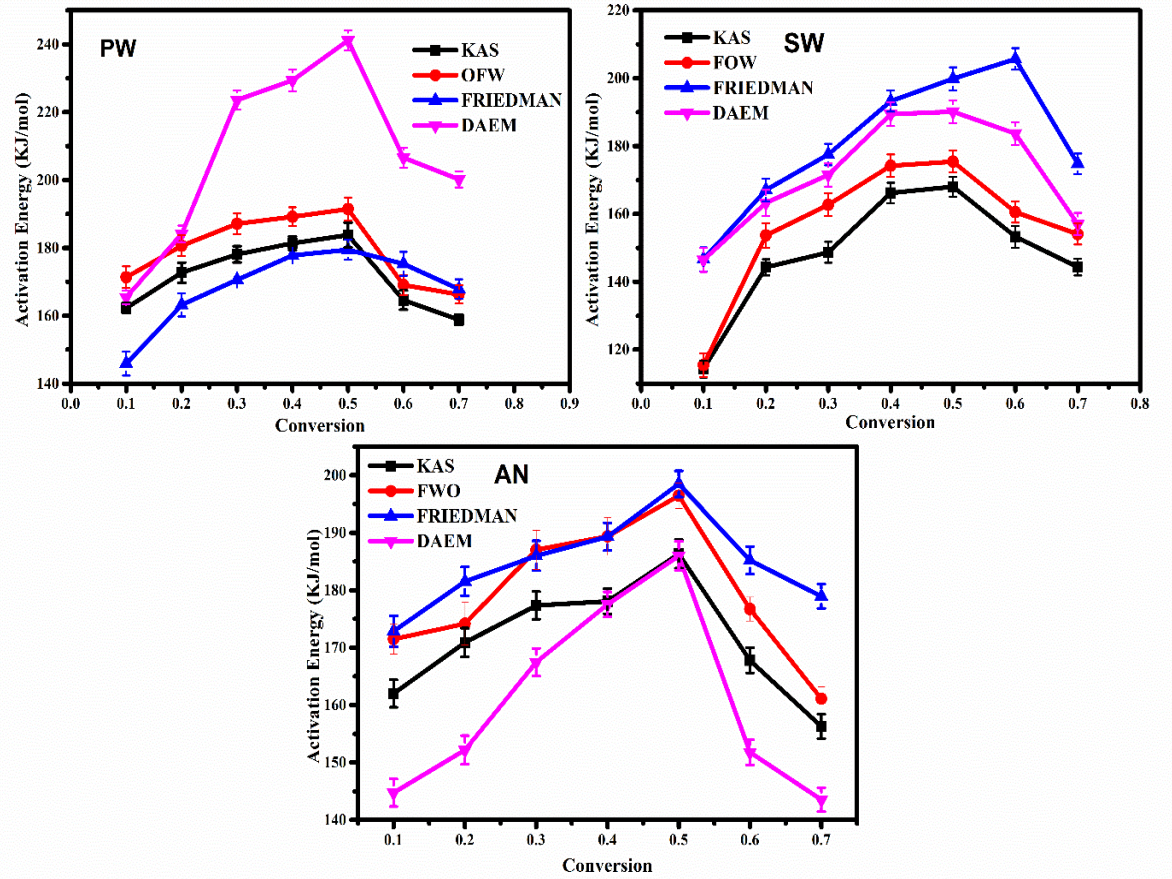

Fig. 4.15. Variation of activation energy with respect to the conversion of PW, SW and AN.

Further, change in Gibbs energy (ΔG) with respect to conversion value was calculated as an average value of Gibbs energy presented in Table 4.13. Studies from Yuan et al. (2017) on cattle manure, [210], and Ahmad et al. (2017), on *Urochloa mutica* biomass reported the variation of Gibbes free energy (161.54 kJ mol^{-1} - 166.24 kJ mol^{-1}, 170 kJ mol^{-1} - 171 kJ mol^{-1}, and 173 kJ mol^{-1} - 177 kJ mol^{-1} respectively). However, the Gibbs free energy of biomass PW, SW and AN have similar values for all the models. This signified that biomass PW, SW and AN have high degree and spontaneity of reactions.

From entropy results, it was confirmed that as conversion value increased (pyrolysis temperature increased) value of entropy increased for all biomass for all models, which indicated that reactivity of system, increased (less residence time). The calculated entropy values were similar in comparison to other reported biomass such as *Urochloa mutica,* and *Urochloa mutica,* [210, 212].

Table 4.11. Kinetic parameters obtained from the distributed activation model (DAEM) for PW, SW, and AN biomass

Conversion	PW			SW			AN		
	E (kJ/mol)	*A* (1/min)	R^2	*E* (kJ/mol)	*A* (1/min)	R^2	*E* (kJ/mol)	*A* (1/min)	R^2
0.1	165.42	1.12696E+12	0.9756	146.44	2.56722E+10	0.9922	144.73	3.32369E+10	0.9984
0.2	184.10	1.24153E+13	0.9597	163.26	3.31669E+11	0.9926	152.18	5.76192E+10	0.9946
0.3	223.57	1.63301E+16	0.9826	171.51	7.99059E+11	0.9787	167.48	6.64914E+11	0.9866
0.4	225.35	8.8546E+15	0.9815	189.39	1.27413E+13	0.997	177.52	2.85800E+12	0.9925
0.5	241.16	8.46685E+16	0.9965	190.13	7.83614E+12	0.9926	185.98	8.47124E+12	0.9912
0.6	206.58	5.69245E+13	0.9871	183.68	1.31552E+12	0.998	151.78	5.05928E+09	0.9923
0.7	200.20	1.01793E+13	0.9720	157.01	5.02840E+9	0.9984	143.52	6.15862+08	0.9945

Table 4.12. Comparison of average values of activation energy of different types of biomass using iso-conversional and model fitting methods

Biomass	Heating rate (°C min^{-1})	Average activation energy (kJ/mol)						References
		KAS	OFW	Friedman	DAEM	CR	CR	
PW	5-25	171.66	179.29	168.58	206.62	50.19	64.13	Present study
SW	5-25	148.44	156.58	181.53	171.63	43.89	57.97	Present study
AN	5-25	171.24	179.47	184.61	160.45	52.90	63.41	Present study
Prosopis juliflora	2, 5-25	281.00	282.00	275.00	283.00	-	-	[58]
Poplar wood	2, 5-15	157.30	158.60	-	-	-	-	[207]
Phlomis bovei	5-15	134.10	134.80	-	-			[208]
Huzelnut husk	5, 10, 20	127.80	131.10	-	-	-	-	[63]
Lignite coal	1, 6, 9, 12, 15, 18	282.00	275.00	283.00	-	-	-	[53]
Cardoon stems	5, 10, 20, 30	229.50	241.50	-	-	-	-	[51]
Cardoon leaves	5, 10, 20, 30	350.17	342.07	-	-	-	-	[51]

Nannochloropsis oculata	5, 10, 20	-	-	-	152.20	-	-	[170]
Tetraselmis sp.	5, 10, 20	-	-	-	334.00	-	-	[170]
Rice husks	5-20	-	169.00	182.20	-	-	-	[206]
Olive cake	5-20	-	141.6	150.0	-	-	-	[206]
Cacao shells	5-20	-	145.6	133.7	-	-	-	[206]
Rice husks	20-100	-	110.7	118.2	-	-	-	[206]
Olive cake	20-100	-	103.2	106.5	-	-	-	[206]
Cacao shells	20-100	-	117.8	119.3	-	-		[206]

Table 4.13. Thermodynamic parameters of PW, SW and AN sawdust using Friedman model

Biomass	Conversion	*A* (1/s)	*ΔH* (kJ/mol)	*ΔG* (kJ/mol)	*ΔS* (J/mol)
	0.1	1.05E+7	140.67	219.04	-124.96
	0.2	3.24E+8	157.96	218.46	-96.46
PW	0.3	1.40E+9	165.38	218.23	-84.26
	0.4	5.80E+9	172.55	218.01	-72.49
	0.5	8.10E+9	174.24	217.96	-69.71
	0.6	3.56E+9	170.08	218.09	-76.54
	0.7	8.19E+8	162.64	218.31	-88.76
Average		2.86E+9	163.36	218.30	-87.60
	0.1	2.31E+7	141.54	214.16	-118.23
	0.2	1.43E+9	161.95	213.49	-83.92
SW	0.3	1.18E+10	172.41	213.18	-66.38
	0.4	2.80294E+11	188.13	212.75	-40.08
	0.5	1.05152E+12	194.71	212.58	-29.09
	0.6	1.13433E+13	206.56	212.28	-9.31
	0.7	6821721325	169.67	213.26	-70.97
Average		1.81361E+12	176.42	213.10	-59.71
	0.1	1.20000E+10	167.86	207.37	-66.04
	0.2	7.25000E+10	176.55	207.12	-51.10
AN	0.3	1.82155E+11	181.01	207.00	-43.44
	0.4	3.60716E+11	184.32	206.91	-37.76
	0.5	2.40554E+12	193.52	206.68	-21.99
	0.6	1.54421E+11	180.21	207.02	-44.82
	0.7	4.25000E+10	173.97	207.19	-55.53
Average		4.61417E+11	179.64	207.04	-45.81

Chapter 5

Thermal and Catalytic Pyrolysis of Biomass

5.1. Thermal Pyrolysis of Selected Biomass

Thermal pyrolysis of PW, SW, AN, SG, CK, SK, NM, MH, and SS was carried out in a semi-batch reactor under an inert atmosphere at optimized conditions. These biomass are abundantly available across the world and have enough potential to produce liquid fuel. Further, pyrolytic oil obtained was characterized using different techniques such as FTIR, and GC-MS analysis.

5.1.1. Optimization of process parameters

Pyrolysis is a process parameter dependent method in which operating parameters such as temperature, heating rate, particle size, sweeping gas flow rate, types of reactor, feed types and its compositions, etc. affect the product yield and quality. Among all process parameters, temperature, heating rate, and particle size have a substantial effect on pyrolytic end products. Therefore, optimization of temperature, heating rate, and particle size become essential to achieve maximum product yield.

In order to optimize the effect of temperature on pyrolytic products yield, 400 °C, 450 °C, 500 °C, 550 °C, and 600 °C were chosen. Thermal pyrolysis confirmed that raising the temperature from 400 °C to 500 °C, liquid and gaseous yields increased, while the char yield was reduced as shown in Fig. 5.1 - 5.8. Further, increasing the temperature from 500 °C to 600 °C, liquid and char yield reduced, while the gaseous product yield increased. At lower temperature (400 °C - 450 °C), partial combustion occurred due to lower heat and mass transfer between particles, which lead to a reduction in liquid yield and an increase in char yield. However, at 500 °C, the maximum liquid yield was achieved (40.45 wt.% for PW, 34.37 wt.% for SW, and 33.75 wt.% for AN, 33.85 wt.% for SG, 64.23 wt.% for SK, 45.22 wt.% for CK, 49.53 wt.% for NM, 51.20 wt.% for MH and 44.20 wt.% for SS) due to complete pyrolysis of biomass (higher heat and mass transfer between particles). Further increase in temperature beyond 500 ^{o}C resulted in rapid endothermic decomposition, which subsequently leads to the formation of gaseous compounds by rapid fractionation of biomass. The results are consistent with previous studies as reported by Wang et al. (2010) [213] and Wang and Brown (2013) [214].

Further, in order to optimize the effect of heating rate on pyrolytic products yield, 50 ^{o}C min^{-1}, 80 ^{o}C min^{-1}, 100 ^{o}C min$^{-1,}$ and 120 ^{o}C min^{-1} were selected. Results revealed that at 80 ^{o}C min^{-1} heating rate, maximum liquid yield was achieved (40.45 wt.% for PW, 34.37 wt.% for SW, and 33.75 wt.% for AN, 33.85 wt.% for SG, 64.23 wt.% for SK, 45.22 wt.% for CK, 49.53 wt.% for NM, 51.20 wt.% for MH and 44.20 wt.% for SS) due to complete pyrolysis of biomass. At a lower heating rate of 50 ^{o}C min^{-1}, the liquid yield was reduced due to incomplete pyrolysis of biomass. However, at higher heating rates 100 ^{o}C min$^{-1,}$ and 120 ^{o}C min^{-1}, both the liquid yield and char yield were reduced while gas yield increased due to rapid fragmentation of biomass which resulted in the formation of more non-condensable gases. The results demonstrated good consistency with previous studies [213, 214].

In order to optimize the effect of particle size on pyrolytic products yield, 0.5 mm, 1 mm, 1.5 mm and 2 mm particle sizes were chosen. It is important to mention that optimization of the particle size of biomass MH and SK was not possible because they become semisolid (not separable) after grinding. Results confirmed that biomass with a smaller particle size (0.5 mm) produced maximum liquid yield (40.45 wt.% for PW, 34.37 wt.% for SW, and 33.75 wt.% for AN, 33.85 wt.% for SG, 64.23 wt.% for SK, 45.22 wt.% for CK, 49.53 wt.% for NM, 51.20 wt.% for MH and 44.20 wt. % for SS), possibly due to higher heat and mass transfer between the particles (Fig. 5.1 - 5.8). A further increase in particle size from 1 mm - 2 mm resulted in a reduction of liquid and gas yields, however with an increase in char yield due to lower heat transfer between biomass particles.

The sweeping gas flow rate was kept constant (100 mL min^{-1}) because literature confirmed that lower flow rate (<100 mL min^{-1}) does not influence liquid yield much [33], whereas an increase in the flow rate of sweeping gas leads to a reduction in liquid yield. Based on the results, 500 °C temperature, 0.5 mm particle size, 80 °C min^{-1} heating rate, and 100 mL min^{-1} sweeping gas flow rate were selected as optimum pyrolysis conditions. Furthermore, Table 5.1 showed the pyrolytic products yield at the optimized condition for all biomass.

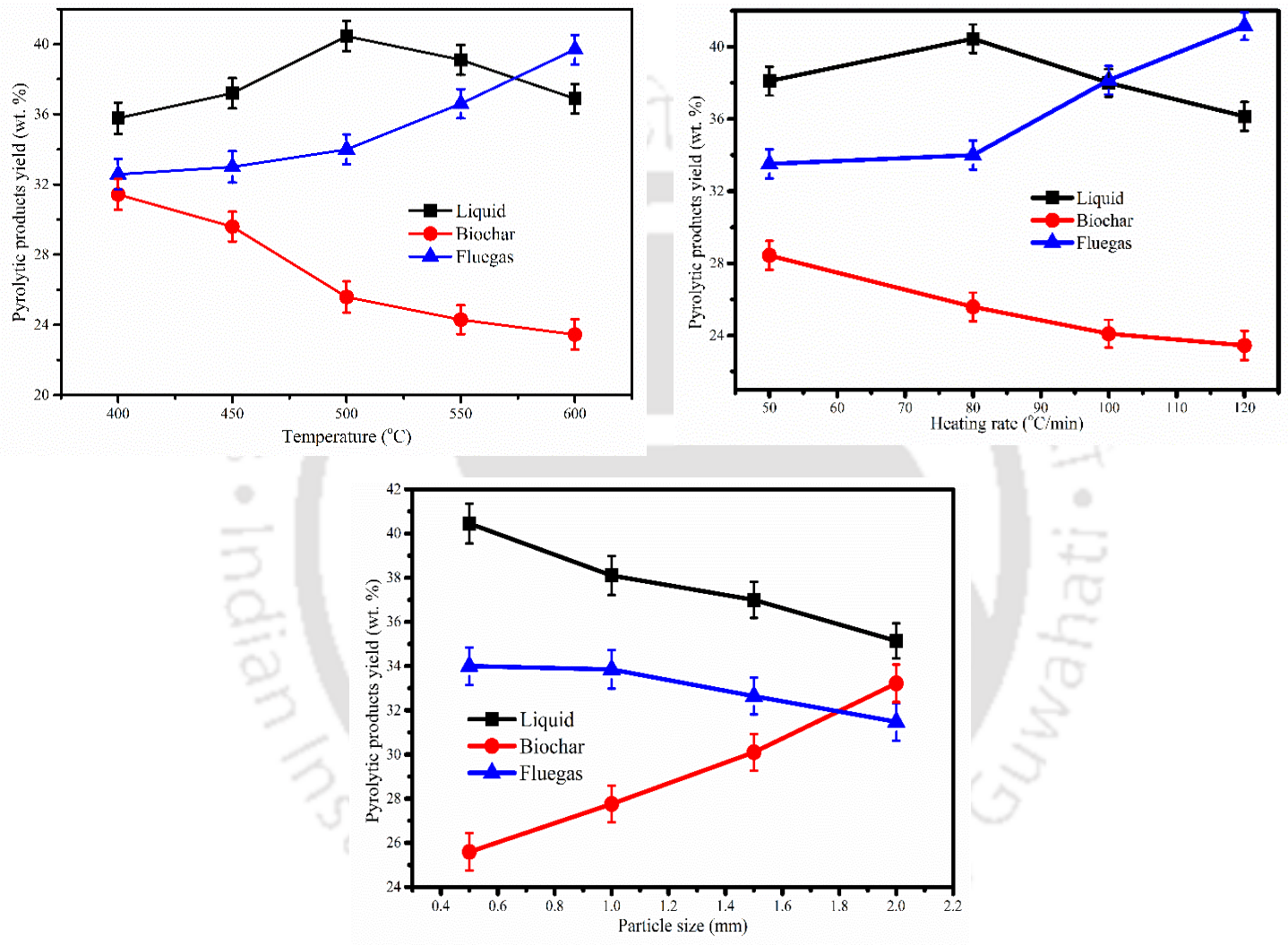

Fig. 5.1. Optimization of temperature, heating rates and particle size of PW biomass

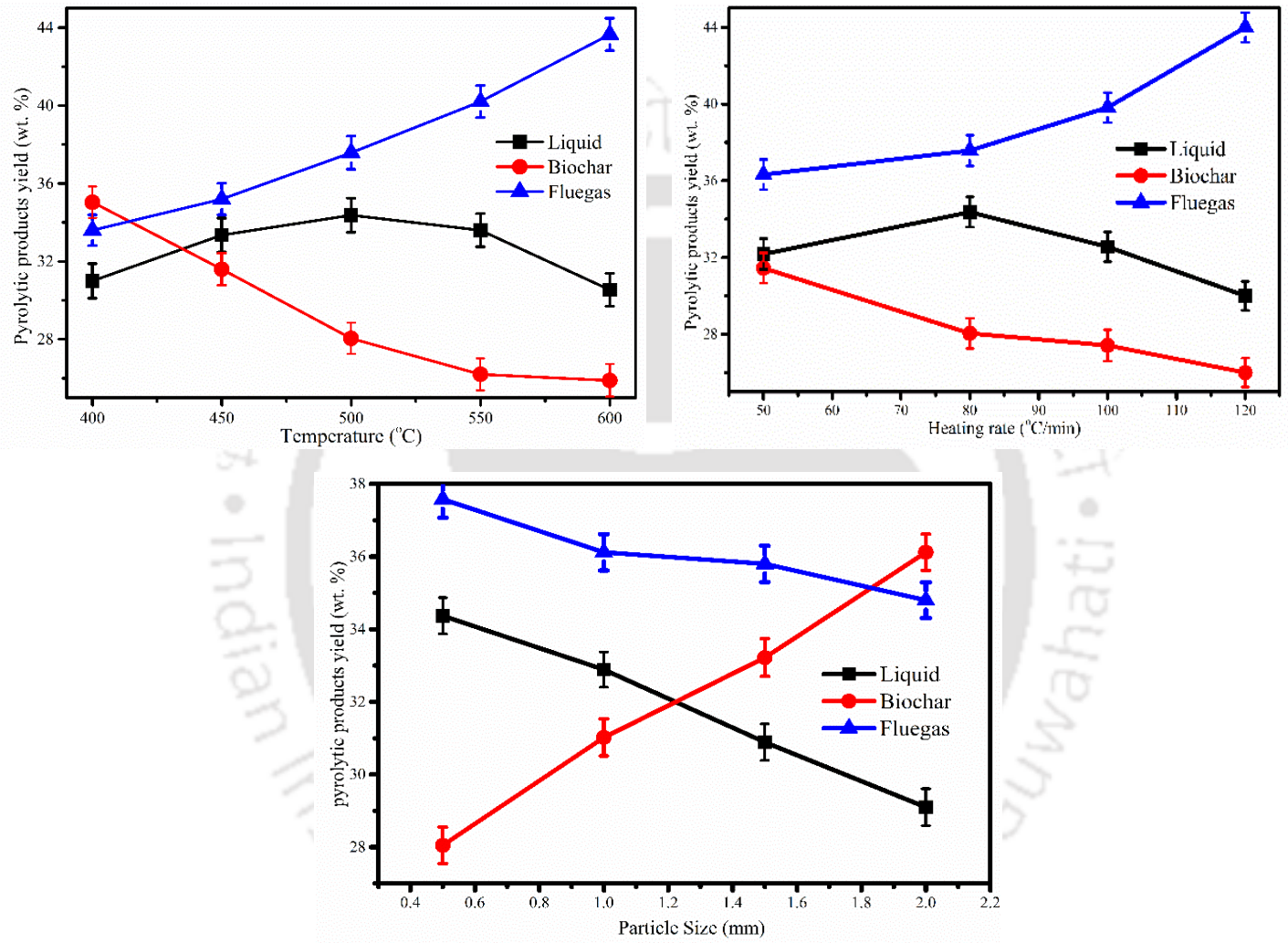

Fig. 5.2. Optimization of temperature, heating rates and particle size of SW biomass

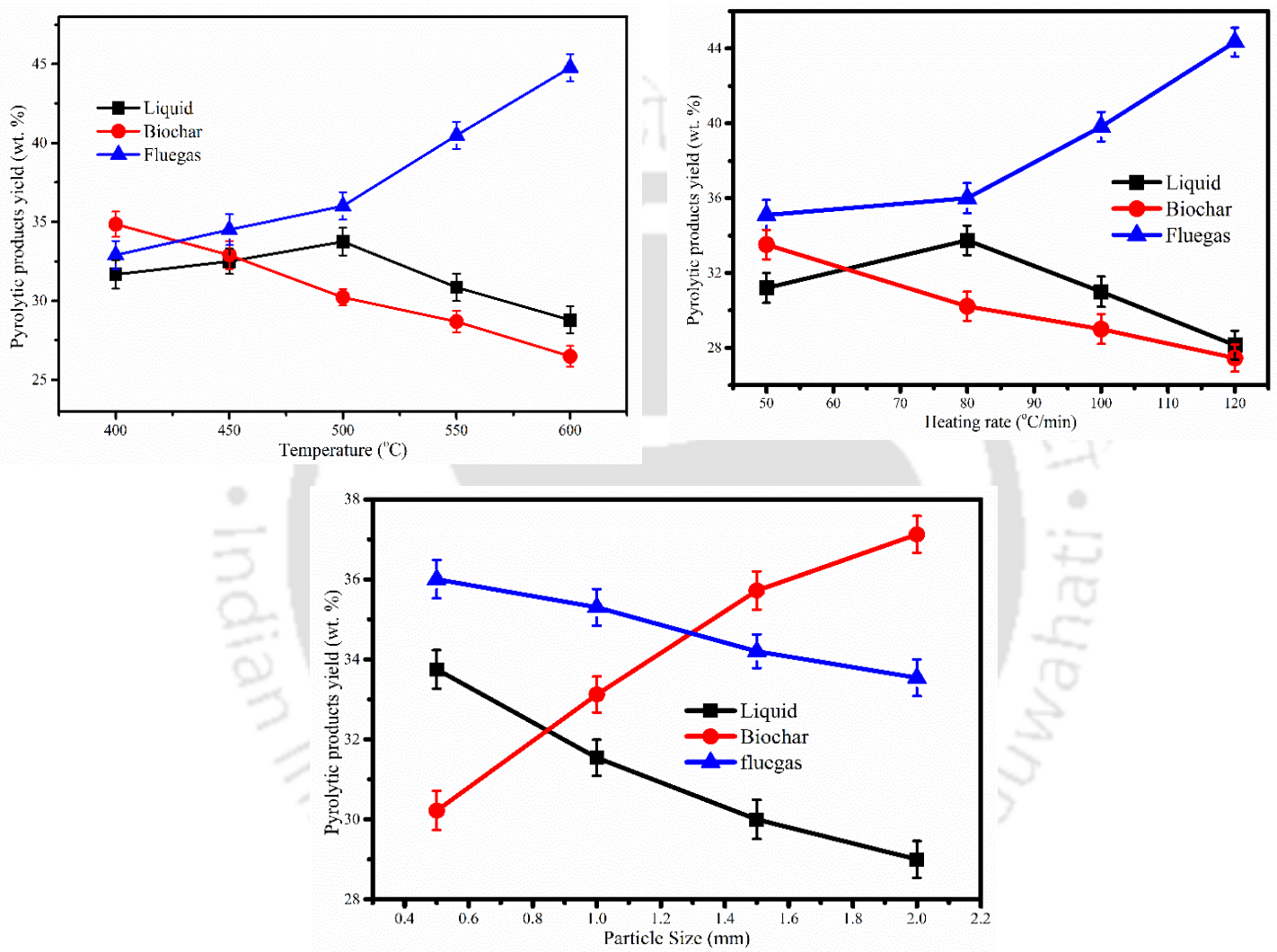

Fig. 5.3. Optimization of temperature, heating rates and particle size of AN biomass

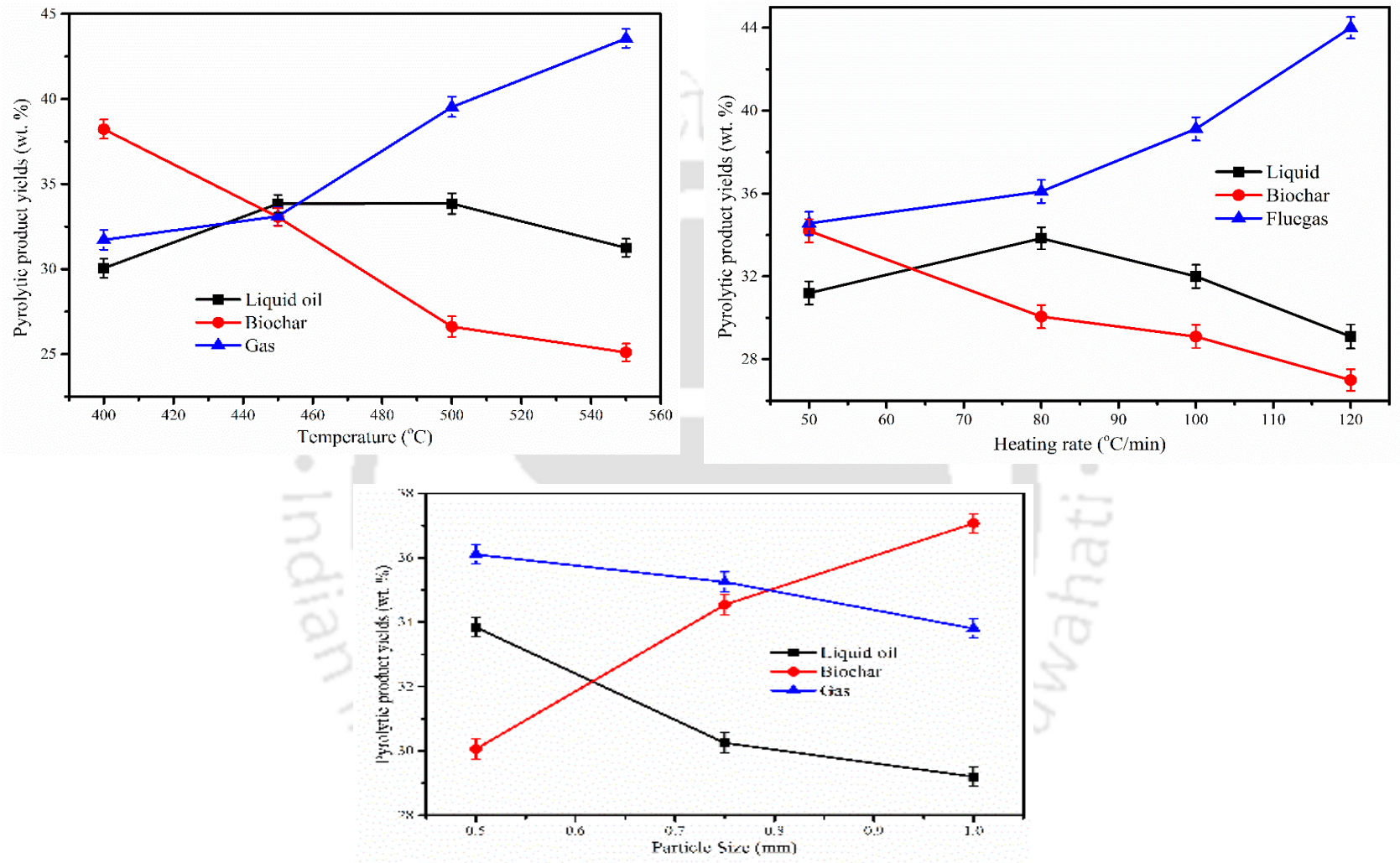

Fig. 5.4. Optimization of temperature, heating rates and particle size of SG biomass

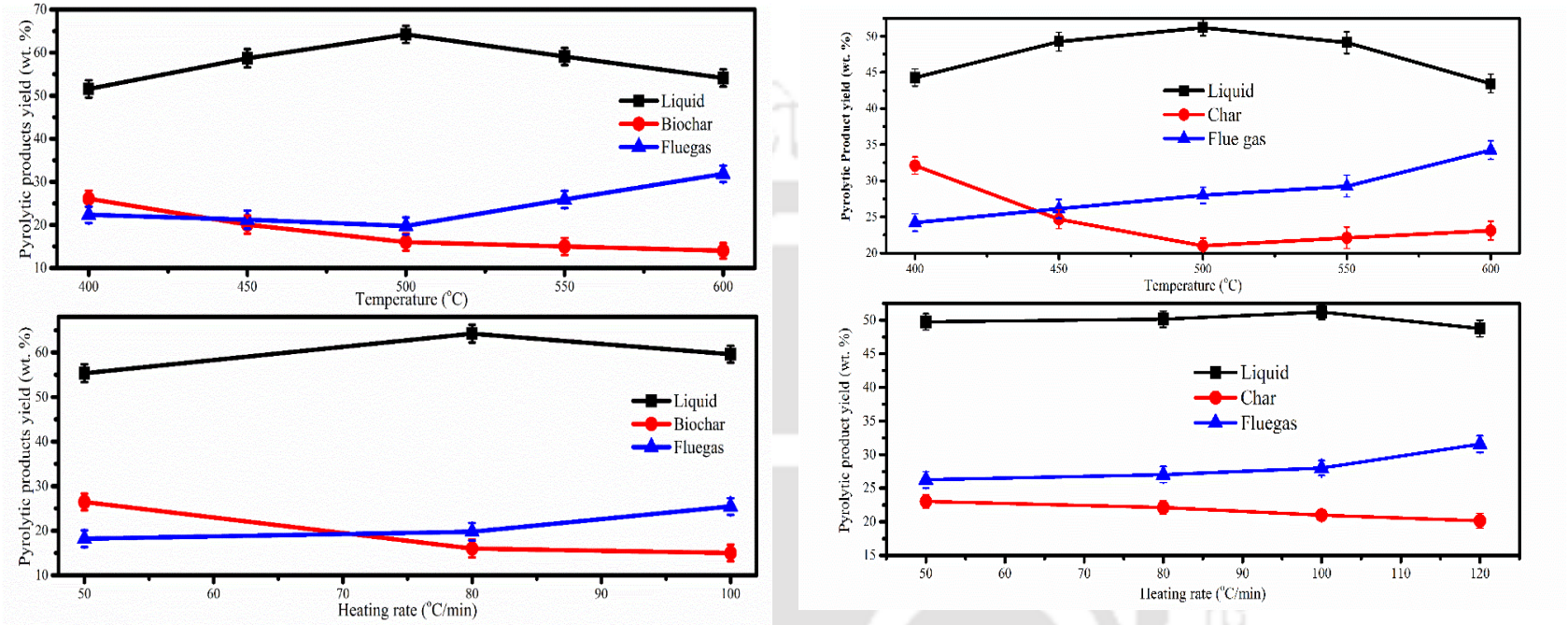

(a) (b)

Fig. 5.5. (a) Optimization of temperature and heating rates of SK biomass (b) Optimization of temperature and heating rate of MH biomass

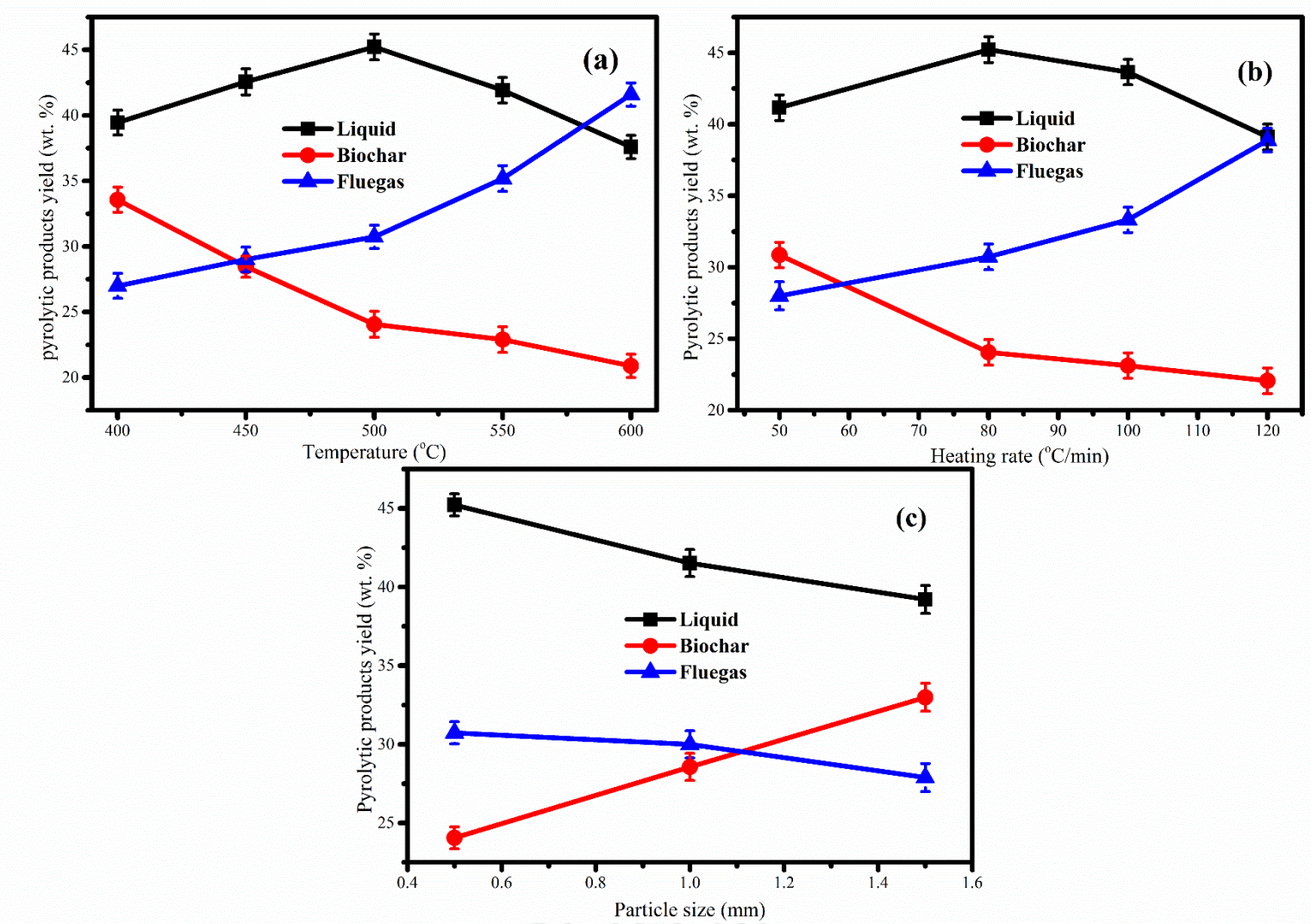

Fig. 5.6. Optimization of temperature, heating rates and particle size of CK biomass

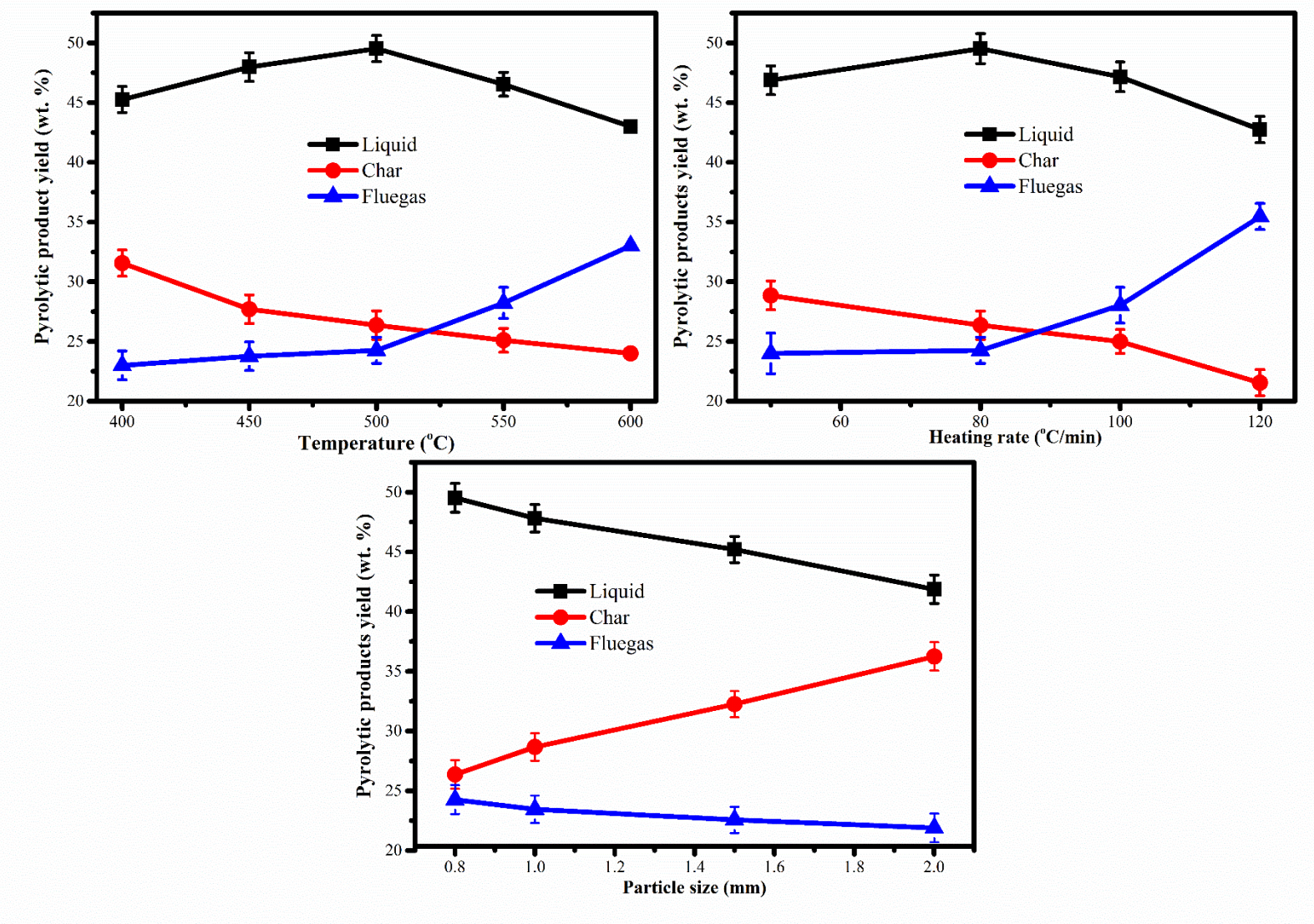

Fig. 5.7. Optimization of temperature, heating rates and particle size of NM biomass

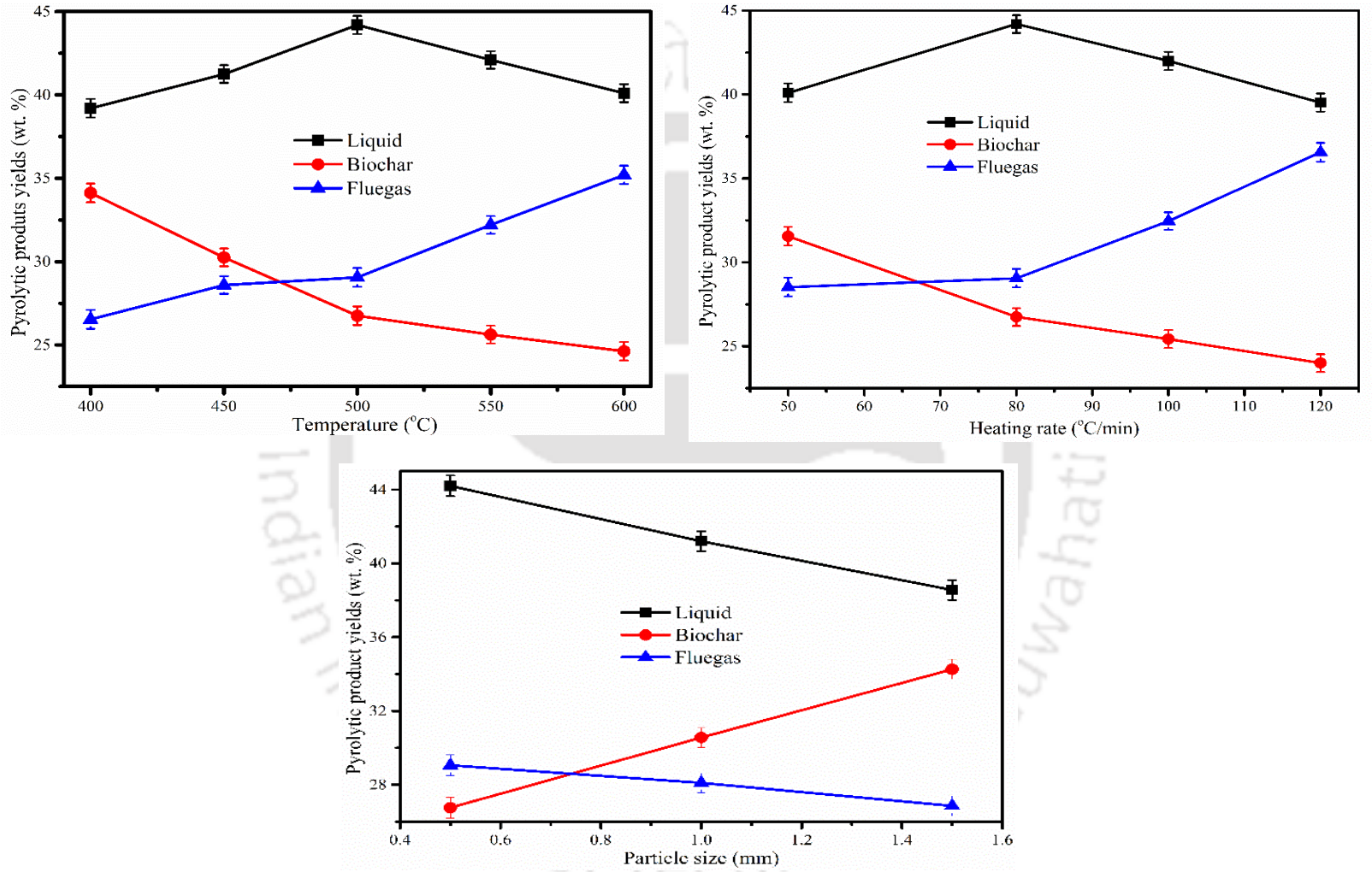

Fig. 5.8. Optimization of temperature, heating rates and particle size of SS biomass

Table 5.1. Thermal pyrolytic products yield obtained at optimized conditions

Biomass	Liquid fuel (wt.%)	Biochar (wt.%)	Fluegas (wt.%)
PW	40.45±1.5	25.59±1.3	34.00±1.6
SW	34.37±1.6	28.05±1.2	37.58±1.4
AN	33.75±1.4	30.22±1.6	36.00±1.5
SG	33.85±1.3	26.62±1.5	39.53±1.4
SK	64.23±1.8	16.00±1.6	19.77±1.6
CK	45.22±1.6	24.05±1.3	30.73±1.4
NM	49.83±1.5	26.36±1.2	24.26±1.3
MH	51.20±1.9	21.00±1.4	28.00±1.5
SS	44.20±1.2	26.75±1.3	29.05±1.3

5.1.2. FTIR analysis of thermal pyrolytic oil

Functional groups present in pyrolytic oil was identified using FTIR analysis. The transmittance against wavenumber curves were plotted and presented in Fig. 5.9. The adsorption band 3000 cm^{-1} - 3750 cm^{-1} attributed to -OH vibration which indicated the presence of water, phenols, alcohol, aromatics, and protein [45]. The peak 2925 cm^{-1} represents the axial deformation of the C-H group. The peak at 2612 cm^{-1} showed the C-H and =C-H stretching vibrations, which indicated the presence of alkanes and alkenes. The presence of carbonyl group like ester (C=O) was observed at peak 1730 cm^{-1} which signified the presence of carboxylic acid and ether [215]. The peak in the region 1400 cm^{-1} - 1595 cm^{-1} suggested the presence of methyl C-H asymmetric stretch. The peak in the region of 1275 cm^{-1} - 1378 cm^{-1} indicated the presence of alcohol and saturated aliphatic compounds [216]. The peak around 606 cm^{-1} - 880 cm^{-1} suggested the presence of alkenes and monocyclic aromatic compounds [45].

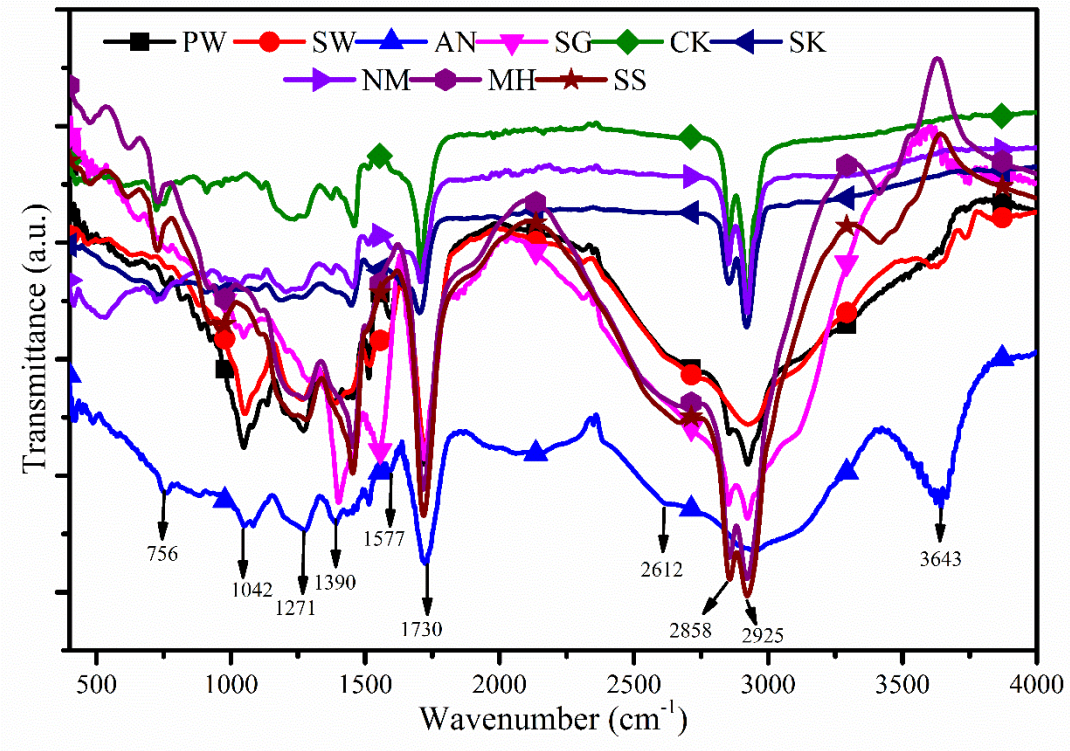

Fig. 5.9. FTIR analysis of thermal pyrolytic oil

5.1.3. Characterization of thermal pyrolytic oil

Thermal pyrolytic oil was characterized and compared with diesel fuel [217, 218] and gasoline [219] and listed in Table 5.2. Results confirmed that all thermal pyrolytic oil had higher viscosity (39.45 cSt) which affects the stability and reduced the fluidity of pyrolytic oil. Results also confirmed that seed pyrolytic oil had a higher viscosity than sawdust as this happened due to the variation of the composition of biomass. Further, the heating value of all pyrolytic oil varied from 23.20 MJ kg^{-1} - 28.32 MJ kg^{-1} which signified that these oil can be used as furnace fuel. All thermal pyrolytic oil had a higher heating value closer to the diesel. The density of all thermal pyrolytic oil was higher than diesel and gasoline. The acidity of thermal pyrolytic oil varied from 2.87 - 6.38, mostly acidic which reduced the heating value of fuel [33]. Finally, moisture varied from 1.20 % - 1.70 % for all thermal pyrolytic oil. It was also reported that the presence of moisture in pyrolytic oil, reduced the heating value which may reduce the quality of fuel [33].

Table 5.2. Characterization of all thermal pyrolytic oil

Biomass	Viscosity (cSt)	Heating value (MJ/kg)	Density (kg/m^3)	Acidity (-)	Moisture (%)
PW	48.89±0.02	23.20±0.02	819.0±3.39	3.02±0.14	1.32±0.20
SW	47.32±0.02	24.12±0.02	824.0±2.14	3.85±0.14	1.33±0.18
AN	45.48±0.02	28.32±0.01	841.0±3.14	2.87±0.12	1.30±0.20
SG	52.45±0.34	23.62±1.3	981.0±2.14	4.90±0.13	1.55±0.17
SK	87.96±0.42	27.07±1.4	921.0±2.49	6.38±0.07	1.5±0.15
CK	63.71±0.18	29.89±1.6	921.72±2.86	6.38±0.01	1.5±0.20
NM	47.56±0.20	25.31±1.4	976.0±2.24	5.21±0.14	1.30±0.18
MH	49.12±1.2	25.63±1.2	904.0±2.20	4.20±0.18	1.20±0.04
SS	39.45±1.2	24.56±1.2	927.0±2.20	4.30±0.14	1.4±0.16
Diesel	2-6	44.50	825.00	-	-
Gasoline	0.12	47.30	838.00	-	<0.10

5.1.4. GC-MS analysis

The chromatograph obtained from thermal pyrolytic oil of all biomass by GC-MS analysis were compared with NIST library and presented in Fig. 5.10. The pyrolytic oil contained more than 300 different types of organic compounds due to its diverse nature. Therefore, they were divided into six major categories: monoaromatics, polyaromatics, aliphatic, heterocyclic, oxygenates and nitrogenates. The pyrolytic oil is a complex mixture of highly oxygenated compounds with large size of molecules, which involves almost all species of oxygenated organics, such as esters, ethers, aldehydes, ketones, phenols, carboxylic acids, amide group, and alcohols. From GC-MS results, it was noticed that the amount of phenols was higher in sawdust than seed biomass and this difference was due to the composition of biomass. However, it is important to mention that phenol is the raw material for several important industrial chemicals. Phenols are used for preparations of reagents used in plastic manufacturing industries, synthesis of various epoxide resins and polycarbonates, making of bakelite (phenol-formaldehyde resin), extraction of bio-molecules, and cosmetic industry in the manufacturing of sunscreens, skin lightening creams, and hair coloring solution. Further, it was noticed that seed thermal pyrolytic oil had higher amount of hydrocarbons than sawdust,

again due to the difference in composition of biomass. Almost all the pyrolytic oil associated with oxygenated compounds such as ethers, esters, and ketones, which had a negative impact on the pyrolytic oil when the intended use is as a transportation fuel. Presence of these oxygenated compounds reduced the fluidity and stability of pyrolytic oil [24, 220]. Acid is another compound found in pyrolytic oil in higher amounts. The presence of higher acidity in pyrolytic oil reduced the heating value of fuel [220]. Also, thermal pyrolytic oil associated with various other compounds such as octadecanenitrile, oleanitrile, 9-octadecenoic acid methyl ester, stearic acid methyl ester, heptadecane, 9-octadecenamide, 11-hexadecenal, and pentadecane, etc. Most of these compounds can be used in various applications, which increase the value of pyrolytic oil. Octadecanenitrile is used as the chemical intermediate for fatty amines; while 9-octadecenoic acid methyl ester is a primary raw material of emulsifiers or oiling agents for foods, spin finishes and textiles, lubricants for plastics, paint and ink additives, surfactants and even forms a base material for perfumery. Stearic acid has numerous value-added application such as slip agent, anti-block agent for LDPE, HDPE, PP, mold release agent, internal lubricant for coatings and films. It is also used in several other applications such as foam builder/stabilizer, viscosity stabilizer in synthetic detergent formulations, cosmetics, water repellent for textiles, oil-well corrosion inhibitor, improves dye solubility in printing inks, carbon paper coatings and fusible coatings for glassware and ceramics, pigment dispersant, thickener for paints, release agent for food packaging, intermediate for synthetic waxes, in food packaging adhesives, in surfing lubricants for manufacturing of food contact metallic articles, enclosure sealing gaskets for food containers, packaging material for irradiated foods etc. [16]. Hexadecanoic acid has many applications which include making of soaps, various cosmetics products, and release agents. Nitrogen-containing groups are one of them which was found to be in less amount which signified that there will be lower NO_x formation during engine application.

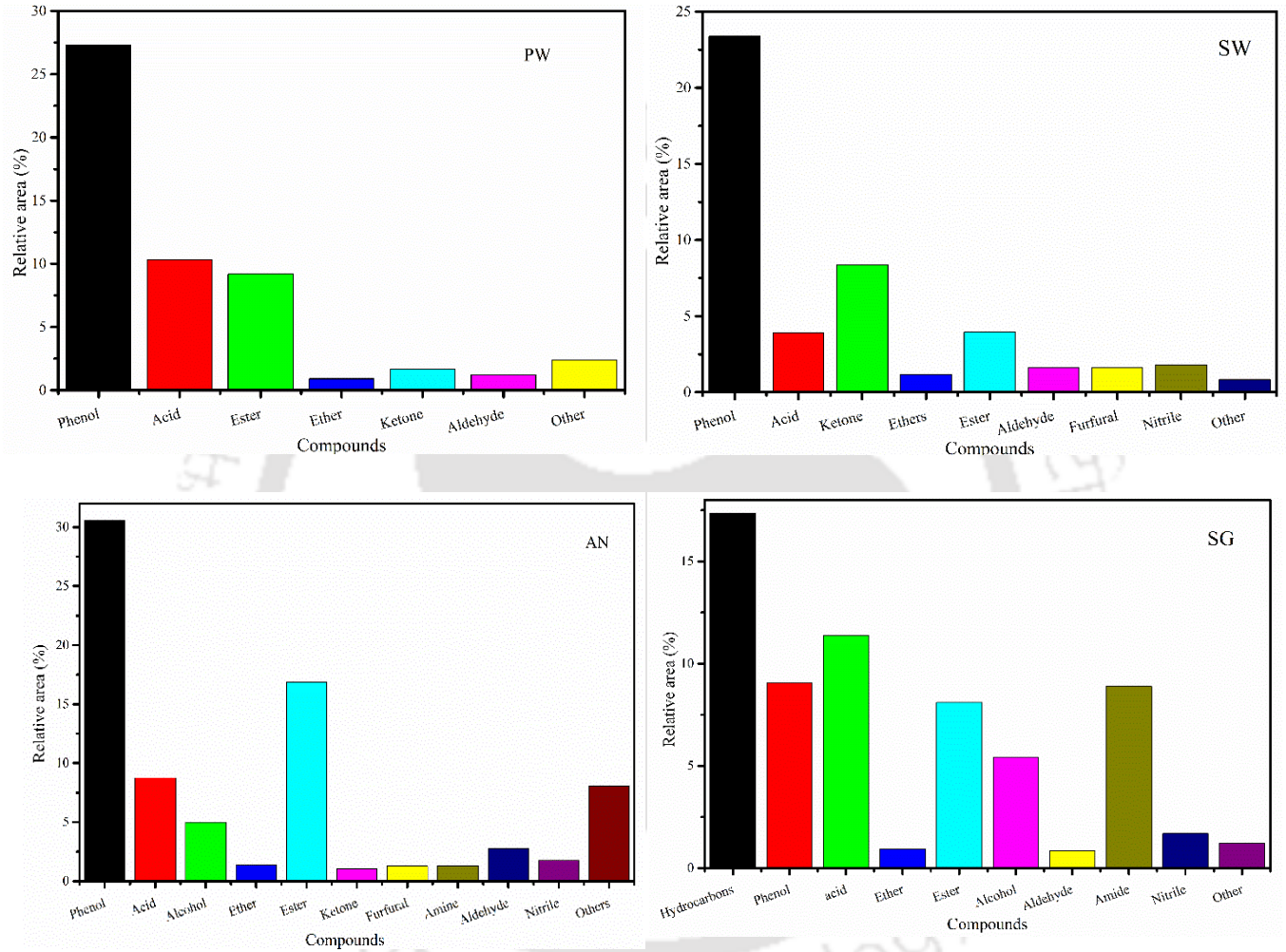

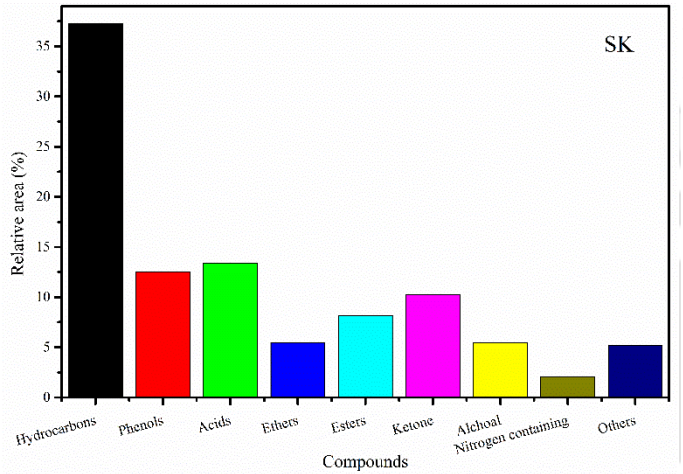

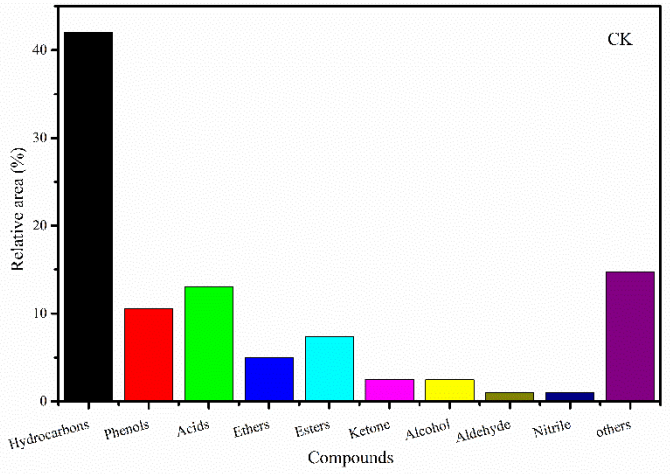

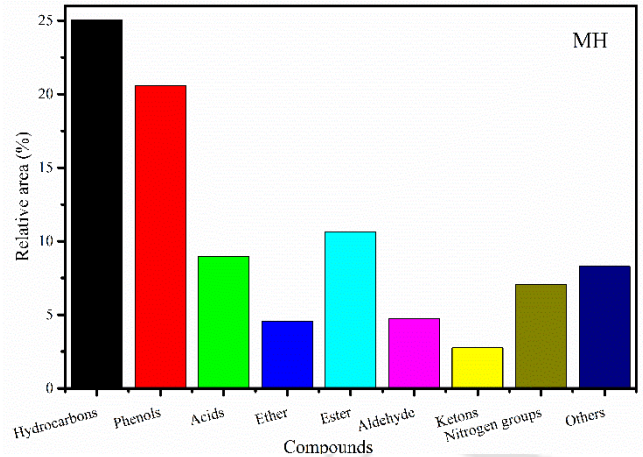

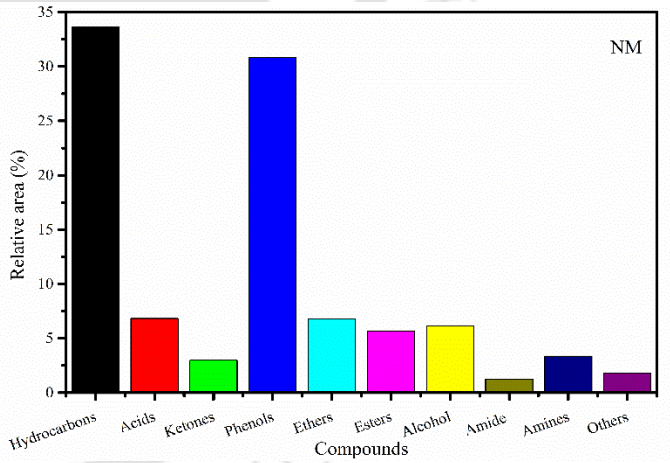

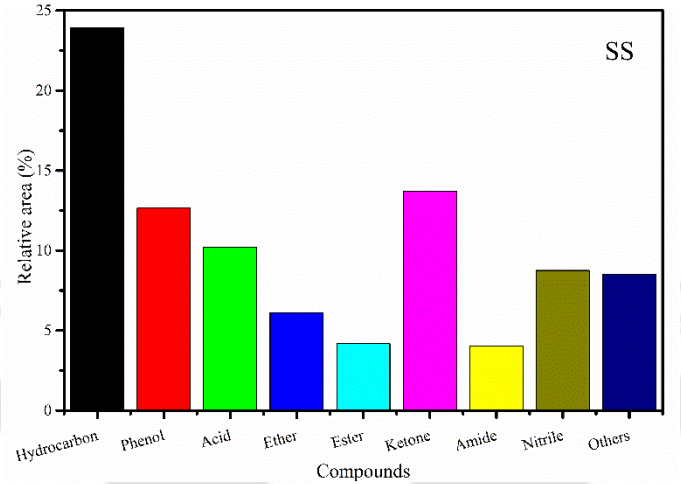

Fig. 5.10. GC-MS analysis of thermal pyrolytic oil of PW, SW, AN, SG, SK, CK, MH, NM, and SS biomass

5.2. Effect of Biomass Bed Thickness and Height on Pyrolytic Products Yield

In this section, three biomass PW, SW and AN were used to study the effect of biomass bed thickness and height on pyrolytic products yield. These biomass are abundantly available across the country and has enough potential to produce liquid fuel.

5.2.1. Process parameters optimization

The process parameters such as temperature, heating rate, inert gas flow rate and particle size of PW, SW and AN were optimized in section 5.1. Results confirmed that 500 ^{o}C temperature, 80 ^{o}C min^{-1} heating rate 0.5 mm particle size and 100 mL gas flow rate produced maximum pyrolytic liquid.

5.2.2. Effect of biomass bed thickness and distance between successive beds on pyrolytic products yield

In the present study, the effect of biomass bed thickness and distance between successive beds on pyrolysis products yield was studied. At the beginning, 50 g of biomass was placed in the reactor in a single bed. Further, the same amount of biomass was placed in the reactor in two beds as depicted in Fig. 5.11(a) and so on. Based on the reactor length, this process was carried out up to sixth bed. The details arrangements of bed thickness and distance between two beds are listed in Table 5.3. It is important to mention that each and every bed has equal biomass bed thickness and equal distance between successive beds for each experiment. The detailed sketch of the experimental setup is shown in Fig. 5.11(b).

The results (Fig. 5.12a) demonstrated that pyrolytic liquid yield changed with the increase in number of biomass beds (40.45 wt.%, 43.96 wt.%, 46.73 wt.%, 50.63 wt.%, 49.78 wt.%, and 47.20 wt.%, for PW; 34.37 wt.%, 39.54 wt.%, 45.59 wt.%, 47.21 wt.%, 46.01 wt.%, 45.62 wt.% for SW and 33.75 wt.%, 36.39 wt.%, 42.44 wt.%, 45.25 wt.%, 43.19 wt.%, 42.29 wt.% for AN respectively for a single bed, double bed, triple bed, fourth bed, fifth bed, and six bed). Results showed that PW, SW, and AN resulted in higher liquid yield at the fourth bed arrangement. Therefore, the fourth bed was considered as the optimum bed in the present study. With the increasing number of biomass beds at optimized bed condition (up to fourth bed for PW, SW, AN,) liquid yield also increased (Fig. 5.12a). The released hot volatiles from the biomass escaped from the reactor easily at the optimized condition, thus, liquid yield increased.

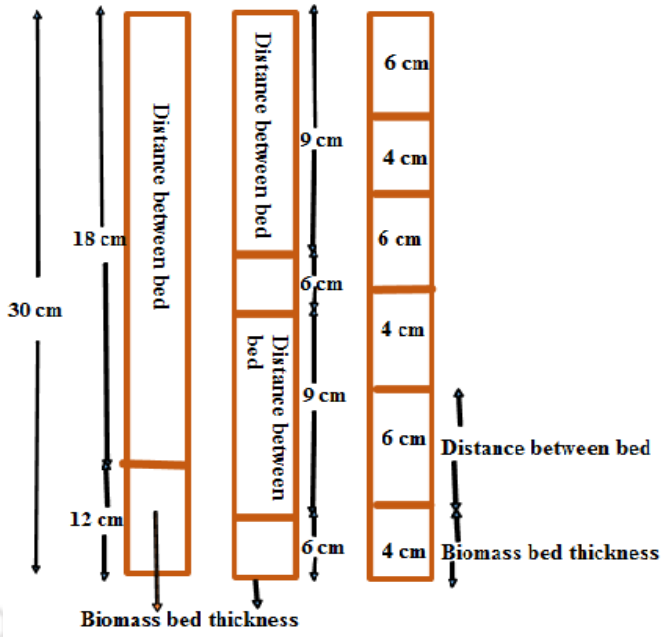

(a)

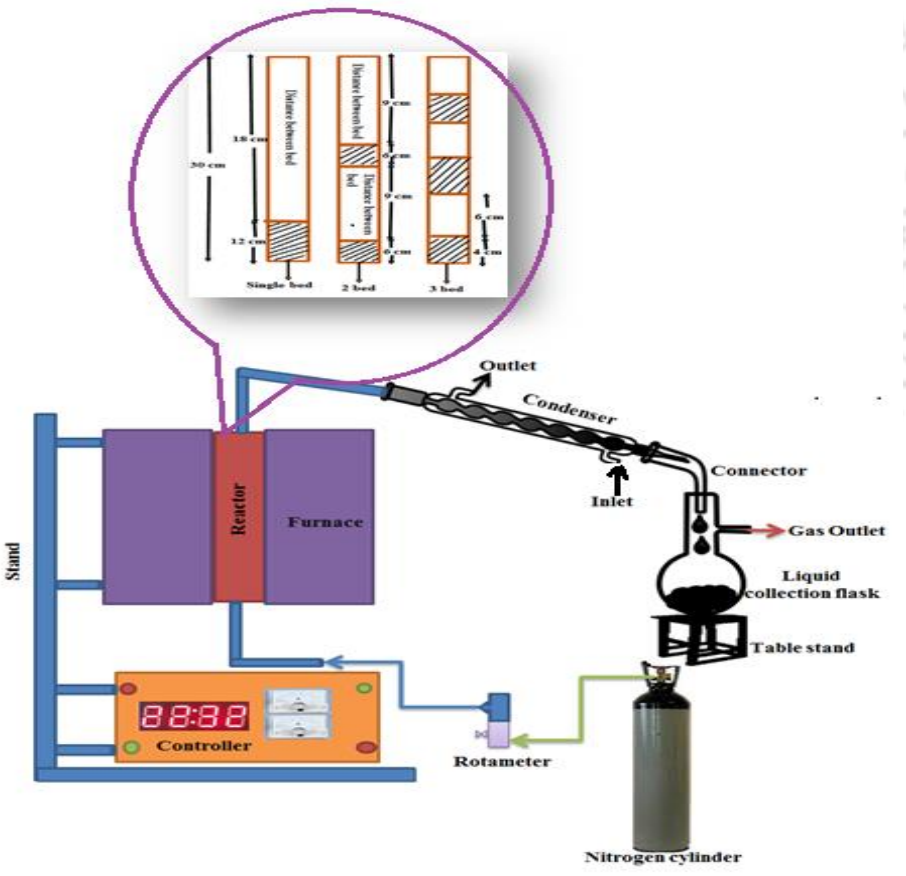

(b)

Fig. 5.11. (a) Systematic arrangement of beds and (b) detail sketch of experimental setup

Table 5.3. Details of biomass bed arrangements in the reactor

Bed arrangements	Single	Double	Triple	Fourth	Fifth	Sixth
Biomass bed thickness (cm)	12.0	6.0	4.0	3.0	2.4	2.0
Distance between successive beds (cm)	18.0	9.0	6.0	4.5	3.6	3.0

At the optimized condition of 4th bed system, the thickness of each bed was kept at 3 cm while the distance between successive beds was 4.5 cm. It was noticed that for this arrangement, the bed thickness, as well as the distance between successive beds, was such that the vapors generated passed through the beds easily. Once the bed thickness, as well as the distance between the beds reduced (as in the case of 5th bed and 6th bed system), the released volatiles were trapped in more numbers of beds and stayed for longer time (higher vapor residence time) which led to secondary reactions (such as dehydrogenation, depolymerisation, and fragmentation), thereby reducing the overall liquid yield. The sweeping gas nitrogen has a role to play in pyrolysis apart from being the inert gas that it helps in flushing out the vapors generated without allowing them to undergo secondary reactions. Precisely, at 5th bed and 6th bed system, due to increase in a number of beds, the velocity of nitrogen gas was not enough to push the vapors out of the reactor which led to secondary reactions probably at the top of the reactor.

Further, beyond optimized bed conditions again liquid and gas yield decreased while char yield increased probably due to initiation of secondary cracking as a result of the increase in vapor residence time. Raja et al. (2010) [221] explained that reduction in liquid yield and increasing char and gas yields were due to secondary cracking of volatiles. Aquino et al. (2007) [222] also elucidated that secondary thermal cracking led fragmentation of biomass into non-condensable gases, which influenced the generation of a higher percentage of gases.

Formation of non-condensable gases found to be higher at first and sixth beds. Further increase in the number of beds beyond the optimum bed decreased the formation of gaseous products (Fig. 5.12b). However, it was noticed that the yield of non-condensable gases

increased (Fig. 5.12b). The alteration in gaseous yield was observed due to the formation of secondary reactions, which changed the volatile gases to non-condensable gases during pyrolysis. During secondary cracking, biomass fragmented into non-condensable gases which resulted in the formation of higher gases.

From Fig. 5.12c, it was confirmed that at optimized bed condition, char formation was decreased while further increasing the number of beds the char yield increased. Possibly initiation of secondary cracking led to the formation of higher char yield due to the increase in vapor residence time. At optimized bed condition, biomass offered higher heat and mass transfer, which led to the reduction in biochar and non-condensable gases. However, As the report suggests, secondary cracking reaction changes the quality and quantity of pyrolytic products [33].

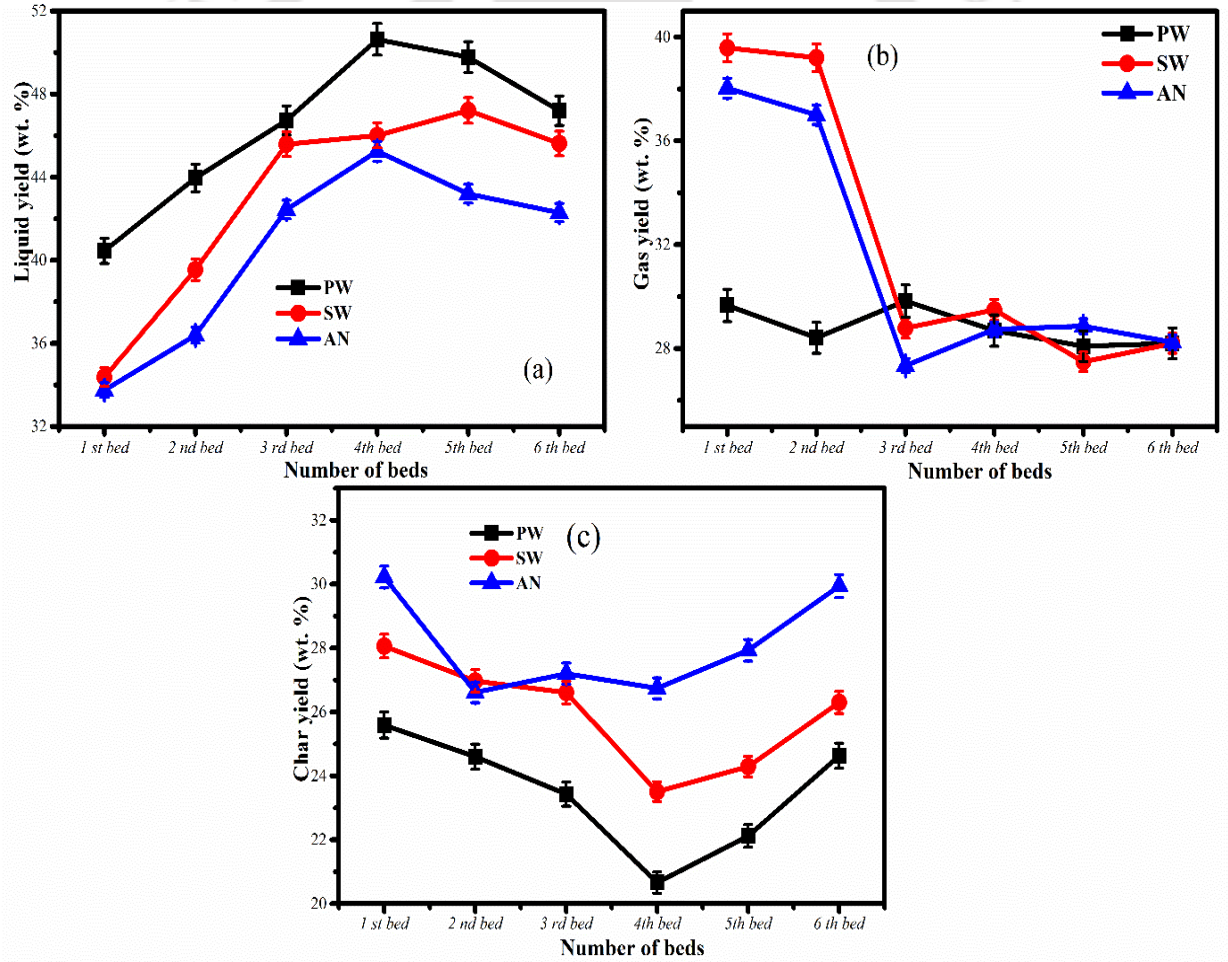

Fig. 5.12. Effect of biomass bed thickness and distance between successive beds on pyrolytic products yield (a) liquid yield, (b) gas yield, (c) char yield

5.2.3. Characterization of pyrolytic oil

At optimized process conditions, the produced pyrolytic oil has a smoky and irritable smell. The pyrolytic oil has a strong brown color with viscous nature, while the aqueous phase looks slightly cloudy yellow-brown solution. As reported in Table 5.4, all biomass showed lower viscosity (48.10 cSt for PW, 46.89 cSt for SW, and 45.14 cSt for AN at 40 ^{o}C with 50 RPM) at the fourth bed, while at first and sixth beds viscosity was slightly higher. The possible reason for the increase in viscosity could be due to secondary reactions. However, at optimized bed conditions, the total bed thickness was less, which helped in the easy escape of volatiles, thus resulted in lower viscosity. Table 5.4 shows that density of first and sixth beds was higher than that of fourth bed. Formation of secondary reaction may be one of the possible reasons for variation in density. However, how these reaction influenced the density of pyrolytic oil is still uncertain. Further, acidity and moisture were higher at first and sixth beds than that of fourth bed again due to the secondary reactions which may lead to depolymerization reactions. The heating value of pyrolytic oil at optimized condition was higher than the first and sixth beds because at optimized conditions formation of acidic compounds were reduced (as evident from GC-MS analysis).

Table 5.4. The physicochemical properties of pyrolytic oil of PW, SW, and AN sawdust

No. of beds	Viscosity (cSt)	Density (kg/m^3)	Acidity (-)	Moisture (%)	Calorific value (MJ/kg)
			PW		
1st bed	48.89±0.02	819.0±3.39	3.02±0.04	1.32±0.20	23.20±0.02
4th bed	48.30±0.02	806.0±2.89	3.05±0.02	1.29±0.12	23.24±0.01
6th bed	48.96±0.02	819.0±2.14	3.85±0.04	1.33±0.18	23.22±0.01
			SW		
1st bed	47.32±0.02	824.0±2.14	2.65±0.03	1.31±0.16	24.12±0.02
4th bed	46.98±0.01	810.0±2.43	2.45±0.04	1.18±0.10	24.16±0.02
6th bed	47.60±0.02	831.0±3.12	2.72±0.03	1.30±0.20	24.15±0.01
			AN		
1st bed	45.48±0.02	841.0±3.14	2.87±0.04	1.30±0.020	28.32±0.01
4th bed	45.14±0.01	821.0±2.14	3.05±0.01	1.10±0.14	28.36±0.01
6th bed	45.71±0.02	831.0±3.17	3.50±0.02	1.30±0.18	28.34±0.02

5.2.4. FTIR analysis

To estimate the presence of various functional groups, FTIR analysis was performed. Wave number versus transmittance spectra were plotted and presented in Fig. 5.13. The peak in the region of 3000 cm^{-1} - 3750 cm^{-1} ascribed to the axial deformation of -OH group which indicated the presence of water, phenol, alcohol, protein, and aromatic compounds [45]. The peak at 2943 cm^{-1} represented axial deformation of the C-H group. The peak at 2619 cm^{-1} showed the C-H and =C-H stretching vibrations, which indicated the presence of alkanes and alkenes. The presence of carbonyl group like ester (C=O) was observed at peak 1727 cm^{-1} which signified the presence of carboxylic acid groups [215]. The peak in the region of 1400 cm^{-1} - 1595 cm^{-1} suggested the presence of methyl C-H asymmetric stretch. The peak in the region of 1275 cm^{-1} - 1378 cm^{-1} indicated the presence of alcohol and saturated aliphatic compounds [216]. The peak around 606 cm^{-1} - 880 cm^{-1} indicated the presence of aromatics.

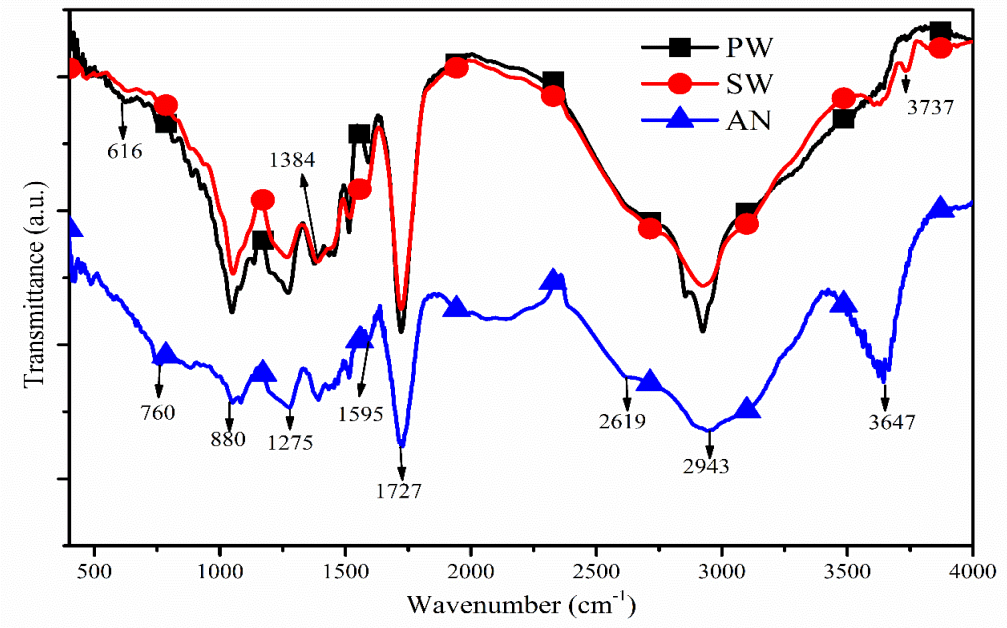

Fig. 5.13. FTIR analysis of pyrolytic oil produced from PW, SW and AN biomass

5.2.5. Gas chromatography analysis (GC)

The non-condensable gases generated at different temperatures via pyrolysis were analyzed by using GC analysis. During pyrolysis, a number of combustible gases such as hydrogen, hydrocarbons, and carbon dioxide were generated (Fig. 5.14). Thus, it can be concluded that hydrogen and hydrocarbons increased significantly with increasing temperature and at the same time, the formation of carbon dioxide was reduced with increasing pyrolysis temperature. At higher temperature, secondary cracking reaction influenced the volatile content

and offered an atmosphere to release hydrogen and hydrocarbons [223]. When pyrolysis temperature increased from 400 ºC to 600 °C, the formation of more hydrogen and hydrocarbons were observed. However, the release of carbon dioxide gas decreased with increase in pyrolysis temperature because the number of combustible gases such as CO_2 released at a lower temperature (400 °C) due to the presence of the oxygenated compound in the biomass by the process of decarboxylation [224]. Similar results were also reported by Zhang et al. (2015) [225] and Kongkasawan et al. (2016) [224].

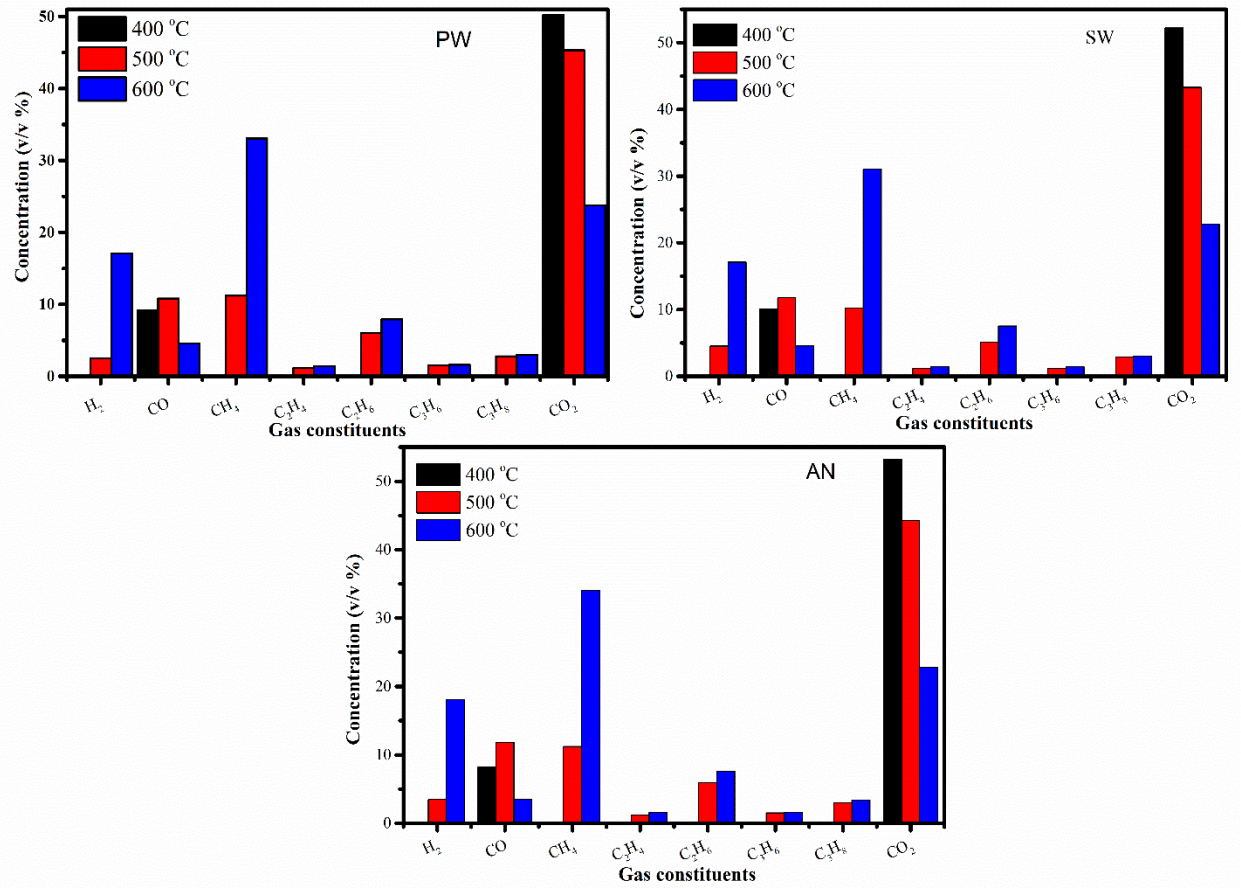

Fig. 5.14. Variation of gas composition with respect to a pyrolysis temperature

5.2.6. GC-MS analysis

GC-MS was used to identify the composition of pyrolytic oil or bio-oil. National Institute of Standards and Technology (NIST) library was used to identify the compounds and their compositions. The results presented in Fig. 5.15, demonstrated the formation of phenol, ester, alcohol, ketones, aromatics, aldehyde, carboxylic acid, and amide during pyrolysis. The produced pyrolytic oil was associated with various valuable chemicals such as nitrile, methyl ester, carboxylic acid methyl ester, heptadecane, and amide. Application of the obtained

chemicals in pyrolytic oil is already described earlier. Furthermore, GC-MS analysis confirmed that in first and sixth beds, formation of phenol was higher (27.28 % for the first bed and 43 % for the sixth bed of PW; 24.14 % for the first bed and 24.07 % for the sixth bed for SW; and 30.59 % for the first bed and 35.55 % for the sixth bed for AN), while at optimized bed conditions (4^{th} bed) formation of phenol was lesser, PW (14.85 %), SW (22.9 %), and AN (13.92 %). It was reported that at optimized condition phenolic compounds varied from 20 % - 30% however, it changes with types of feedstocks, reactors and operating conditions [226]. In the first and sixth beds, the thicknesses of beds were higher, which prevented the release of volatile compounds. At the same time, the residence time of volatile compounds increased, which led to the start of secondary cracking reactions and subsequently the formation of phenolic compounds. Zhang et al. (2017) [227] studied the pyrolysis of pine wood biomass in a fixed bed reactor (two-stage method) for improving hydrocarbon yield and reported that at moderate temperature (600 °C) formation of phenolic compounds and acids were higher. The study also suggested that pyrolysis of wood biomass resulted in the formation of higher phenolic compounds at higher temperature [228].

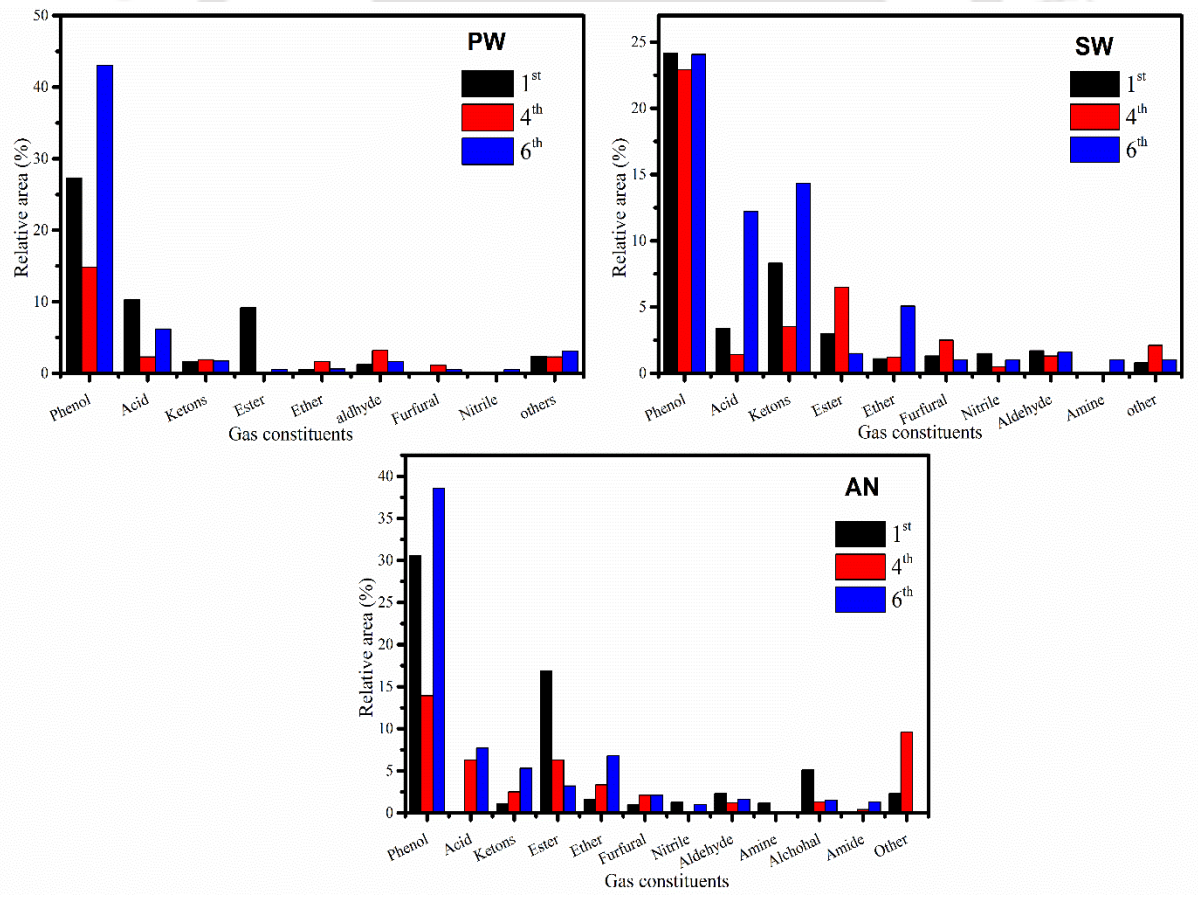

Fig. 5.15. GC-MS analysis of pyrolytic oil of PW, SW and AN

5.3. Catalytic Pyrolysis of *Cascabela thevetia* Seeds

Cascabela thevetia seeds were pyrolyzed over ZSM-5 catalysts at different proportions (3:1, 6:1, 8:1 and 10:1). Zeolite catalysts have the potential to alter the quality and quantity of pyrolytic liquid. In this study, *Cascabela thevetia* seeds were chosen because it produced maximum liquid yield among all the biomass studied.

5.3.1. Process parameter optimizations

The process parameters optimization such as temperature and heating rate was optimized in section 4.3. Results confirmed that 500 ^{o}C temperature, 80 ^{o}C min^{-1} heating rate and 100 mL min^{-1} sweeping gas flow rate produced maximum liquid yield.

5.3.2. Optimization of biomass to catalyst (B/C) ratio

Catalytic pyrolysis of *cascabela thevetia* seeds (SK) was carried out to enhance the properties of liquid fuel (bio-oil). Since catalyst has a significant effect on pyrolytic products yield, therefore the optimization of catalyst loading becomes essential. Fig. 5.16 demonstrated that liquid yield increased when B/C ratio was varied from 3:1 to 10:1. B/C ratio 3:1 produced minimum liquid yield while B/C ratio 10:1 produced maximum liquid yield. Results confirmed that at B/C ratio 3:1, liquid and gas yield decreased while char yield increased. On the other side, the liquid yield increased and solid and gas yield decreased when B/C ratio increased (10:1). Higher B/C ratio (3:1) might have blocked the active sites of the biomass (pore) which helped the volatiles to escape from the biomass. However, at 8:1 ratio, the reaction reactivity was boosted significantly which resulted in an increase in liquid yield and decreased the char yield. However, use of catalyst enhanced the yield of pyrolytic oil via two ways: surface reaction and pore reaction. Lower amount of catalyst involved surface reaction whereas higher catalyst loading involved pore reaction [229]. It was also noted that, higher catalyst to biomass ratio reduced the oxygen content which resulted in the formation of higher aqueous fraction (water) while other B/C ratio reduced it, however, comparatively less [229].

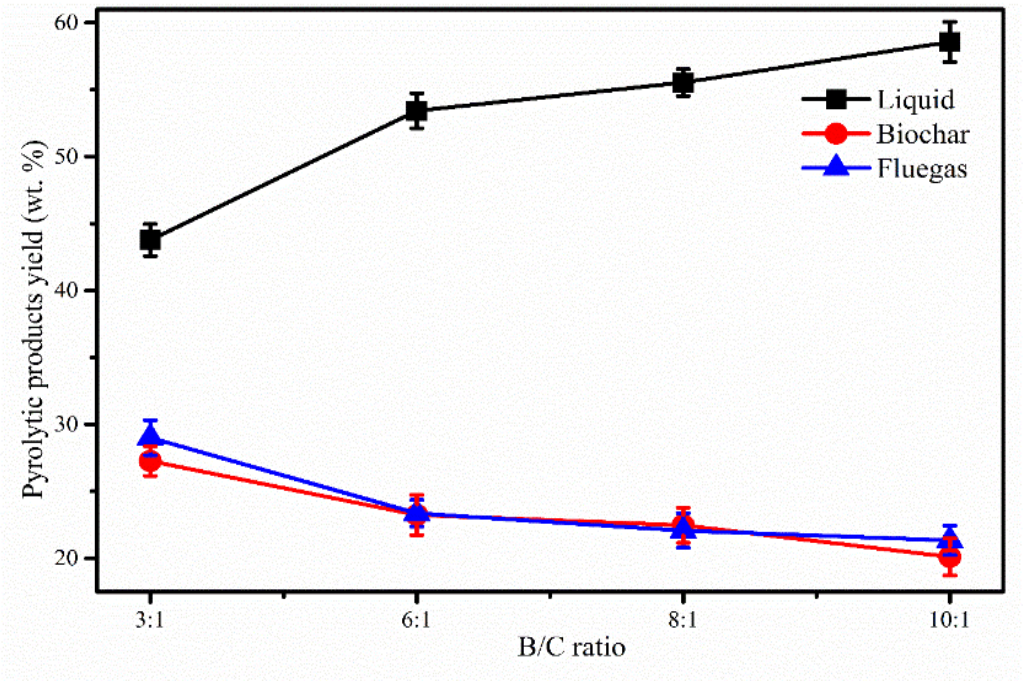

Fig. 5.16. Effect of catalyst loading on pyrolytic products yield

5.3.3. Characterization of pyrolytic oil

The characterization of thermal and catalytic pyrolytic oils derived from different biomass to catalyst ratios (3:1, 6:1, 8:1 and 10:1) are presented in Table 5.5. Characterization of pyrolytic oil confirmed that thermal pyrolytic oil was associated with higher viscosity (63.71 cSt), and density (921.72 kg m^{-3}), however with lower heating value (29.89 MJ kg^{-1}). Pyrolytic oil having a higher viscosity, density and lower heating value cannot be used as a transportation fuel because of the presence of unsaturated oxygen which affects the stability and fluidity of a pyrolytic oil. Further, the use of catalyst significantly enhanced the properties of the pyrolytic oil such as an increase in heating value and reduction in viscosity and densities. Results (Table 5.5) also confirmed that lower biomass to catalyst ratio (3:1) significantly enhanced the properties of the pyrolytic oil such as heating value, viscosity, and density, however, at this ratio the yield of oil fuel got reduced (43.77 %). A similar pattern was also noticed for 6:1, 8:1 and 10:1 ratio. Among all the biomass to catalyst ratio, 3:1 significantly increased the properties of oil yield while 10:1 produced maximum liquid yield. Based on the properties of pyrolytic oil and yield, it can be concluded that B/C ratio 8:1 produced maximum oil yield.

Table 5.5. Characterization of thermal and catalytic pyrolytic oil at various B/C ratios

Analysis	Thermal	ZSM-5(3:1)	ZSM-5(6:1)	ZSM-5(8:1)	ZSM-5(10:1)
Calorific value (MJ/kg)	29.89±0.20	41.52±0.14	39.14±0.12	38.80±0.16	33.72±0.14
Viscosity at 40 ^{o}C at 50 rpm (cSt)	63.71±0.30	38.12±0.16	40.40±0.41	41.20±0.21	52.65±0.32
Density (kg/m^3)	921.72±1.6	811±1.2	826±1.1	831±1.6	885±1.2
Moisture (%)	1.5±0.10	3.2±0.12	2.9±0.02	2.1±0.12	1.8±0.11
Acidity(-)	6.38±0.12	5.46±0.16	5.98±0.32	5.7±0.21	5.98±0.42

5.3.4. FTIR analysis of pyrolytic oil

The FTIR analysis of thermal and catalytic pyrolytic oil derived from of *cascabela thevetia* seeds is presented in Fig. 5.17. The adsorption band 3201 cm^{-1} - 3743 cm^{-1} showed the presences of -OH group which confirmed the existence of water, phenols, alcohol, and protein [45]. Peak 2919 cm^{-1} was associated with C-H stretching vibration which showed the existence of alkane and saturated aliphatic groups while peak 2180 cm^{-1} suggested the presence of aliphatic cyanide and aliphatic nitrile. The peak at 2846 cm^{-1} confirmed the presence of alkanes. The peak 1705 cm^{-1} confirmed the presences of C=O stretching vibration which indicated the existence of aldehyde, ketone, and ester [230]. The peak 1440 cm^{-1} associated with C-H was bending vibration, CH_2, and CH_3 bending vibration which confirmed the existence of alkanes while peaks 1171 cm^{-1} confirmed the presence of esters due to C-O-C stretching vibration. Further, peaks at 911 cm^{-1} and 729 cm^{-1} showed the presence of an aromatic compound in pyrolytic oil. Capunitan and Capareda (2012) [223]; Onay and Koçkar (2004) [102] and Seal et al. (2015) [92], reported the presence of aliphatic compounds and a lower percentage of aromatics and confirmed the presence of useful compounds such as hemicellulose, cellulose, lignin which can be used for various applications.

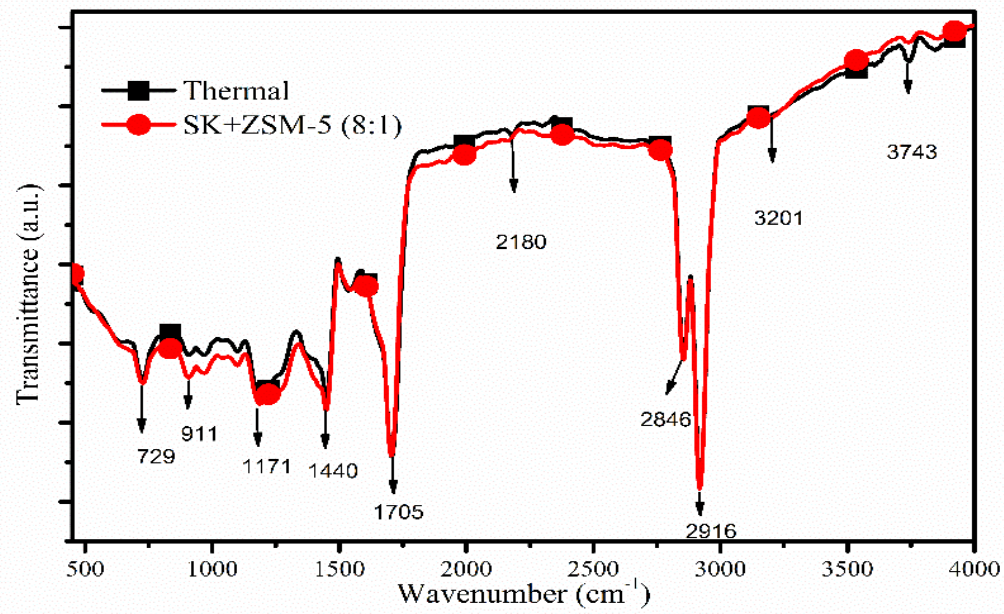

Fig. 5.17. FTIR analysis of thermal and catalytic pyrolytic oil at different proportions

5.3.5. NMR analysis of thermal and catalytic pyrolytic oil

^{1}H NMR analysis of thermal and catalytic pyrolytic oil at 8:1 B/C ratio is presented in Fig. 5.18 while the identified compounds are listed in Table 5.6. ^{1}H NMR analysis of the thermal pyrolytic oil confirmed the presence of –CH, -$CH_{3\alpha}$ to the aromatic ring while catalytic pyrolytic oil at 3:1 confirmed the presence of tri and tetra aromatic rings. The pyrolytic oil associated with aromatics, phenolic or olefinics, CH_2, CH_β to an aromatic ring, CH_3, CH_2, and CH_α to an aromatic ring, β-CH_3, CH_2, and CHγ or an aromatic ring, and $CH_{3\gamma}$. Based on the proton analysis three major groups were identified as aromatics, olefinics and aliphatic. The major aliphatic compound listed as methylene groups, CH_3, CH_2, and CHγ or form an aromatic ring and $CH_{3\gamma}$ [230, 231]. Further, from results (Table 5.6), it was confirmed that thermal pyrolytic oil had 1.89 mol % of hydrogen at 5.38 ppm - 5.27 ppm chemical shift. Similarly, 13.55 mol %, 4.94 mol %, 69.24 mol % and 14.46 mol % of hydrogen at 2.79 ppm - 2.32 ppm, 2.05 ppm - 1.95 ppm, 1.66 ppm - 1.29 ppm and 0.91 ppm - 0.87 ppm chemical shift were noticed. However, for catalytic pyrolytic oil, the same chemical shift was found at 2.97 mol %, 3.96 mol %, 7.92 mol %, 13.86 mol %, 36.36 mol % and 13.86 mol % of hydrogen at 3:1 B/C ratio and 1.50 mol %, 9.52 mol %, 4.67 mol %, 68.25 mol % and 12.46 mol % of hydrogen at 8:1 B/C ratio. The results are similar to that reported by Demiral and Ayan (2011); Onay and Kockar (2003) [14, 232].

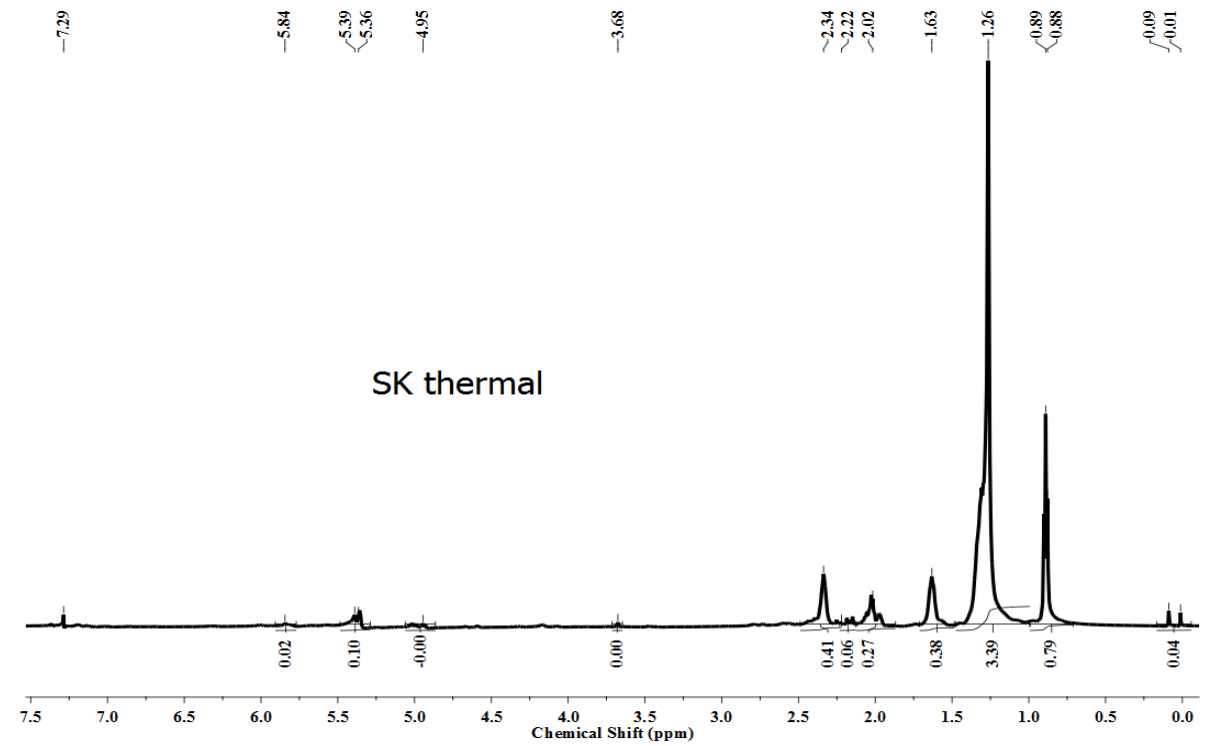

(a)

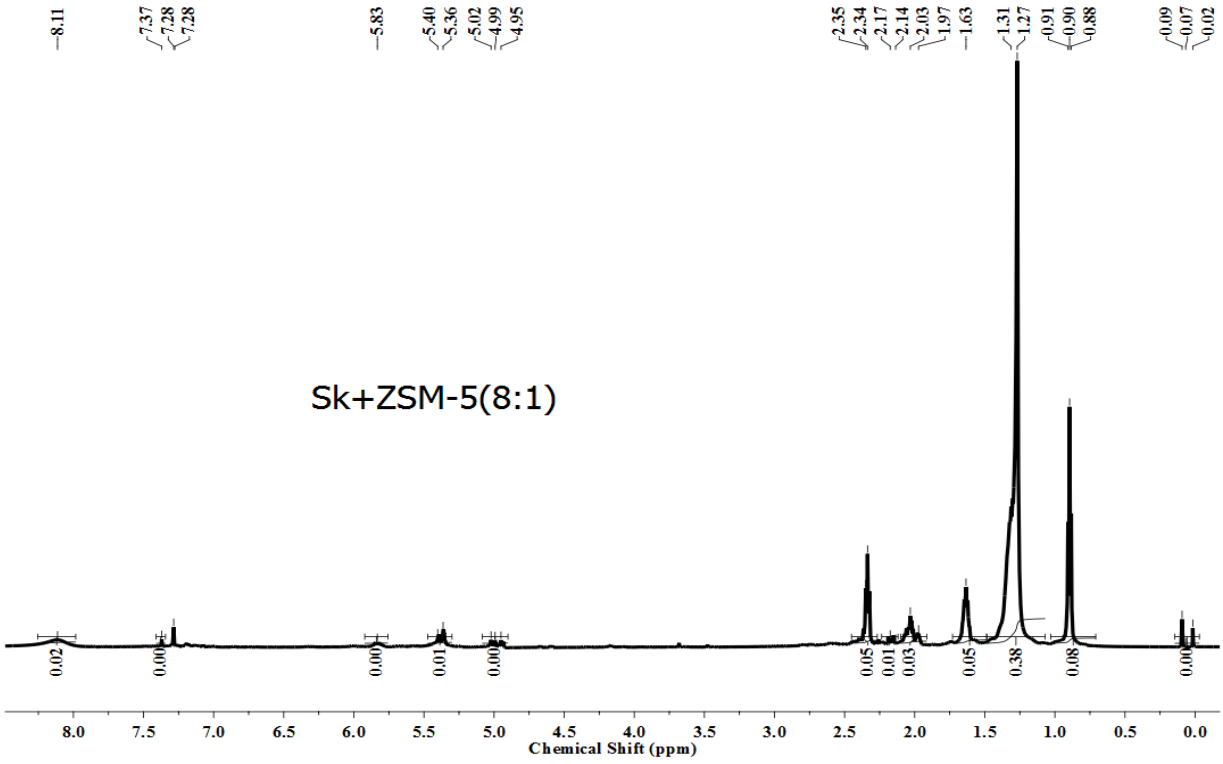

(b)

Fig. 5.18. ^{1}H NMR analysis of (a) thermal and (b) catalytic (ZSM-5 (8:1)) pyrolytic oil

Table 5.6. ^{1}H NMR analysis of thermal and catalytic pyrolytic oil

Type of hydrogen	Chemical shift (ppm)	mol % of hydrogen
Thermal pyrolytic oil		
Phenolic (OH) or olefinic proton	5.38-5.27	1.89
CH_2 bridge (diphenylmethane) and Methoxy Carbohydrates	4.31-4.14	-
CH_3 CH_2 and CH to an aromatic ring	2.79-2.32	13.55
CH_2 and CH_β to an aromatic ring (naphthenic)	2.05-1.95	4.94
β-CH3, CH_2 and CH γ to an aromatic ring and some β-CH with C–C–H, Ar–C–H, C–CCH_3, H–C–COOR, H–C–COOH, H–C–C=O, CH_2, CH_γ, methyl and methylene groups, and for normal, branched alkanes	1.66-1.29	69.24
CH_3 γ or further from an aromatic ring and naphthenic-CH and CH_2	0.91-0.87	14.46
Catalytic Pyrolysis (SK+ZSM-5 (8:1))		
Phenolic (OH) or olefinic proton	5.38-5.27	1.50
CH_2 bridge (diphenylmethane) and Methoxy Carbohydrates	4.31-4.14	-
CH_3 CH_2 and CH to an aromatic ring	2.79-2.32	9.52
CH_2 and CH_β to an aromatic ring (naphthenic)	2.05-1.95	4.67
β-CH3, CH_2 and CH γ to an aromatic ring and some β-CH with C–C–H, Ar–C–H, C–CCH_3, H–C–COOR, H–C–COOH, H–C–C=O, CH_2, CH_γ, methyl and methylene groups, and for normal, branched alkanes	1.66-1.29	68.25
CH_3 γ or further from an aromatic ring and naphthenic-CH and CH_2	0.91-0.87	12.46

5.3.6. GC-MS analysis

GC-MS of thermal and catalytic pyrolytic oil carried out and presented in Fig. 5.19. Results confirmed that thermal pyrolytic oil associated with various oxygenated compounds such as ethers, esters, ketones. Also, it was found to be associated with a higher percentage of acids and phenols. The thermal pyrolytic oil had various acidic compounds such as octadecanenitrile, oleanitrile, 9-octadecenoic acid methyl ester, stearic acid methyl ester, heptadecane, 9-octadecenamide, 11-hexadecenal, and pentadecane, etc. It is important to mention the intended application of pyrolytic oil which decide whether the oil is attractive or unattractive, like, if used as transportation fuel oxygenated and acidic compounds considered as drawback while it will be good for extraction of value-added chemicals. Application of phenols and other valuable compounds is already discussed. Use of pyrolytic oil as transportation fuel requires upgradation such as cracking by using catalysts. Catalytic pyrolytic oil confirmed a reduction in oxygenated compounds such as ethers, esters, ketones while the increase in alcohols and aldehydes (Fig. 5.19). However, the use of catalysts (ZSM-5) also indicated the increased percentage of aromatic hydrocarbons. Based on the results, it can be concluded that catalytic pyrolytic oil can be used as transportation fuel after suitably blending with diesel.

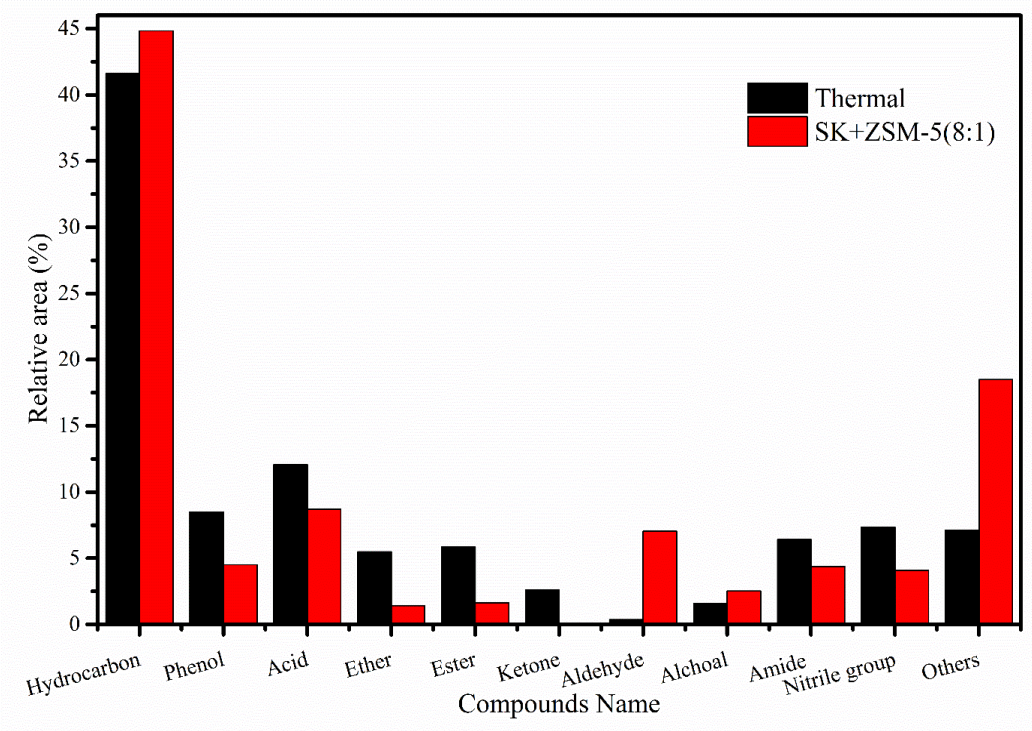

Fig. 5.19. GC-MS analysis of thermal and catalytic pyrolytic oil at 8:1 B/C ratio

Chapter 6

Thermal and Catalytic Pyrolysis of Neem seed and Waste Nitrile Gloves

6.1. Thermocatalytic Co-pyrolysis of Biomass and Waste Plastic

Non-edible neem seeds (NM) and waste nitrile gloves (WNG) were co-pyrolyzed to understand the effect of synergistic effect during conversion between biomass and waste plastic. Also, two low-cost catalysts, CaO and Al_2O_3 were used to observe the effect of a catalyst on pyrolytic products yield and pyrolytic oil properties.

6.1.1. Characterization of Neem seeds and Waste nitrile gloves

Physicochemical characterization of NM and WNG along with that of jatropha seeds [224], castor seeds [62], pine nut shells, scrap tires [233], polyethylene terephthalate, and low-density polyethylene [234] is presented in Table 6.1. The results confirmed that NM and WNG had a high content of volatile matter (77.20 % and 93.63 %, respectively) and low ash content (3.16 % and 5.57 %, respectively), indicating high ignition efficiency. The lower ash content also reduces the slagging and fouling indices, which enhances boiler operation. In addition, ash content is inversely related to the heating value, indicating that NM and WNG have a high heating value. Further, the low moisture (<10 %) of NM and WNG makes them suitable candidates for pyrolysis. The calculated moisture, volatile matter, and ash contents were similar to those of other reported biomass in Table 6.1. NM and WNG were also found to have a high carbon content (51.36 % and 75.99 %, respectively), indicating a high burning capacity, as well as 7.36 % and 8.26 % hydrogen content, respectively. WNG showed a high nitrogen content (6.34 %), which increased the content of nitrogen-containing compounds in the pyrolytic liquid, as revealed by the GC-MS analysis. NM showed a higher oxygen content (36.68 %) than WNG (9.41%), indicating that the blending of NM and WNG reduced the oxygen content and enhanced the pyrolytic liquid properties. Our results showed that NM has a lower heating value (23.19 MJ kg^{-1}) than WNG (36.89 MJ kg^{-1}), probably because of their high moisture content and low carbon content. The compositional analysis of NM confirmed the presence of hemicellulose (22.94 %), cellulose (40.04 %), and lignin (10.58 %). Further, the extractive analysis of NM confirmed high amounts of extractives (37.24 %), indicating the generation of high liquid yield during pyrolysis. The composition and extractive analysis results of NM are consistent with those of other reported biomass presented in Table 6.1.

Table 6.1. Physicochemical characterization of NM and WNG along with other biomass and plastics waste

Analysis	Neem seeds (present work)	Waste Nitrile Gloves (present work)	Jatropha seed [224]	Castor seed [62]	Pine nut Shells [233]	Scrap tires [233]	Polyethylene terephthalate [234]
Proximate analysis (wt.%)							
Moisture	7.32±0.02	0.66±0.02	7.5±0.12	7.24	7.85	0.88	0.22
Volatile matter	75.20±0.03	93.63±0.33	77.1±0.95	65.21	72.06	66.51	86.75
Ash content	2.16±0.02	5.57±0.03	5.9±0.55	4.22	1.46	4.48	6.83
Fixed carbon	15.42±0.02	0.14±0.02	9.4±0.53	23.33	18.63	28.13	6.2
Ultimate analysis (wt.%)							
C	51.36	75.99	53.7	48.96	52.04	87.04	63.94
H	7.36	8.26	8.0	5.52	6.95	7.94	4.52
O	36.68	9.41	27.9	42.61	40.64	2.81	31.49
N	3.89	6.34	4.5	2.79	0.29	0.75	0.01
S	0.7	-	-	0.12	0.08	1.46	0.04

Heating value* (MJ/kg)	23.19±0.1	36.89	24.0±0.24		18.50	38.60	-
Bulk density (kg/m^3)	600.05±3.5	428.29			-	-	-
Compositional analysis (wt. %)							
Hemicellulose	25.94±0.28	-	-	4.6	6.90	-	-
Cellulose	43.04±0.16	-	-	46.95	41.42	-	-
Lignin	9.58±0.13	-	26.1	32.31	48.97	-	-
Total Extractives (wt. %)	39.24±0.60	-	44.6	16.07	1.36	-	-
Hexane	30.80±0.15	-	15.5		-	-	-
Ethanol	12.10 ± 0.45	-	29.1		-	-	-

* heating value was determine on dry basis.

6.2. Thermal Analysis

Thermal degradation of NM and WNG were carried out in a thermogravimetric analyzer under non-isothermal condition. The thermal degradation pattern is shown in Fig. 6.1. The results confirmed that NM biomass underwent three major degradation stages, such as drying, devolatilization (active pyrolytic zone), and char formation stage. In the first stage (up to 150 °C), water molecules and low-molecular-weight compounds got removed. However, negligible weight loss was observed up to 300 °C, which indicated that WNG was thermostable up to 300 °C and have almost negligible moisture. In the second stage (150 °C - 550 °C), 73.13 % of NM decomposed, and during 300 °C - 600 °C, 85.90 % of WNG decomposed. This decomposition occurred due to the evaporation of light organic compounds and other heavy carbonaceous organic compounds. An additional 3.63 % and 5.76 % weight loss of NM and WNG occurred at 550 °C and 600 °C, respectively. In case of NM, hemicellulose and cellulose were the major compounds that decomposed in the second stage (150 °C - 550 °C), and in the third stage at <550 °C, lignin decomposed at a slower rate. In the DTG thermograph in Fig. 6.1, the first peak appeared due to the removal of water molecules and light volatile compounds, which was missing in DTG of WNG. However, 2.16 % decomposition was observed in WNG which may have occurred due to the removal of low-molecular-weight compounds. In the second stage of NM, two peaks were observed due to the decomposition of hemicellulose and cellulose. In this stage, high-molecular-weight compounds fragmented into low-molecular-weight compounds due to continuous heat supply. A similar pattern was also obtained at 300 °C - 600 °C, as shown in WNG thermograph. In the third stage, lignin of NM and high-molecular-weight compounds of WNG decomposed at a higher temperature.

6.3. Synergistic Effect and Reactivity of NM+WNG along with Catalysts in Different Ratios

Synergistic interactions occurred during co-pyrolysis due to the high reactivity of the biomass and the presence of higher amounts of volatile matter in it. Moreover, the presence of metals in the biomass and catalysts causes synergistic effects on the biomass because these metals function as catalysts and enhance the pyrolysis reactions [235]. Synergistic interactions occurred during co-pyrolysis due to the high reactivity of the biomass and the presence of higher amounts of volatile matter in it.

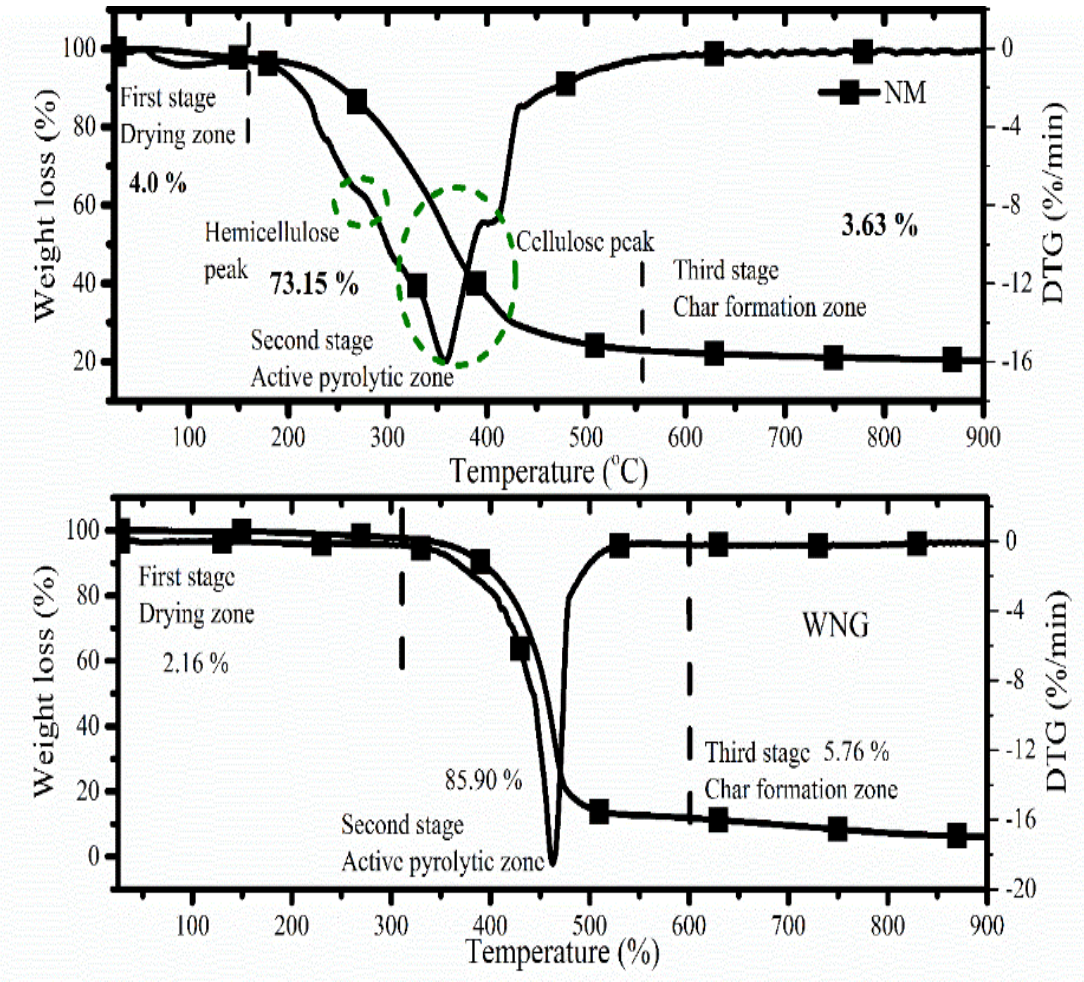

Fig. 6.1. TGA and DTG analysis of neem seeds (NM), and waste nitrile gloves (WNG)

Moreover, the presence of metals in the biomass and catalysts causes synergistic effects on the biomass because these metals function as catalysts and enhance the pyrolysis reactions [235]. The comparison of the non-catalytic and catalytic blending of NM and WNG at different proportions is shown in Fig. 6.2. The figure shows that the ΔW value of the blends first decreased and then increased rapidly as the temperature increased. When the temperature was between 220 °C and 365 °C, the ΔW value was negative (<0), indicating a negative synergistic effect. Further, the ΔW value became positive when the temperature exceeded 410 °C, indicating a positive synergistic effect. Among the NM+WNG blending ratios (1:1, 3:1, and 5:1), the interaction between NM and WNG at 3:1 was positive, indicating a positive synergistic effect between NM and WNG, which confirmed the formation of higher amounts of volatile matter (negative synergistic effect indicated reduced formation of volatile matter) [236]. At the final temperature, the $W_{expt.}$ value was larger than the $W_{calc.}$ value, indicating that

a lower amount of volatile matter was formed during the entire degradation process due to the positive synergistic effect. Blending of NM+WNG with the catalyst at different proportions (3:1, 5:1, and 8:1) showed a positive synergistic effect, causing the formation of high amounts of volatile matter. Further, the ΔW value was positive at a lower temperature, as opposed to that in non-catalytic blending. The catalytic blending showed that NM+WNG(3:1)+CaO(3:1) and NM+WNG(3:1)+CaO (5:1) was higher than NM+WNG(3:1) +CaO(8:1); however, although NM+WNG (3:1)+CaO (3:1) and NM+WNG(3:1)+CaO(8:1) affected the properties of the pyrolytic liquid, only NM+WNG(3:1)+CaO(5:1) had a considerable effect. A similar result was found for NM+WNG(3:1)+Al_2O_3(5:1). Therefore, NM+WNG(3:1)+CaO(5:1) and NM+WNG (3:1)+Al_2O_3 (5:1) were considered as the optimal ratios for further experiments.

6.4. FTIR Analysis of Raw Sample

The wavenumber vs. transmittance spectra is plotted and presented in Fig. 6.3. The peak at 3296 cm^{-1} - 3616 cm^{-1} indicated the presence of water, aromatics, acids, phenols, and proteins in the biomass, which was ascribed to the axial deformation of -OH groups [45]. The peak at 2929 cm^{-1} was attributed to the C-H_2 and C-H_3 asymmetric and symmetric vibrations, which confirmed the presence of alkanes [45]. Further, the peak at 1720 cm^{-1} is attributed to the C=O stretching vibration, indicating the presence of ketone, carbonyl, and aliphatic groups in the biomass [215]. The peak at 1153 cm^{-1} was attributed to the symmetric deformation of CH_2 groups, indicating the presence of alkenes in the biomass [216]. The peaks at 1038 cm^{-1} and 714 cm^{-1} indicated the presence of aromatic compounds.

6.5. Process Parameter Optimization and Co-Pyrolysis

For finding out the optimal pyrolysis conditions, 400 °C, 450 °C, 500 °C, 550 °C, and 600 °C temperatures were used; the heating rates of 50 °C min^{-1}, 80 °C min^{-1}, and 100 °C min^{-1} were used; the particle size of biomass was maintained at >1.0 mm; and the sweeping gas flow rate was maintained 100 mL min^{-1}. The optimization of process parameters, such as temperature and heating rate, is presented in Fig. 6.4. The results showed that maximum liquid yield [43.52 ±2.20 wt.% for NM+WNG (3:1)] was achieved at 500 °C. At lower temperatures of 400 °C and 450 °C, liquid and gas yields were lower than char yield due to partial or incomplete pyrolysis (release of less volatiles), which occurred due to lower heat and mass transfer. However, by increasing the temperature from 450 °C to 500 °C, the liquid yield increased from 39.10 wt.% to 43.52 wt.% due to increased heat and mass transfer between biomass and waste plastic particles.

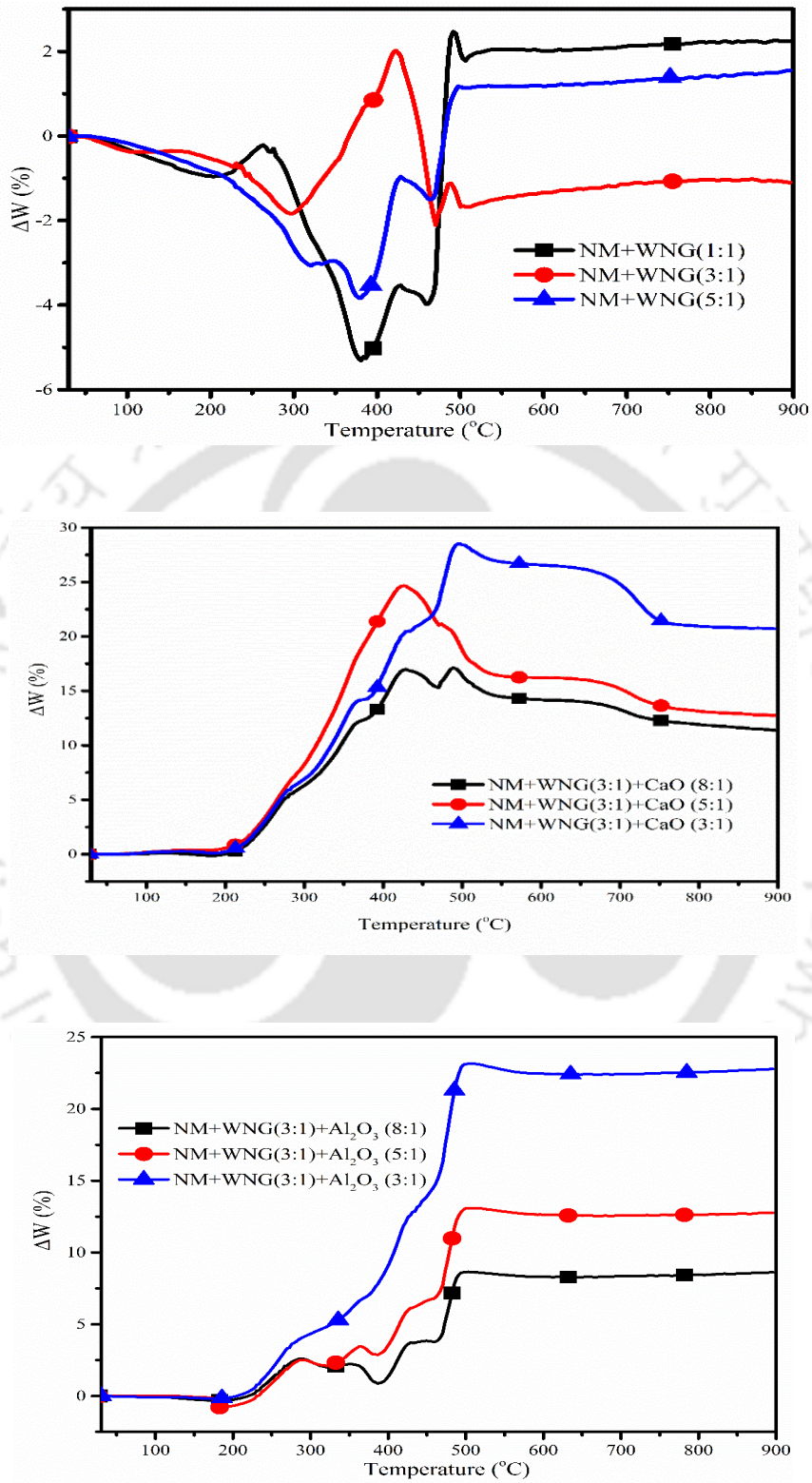

Fig. 6.2. Synergistic effect of NM+WNG(1:1, 3:1 and 5:1), NM+WNG(3:1)+CaO(3:1, 5:1 and 8:1) and, NM+WNG(3:1)+Al_2O_3(3:1, 5:1 and 8:1)

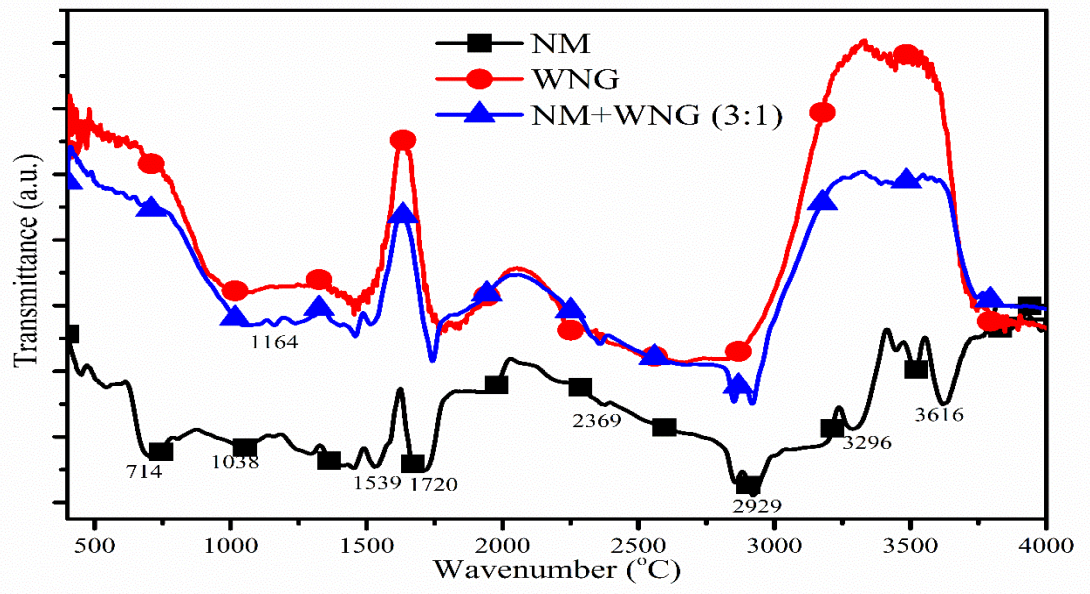

Fig. 6.3. FTIR analysis of raw NM, WNG and NM+WNG(3:1)

Further increase in the temperature from 500 °C to 600 °C decreased the liquid and char yields due to rapid biomass fragmentation (due to rapid heat transfer), which increased the formation of non-condensable gases and consequently decreased the liquid yield. The present results are inconsistent with previous studies by Wang et al. (2010) [213] and Wang and Brown (2013) [214].

The heating rate also significantly affected the pyrolytic liquid yield. Fig. 6.4 shows that a low heating rate (50 °C min^{-1}) reduced the liquid yield and increased the char yield due to incomplete biomass pyrolysis (low heat and mass transfer). Further, by increasing the heating rate from 50 °C min^{-1} to 80 °C min^{-1}, the liquid yield increased [40.96 wt.% to 43.52 wt.% for NM+WNG (3:1)] and the char yield decreased (27.99 wt.% to 24.0 wt.%). At the heating rate of 80 °C min^{-1}, the maximum volatile matter was released due to sufficient heat and mass transfer, leading to increased liquid yield and decreased char yield. Further, increase in heating rate from 80 °C min^{-1} to 100 °C min^{-1} reduced the liquid yield from 43.52 wt.% to 39.48 wt.% and increased the gas yield from 32.55 % to 38.56 %. The use of high heating rate results in rapid fragmentation (high rate of heat and mass transfer) of biomass, leading to the formation of non-condensable gases, thereby increasing the gas yield and reducing the liquid yield. The present results are also inconsistent with those of previous studies by Wang et al. (2010) [213] and Wang and Brown (2013) [214]. The particle size of biomass (<1.0 mm) and the sweeping gas flow rate (100 mL min^{-1}) were kept constant throughout the experiment. Based on these results, the temperature of 500 °C, a heating rate of 80 °C min^{-1}, the particle

size of <1.0 mm, and sweeping gas flow rate of 100 mL min^{-1} were considered as optimal pyrolysis condition.

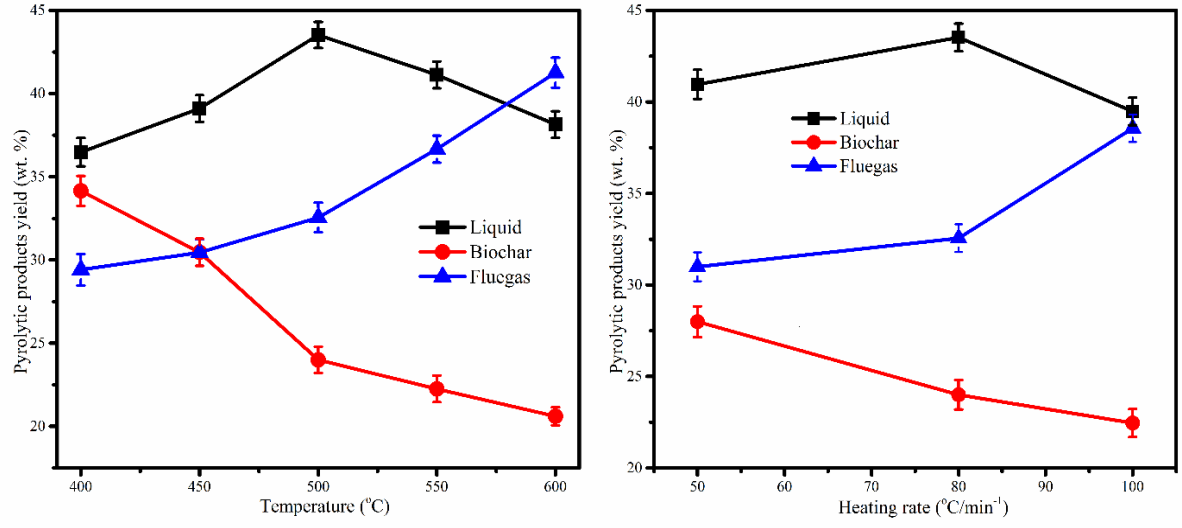

Fig. 6.4. Effect of temperature and heating rates on pyrolytic products yield

6.6. Effect of Catalyst on Thermal Decomposition Profile of NM+WNG at Different Ratios

Catalysts were used to increase the quality and yield of the pyrolytic liquid because the thermal pyrolytic liquid has various drawbacks, such as high oxygen content, high viscosity, and low calorific value. Moreover, the use of catalysts at an appropriate ratio reduces the thermal degradation temperature, which reduces the energy cost. Fig. 6.5(a) shows that the use of the optimal catalyst ratio significantly reduced the thermal degradation temperature in our study. Fig. 6.5(a) showed that the first peak appeared at 357 °C, 335 °C, 342 °C, and 349 °C and the second peak appeared at 408 °C, 455 °C, 456 °C, and 457 °C for NM, NM+WNG(3:1), NM+WNG(3:1)+CaO(5:1), and NM+WNG(3:1)+Al_2O_3(5:1), respectively. The results demonstrated that the blending of WNG with the NM biomass also reduced the thermal degradation temperature (335 °C and 456 °C for the first and second peaks, respectively). Further, it is known that the use of catalysts boosts the reaction rate, promoting material decomposition at lower temperatures. Catalysts may also attack the active site of biomass or waste, leading to decomposition at lower temperatures. In this study, catalytic co-pyrolysis of NM+WNG was performed at different catalytic ratios (3:1, 5:1, and 8:1). The results (Fig. 6.5 b) confirmed that compared with the liquid yield (43.52 %) by thermal co-pyrolysis, the catalytic co-pyrolysis of NM+WNG at optimized conditions reduced the co-pyrolytic liquid

yield [40.42 % ± 2.03 % and 37.14 % ± 1.41 % for CaO(5:1) and Al_2O_3(5:1), respectively]. A high B/C ratio (3:1) may make the active site inaccessible, thus, reducing the liquid yield and increasing the char yield, whereas a low B/C ratio (8:1) may not enhance the reaction rate, which also reduces the liquid yield.

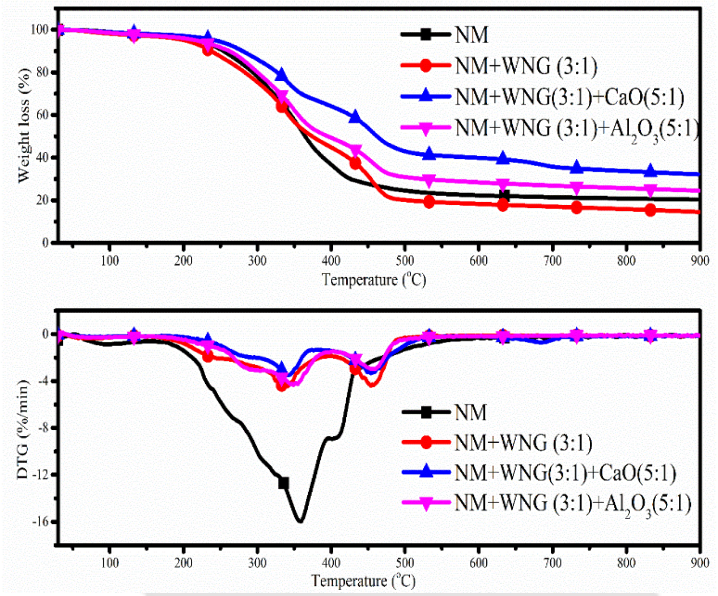

(a)

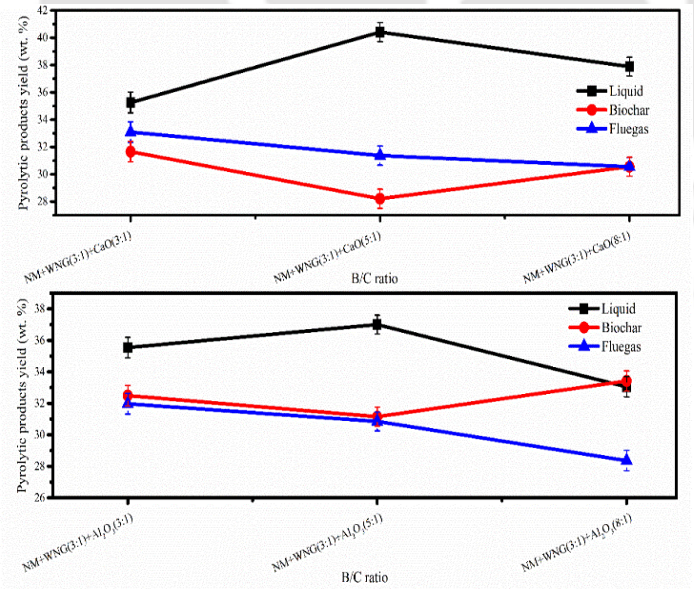

(b)

Fig. 6.5. (a) Effect of catalysts on NM, NM+WNG(3:1), NM+WNG(3:1)+CaO(5:1) and NM+WNG(3:1)+Al_2O_3(5:1), (b) Effect of catalyst of co-pyrolytic products yield

6.7. Physicochemical Characterization of Pyrolytic Oil

Physicochemical characteristics of thermal and catalytic co-pyrolytic oil obtained at optimal conditions in this study along with those of Karanja+Polystyrene (8:1), Niger+Polystyrene (8:1) [112] and palm shell+Polystyrene (40:60 - 60:40) [111] co-pyrolytic oil is presented in Table 6.2. The results showed that the oxygen content significantly reduced, and the carbon content increased by thermal pyrolysis of NM+WNG(3:1) and that the use of catalysts (CaO and Al_2O_3) further reduced the oxygen content and increased the carbon content resulting in increased heating value and ignition efficiency of the fuel, respectively [111]. The carbon and oxygen contents of the pyrolytic oil are inconsistent with those of other previously reported fuels as evident from Table 6.2. NM pyrolytic oil had a low heating value (25.48 MJ kg^{-1}) due to a high oxygen content (33.11 %), and the mixing of WNG at an appropriate ratio increased the heating value (34.15 MJ kg^{-1}). However, co-pyrolytic oil of NM+WNG(1:1) had higher viscosity (due to a high carbon-to-hydrogen ratio) than that of NM+WNG(3:1), making it unsuitable for engine or boiler application. Further, the use of catalysts CaO and Al_2O_3 at 5:1 B/C ratio significantly increased the heating value of the fuel (40.36 MJ kg^{-1} and 39.21 MJ kg^{-1}, respectively), which became closer to that of diesel fuel (45.00 MJ kg^{-1}). NM pyrolytic oil showed higher acidity (4.87), which may lead to corrosion problems in both vessels and piping systems, whereas the co-pyrolytic and catalytic oils showed lower acidity (7.5 - 9.5). The presence of acids (mainly acetic and formic acid) in the pyrolytic oil reduces the heating value. Further, NM pyrolytic oil demonstrated a higher density (976 kg m^{-3}) than the co-pyrolytic oil (868 kg m^{-3}) and catalytic co-pyrolytic oil (772 kg m^{-3} for CaO and 754 kg m^{-3} for Al_2O_3). These increased densities of NM+WNG(3:1) co-pyrolytic and catalytic co-pyrolytic oil suggest that a smaller area is needed for oil storage compared to that of the large land needed for dumping waste. NM pyrolytic liquid showed a high viscosity (47.56 cSt), which decreased with the addition of WNG (3:1) and the catalysts CaO and Al_2O_3(5:1) (Table 6.2). However, the co-pyrolytic oil of NM+WNG (1:1) showed higher viscosity (68.98 cSt) than NM pyrolytic oil. The degradation of inorganic compounds in WNG may have contributed to the higher viscosity. Further, the NM pyrolytic oil showed higher moisture (1.3) than the co-pyrolytic oil (1.0); the catalytic co-pyrolytic oil showed even higher moisture (1.8 and 1.7 for CaO and Al_2O_3). These results indicated that NM+WNG significantly reduced the moisture, thus, increasing the heating value of the co-pyrolytic oil. The carbon content of the co-pyrolytic oil was also found to be high, consistent with the carbon contents previously reported (Table 6.2).

Table 6.2. Characterization of NM, co-pyrolytic and catalytic pyrolytic oil

Analysis	NM	(NM+WNG (3:1) (present work)	NM+WNG (3:1)+CaO (5:1) (present work)	NM+WNG (3:1)+Al_2O_3 (5:1) (present work)	Palm shell+ Polystyrene [111]	Karanja+Polystyrene (8:1) [112]	Niger+Polystyrene (8:1) [112]
C (%)	53.36	74.12	82.56	83.47	81.34	-	-
H (%)	9.36	7.02	7.14	7.04	7.79	-	-
O (%)	32.68	13.18	7.09	6.31	10.50	-	-
N (%)	3.89	5.68	3.21	3.18	0.38	-	-
S (%)	0.70	-	-	-	-	-	-
Heating value (MJ/kg)	25.48±1.2	34.15±1.6	40.36±1.4	39.21±1.2	40.34	26.53[a]	29.77[a]
Viscosity (cSt)	47.56±1.8	29.45±1.4	21.59±1.9	19.89±2.0	8.28	12.84	11.20
Density (Kg/m^3)	976.0±2.3	868.0±2.4	772.0±1.8	754.0±2.0	10.58	0.98 (mg/cc)	0.85(mg/cc)
Acidity (-)	4.87±1.2	5.58±1.1	9.5±1.6	7.5±1.2	2.8	7.57	8.21
Moisture (%)	1.3±0.2	1.0±0.6	1.8±0.2	1.7±0.2	1.9	0.0	0.0
Ash content (wt. %)	0.49±0.02	0.43±0.03	0.28±0.01	0.35±0.02	-	1.71	1.13

6.8. FTIR Analysis of Pyrolytic Oil

FTIR spectroscopy results of the thermal, co-pyrolytic, and catalytic co-pyrolytic liquids is presented in Fig. 6.6. The peak at 3749 cm^{-1} - 3293 cm^{-1} represents the presence of -OH groups, indicating the presence of water, phenols, protein, and water in the pyrolytic oil [45]. The peak at 2919 cm^{-1} indicated the presence of alkane and saturated aliphatic groups, whereas the peak at 1700 cm^{-1} - 1600 cm^{-1} (1646 cm^{-1}) confirmed the presence of C=O stretching vibration, indicating the presence of acid groups (mainly carboxylic and formic acid), aldehydes, ketones, and esters. The peak at 1454 cm^{-1} showed the presence of C-H bending vibration, CH_2, and CH_3 bending vibration, indicating the presence of alkanes [216]. The peak at 1281 cm^{-1} - 1160 cm^{-1} indicated the presence of alcohol. The peak at 1036 cm^{-1} - 950 cm^{-1} represents the presence of aromatic C-H plane bending. Lastly, the peaks at 735 cm^{-1} and 622 cm^{-1} indicated the presence of aromatic compounds in the pyrolytic oil.

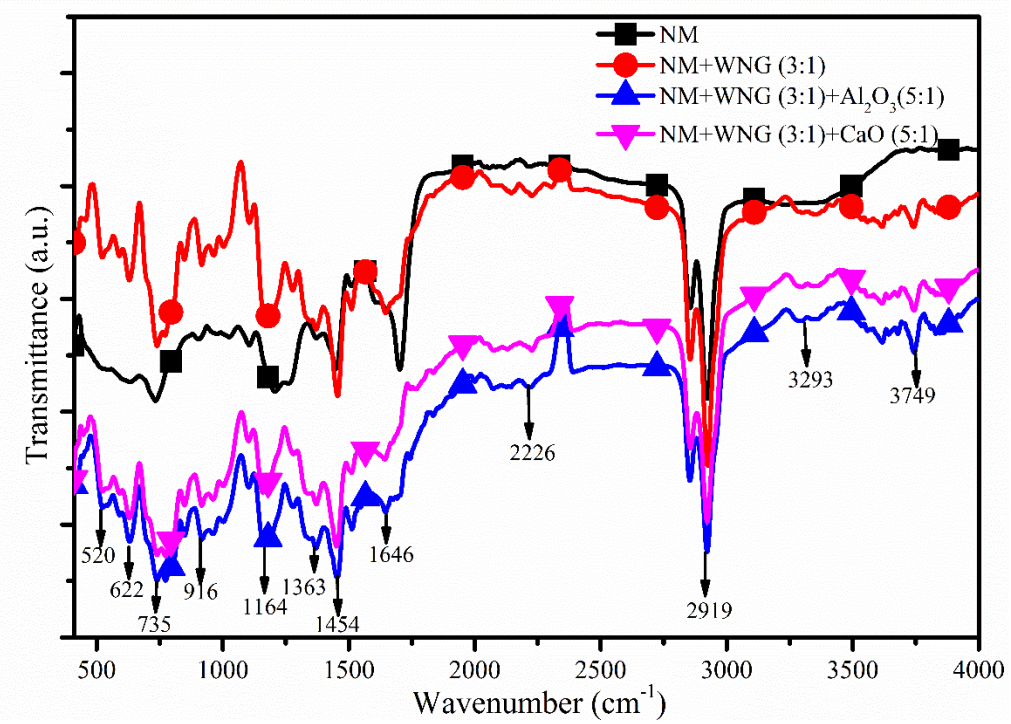

Fig. 6.6. FTIR analysis of thermal, co-pyrolytic and catalytic co-pyrolytic oil

6.9. ^{1}H NMR Analysis of Pyrolytic Oil

The quantification of product composition of NM, NM+WNG(3:1), NM+WNG(3:1)+CaO(5:1), and NM+WNG(3:1)+Al_2O_3(5:1) pyrolytic products was performed using ^{1}H NMR with Myers's correlation (1975b) [174], and the results are presented in Fig. 6.7. The product composition revealed by ^{1}H NMR analysis is reported in Table 6.3.

The results indicated that the paraffin content was higher (29.94 % - 83.87 %) than the aromatic (11.34 % - 26.62 %) and olefin (4.94 % - 53.48 %) contents. Table 6.3 showed that the aromatic content was slightly higher in the co-pyrolytic oil than in the NM pyrolytic oil. The presence of nitrogen in WNG might have led to increased aromatic content. The results are inconsistent with those reported by Das and Tiwari (2018) [237]. Further, the H/C ratio (2.27) was high in the NM pyrolytic oil, probably because of the high paraffin content of NM. The iso-paraffin index was lower for the NM pyrolytic oil than for the co-pyrolytic and catalytic co-pyrolytic oil. This difference was primarily due to the presence of high olefin content in the co-pyrolytic and catalytic pyrolytic oil.

Table 6.3. The product distribution of blending of non-catalytic and catalytic pyrolytic oil through ^{1}H NMR analysis

Sample	Aromatic, Vol. %	Paraffins, vol. %	Olefins, vol. %	H/C	Iso-paraffins Index
NM	11.34	83.87	4.93	2.27	0.27
NM+WNG(3:1)	25.78	52.05	22.49	1.55	3.15
NM+WNG (3:1)+CaO(5:1)	26.62	70.04	3.65	1.65	1.94
NM+WNG (3:1)+Al_2O_3(5:1)	17.06	29.94	53.47	1.32	2.10

6.10. GC-MS Analysis of Pyrolytic Oil

The chromatograms obtained from the thermal pyrolysis, co-pyrolysis, and catalytic co-pyrolysis of NM and WNG at optimized conditions [NM, NM+WNG(3:1), NM+WNG(3:1)+CaO(5:1), and NM+WNG(3:1)+Al_2O_3(5:1)] were compared with those of the compounds from the NIST library (Fig. 6.8). The pyrolytic oil is a complex mixture that is highly oxygenated and contains large-sized molecules of almost all species of oxygenated organics, such as esters, ethers, aldehydes, ketones, phenols, carboxylic acids, amide group, and alcohols [238]. The results demonstrated that the thermal pyrolysis of NM produced undesirable components such as esters, ethers, and acids, and nitrogen-containing groups.

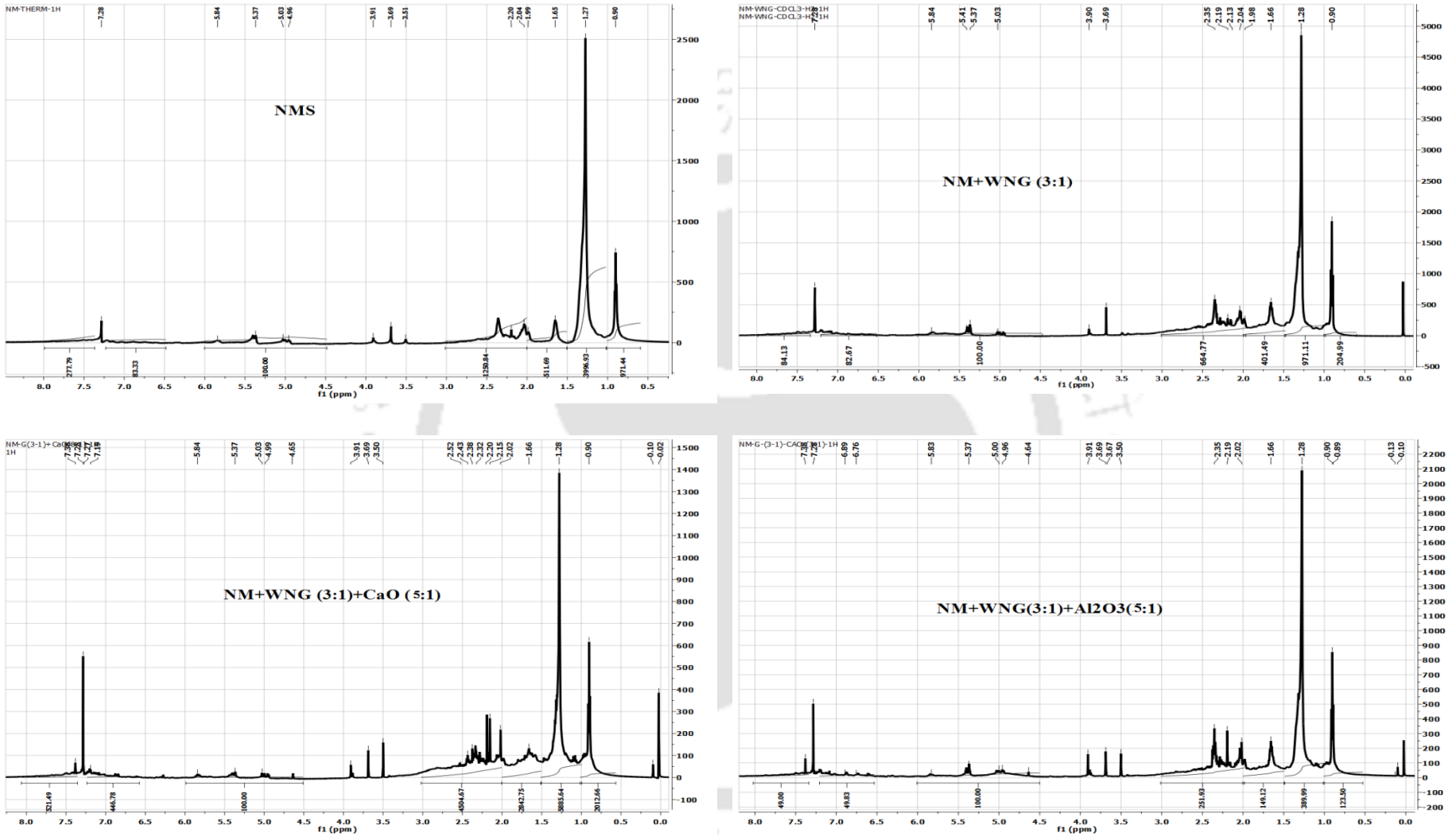

Fig. 6.7. NMR analysis of thermal and catalytic co-pyrolytic oils

In this study, the NM pyrolytic oil showed the maximum percentage of phenols, which is considered as an important raw material for extracting various chemicals. Fig. 6.8 showed that the NM pyrolytic oil has 17.74 % aromatic hydrocarbon content and 16.11 % hydrocarbon content, which makes it suitable for such applications. Further, the co-pyrolysis of NM+WNG (3:1) significantly increased the contents of aromatic hydrocarbons (37.24 %) and nitrogen-containing compounds, whereas reduced those of phenols (15.34 %) and hydrocarbons (10.95 %). It also significantly reduced the content of oxygenated compounds. Use of catalysts CaO and Al_2O_3 at an optimal ratio significantly enhanced the properties of the pyrolytic oil. The use of CaO and Al_2O_3 reduced the content of oxygenated compounds, such as acids (2.91 % and 3.24 %), esters (2.92 % and 0.72 %), ethers (3.78 % and 4.07 %), and ketones (3.58 % and 0.67 %, respectively). At the same time, the amounts of useful compounds, such as aldehydes (4.29 % and 2.58 %) and alcohol (5.38 % and 7.11 %, respectively) increased significantly by catalytic co-pyrolysis compared with that by thermal pyrolysis or NM+WNG co-pyrolysis. The use of catalysts at optimal ratio also significantly reduced the content of nitrogen-containing compounds (3.25 % and 2.35 % for CaO and Al_2O_3, respectively), which makes the pyrolytic oil suitable for use as a transportation fuel.

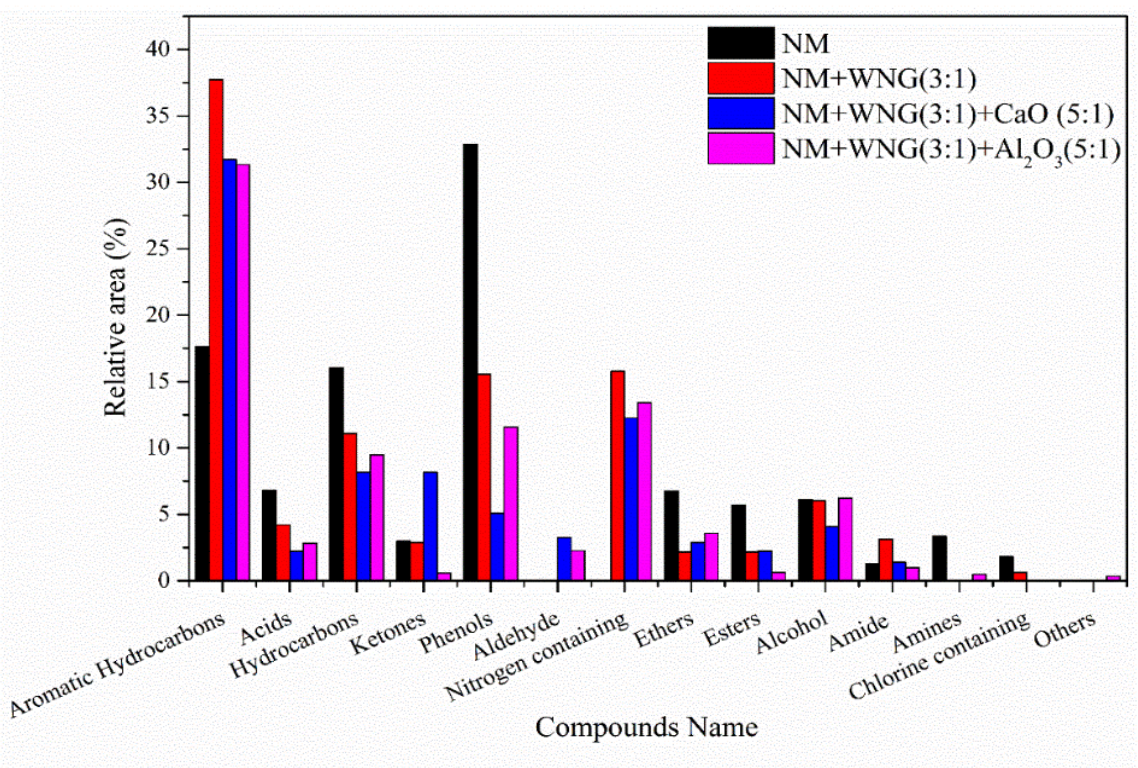

Fig. 6.8. GC-MS analysis of pyrolytic oil (a) NM, (b) NM+WNG(3:1), (C) NM+WNG(3:1)+CaO(5:1), and (d) NM+WNG(3:1)+Al_2O_3(5:1)

Chapter 7

Characterization of Biochar

7. Characterization of Biochar

In this section, Pine sawdust char (PWC), Sal sawdust char (SWC), Areca nut husk char (ANC), *Cascabela thevetia* seed char (SKC), *Delonix regia* seed char (SGC), *Manilkara zapota* seed char (CKC), *Azadirachta indica* seed char (NMC), and *Madhuca longifolia* seed char (MHC) were characterised which were obtained from pyrolysis at optimized conditions (500 ^{o}C temperature, 80 ^{o}C min^{-1} heating rate, 0.5 mm particle size and 100 mL min^{-1} sweep gas flow rate). The characterization of all these selected biochar was done based on their physical and chemical properties.

7.1. Thermal Analysis

Thermal analysis of all selected biochar are presented in Fig. 7.1. It was noticed that biochar decomposed into three major steps: drying (30 ^{o}C - 120 ^{o}C), maximum decomposition (120 ^{o}C - 700 ^{o}C), and char formation or passive stage (>700 ^{o}C). From Fig. 7.1, it was noticed that temperature up to 120 ^{o}C, moisture, and light volatile matter were removed in the first stage. In this stage, all biochar had <10 % moisture (9.23 %, 2.7 %, 1.51 %, 2.1 %, 3.23 %, 3.0 %, 2.8 %, and 3.18 % for PWC, SWC, ANC, SGC, NMC, MHC, CKC and SKC respectively) which make it an ideal feedstock for combustion and pyrolysis while biochar AWAC had higher moisture content (15.84 %) due to its hydrophilic nature. Further, in the second stage, known as the maximum decomposition stage where 60.85 %, 15.47 %, 11.49 %, 14.99 %, 18.99 %, 20.05 %, 39.28 %, 9.30 % and 5.14 % for PWC, SWC, ANC, SGC, NMC, MHC, CKC SKC and AWAC degradation took place due to fragmentation of higher molecular weight compounds into lower molecular weight compounds. In the final stage, decomposition occurred at higher temperature with slower rate which indicated the formation of maximum char. TGA analysis confirmed that all biochar produced had higher fixed carbon which was also confirmed by proximate analysis. The results are in good agreement with the results of Missio et al. (2014) and Yargicoglu et al. (2015) [123, 239].

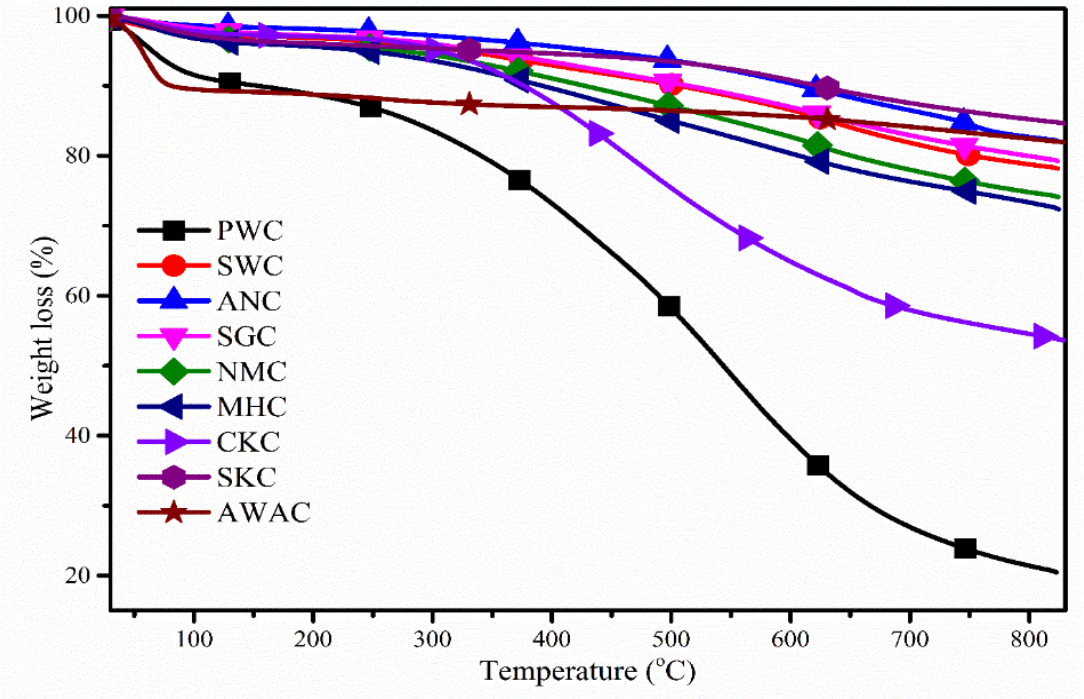

Fig. 7.1. Thermal analysis of biochars obtained from pyrolysis of selected biomass

7.2. Organic Matter, Proximate and Elemental Analysis

The proximate and elemental analysis of all biochar is presented in Table 7.1. From the table, it was confirmed that organic matter of all biochar varied from 12.74 % - 28.04 % which showed that these biochar can be used for soil amendments. Among all biochar, areca nut husk char (ANC) contained lower organic matter (12.74 %) while mahua seed char (MHC) contained higher organic matter (28.04 %). Further, it was also observed that all biochar had <10 % moisture (2.56 % - 21.81 %) which indicated that burning of biochar would be the easier and calorific value of the fuel will be higher. Volatile matter of all the biochars were varied from 16.69 % - 40.08 % which suggested that the ignition efficiency would be higher during combustion. Ash content was found slightly higher which varied from 7.86 % - 21.50 % which had a negative impact on the heating value of biochar. Ash content has an inverse relationship to the heating value of char which means that higher the ash content, lower will be the heating value. Fixed carbon also varied from 36.92 % - 62.12 %. The volatile matter to fixed carbon ratio (VM/FC) also varied from 0.306 - 1.007. Our results are inconsistent with other reported studies [123].

Ultimate analysis of all the biochars are also reported in Table 7.1. It can be seen that; carbon content was higher (51.42 % - 85.55 %) which indicated the higher ignition efficiency of these chars. Biochars activated with acids had higher carbon content (85.55 %) than those

not treated with acids. Further, the oxygen content was found to be slightly higher (12.96 % - 42.34 %) which has a negative impact as solid fuel. From results, it was also noticed that all biochars had lower nitrogen content (0.34 % - 4.12 %), however, sulpher was absent which indicated SO_x and NO_x gases will be lesser during combustion. All the biochar had higher heating value varied from 21.78 MJ kg^{-1} - 30.65 MJ kg^{-1} which indicated their burning potential. Moreover, biochars can be used as solid fuel in domestic heating and cooking due to higher heating value. The obtained results are in good agreement with other biochars reported in the literature [123].

7.3. Particle Size, Zeta Potential, Acidity (pH), Oxidation and Reduction Potential (ORP) and Electrical Conductivity (EC) of Biochars

The particle size analysis of biochars are reported in Table 7.1. From the table, it was confirmed that all the biochars had a smaller particle size (21.29 nm - 3895.7 nm) which were smaller to those reported by Yargicoglu et al. (2015) [123]. However, it is important to mention that the particle size of biochar depends on the nature of pyrolysis and operating conditions. The smaller particle size of biochars indicates the higher surface area of biochars [123]. From results, it was noticed that CKC biochar had 3895.7 nm particle size which leads to higher surface area (20.26 m^2 g^{-1}) as compared to other biochars reported in Table 7.1. Further, zeta potential varied from (-28.57 mV to - 46.87 mV) which showed that these biochars could be used as bio-adsorbents for the removal of various pollutants from water and wastewater. It was reported that higher the negative zeta potential, higher will be the removal of pollutants [123]. The acidity of acid treated biochars were lower (4.26) while without treated biochar had a higher acidity (7.78 - 9.96), however, oxidation-reduction potential was found to be significant (-269 mV to -332 mV). The electrical conductivity of all biochars were also varied from 280 uS - 1972 uS. The acid treated biochar had lower electrical conductivity (280 uS) where CKC biochar had higher electrical conductivity (1972 uS). The electrical conductivity (EC) of biochar showed that these chars can be used for making superconductors [240]. EC depends on the effective interaction between all carbon particles. The closer the particles after expulsion of air from the pores, lesser the void space, higher is the electrical conductivity. Electrical conductivity of biochar was found to be highly dependent on its degree of carbonization [240]. Moreover, biochar if used as a solid fuel for combustion, then electrical conductivity is largely irrelevant and ignored [240].

7.4. Bulk Density and Specific Gravity

The bulk density of biochar is an essential property as it is directly related to biochar transportation and storage cost. From results (Table 7.1), it was confirmed that all the biochars had a lower bulk density (221 kg m^{-3} - 614 kg m^{-3}) which may create storage and transportation difficulties. Also, lower densities indicate higher integral properties of biochar [123]. The specific gravity of biochars varied from 0.221- 0.614. It was confirmed that biochar with the highest specific gravity had the lowest H:C ratio. Higher H:C ratio represents the charging intensity of biochar [241], this was likely due to the concentration of heavier biomass components (ash and metal) due to the greater extent of pyrolysis.

7.5. Water Holding Capacity and Surface Area Analysis

Water holding capacity (WHC) of all the biochars are listed in Table 7.1. From the results, it was noticed that WHC varied from 39.48 % - 61.60 % which indicated that it can be used for soil abetments and as fertilizers. Among all the biochars, PWC had higher WHC (61.60 %) while SKC had lower WHC (39.48 %). Surface analysis of biochars confirmed that all the biochars without acid treated had a lower surface area (1.64 m^2 g^{-1} - 20.26 m^2 g^{-1}) than acid treated biochar (873.21 m^2 g^{-1}). The lower surface area might be due to the poor construction of materials which can leads to difficulties for N_2 adsorption especially for coal and carbonaceous material [242]. The lower surface area indicated that these biochars cannot be used as bio-adsorbents. However, it is important to mention that selection of bio-adsorbents depends on various other parameters too.

Table 7.1. Physiochemical characterization of biochars obtained from pyrolysis at optimized condition

Types of analysis	PWC	SWC	ANC	SGC	MHC	NMC	SKC	CKC	ACWC
Proximate analysis (wt.%)									
Organic matter (LOI) (%)	17.78±0.80	19.05±0.60	12.74±1.1	27.42±1.0	28.04±0.6	19.45±0.80	19.56±1.1	14.38±1.2	21.08±1.3
Moisture	3.82±0.8	6.45±1.2	4.27±0.6	4.15±0.6	4.39±0.4	5.14±0.7	6.32±0.6	2.56±0.2	21.08±1.2
Volatile matter	40.08±1.0	28.33±1.2	22.83±1.2	33.08±0.8	37.19±1.2	34.14±1.6	36.12±1.4	25.32±0.9	16.69±0.6
Ash	12.18±0.6	12.25±0.4	10.78±0.3	16.40±1.0	21.50±1.1	13.18±0.6	12.45±0.8	10.62±0.6	7.86±0.4
Fixed carbon	43.92±0.6	52.97±0.5	62.12±0.4	46.37±0.3	36.92±0.6	47.54±0.4	45.11±0.6	61.5±1.2	54.37±1.2
VM/FC	0.912	0.534	0.367	0.713	1.007	0.718	0.8	0.411	0.306
Ultimate analysis (wt %)									
C	68.17	70.61	73.14	56.62	60.27	62.66	51.42	52.59	85.55
H	2.58	2.27	2.5	2.54	2.27	2.06	2.12	3.58	0.9
O	27.68	26.78	22.82	37.2	34.27	31.83	42.34	41.46	12.96
N	1.57	0.34	1.54	3.64	3.19	3.45	4.12	2.37	0.59
S	-	-	-	-	-	-	-	-	-
O/C	0.3	0.28	0.23	0.49	0.43	0.38	0.62	0.59	0.11
H/C	1.12	1.02	1.31	0.82	0.79	0.78	0.6	1.04	0.83
Heating value (MJ/kg)	26.73±1.2	30.65±1.4	28.21±1.1	21.78±1.2	24.68±1.4	23.14±1.2	22.63±1.2	24.76±1.3	24.77±1.4
Particle size (nm)	777.4±2.6	1282.1±2.8	708.6±1.6	871.7±1.8	770.1±1.8	631.4±1.6	857.4±1.6	3895.7±2.8	21.29±1.1

Zeta potential (mV)	-28.57±1.2	-29.60±2.0	-31.04±2.1	-30.84±2.2	-46.87±1.8	-31.68±1.8	-33.29±2.0	-30.97±2.4	-29.05±1.8
Bulk density (Kg/m^3)	267.0±2.6	257.0±1.6	280.0±1.8	585.0±2.4	512.0±2.4	478.0±1.8	614.0±2.6	547.0±1.8	221.0±1.2
Specific gravity	0.267	0.257	0.280	0.585	0.512	0.478	0.614	0.547	0.221
Water holding capacity (WHC) (%)	61.60±2.0	58.40±1.8	57.56±2.6	39.56±1.8	42.87±2.4	41.50±2.0	39.48±1.6	40.15±1.8	57.59±2.3
Acidity (-)	8.56±1.2	7.87±1.1	7.79±0.8	9.96±0.6	9.32±1.0	7.78±1.1	7.81±1.0	9.49±1.4	4.26±1.0
Oxidation reduction potential (mV)	-269±1.1	-274±0.9	-310±1.4	-290±1.2	-310±1.2	-297±1.6	-332±1.8	-294±1.2	-301±1.6
Electrical conductivity (uS)	426±1.6	339±1.8	1970±2.0	1966±2.0	1865±1.8	1798±1.6	540±1.0	1972±1.8	280±0.8
Surface area (m^2/g)	5.83±0.8	5.50±1.1	5.49±1.0	1.64±1.1	4.81±1.2	4.60±1.2	3.19±1.0	20.26±1.0	873.21±1.6

7.6. FESEM Analysis

FESEM analysis of all the biochars obtained at optimized pyrolysis condition is presented in Fig. 7.2. FESEM image was taken at various magnifications varied from 1.5 KX - 500 KX. From the results, it was confirmed that all the biochars varied with different pore sizes (7.97 µm, 44.0 µm, 2.76 µm, 37.13 µm, 4.52 µm, 6.16 µm, 2.39 µm, 31.23 µm, and 21.1 µm for PWC, SWC, ANC, SGC, NMC, MHC, CKC, SKC, and AWAC respectively). Moreover, these FESEM images look like honeycombs with varying pore diameter on the surface of biochars. It was also observed that AWAC biochar had a uniform and smooth surface area while other biochars had a rough and varying surface area. Fig. 7.2 confirmed that these pores are cross-linked and known as hardwood materials [243]. Since pyrolysis operating conditions are almost the same which did not affect the surface area and pore sizes of biochars, however, the structure of biomass may be one of the possible reason for varying surface and pore. From Fig. 7.2, it was confirmed that temperature 450 ^{o}C - 850 ^{o}C caused the formation of micropores which attributed to the phenomenon where micropores become filled with tars (condensed volatiles) and other decomposition products, partially blocking porosity [244].

7.7. Van Krevelen Diagram

A plot of Van-Krevelen diagram is shown in Fig. 7.3. It was confirmed that hydrogen to carbon ratio (H:C) varied from (0.60 - 1.31) which was similar to that reported by Yargicoglu et al. (2015) [123]. Higher hydrogen to carbon ratio of biochars showed easer ignition of the fuel. The atomic ratio of biochars were found to be in decreasing order as ANC>PWC>SWC>ACWA>MHC>SGC>CKC>SKC respectively. From Fig. 7.3, it was confirmed that among all the biochars, ANC had higher H:C ratio which indicated that burning of ANC as solid fuel will be much easier compared to other biochars.

7.8. Biochar Reactivity

Biochar reactivity was calculated from the molar ratio of O/C, H/C and VM/FC for each biochar sample and presented in Fig. 7.4. It was confirmed that volatile matter to fixed carbon ratio (VM: FC) varied from 0.31 % - 1.0 %. From the results (Fig. 7.4), it was confirmed that biochar that had a higher volatile matter to fixed carbon ratio was more reactive than having a lower volatile matter to fixed carbon ratio. In addition, these biochars showed better advantages over other biochars for utilization as solid fuel, biofuel, and chemicals.

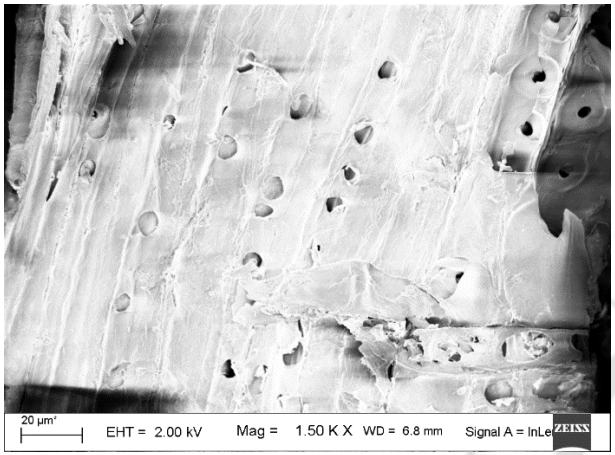

PWC

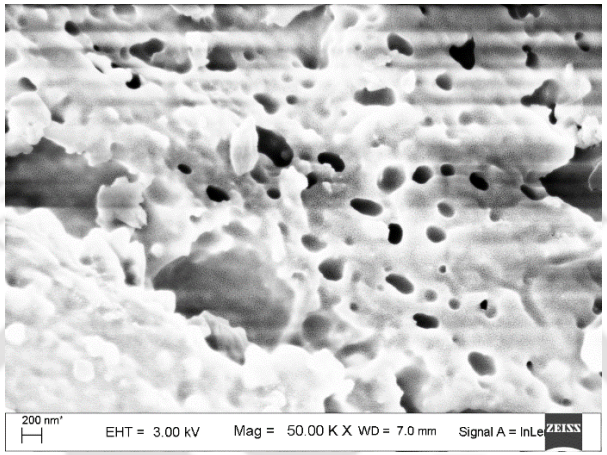

SWC

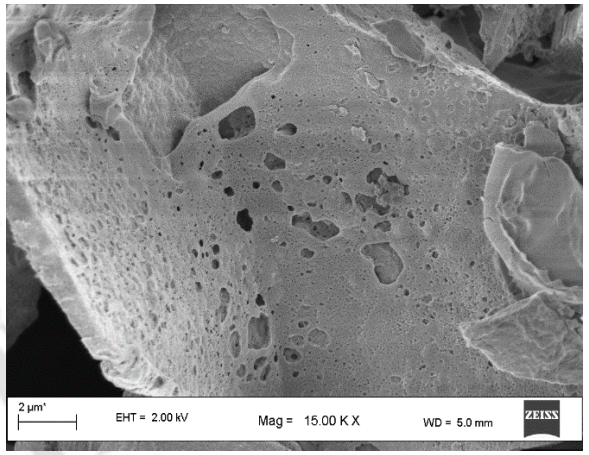

ANC

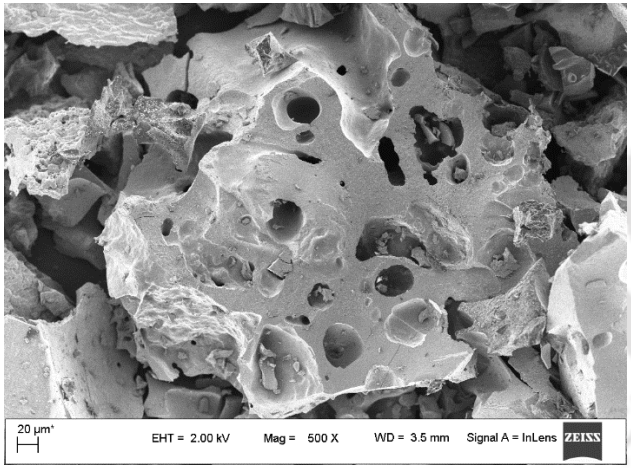

SGC

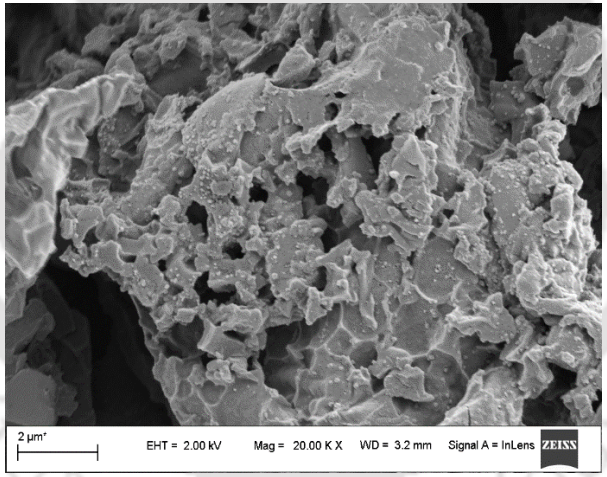

MHC

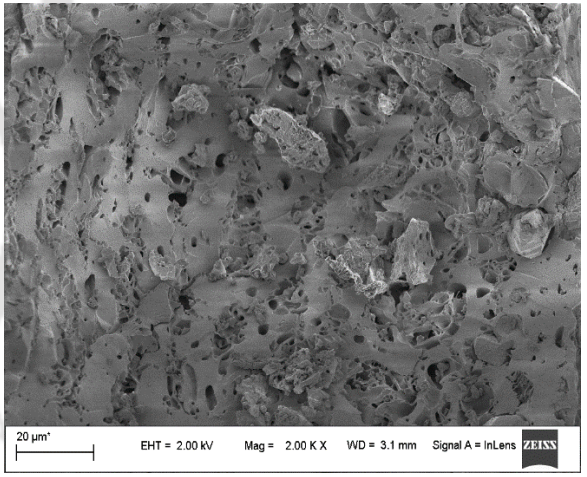

NMC

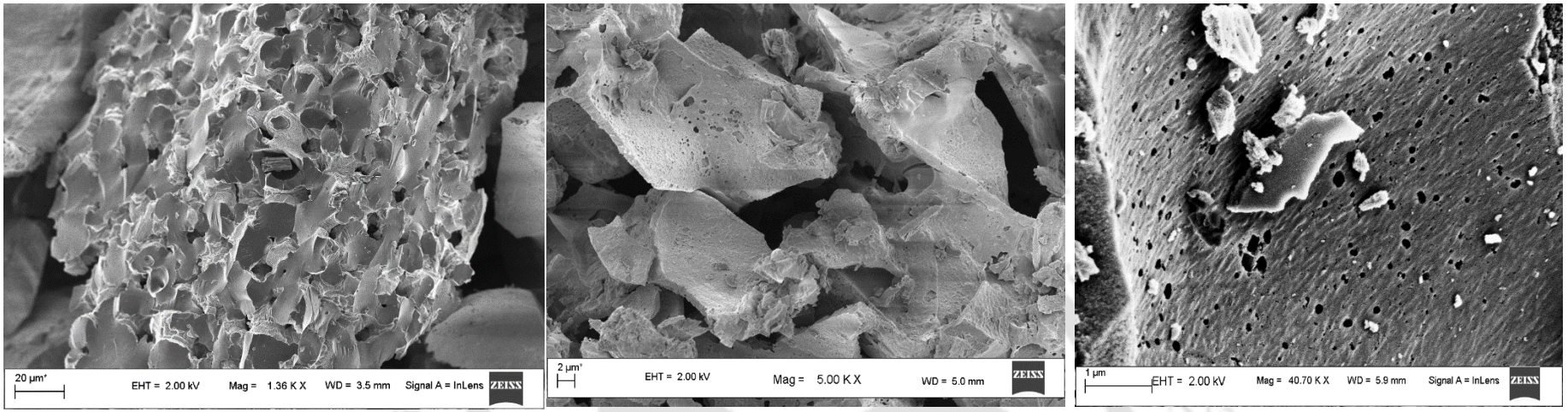

SKC CKC ACWA

Fig. 7.2. FESEM analysis of biochars obtained at optimized condition

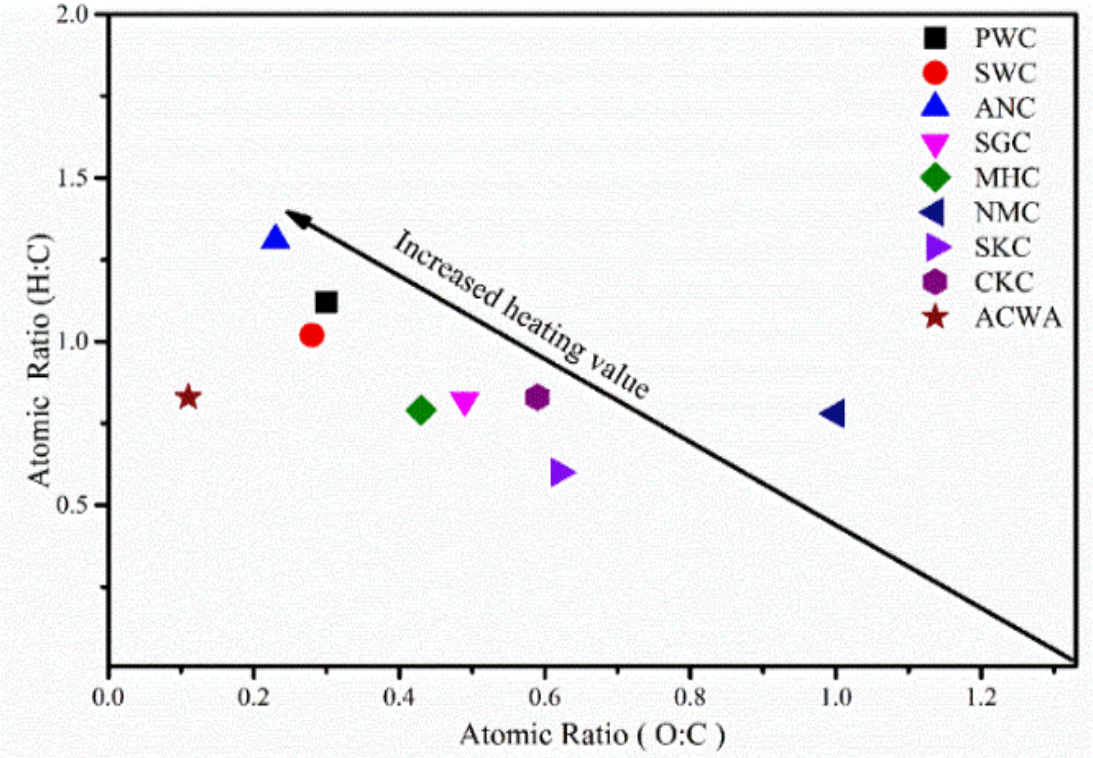

Fig. 7.3. Van-Krevelen diagram of biochars obtained from pyrolysis of selected biomass

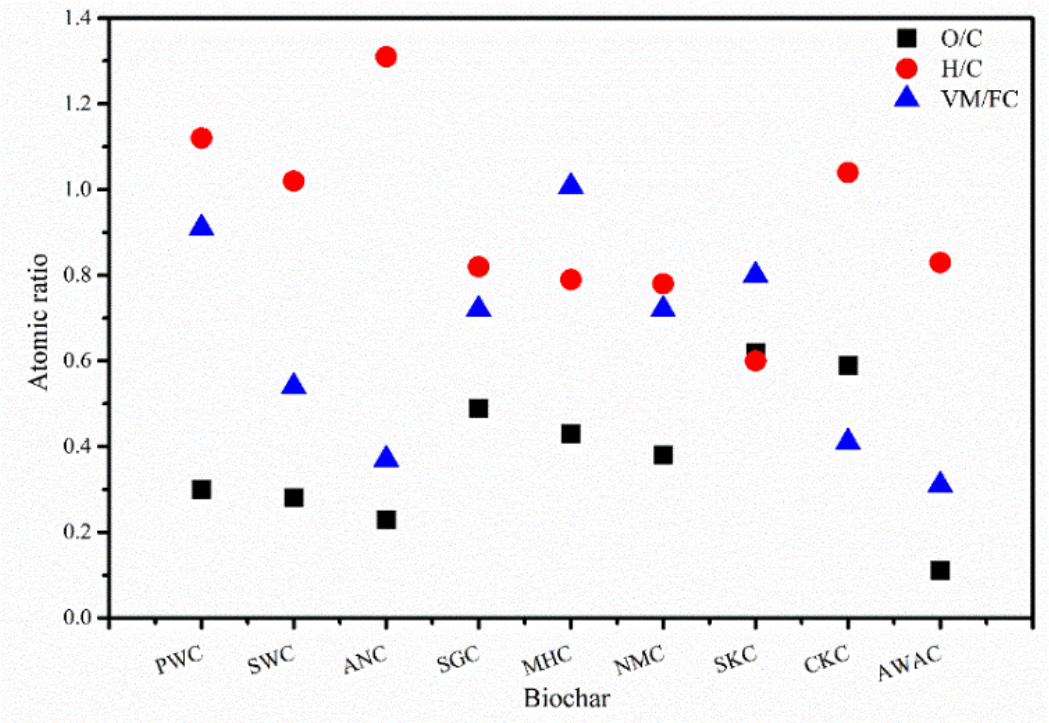

Fig. 7.4. Biofuel reactivity of biochar obtained from pyrolysisof slected biomass

7.9. FTIR Analysis of Biochar

FTIR analysis was used to identify the presence of useful functional groups. The wave number against transmittance plot is presented in Fig. 7.5. The peak 3432 cm^{-1} attributed with H-bonded O-H stretching vibrations of hydroxyl groups which confirmed the presence of alcohols, phenols, organic acids, and water [245-249]. Further, peak 2850 cm^{-1} - 2950 cm^{-1} associated with alkyl structures, and peak 1642 cm^{-1} attributed to C=C vibrations and N-H acids which represents aromatics, olefinic compounds [249] and amides [127]. Peak 1000 cm^{-1} - 1100 cm^{-1} showed bending of Si-O stretching while peak 1332 cm^{-1} showed O-H stretching of phenolic and acids compounds.

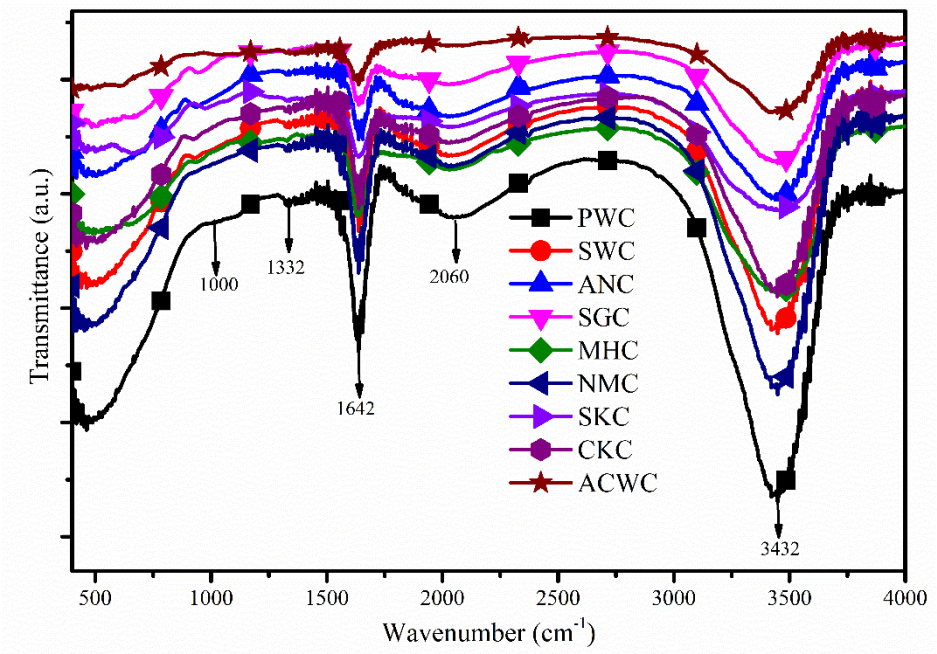

Fig. 7.5. FTIR analysis of biochars PWC, SWC, ANC, SGC, MHC, NMC, SKC, CKC and ACWC

Chapter 8

Conclusions and Recommendations for Future Study

8. Conclusions and Recommendations for Future Study

This chapter summarizes the inferences drawn from the present work and recommendations for future works.

8.1. Conclusions

The present study demonstrated potentials of *Cascabela thevetia* seeds, *Delonix regia* seeds, *Samanea saman* seeds, *Phyllanthus emblica* kernel, *Azadirachta indica* seeds, Manilkara *zapota* seed seeds, *Madhuca longifolia* seeds, *Pinus ponderosa* sawdust, *Shorea robusta* sawdust and *Areca catechu* husk towards the production of renewable fuel and value-added chemicals. Characterization revealed that all biomass have <10 % moisture, higher volatile matter (75.05 % - 79.03 %) and lower ash content (1.14 % - 3.26 %). Heating values and bulk densities of these biomass were found to be 17.10 MJ kg^{-1} - 24.50 MJ kg^{-1} and 249.56 kg m^3 - 657.41 kg m^3. The thermal analysis confirmed biomass decomposed into three main stages, however, their decomposition profile was altered which might be due to the composition of feedstocks. Chemical analysis of biomass confirmed that all biomass have lower lignin content while higher cellulose (30.81 % - 49.36 %) and hemicellulose (16.59 % - 27.22 %) content. FTIR analysis confirmed the presence of useful compounds such as phenols, aromatics, alcohol, ethers, ester, and acid. XRF analysis showed that the presence of useful inorganic compounds which acts as catalysts during pyrolysis.

Thermal analysis of selected biomass confirmed that with an increase in heating rate, degradation peak shifted towards higher region without altering decomposition behaviors. From results, it was confirmed that by increasing the rate of heating, the total volume of volatile products increased while at a lower rate of heating, volatiles was retained longer in the reactor which may change the product's composition. Furthermore, it was observed that activation energy increased up to a certain conversion value and then reduced. The variation of activation energy confirmed that during pyrolysis, the reaction does not follow the same reaction path, instead, it followed a multistep reaction path. The change in enthalpy, entropy, and Gibbs free energy confirmed the spontaneity of reactions, nature of the reaction process and reactivity of the reaction system. DSC analysis confirmed the evolution of moisture resulted in an exothermic peak whereas hemicellulose, cellulose, and lignin provided the endothermic peaks.

Thermal pyrolysis of PW, SW, AN, SG, SK, CK, NM, MH and SS biomass produced maximum liquid yield at optimum condition (500 ^{o}C, 80 ^{o}C min^{-1}, 0.5 mm - 1.0 mm particle size and 100 mL min^{-1} gas flow rate). Characterization results showed that thermal pyrolytic oil engaged with higher viscosity, higher oxygen content, and lower heating value which had a negative impact on pyrolytic oil. FTIR analysis confirmed the presence of aromatics, alcohols, water, proteins, alkenes, and acids while GC-MS confirmed the presence of phenols, acids, ethers, esters, alcohols, aromatics, hydrocarbons, amides and nitrogen-containing compounds.

Study of the effect of biomass bed thickness and distance between beds confirmed that pyrolytic liquid yield changed with the increase in number of biomass beds for a single bed, double bed, triple bed, fourth bed, fifth bed, and sixth bed. Results showed that *PW*, *SW*, and *AN* resulted in higher liquid yield in the fourth bed. Therefore, the fourth bed was considered as an optimum bed in the present study. Further, characterization results showed that the quality and quantity of pyrolytic oil was found to be better at the fourth bed. GC confirmed that with increasing temperature, the amount of hydrogen and hydrocarbons increased significantly and at the same time the formation of CO_2 was reduced.

Catalytic pyrolysis results confirmed that with varied B/C ratios from 3:1 - 10:1, the yield of pyrolytic liquid increased. However, it was noticed that at 3:1 B/C ratio, the yield of pyrolytic oil reduced but improved the properties of pyrolytic oil than 6:1, 8:1 and 10:1 B/C ratios. It was also noticed that B/C ratio 3:1 gave a higher grade fuel but lower liquid yield while at 8:1 higher liquid yield was observed. GC-MS analysis confirmed that the use of catalysts at optimized condition significantly reduced the oxygenated compounds and increased the percentage of alcohol and hydrocarbons.

Co-pyrolysis of waste nitrile gloves with biomass seems one of the prominent ways to reduce waste and increased the economy. Physicochemical results of NM and WNG confirmed their potential towards the production of fuels and value-added chemicals. The synergistic effect confirmed that the value of ΔW becomes positive when the temperature reached beyond 410 ^{o}C, demonstrated the positive synergistic effect. Among blending ratio NM+WNG (1:1, 3:1, and 5:1), the interaction between NM+WNG(3:1) was positive which indicated good synergistic effect between NM and WNG. Similarly, NM+WNG(3:1)+CaO(5:1) and NM+WNG(3:1)+Al_2O_3(5:1) also resulted in a higher synergistic effect. It was noticed that co-pyrolysis of NM and WNG increased the liquid yield along with enhanced properties of fuels.

Introduction of catalysts enhanced the properties of fuels. FTIR analysis confirmed the presence of useful functional groups while NMR analysis confirmed the maximum amount of paraffin and aromatics. GC-MS analysis of all pyrolytic oils revealed a reduction in oxygenated compounds, acids, and an increase in alcohol and aldehyde.

The characterization of biochars confirmed the presence of higher organic matter, volatile matter, and carbon content. Further, gross heating value and bulk density of biochars were found to be 21.78 MJ kg^{-1} - 30.65 MJ kg^{-1} and 221 kg m^{-3} - 614 kg m^{-3}. The characterized biochars showed high variability in surface area 1.64 m^2 g^{-1} - 20.26 m^2 g^{-1}, zeta potential -28.57 mV to -46.87 mV, and water holding capacity 39.48 % - 61.60 %. The morphology of all biochars varied with different sizes (7.97 µm, 44.0 µm, 2.76 µm, 37.13 µm, 4.52 µm, 6.16 µm, 2.39 µm, 31.23 µm, and 21.1 µm for *PWC*, *SWC*, *ANC*, *SGC*, *NMC*, *MHC*, *CKC*, *SKC*, and *AWAC* respectively).

8.2. Recommendations for Future Investigation

The current study emphasizes the utilization of biomass towards the production of fuel and valuable chemicals. Based on the present study following work to be carried out in the future,

- Development and scale-up of new pyrolyzer for production of higher liquid yield.
- To develop a new mathematical model to investigate the pyrolysis characteristics of biomass by using thermogravimetric analysis which produces minimum or negligible error.
- Development of new low-cost metal and zeolite catalysts for enhancing pyrolytic liquid yield and properties.
- Extraction of various useful chemicals such as acids and some hydrocarbons from the aqueous fraction of pyrolytic liquid.
- Investigation and performance evaluation of pyrolytic liquid fuel using an engine.
- Development of new routes for the better efficiency of utilization of char.
- Techno-economic analysis (*TEA*) and lifecycle assessments (*LCA*) of the pyrolysis process.

References

1. Dufour, A., *Thermochemical conversion of biomass for the production of energy and chemicals*. 2016: John Wiley & Sons.
2. Energy, S.R.o.W., *Statistical Review of World Energy* 2016.
3. Nigam, P.S. and A. Singh, *Production of liquid biofuels from renewable resources.* Progress in energy and combustion science, 2011. **37**(1): p. 52-68.
4. Chan, Y.H., et al., *An overview of biomass thermochemical conversion technologies in Malaysia.* Science of The Total Environment, 2019.
5. Mythili, R., et al., *Characterization of bioresidues for biooil production through pyrolysis.* Bioresource Technology, 2013. **138**: p. 71-78.
6. Singh, N., A. Kumar, and S. Rai, *Potential production of bioenergy from biomass in an Indian perspective.* Renewable and Sustainable Energy Reviews, 2014. **39**: p. 65-78.
7. Park, J., et al., *Slow pyrolysis of rice straw: Analysis of products properties, carbon and energy yields.* Bioresource Technology, 2014. **155**: p. 63-70.
8. Burra, K. and A. Gupta, *Kinetics of synergistic effects in co-pyrolysis of biomass with plastic wastes.* Applied Energy, 2018. **220**: p. 408-418.
9. Bridgwater, A., *Production of high grade fuels and chemicals from catalytic pyrolysis of biomass.* Catalysis Today, 1996. **29**(1): p. 285-295.
10. Czernik, S. and A. Bridgwater, *Overview of applications of biomass fast pyrolysis oil.* Energy & fuels, 2004. **18**(2): p. 590-598.
11. Park, C.S., P.S. Roy, and S.H. Kim, *Current developments in thermochemical conversion of biomass to fuels and chemicals*, in *Gasification for Low-grade Feedstock.* 2018, IntechOpen.
12. Duman, G., et al., *The slow and fast pyrolysis of cherry seed.* Bioresource Technology, 2011. **102**(2): p. 1869-1878.
13. Shadangi, K.P. and K. Mohanty, *Thermal and catalytic pyrolysis of Karanja seed to produce liquid fuel.* Fuel, 2014. **115**: p. 434-442.
14. Onay, O. and O.M. Kockar, *Slow, fast and flash pyrolysis of rapeseed.* Renewable Energy, 2003. **28**(15): p. 2417-2433.
15. Singh, R. and K. Shadangi, *Liquid fuel from castor seeds by pyrolysis.* Fuel, 2011. **90**(7): p. 2538-2544.
16. Nayan, N.K., S. Kumar, and R. Singh, *Production of the liquid fuel by thermal pyrolysis of neem seed.* Fuel, 2013. **103**: p. 437-443.

17. Alagu, R. and E.G. Sundaram, *Preparation and characterization of pyrolytic oil through pyrolysis of neem seed and study of performance, combustion and emission characteristics in CI engine.* Journal of the Energy Institute, 2016.
18. Shadangi, K.P. and K. Mohanty, *Comparison of yield and fuel properties of thermal and catalytic Mahua seed pyrolytic oil.* Fuel, 2014. **117**: p. 372-380.
19. Das, S., J.A. Priess, and C. Schweitzer, *Biofuel Options for India—Perspectives on Land Availability, Land Management and Land-Use Change.* Journal of Biobased Materials and Bioenergy, 2010. **4**(3): p. 243-255.
20. Shadangi, K.P. and K. Mohanty, *Characterization of nonconventional oil containing seeds towards the production of bio-fuel.* Journal of Renewable and Sustainable Energy, 2013. **5**(3): p. 033111.
21. Kumar, A., et al., *A review on biomass energy resources, potential, conversion and policy in India.* Renewable and Sustainable Energy Reviews, 2015. **45**: p. 530-539.
22. Chiranjeevi, P., S. Dahiya, and N. Kumar, *Waste derived bioeconomy in India: A perspective.* New biotechnology, 2018. **40**: p. 60-69.
23. Butler, E., et al., *A review of recent laboratory research and commercial developments in fast pyrolysis and upgrading.* Renewable and Sustainable Energy Reviews, 2011. **15**(8): p. 4171-4186.
24. Mohan, D., C.U. Pittman, and P.H. Steele, *Pyrolysis of wood/biomass for bio-oil: a critical review.* Energy & fuels, 2006. **20**(3): p. 848-889.
25. Ganesh, A. and R. Banerjee, *Biomass pyrolysis for power generation—a potential technology.* Renewable Energy, 2001. **22**(1): p. 9-14.
26. Mohan, D., et al., *Organic and inorganic contaminants removal from water with biochar, a renewable, low cost and sustainable adsorbent–a critical review.* Bioresource Technology, 2014. **160**: p. 191-202.
27. Huang, Y.-F., et al., *Microwave pyrolysis of rice straw to produce biochar as an adsorbent for CO2 capture.* Energy, 2015. **84**: p. 75-82.
28. Dhyani, V. and T. Bhaskar, *A comprehensive review on the pyrolysis of lignocellulosic biomass.* Renewable Energy, 2017.
29. Zhang, B., M. von Keitz, and K. Valentas, *Thermochemical liquefaction of high-diversity grassland perennials.* Journal of Analytical and Applied Pyrolysis, 2009. **84**(1): p. 18-24.

30. Berndes, G., M. Hoogwijk, and R. Van den Broek, *The contribution of biomass in the future global energy supply: a review of 17 studies.* Biomass and Bioenergy, 2003. **25**(1): p. 1-28.
31. Vamvuka, D., et al., *Pyrolysis characteristics and kinetics of biomass residuals mixtures with lignite☆.* Fuel, 2003. **82**(15-17): p. 1949-1960.
32. Collard, F.-X. and J. Blin, *A review on pyrolysis of biomass constituents: Mechanisms and composition of the products obtained from the conversion of cellulose, hemicelluloses and lignin.* Renewable and Sustainable Energy Reviews, 2014. **38**: p. 594-608.
33. Akhtar, J. and N.S. Amin, *A review on operating parameters for optimum liquid oil yield in biomass pyrolysis.* Renewable and Sustainable Energy Reviews, 2012. **16**(7): p. 5101-5109.
34. Bridgwater, A.V., *Review of fast pyrolysis of biomass and product upgrading.* Biomass and Bioenergy, 2012. **38**: p. 68-94.
35. Pakdel, H., C. Roy, and W. Kalkreuth, *Oil production by vacuum pyrolysis of Canadian oil shales and fate of the biological markers.* Fuel, 1999. **78**(3): p. 365-375.
36. Raveendran, K. and A. Ganesh, *Heating value of biomass and biomass pyrolysis products.* Fuel, 1996. **75**(15): p. 1715-1720.
37. Uzoejinwa, B.B., et al., *Co-pyrolysis of biomass and waste plastics as a thermochemical conversion technology for high-grade biofuel production: Recent progress and future directions elsewhere worldwide.* Energy Conversion and Management, 2018. **163**: p. 468-492.
38. Johansson, A.-C., et al., *Co-pyrolysis of woody biomass and plastic waste in both analytical and pilot scale.* Journal of Analytical and Applied Pyrolysis, 2018. **134**: p. 102-113.
39. CRIQUI, P., et al., *World Energy Scenarios.* Shared Analysis Project: Economic Foundations for Energy Policy, Volume, (2).
40. Agarwal, A.K., *Biofuels (alcohols and biodiesel) applications as fuels for internal combustion engines.* Progress in Energy and Combustion Science, 2007. **33**(3): p. 233-271.
41. Demirbaş, A., *Biomass resource facilities and biomass conversion processing for fuels and chemicals.* Energy Conversion and Management, 2001. **42**(11): p. 1357-1378.

42. Verrastro, F. and S. Ladislaw, *Providing energy security in an interdependent world.* Washington Quarterly, 2007. **30**(4): p. 95-104.
43. Sharma, Y. and B. Singh, *Development of biodiesel from karanja, a tree found in rural India.* Fuel, 2008. **87**(8-9): p. 1740-1742.
44. Islam, A.K.M.A., S.R.P. Primandari, and Z. Yaakob, *Non-Edible Vegetable Oils as Renewable Resources for Biodiesel Production: South-East Asia Perspective*, in *Advances in Biofuels and Bioenergy*. 2018, IntechOpen.
45. Doshi, P., et al., *Physicochemical and thermal characterization of nonedible oilseed residual waste as sustainable solid biofuel.* Waste Management, 2014. **34**(10): p. 1836-1846.
46. Nanda, S., et al., *Characterization of North American lignocellulosic biomass and biochars in terms of their candidacy for alternate renewable fuels.* Bioenergy Research, 2013. **6**(2): p. 663-677.
47. Sasmal, S., V.V. Goud, and K. Mohanty, *Characterization of biomasses available in the region of North-East India for production of biofuels.* Biomass and Bioenergy, 2012. **45**: p. 212-220.
48. Kumar, M., S. Upadhyay, and P. Mishra, *A comparative study of thermochemical characteristics of lignocellulosic biomasses.* Bioresource Technology Reports, 2019: p. 100186.
49. Naik, S., et al., *Characterization of Canadian biomass for alternative renewable biofuel.* Renewable Energy, 2010. **35**(8): p. 1624-1631.
50. Raj, T., et al., *Physical and chemical characterization of various Indian agriculture residues for biofuels production.* Energy & Fuels, 2015. **29**(5): p. 3111-3118.
51. Damartzis, T., et al., *Thermal degradation studies and kinetic modeling of cardoon (Cynara cardunculus) pyrolysis using thermogravimetric analysis (TGA).* Bioresource Technology, 2011. **102**(10): p. 6230-6238.
52. White, J.E., W.J. Catallo, and B.L. Legendre, *Biomass pyrolysis kinetics: a comparative critical review with relevant agricultural residue case studies.* Journal of Analytical and Applied Pyrolysis, 2011. **91**(1): p. 1-33.
53. Heydari, M., M. Rahman, and R. Gupta, *Kinetic study and thermal decomposition behavior of lignite coal.* International Journal of Chemical Engineering, 2015. **2015**.
54. Mehmood, M.A., et al., *Pyrolysis and kinetic analyses of Camel grass (Cymbopogon schoenanthus) for bioenergy.* Bioresource Technology, 2017. **228**: p. 18-24.

55. Ceylan, S., Y. Topcu, and Z. Ceylan, *Thermal behaviour and kinetics of alga Polysiphonia elongata biomass during pyrolysis.* Bioresource Technology, 2014. **171**: p. 193-198.
56. Huang, X., et al., *Pyrolysis kinetics of soybean straw using thermogravimetric analysis.* Fuel, 2016. **169**: p. 93-98.
57. Varma, A.K. and P. Mondal, *Physicochemical characterization and pyrolysis kinetic study of sugarcane bagasse using thermogravimetric analysis.* Journal of Energy Resources Technology, 2016. **138**(5): p. 052205.
58. Chandrasekaran, A., S. Ramachandran, and S. Subbiah, *Determination of kinetic parameters in the pyrolysis operation and thermal behavior of Prosopis juliflora using thermogravimetric analysis.* Bioresource Technology, 2017. **233**: p. 413-422.
59. Oladokun, O., et al., *Multicomponent devolatilization kinetics and thermal conversion of Imperata cylindrica.* Applied Thermal Engineering, 2016. **105**: p. 931-940.
60. Zhang, Z., et al., *Thermo-physical properties of pretreated agricultural residues for bio-hydrogen production using thermo-gravimetric analysis.* International Journal of Hydrogen Energy, 2016. **41**(10): p. 5234-5242.
61. Ma, Z., et al., *Determination of pyrolysis characteristics and kinetics of palm kernel shell using TGA–FTIR and model-free integral methods.* Energy Conversion and Management, 2015. **89**: p. 251-259.
62. Santos, N.A., et al., *Kinetic study of pyrolysis of castor beans (Ricinus communis L.) presscake: an alternative use for solid waste arising from the biodiesel production.* Energy & Fuels, 2015. **29**(4): p. 2351-2357.
63. Ceylan, S. and Y. Topçu, *Pyrolysis kinetics of hazelnut husk using thermogravimetric analysis.* Bioresource Technology, 2014. **156**: p. 182-188.
64. Xu, L., Y. Jiang, and L. Wang, *Thermal decomposition of rape straw: Pyrolysis modeling and kinetic study via particle swarm optimization.* Energy Conversion and Management, 2017. **146**: p. 124-133.
65. Rony, A.H., et al., *Kinetics, thermodynamics, and physical characterization of corn stover (Zea mays) for solar biomass pyrolysis potential analysis.* Bioresource Technology, 2019.
66. Uçar, S. and S. Karagöz, *The slow pyrolysis of pomegranate seeds: the effect of temperature on the product yields and bio-oil properties.* Journal of Analytical and Applied Pyrolysis, 2009. **84**(2): p. 151-156.

67. Garcia-Perez, M., et al., *Fast pyrolysis of oil mallee woody biomass: effect of temperature on the yield and quality of pyrolysis products.* Industrial & Engineering Chemistry Research, 2008. **47**(6): p. 1846-1854.
68. Pütün, E., *Catalytic pyrolysis of biomass: Effects of pyrolysis temperature, sweeping gas flow rate and MgO catalyst.* Energy, 2010. **35**(7): p. 2761-2766.
69. Ozbay, N., A.E. Pütün, and E. Pütün, *Bio-oil production from rapid pyrolysis of cottonseed cake: product yields and compositions.* International Journal of Energy Research, 2006. **30**(7): p. 501-510.
70. Gibbins-Matham, J. and R. Kandiyoti, *Coal pyrolysis yields from fast and slow heating in a wire-mesh apparatus with a gas sweep.* Energy & fuels, 1988. **2**(4): p. 505-511.
71. Seebauer, V., J. Petek, and G. Staudinger, *Effects of particle size, heating rate and pressure on measurement of pyrolysis kinetics by thermogravimetric analysis.* Fuel, 1997. **76**(13): p. 1277-1282.
72. Yorgun, S., S. Şensöz, and Ö. Koçkar, *Flash pyrolysis of sunflower oil cake for production of liquid fuels.* Journal of Analytical and Applied Pyrolysis, 2001. **60**(1): p. 1-12.
73. Haykiri-Acma, H., *The role of particle size in the non-isothermal pyrolysis of hazelnut shell.* Journal of Analytical and Applied Pyrolysis, 2006. **75**(2): p. 211-216.
74. Bridgwater, A. and G. Peacocke, *Fast pyrolysis processes for biomass.* Renewable and Sustainable Energy Reviews, 2000. **4**(1): p. 1-73.
75. Encinar, J., J. Gonzalez, and J. Gonzalez, *Fixed-bed pyrolysis of Cynara cardunculus L. Product yields and compositions.* Fuel Processing Technology, 2000. **68**(3): p. 209-222.
76. Acıkgoz, C., O. Onay, and O. Kockar, *Fast pyrolysis of linseed: product yields and compositions.* Journal of Analytical and Applied Pyrolysis, 2004. **71**(2): p. 417-429.
77. Demiral, İ. and S. Şensöz, *Fixed-bed pyrolysis of hazelnut (Corylus avellana L.) bagasse: influence of pyrolysis parameters on product yields.* Energy Sources, Part A: Recovery, Utilization, and Environmental Effects, 2006. **28**(12): p. 1149-1158.
78. Olukcu, N., et al., *Liquefaction of Beypazari oil shale by pyrolysis.* Journal of Analytical and Applied Pyrolysis, 2002. **64**(1): p. 29-41.
79. Shadangi, K.P. and K. Mohanty, *Production and characterization of pyrolytic oil by catalytic pyrolysis of Niger seed.* Fuel, 2014. **126**: p. 109-115.

80. Li, H., P. Yu, and B. Shen, *Biofuel potential production from cottonseed oil: a comparison of non-catalytic and catalytic pyrolysis on fixed-fluidized bed reactor.* Fuel Processing Technology, 2009. **90**(9): p. 1087-1092.
81. Onay, O., *Fast and catalytic pyrolysis of pistacia khinjuk seed in a well-swept fixed bed reactor.* Fuel, 2007. **86**(10-11): p. 1452-1460.
82. Özbay, G., *Catalytic Pyrolysis of Pine Wood Sawdust to Produce Bio-oil: Effect of Temperature and Catalyst Additives.* Journal of Wood Chemistry and Technology, 2015. **35**(4): p. 302-313.
83. Chen, X., et al., *Fast pyrolysis of cotton stalk biomass using calcium oxide.* Bioresource Technology, 2017. **233**: p. 15-20.
84. Zhang, L., C.C. Xu, and P. Champagne, *Overview of recent advances in thermo-chemical conversion of biomass.* Energy Conversion and Management, 2010. **51**(5): p. 969-982.
85. Schroeder, P., et al., *Chemical and physical analysis of the liquid fractions from soursop seed cake obtained using slow pyrolysis conditions.* Journal of Analytical and Applied Pyrolysis, 2017. **124**: p. 161-174.
86. Pradhan, D., et al., *Pyrolysis of Mahua seed (Madhuca indica)–production of biofuel and its characterization.* Energy conversion and management, 2016. **108**: p. 529-538.
87. Rout, T.K., *Pyrolysis of coconut shell*. 2013.
88. Alper, K., K. Tekin, and S. Karagöz, *Pyrolysis of agricultural residues for bio-oil production.* Clean Technologies and Environmental Policy, 2015. **17**(1): p. 211-223.
89. Aysu, T. and H. Durak, *Catalytic pyrolysis of liquorice (Glycyrrhiza glabra L.) in a fixed-bed reactor: effects of pyrolysis parameters on product yields and character.* Journal of Analytical and Applied Pyrolysis, 2015. **111**: p. 156-172.
90. Chouhan, A.P.S., *A slow pyrolysis of cotton stalk (Gossypium arboretum) waste for bio-oil production.* J Pharm Chem Biol Sci, 2015. **3**: p. 143-149.
91. Majhi, A., et al., *The production and evaluation of bio-oil obtained from the Jatropha curcas cake.* Energy Sources, Part A: Recovery, Utilization, and Environmental Effects, 2015. **37**(16): p. 1782-1789.
92. Seal, S., et al., *Production and characterization of bio oil from cotton seed.* Environmental Progress & Sustainable Energy, 2015. **34**(2): p. 542-547.
93. Chutia, R.S., R. Kataki, and T. Bhaskar, *Characterization of liquid and solid product from pyrolysis of Pongamia glabra deoiled cake.* Bioresource Technology, 2014. **165**: p. 336-342.

94. Mohammed, T.H., et al., *Bio-oil from pyrolysis of castor shell.* Int J Basic Appl Sci, 2014: p. 1-5.
95. Singh, V., et al., *Pyrolysis of sal seed to liquid product.* Bioresource Technology, 2014. **151**: p. 432-435.
96. Sinha, R., S. Kumar, and R. Singh, *Production of biofuel and biochar by thermal pyrolysis of linseed seed.* Biomass Conversion and Biorefinery, 2013. **3**(4): p. 327-335.
97. Azduwin, K., et al., *Slow pyrolysis of Imperata cylindrica in a fixed bed reactor.* International Journal of Biological, Ecological, and Environment Science, 2012: p. 176-180.
98. Nayan, N.K., S. Kumar, and R. Singh, *Characterization of the liquid product obtained by pyrolysis of karanja seed.* Bioresource Technology, 2012. **124**: p. 186-189.
99. Ucar, S. and A.R. Ozkan, *Characterization of products from the pyrolysis of rapeseed oil cake.* Bioresource Technology, 2008. **99**(18): p. 8771-8776.
100. Onay, O., *Influence of pyrolysis temperature and heating rate on the production of bio-oil and char from safflower seed by pyrolysis, using a well-swept fixed-bed reactor.* Fuel Processing Technology, 2007. **88**(5): p. 523-531.
101. Onay, O. and O.M. Koçkar, *Pyrolysis of rapeseed in a free fall reactor for production of bio-oil.* Fuel, 2006. **85**(12): p. 1921-1928.
102. Onay, O. and O.M. Koçkar, *Fixed-bed pyrolysis of rapeseed (Brassica napus L.).* Biomass and Bioenergy, 2004. **26**(3): p. 289-299.
103. Beis, S., Ö. Onay, and Ö. Koçkar, *Fixed-bed pyrolysis of safflower seed: influence of pyrolysis parameters on product yields and compositions.* Renewable Energy, 2002. **26**(1): p. 21-32.
104. Pütün, A.E., E. Apaydin, and E. Pütün, *Bio-oil production from pyrolysis and steam pyrolysis of soybean-cake: product yields and composition.* Energy, 2002. **27**(7): p. 703-713.
105. Özbay, N., et al., *Biocrude from biomass: pyrolysis of cottonseed cake.* Renewable Energy, 2001. **24**(3-4): p. 615-625.
106. Şensöz, S., D. Angın, and S. Yorgun, *Influence of particle size on the pyrolysis of rapeseed (Brassica napus L.): fuel properties of bio-oil.* Biomass and Bioenergy, 2000. **19**(4): p. 271-279.
107. Tat, M.E. and J.H. Van Gerpen, *The specific gravity of biodiesel and its blends with diesel fuel.* Journal of the American Oil Chemists' Society, 2000. **77**(2): p. 115-119.

108. Bahadur, N.P., D.G. Boocock, and S.K. Konar, *Liquid hydrocarbons from catalytic pyrolysis of sewage sludge lipid and canola oil: evaluation of fuel properties.* Energy & fuels, 1995. **9**(2): p. 248-256.
109. Kumar, S., et al., *Performance and emission analysis of blends of waste plastic oil obtained by catalytic pyrolysis of waste HDPE with diesel in a CI engine.* Energy Conversion and Management, 2013. **74**: p. 323-331.
110. Sharypov, V., et al., *Co-pyrolysis of wood biomass and synthetic polymer mixtures. Part I: influence of experimental conditions on the evolution of solids, liquids and gases.* Journal of Analytical and Applied Pyrolysis, 2002. **64**(1): p. 15-28.
111. Abnisa, F., et al., *Co-pyrolysis of palm shell and polystyrene waste mixtures to synthesis liquid fuel.* Fuel, 2013. **108**: p. 311-318.
112. Shadangi, K.P. and K. Mohanty, *Co-pyrolysis of Karanja and Niger seeds with waste polystyrene to produce liquid fuel.* Fuel, 2015. **153**: p. 492-498.
113. Domínguez, A., et al., *Investigations into the characteristics of oils produced from microwave pyrolysis of sewage sludge.* Fuel Processing Technology, 2005. **86**(9): p. 1007-1020.
114. Dewangan, A., D. Pradhan, and R. Singh, *Co-pyrolysis of sugarcane bagasse and low-density polyethylene: Influence of plastic on pyrolysis product yield.* Fuel, 2016. **185**: p. 508-516.
115. Yang, J., et al., *Fast co-pyrolysis of low density polyethylene and biomass residue for oil production.* Energy Conversion and Management, 2016. **120**: p. 422-429.
116. Chattopadhyay, J., et al., *Catalytic co-pyrolysis of paper biomass and plastic mixtures (HDPE (high density polyethylene), PP (polypropylene) and PET (polyethylene terephthalate)) and product analysis.* Energy, 2016. **103**: p. 513-521.
117. Önal, E., B.B. Uzun, and A.E. Pütün, *An experimental study on bio-oil production from co-pyrolysis with potato skin and high-density polyethylene (HDPE).* Fuel Processing Technology, 2012. **104**: p. 365-370.
118. Xue, Y. and X. Bai, *Synergistic enhancement of product quality through fast co-pyrolysis of acid pretreated biomass and waste plastic.* Energy Conversion and Management, 2018. **164**: p. 629-638.
119. Wang, J., et al., *Co-pyrolysis of bamboo residual with waste tire over dual catalytic stage of CaO and co-modified HZSM-5.* Energy, 2017. **133**: p. 90-98.
120. Lu, P., et al., *Synergistic effects on char and oil produced by the co-pyrolysis of pine wood, polyethylene and polyvinyl chloride.* Fuel, 2018. **230**: p. 359-367.

121. Ding, K., et al., *Improving hydrocarbon yield from catalytic fast co-pyrolysis of hemicellulose and plastic in the dual-catalyst bed of CaO and HZSM-5.* Bioresource Technology, 2018. **261**: p. 86-92.
122. Lee, J.W., et al., *Characterization of biochars produced from cornstovers for soil amendment.* Environmental Science & Technology, 2010. **44**(20): p. 7970-7974.
123. Yargicoglu, E.N., et al., *Physical and chemical characterization of waste wood derived biochars.* Waste Management, 2015. **36**: p. 256-268.
124. Jindo, K., et al., *Physical and chemical characterization of biochars derived from different agricultural residues.* Biogeosciences, 2014. **11**(23): p. 6613-6621.
125. Hmid, A., et al., *Production and characterization of biochar from three-phase olive mill waste through slow pyrolysis.* Biomass and Bioenergy, 2014. **71**: p. 330-339.
126. Sadaka, S., et al., *Characterization of biochar from switchgrass carbonization.* Energies, 2014. **7**(2): p. 548-567.
127. Wang, Y., R. Yin, and R. Liu, *Characterization of biochar from fast pyrolysis and its effect on chemical properties of the tea garden soil.* Journal of Analytical and Applied Pyrolysis, 2014. **110**: p. 375-381.
128. Pattanaik, L., N.K. Sahoo, and S. Naik, *Thevetia peruviana (Yellow oleander)–A non-edible biodiesel feedstock.* Journal of Thermal Energy Systems, 2017. **2**(1): p. 47-55.
129. *http://www.flowersofindia.net/catalog/slides/Mexican%20Oleander.html*.
130. Van Parijs, J., et al., *Hevein: an antifungal protein from rubber-tree (Hevea brasiliensis) latex.* Planta, 1991. **183**(2): p. 258-264.
131. *http://www.tradeindia.com/fp1269091/Gulmohar-Ornamental-Tree-Seeds-Delonix-Regia-.html*.
132. Gardens, R.B. and M.B.G. Kew, *The plant list. A working list of all plant species*. 2017.
133. *Species profile for pacific island agroforestry (www.traditionaltree.org).*
134. Mirunalini, S., V. Vaithiyanathan, and M. Krishnaveni, *AMLA: A novel Ayurvedic herb as a functional food for health benefits"-A mini review.* International Journal of Pharmacy and Pharmaceutical Sciences, 2013. **5**(Suppl 1).
135. Zhang, Y.-J., et al., *Phyllaemblic acid, a novel highly oxygenated norbisabolane from the roots of Phyllanthus emblica.* Tetrahedron Letters, 2000. **41**(11): p. 1781-1784.
136. Girish, K. and S. Shankara Bhat, *Neem–a green treasure.* Electronic journal of Biology, 2008. **4**(3): p. 201-111.
137. Kumar, R. and V. Gupta, *Thrust on neem is need of today.* Employment news, 2002: p. 20-26.

138. Balerdi, C.F., J.H. Crane, and I. Maguire, *Sapodilla Growing in the Florida Home Landscape.* Horticultural Sciences Department Document HS1. Florida Cooperative Extension Service, Institute of Food and Agricultural Sciences, University of Florida, 2008.
139. Paramathma, M., K. Parthiban, and K. Neelakantan, *Jatropha-curcas*. 2004: Tamil Nadu Agricultural University.
140. Prasad Shadangi, K. and K. Mohanty, *Characterization of nonconventional oil containing seeds towards the production of bio-fuel.* Journal of Renewable and Sustainable Energy, 2013. **5**(3): p. 033111.
141. *https://en.wikipedia.org/wiki/Madhuca_longifolia.*
142. Razon, L.F., *Alternative crops for biodiesel feedstock.* CAB Reviews: Perspectives in agriculture, veterinary science, nutrition and natural resources, 2009. **4**(56): p. 1-15.
143. seeds, F.a.c.o.v.n.e., *https://www.chempro.in/fattyacid.htm for fatty acid composition.* 2018.
144. Lone, J.K., M. Lekha, and K. Chandrashekharaiah, *Studies on proteolytic inhibitory peptides from the seeds Ricinus communis.*
145. Dorado, J., et al., *Elimination and detoxification of softwood extractives by white-rot fungi*. Journal of Biotechnology, 2000. **80**(3): p. 231-240.
146. *https.//en.wikipedia.org/wiki/Shorea_robusta.*
147. *https.//en.wikipedia.org/wiki/Areca_catechu.*
148. Singh, A. and I. Singh, *Chemical evaluation of mahua (Madhuca indica) seed.* Food chemistry, 1991. **40**(2): p. 221-228.
149. Sanchez-Jimenez, P., et al., *Combined kinetic analysis of thermal degradation of polymeric materials under any thermal pathway.* Polymer Degradation and Stability, 2009. **94**(11): p. 2079-2085.
150. Olmstead, R.G., et al., *Phylogeny and provisional classification of the Solanaceae based on chloroplast DNA.* Solanaceae IV, 1999. **1**(1): p. 1-137.
151. Mandal, B., S.G. Majumdar, and C. Maity, *Chemical and nutritional evaluation ofPongamia glabra oil andAcacia auriculaeformis oil.* Journal of the American Oil Chemists Society, 1984. **61**(9): p. 1447-1449.
152. Dutta, P.C., et al., *Variation in lipid composition of niger seed (Guizotia abyssinica Cass.) samples collected from different regions in Ethiopia.* Journal of the American Oil Chemists' Society, 1994. **71**(8): p. 839-843.

153. Kaushik, N. and S. Vir, *Variations in fatty acid composition of neem seeds collected from the Rajasthan state of India*. 2000, Portland Press Limited.
154. Padhee, D. and H. Raheman, *Performance, Emissions and Combustion Characteristics of a Single Cylinder Diesel Engine Fuelled with Blends of Jatropha Methyl Ester and Diesel*. Vol. 3. 2015.
155. Kittigowittana, K., et al., *Fatty acid composition and biological activities of seed oil from rubber (Hevea brasiliensis) cultivar RRIM 600.* International Journal of Applied Research in Natural Products, 2013. **6**(2): p. 1-7.
156. Dhar, D., *Chemical Examination of Schleichera trijuga Seeds.* Fette, Seifen, Anstrichmittel, 1968. **70**(12): p. 942-943.
157. Ali, M.R., et al., *Fatty Acid Composition of the Seed Pods of Albizia lebbeck and the Leaves of Samanea saman.*
158. McKendry, P., *Energy production from biomass (part 1): overview of biomass.* Bioresource Technology, 2002. **83**(1): p. 37-46.
159. Greenhalf, C., et al., *Thermochemical characterisation of straws and high yielding perennial grasses.* Industrial crops and products, 2012. **36**(1): p. 449-459.
160. Zabaniotou, A., et al., *Experimental study of pyrolysis for potential energy, hydrogen and carbon material production from lignocellulosic biomass.* International Journal of Hydrogen Energy, 2008. **33**(10): p. 2433-2444.
161. Poletto, M., *Effect of extractive content on the thermal stability of two wood species from Brazil.* Maderas. Ciencia y tecnología, 2016. **18**(3): p. 435-442.
162. Horowitz, H.H. and G. Metzger, *A new analysis of thermogravimetric traces.* Analytical Chemistry, 1963. **35**(10): p. 1464-1468.
163. Vassilev, S.V., et al., *An overview of the chemical composition of biomass.* Fuel, 2010. **89**(5): p. 913-933.
164. Carpenter, A.M., *Switching to cheaper coals for power generation*. 1998: IEA Coal Research London.
165. Idris, S.S., N.A. Rahman, and K. Ismail, *Combustion characteristics of Malaysian oil palm biomass, sub-bituminous coal and their respective blends via thermogravimetric analysis (TGA).* Bioresource Technology, 2012. **123**: p. 581-591.
166. Cai, J. and L. Bi, *Kinetic analysis of wheat straw pyrolysis using isoconversional methods.* Journal of Thermal Analysis and Calorimetry, 2009. **98**(1): p. 325-330.
167. Doyle, C.D., *Series approximations to the equation of thermogravimetric data.* 1965.

168. Vand, V., *A theory of the irreversible electrical resistance changes of metallic films evaporated in vacuum.* Proceedings of the Physical Society, 1943. **55**(3): p. 222.
169. Bhavanam, A. and R. Sastry, *Kinetic study of solid waste pyrolysis using distributed activation energy model.* Bioresource Technology, 2015. **178**: p. 126-131.
170. Ceylan, S. and D. Kazan, *Pyrolysis kinetics and thermal characteristics of microalgae Nannochloropsis oculata and Tetraselmis sp.* Bioresource Technology, 2015. **187**: p. 1-5.
171. Soria-Verdugo, A., et al., *Evaluating the accuracy of the distributed activation energy model for biomass devolatilization curves obtained at high heating rates.* Energy Conversion and Management, 2014. **86**: p. 1045-1049.
172. Miura, K., *A new and simple method to estimate F (E) and K (0)(E) in the distributed activation-energy model from 3 sets of experimental-data.* Energy & Fuels, 1995. **9**(2): p. 302-307.
173. Myers, M.E., J. Stollsteimer, and A.M. Wims, *Determination of gasoline octane numbers from chemical composition.* Analytical Chemistry, 1975. **47**(13): p. 2301-2304.
174. Myers, M.E., J. Stollsteimer, and A.M. Wims, *Determination of hydrocarbon-type distribution and hydrogen/carbon ratio of gasolines by nuclear magnetic resonance spectrometry.* Analytical Chemistry, 1975. **47**(12): p. 2010-2015.
175. Sınağ, A., et al., *Characterization of the liquid phase obtained by copyrolysis of Mustafa Kemal Paşa (MKP) lignite (Turkey) with low density polyethylene.* Energy & Fuels, 2006. **20**(5): p. 2093-2098.
176. Albahri, T.A., *Structural group contribution method for predicting the octane number of pure hydrocarbon liquids.* Industrial & Engineering Chemistry Research, 2003. **42**(3): p. 657-662.
177. Yang, H., et al., *Characteristics of hemicellulose, cellulose and lignin pyrolysis.* Fuel, 2007. **86**(12): p. 1781-1788.
178. Ruiz, R., et al., *Determination of extractives in biomass.* NREL Laboratory Analytical Procedure. National Renewable Energy Laboratory Golden, CO, 2005.
179. Wang, Z., et al., *Effect of cellulose crystallinity on the formation of a liquid intermediate and on product distribution during pyrolysis.* Journal of Analytical and Applied Pyrolysis, 2013. **100**: p. 56-66.

180. Shebani, A., A. Van Reenen, and M. Meincken, *The effect of wood extractives on the thermal stability of different wood-LLDPE composites.* Thermochimica Acta, 2009. **481**(1): p. 52-56.
181. GUO, X.-j., et al., *Influence of extractives on mechanism of biomass pyrolysis.* Journal of fuel Chemistry and Technology, 2010. **38**(1): p. 42-46.
182. Kilulya, K.F., et al., *Effect of site, species and tree size on the quantitative variation of lipophilic extractives in Eucalyptus woods used for pulping in South Africa.* Industrial Crops and Products, 2014. **56**: p. 166-174.
183. He, W. and H. Hu, *Prediction of hot-water-soluble extractive, pentosan and cellulose content of various wood species using FT-NIR spectroscopy.* Bioresource Technology, 2013. **140**: p. 299-305.
184. Poletto, M., et al., *Thermal decomposition of wood: Influence of wood components and cellulose crystallite size.* Bioresource Technology, 2012. **109**: p. 148-153.
185. Sheshmani, S., *Effects of extractives on some properties of bagasse/high density polypropylene composite.* Carbohydrate Polymers, 2013. **94**(1): p. 416-419.
186. Silvério, F.O., et al., *Effect of storage time on the composition and content of wood extractives in Eucalyptus cultivated in Brazil.* Bioresource Technology, 2008. **99**(11): p. 4878-4886.
187. Sjöström, E., *Wood chemistry: fundamentals and applications*. 1993: Gulf Professional Publishing.
188. Kumar, R., et al., *Physical and chemical characterizations of corn stover and poplar solids resulting from leading pretreatment technologies.* Bioresource Technology, 2009. **100**(17): p. 3948-3962.
189. Turmanova, S.C., et al., *Non-isothermal degradation kinetics of filled with rise husk ash polypropene composites.* Express Polymer Letters, 2008. **2**(2): p. 133-146.
190. Mothé, C.G. and I.C. de Miranda, *Characterization of sugarcane and coconut fibers by thermal analysis and FTIR.* Journal of Thermal Analysis and Calorimetry, 2009. **97**(2): p. 661-665.
191. Hupa, M., *Interaction of fuels in co-firing in FBC.* Fuel, 2005. **84**(10): p. 1312-1319.
192. Bryers, R.W., *Fireside slagging, fouling, and high-temperature corrosion of heat-transfer surface due to impurities in steam-raising fuels.* Progress in Energy and Combustion Science, 1996. **22**(1): p. 29-120.
193. Yin, C., L.A. Rosendahl, and S.K. Kær, *Grate-firing of biomass for heat and power production.* Progress in Energy and Combustion Science, 2008. **34**(6): p. 725-754.

194. Adánez, J., et al. *Co-combustion of biomass and coal in circulating fluidized bed: modeling and validation*. in *17th International Conference on Fluidized Bed Combustion*. 2003. American Society of Mechanical Engineers.
195. Armesto, L., et al., *Combustion behaviour of rice husk in a bubbling fluidised bed.* Biomass and Bioenergy, 2002. **23**(3): p. 171-179.
196. Moghtaderi, B., *A study on the char burnout characteristics of coal and biomass blends.* Fuel, 2007. **86**(15): p. 2431-2438.
197. El-Sayed, S.A. and M. Mostafa, *Pyrolysis characteristics and kinetic parameters determination of biomass fuel powders by differential thermal gravimetric analysis (TGA/DTG).* Energy Conversion and Management, 2014. **85**: p. 165-172.
198. Maiti, S., S. Purakayastha, and B. Ghosh, *Thermal characterization of mustard straw and stalk in nitrogen at different heating rates.* Fuel, 2007. **86**(10-11): p. 1513-1518.
199. Jüntgen, H., *Review of the kinetics of pyrolysis and hydropyrolysis in relation to the chemical constitution of coal.* Fuel, 1984. **63**(6): p. 731-737.
200. Chutia, R.S., R. Kataki, and T. Bhaskar, *Thermogravimetric and decomposition kinetic studies of Mesua ferrea L. deoiled cake.* Bioresource Technology, 2013. **139**: p. 66-72.
201. Kim, S.-S., et al., *Thermogravimetric characteristics and pyrolysis kinetics of Alga Sagarssum sp. biomass.* Bioresource Technology, 2013. **139**: p. 242-248.
202. Samuelsson, L.N., M.U. Babler, and R. Moriana, *A single model-free rate expression describing both non-isothermal and isothermal pyrolysis of Norway Spruce.* Fuel, 2015. **161**: p. 59-67.
203. Vyazovkin, S., *Computational aspects of kinetic analysis.: Part C. The ICTAC Kinetics Project—the light at the end of the tunnel?* Thermochimica Acta, 2000. **355**(1): p. 155-163.
204. Venkatesh, M., P. Ravi, and S.P. Tewari, *Isoconversional kinetic analysis of decomposition of nitroimidazoles: Friedman method vs Flynn–Wall–Ozawa method.* The Journal of Physical Chemistry A, 2013. **117**(40): p. 10162-10169.
205. Gai, C., Y. Dong, and T. Zhang, *The kinetic analysis of the pyrolysis of agricultural residue under non-isothermal conditions.* Bioresource Technology, 2013. **127**: p. 298-305.
206. Biagini, E., A. Fantei, and L. Tognotti, *Effect of the heating rate on the devolatilization of biomass residues.* Thermochimica Acta, 2008. **472**(1): p. 55-63.
207. Slopiecka, K., P. Bartocci, and F. Fantozzi, *Thermogravimetric analysis and kinetic study of poplar wood pyrolysis.* Applied Energy, 2012. **97**: p. 491-497.

208. Yahiaoui, M., et al., *Determination of kinetic parameters of Phlomis bovei de Noé using thermogravimetric analysis.* Bioresource Technology, 2015. **196**: p. 441-447.
209. Vlaev, L., V. Georgieva, and S. Genieva, *Products and kinetics of non-isothermal decomposition of vanadium (IV) oxide compounds.* Journal of Thermal Analysis and Calorimetry, 2007. **88**(3): p. 805-812.
210. Yuan, X., et al., *Cattle manure pyrolysis process: Kinetic and thermodynamic analysis with isoconversional methods.* Renewable Energy, 2017. **107**: p. 489-496.
211. Ahmad, M.S., et al., *Kinetic analyses and pyrolytic behavior of Para grass (Urochloa mutica) for its bioenergy potential.* Bioresource Technology, 2017. **224**: p. 708-713.
212. Maia, A.A.D. and L.C. de Morais, *Kinetic parameters of red pepper waste as biomass to solid biofuel.* Bioresource Technology, 2016. **204**: p. 157-163.
213. Wang, Z., et al., *Pyrolysis of pine wood in a slowly heating fixed-bed reactor: Potassium carbonate versus calcium hydroxide as a catalyst.* Fuel Processing Technology, 2010. **91**(8): p. 942-950.
214. Wang, K. and R.C. Brown, *Catalytic pyrolysis of microalgae for production of aromatics and ammonia.* Green Chemistry, 2013. **15**(3): p. 675-681.
215. Himmelsbach, D.S., S. Khalili, and D.E. Akin, *The use of FT-IR microspectroscopic mapping to study the effects of enzymatic retting of flax (Linum usitatissimum L) stems.* Journal of the Science of Food and Agriculture, 2002. **82**(7): p. 685-696.
216. Sharma, R.K., et al., *Characterization of chars from pyrolysis of lignin.* Fuel, 2004. **83**(11-12): p. 1469-1482.
217. Miao, X., Q. Wu, and C. Yang, *Fast pyrolysis of microalgae to produce renewable fuels.* Journal of Analytical and Applied Pyrolysis, 2004. **71**(2): p. 855-863.
218. Yusuf, A., *Beef tallow as a biodiesel fuel*. 1995, Ph. D. Thesis.
219. Galiasso, R., D. Tailleur, and L. Resasco. *Switchgrass to Gasoline & Diesel via pyrolysis*. in *Poster presented at Oklahoma Biofuels Conference*. 2008.
220. Bridgwater, A., S. Czernik, and J. Piskorz, *An overview of fast pyrolysis.* Progress in Thermochemical Biomass Conversion, 2001: p. 977-997.
221. Raja, S.A., et al., *Flash pyrolysis of jatropha oil cake in electrically heated fluidized bed reactor.* Energy, 2010. **35**(7): p. 2819-2823.
222. Aquino, F.L., S.C. Capareda, and J.R. Hernandez. *Elucidating the solid, liquid and gaseous products from pyrolysis of cotton gin trash*. in *Beltwide Cotton Conference*. 2007.

223. Capunitan, J.A. and S.C. Capareda, *Assessing the potential for biofuel production of corn stover pyrolysis using a pressurized batch reactor.* Fuel, 2012. **95**: p. 563-572.
224. Kongkasawan, J., H. Nam, and S.C. Capareda, *Jatropha waste meal as an alternative energy source via pressurized pyrolysis: A study on temperature effects.* Energy, 2016. **113**: p. 631-642.
225. Zhang, Z., et al., *Effect of Biochar on the Cracking of Tar from the Pyrolysis of a Pine Sawdust in a Fixed Bed Reactor.* Energy Procedia, 2015. **75**: p. 196-201.
226. Wang, S., et al., *Bio-gasoline production from co-cracking of hydroxypropanone and ethanol.* Fuel Processing Technology, 2013. **111**: p. 86-93.
227. Zhang, H., et al., *Improving hydrocarbon yield by two-step pyrolysis of pinewood in a fluidized-bed reactor.* Fuel Processing Technology, 2017. **159**: p. 19-26.
228. Garg, R., N. Anand, and D. Kumar, *Pyrolysis of babool seeds (Acacia nilotica) in a fixed bed reactor and bio-oil characterization.* Renewable Energy, 2016. **96**: p. 167-171.
229. Liu, C., et al., *Catalytic fast pyrolysis of lignocellulosic biomass.* Chemical Society Reviews, 2014. **43**(22): p. 7594-7623.
230. Nanda, S., et al., *Physico-chemical properties of bio-oils from pyrolysis of lignocellulosic biomass with high and slow heating rate.* Energy and Environment Research, 2014. **4**(3): p. 21.
231. Schnitzer, M.I., et al., *The conversion of chicken manure to biooil by fast pyrolysis I. Analyses of chicken manure, biooils and char by 13C and 1H NMR and FTIR spectrophotometry.* Journal of Environmental Science and Health Part B, 2007. **42**(1): p. 71-77.
232. Demiral, İ. and E.A. Ayan, *Pyrolysis of grape bagasse: effect of pyrolysis conditions on the product yields and characterization of the liquid product.* Bioresource Technology, 2011. **102**(4): p. 3946-3951.
233. Uçar, S. and S. Karagöz, *Co-pyrolysis of pine nut shells with scrap tires.* Fuel, 2014. **137**: p. 85-93.
234. Sharuddin, S.D.A., et al., *Energy recovery from pyrolysis of plastic waste: Study on non-recycled plastics (NRP) data as the real measure of plastic waste.* Energy Conversion and Management, 2017. **148**: p. 925-934.
235. Edreis, E.M., et al., *Synergistic effects and kinetics thermal behaviour of petroleum coke/biomass blends during H 2 O co-gasification.* Energy Conversion and Management, 2014. **79**: p. 355-366.

236. Meng, H., et al., *Investigation on synergistic effects and char morphology during co-pyrolysis of poly (vinyl chloride) blended with different rank coals from Northern China.* Energy & Fuels, 2015. **29**(10): p. 6645-6655.
237. Das, P. and P. Tiwari, *Valorization of packaging plastic waste by slow pyrolysis.* Resources, Conservation and Recycling, 2018. **128**: p. 69-77.
238. Peng, W. and Q. Wu, *Production of fuels from biomass by pyrolysis.* New Energy Sour, 2000. **22**(11): p. 39-44.
239. Missio, A.L., et al., *Thermal analysis of charcoal from fast-growing eucalypt wood: Influence of raw material moisture content.* Journal of Wood Chemistry and Technology, 2014. **34**(3): p. 191-201.
240. Gabhi, R.S., D.W. Kirk, and C.Q. Jia, *Preliminary investigation of electrical conductivity of monolithic biochar.* Carbon, 2017. **116**: p. 435-442.
241. Ameloot, N., et al., *Interactions between biochar stability and soil organisms: review and research needs.* European Journal of Soil Science, 2013. **64**(4): p. 379-390.
242. de Jonge, H. and M.C. Mittelmeijer-Hazeleger, *Adsorption of CO2 and N2 on soil organic matter: nature of porosity, surface area, and diffusion mechanisms.* Environmental Science & Technology, 1996. **30**(2): p. 408-413.
243. Kumar, B.P., et al., *Preparation of steam activated carbon from rubberwood sawdust (Hevea brasiliensis) and its adsorption kinetics.* Journal of Hazardous Materials, 2006. **136**(3): p. 922-929.
244. Bourke, J., et al., *Do all carbonized charcoals have the same chemical structure? 2. A model of the chemical structure of carbonized charcoal.* Industrial & Engineering Chemistry Research, 2007. **46**(18): p. 5954-5967.
245. Chen, B. and Z. Chen, *Sorption of naphthalene and 1-naphthol by biochars of orange peels with different pyrolytic temperatures.* Chemosphere, 2009. **76**(1): p. 127-133.
246. Novak, J.M., et al., *Short-term CO2 mineralization after additions of biochar and switchgrass to a Typic Kandiudult.* Geoderma, 2010. **154**(3-4): p. 281-288.
247. Guo, J. and B. Chen, *Insights on the molecular mechanism for the recalcitrance of biochars: interactive effects of carbon and silicon components.* Environmental Science & Technology, 2014. **48**(16): p. 9103-9112.
248. Wu, W., et al., *Chemical characterization of rice straw-derived biochar for soil amendment.* Biomass and Bioenergy, 2012. **47**: p. 268-276.
249. Santos, L.B., et al., *Characterization of biochar of pine pellet.* Journal of Thermal Analysis and Calorimetry, 2015. **122**(1): p. 21-32.

List of Appendices

Table A1. GC-MS analysis of thermal pyrolytic oil of PW

Compound Name	Relative Area (%)
Phenol	
Phenol	0.497
Phenol, 2-methyl-	2.812
Phenol, 3-methyl-	2.369
Phenol, 2-methoxy-	3.449
Phenol, 2,3-dimethyl-	0.694
Phenol, 3,5-dimethyl	2.433
Phenol, 2-ethyl-6-methyl-	1.051
Phenol, 4-ethyl-2-methoxy-	3.977
2-methoxy-4-vinylphenol	1.385
Phenol, 2,6-dimethoxy	1.58
Phenol, 2-methoxy-3-(2-propenyl)-	0.961
Phenol, 2-methoxy-4-propyl	0.931
Phenol, 2-methoxy-4-(1-propenyl)-	4.506
Phenol, 2,6-dimethoxy-4-(2-propenyl)	0.644
Ketone	
2-ethyl-5-propylcyclopentanone	1.162
2-cyclopenten-1-one, 2,3-dimethyl-	0.497
Ester	
1,2,3-trimethoxybenzene	1.402
Benzene, 1,2,3-trimethoxy-5-methyl-	1.892
Methyl 11-methyl-dodecanoate	0.473
7-oxodehydroabietic acid, methyl ester	0.567
L-(+)-ascorbic acid 2,6-dihexadecanoate	3.778
Methyl 13-octadecenoate	1.065
Acids	
1,2-benzenedicarboxylic acid, bis(2-methylpropyl) ester	5.517
17-octadecynoic acid	1.52
Octadecanoic acid	1.786
1-phenanthrenecarboxylic,acid, 1,2,3,4,4a,9,10,10a-octahydro-1,4a-dime	1.506
Aldehyde	
Butanal, 2-ethyl-	0.6
2,3,4-trimethoxy-benzaldehyde	0.24
Propanal, 2,3-dichloro-2-methyl-	0.38
Ether	
Furan, 2-(2-propenyl)-	0.46
Oxirane, [[4-(1,1-dimethylethyl) phenoxy] methyl]	0.45
Others	
Silanediamine, 1,1-dimethyl-N,N0-diphenyl-	1.71
2,4-Dimethylbenzyl chlorine	0.69

Table A2. GC-MS analysis thermal pyrolytic oil of SW

Compound Name	Relative Area (%)
Phenol	
Phenol	1.754
Phenol, 2-methyl-	1.008
Phenol, 4-methyl- 10	1.668
Phenol, 2-methoxy-	1.688
Phenol, 3,4-dimethyl-, methylcarbamate	1.029
Phenol, 2-methoxy-4-methyl-	1.684
Phenol, 4-ethyl-2-methoxy-	1.598
Phenol, 2,6-dimethoxy	7.815
Phenol, 2-methoxy-3-(2-propenyl)-	0.356
Phenol, 2-methoxy-4-propyl	0.532
Phenol, 2,6-dimethoxy-4-(2-propenyl)-	1.111
Phenol, 2,6-dimethoxy-4-(2-propenyl)	1.144
1,2-benzenedicarboxylic acid, butyl 8-methylnonyl ester	2.006
Acids	
1,2-benzenedicarboxylic acid, bis(2-methylpropyl) ester	1.6
17-octadecynoic acid	1.1
Octadecanoic acid	1.2
Aldehyde	
Benzaldehyde, 4-hydroxy-3,5-dimethoxy	1.633
Ester	
Methyl (3,4-dimethoxyphenyl)(hydroxy)acetate	0.494
L-(+)-ascorbic acid 2,6-dihexadecanoate	1.18
2h-pyran, 3,4-dihydro-	1.1
1,2,4-trimethoxybenzene	0.98
Benzene, 1,2,3-trimethoxy-5-methyl-	0.20
Furfural	
2-furancarboxaldehyde, 5-methyl	0.56
Furancarboxaldehyde, 5-methyl-	0.63

Furfuryl alcohol, tetrahydro-5-methyl-, cis-	0.43
Ether	
Phenol, 2-methoxy-4-methyl-	0.65
Ethanone, 1-(2-hydroxy-6-methoxyphenyl)-	0.53
Ketone	
2-ethyl-5-propylcyclopentanone	4.369
2-cyclopenten-1-one, 3-ethyl-2-hydroxy-	1.139
2-propanone, 1-(4-hydroxy-3-methoxyphenyl)	1.807
Ethanone, 1-(4-hydroxy-3,5-dimethoxyphenyl)	1.038
Nitrile	
Heptanenitrile, 4-acetyl-	0.49
Benzenepropanenitrile	0.32
Dodecanenitrile	0.45
Heptadecanenitrile	0.53
Others	
3,5-dimethoxy-4-hydroxyphenylacetic acid	0.52
Cyclohexylmethylsilane	0.32

Table A3. GC-MS analysis of thermal pyrolytic oil of AN

Compound Name	Relative Area (%)
Phenols	
Phenol	2.364
Phenol, 2-methyl	3.799
Phenol, 2-methyl	3.117
Phenol, 2-methoxy	3.187
Phenol, 2,3-dimethyl	1.112
Phenol, 2,3-dimethyl	3.533
Phenol, 2-methoxy-4-methyl	2.52
Phenol, 2,3,6-trimethyl	1.148
Phenol, 3,4,5-trimethyl	0.693
Phenol, 4-ethyl-2-methoxy-	3.684
Phenol, 2,6-dimethoxy	5.442
Alcohol	
1,2-benzenediol	3.184
3-methyl-2-(3-methylpentyl)-3-buten-1-ol	1.814
Ester	
2-buten-1-ol, propanoate	10.763
Nicotinic acid, 2-ethylcyclohexyl ester	5.523
Heptane, 1,1'-oxybis	0.603
Ether	
1,2,4-trimethoxybenzene	0.35
Benzene, 1,2,3-trimethoxy-5-methyl	0.46
Phenol, 2,6-dimethoxy-4-(2-propenyl)	0.53
Ketone	
Cyclopentanone, 2-(1-methylpropyl)-	0.429
2-ethyl-5-propylcyclopentanone	0.638
Furfural	
Furancarboxaldehyde, 5-methyl-	0.36
Furfural	0.26

Furfuryl alcohol, tetrahydro-5-methyl-, cis-	0.65
Amine	
3,5-dimethoxy-4-hydroxyphenethylamine	0.62
1-Decanamine	0.43
1-Octadecanamine	0.26
Others	
1,4:3,6-dianhydro-.alpha.-d-glucopyranose	6.13
1,6-anhydro-3,4-o-isopropylidene-.beta.-d-galactopyranose	0.68
D-allose	1.26
Nitrile	
Butanenitrile, 2-methyl-	0.33
Oleanitrile	0.21
Butanenitrile, 3-methyl-	0.86
Hexanenitrile	0.35
Aldehyde	
Butanal, 2-ethyl-	0.35
hydroxyacetaldehyde	0.53
glyceraldehyde	0.29
2,3,4-trimethoxy-benzaldehyde	0.62
methylindole	0.35
Dodecanal	0.62
Acid	
1,2-benzenedicarboxylic acid, bis(2-methylpropyl) ester	2.6
17-octadecynoic acid	2.4
Octadecanoic acid	2.9

Table A4. GC-MS analysis of thermal pyrolytic oil of SG

Compounds Name	Relative area (%)
Alcohol	
Oleyl alcohol, trifluoroacetate	5.42
Aldehyde	
Benzaldehyde, 3-[4-(1,1-dimethylethyl)phenoxy]-	0.869
amide	
Hexadecanamide	2.418
9-octadecenamide, (z	3.64
9-octadecenamide	1.637
n,n'-bis-(2,2,6,6-tetramethylpiperid-4-yl)phthalamide	1.198
Acids	
Phosphonic acid, methyl-, bis(trimethylsilyl) ester	1.088
1,2-benzenedicarboxylic acid, bis(2-methylpropyl) ester	1.393
Oleic acid	2.71
Octanoic acid	0.66
n-dodecane	0.62
n-octadecane	2.36
6-octadecenoic acid	1.32
n-octadecanoic acid	1.23
Ester	
Cyclohexyl methyl ethylphosphonate	5.72
Methyl 8,9-octadecadienoate	0.89
Octadecanoic acid, methyl ester	1.14
1,2,4-benzenetricarboxylic acid, 4-dodecyl dimethyl ester	0.36
Ether	
Furan, 2-(2-propenyl)-	0.466
Oxirane, [[4-(1,1-dimethylethyl)phenoxy]methyl]	0.457
Nitrile	
Dodecanenitrile	1
Octahydropyrrolo[1,2-a]pyrazine	0.686
Phenols	
O-cresol	0.48
Phenol	1.2
Phenol, 2-methoxy-4-(1-propenyl)	1.113
Phenol, 2-methoxy-4-(1-propenyl)	1.011
Phenol, 3,5-bis(1,1-dimethylethyl)	1.128
Phenol, 2-methoxy-4-propyl	1.254
Phenol, 2,6-dimethoxy-4-(2-propenyl)-	0.545
Phenol, 2,6-dimethyl-4-nitro-	0.425
Phenol, 2,6-dimethoxy-4-(2-propenyl)	0.697
Phenol, 2,6-dimethoxy-4-(2-propenyl)-	0.632
Phenol, 2-methoxy-4-methyl-	0.596
others	
Trans-2-methyl-4-n-pentylthiane, s,s-dioxide	0.834

Trans-2-methyl-4-n-butylthiane, s,s-dioxide	0.387
Hydrocarbons	
5-Undecene	0.46
n-Undecane	0.83
Cyclooctene	1.00
1-Dodecene	0.63
n-Dodecane	0.66
n-Tetradecan	2.24
Pentadecane	2.85
Hexadecane	2.41
n-Heptadecane	3.21
n-Octadecane	2.0
Cyclopentane, 1,1 0-[3-(2-Cyclopentylethyl)-1,5-pentanediyl]bis	1.08

Table A5. GC-MS analysis of thermal pyrolytic oil of SK

Compounds name	Relative area
Hydrocarbons	
Benzene, propyl	0.75
Benzene, n-butyl	1.04
E-11-Tetradecen-1-ol trifluoroacetate	0.72
Benzene, pentyl	0.26
Naphthalene	0.11
5,7-Dodecadiene, (Z,Z)-	0.32
Indole	0.2
1H-Indene, 1-ethylidene	0.23
Benzocycloheptatriene	0.86
Hexatriacontane	1.25
Indole, 3-methyl	2.33
3-Tetradecene, (E)-	0.89
Dotriacontane	0.25
8-Hexadecyne	0.98
5-Tetradecene, (E)-	2.69
Nonadecane	0.62
Benzene, (1-methylnonyl)-	0.27
Benzene, (1-butyloctyl)-	0.69
Benzene, (1-propylnonyl)-	0.78
9-Tricosene, (Z)-	2.82
1,19-Eicosadiene	0.55
17-Pentatriacontene	1.02
Tetratetracontane	1.2
Benzene, (1-methyldecyl)-	0.62
7-Tetradecyne	0.25
Benzene, (1-methylundecyl)-	0.63
Hexacosane	0.89
Benzene, 2-propenyl	0.46
Benzene, pentyl-	0.82
1H-Indene, 3-methyl-	0.45
6-Dodecene, (E)-	1.16
7-Tetradecene	0.56
Heptadecane, 2-methyl	0.53
Naphthalene, 2-methyl	0.59
5,7-Dodecadiene, (E,Z)-	0.42
1H-Indene, 1-ethylidene	0.38
6-Tridecene, (Z)-	0.42
Cyclopentene, 1-pentyl	0.83
1,7-Dimethyl-4-(1-methylethyl) cyclodecane	0.52
1-Tridecyne	0.33

Cyclohexane, 2-butyl-1,1,3-trimethyl	0.23
Cyclohexene, 1-butyl	0.24
1-Octadecyne	0.68
17-Pentatriacontene	0.77
Dotriacontane	0.02
Octacosane	0.29
3-Dodecene, (Z)-	0.25
Naphthalene, 1-methyl	0.12
6-Dodecene, (E)-	0.25
Biphenyl	0.57
Naphthalene, 1-ethyl	0.2
Cyclopentene, 1-butyl	0.89
Heptadecane, 2-methyl	0.8
Benzene, (1-methyldecyl)-	0.41
Phenanthrene, 1-methyl	0.22
7-Oxabicyclo[4.1.0]heptane, 1-methyl	0.65
	37.28
Alcohol	
1-Octanol, 2,7-dimethyl	0.79
1-Octyn-3-ol, 4-ethyl	0.32
1-Hexadecanol	0.41
11-Hexadecyn-1-ol	1.03
Benzyl alcohol	1.09
1,2-Ethanediol, 1,2-diphenyl	0.56
1,22-Docosanediol	1.05
n-Tridecan-1-ol	0.18
	5.43
Ketone	
2-Cyclopenten-1-one, 2,3-dimethyl	0.25
Cyclohexanone, 2-ethyl	2.04
4-Piperidinone, 2,2,6,6-tetramethyl	2.81
2-Tridecanone	0.35
2-Cyclopenten-1-one, 2,3-dimethyl	0.25
4-Piperidinone, 2,2,6,6-tetramethyl	2.88
2-Dodecanone	0.26
2-Pentadecanone, 6,10,14-trimethyl	1.05
2-Nonadecanone	0.22
Octadecanophenone	0.14
	10.25
Phenols	
Phenol, 2-methyl	1.02
p-Cresol	4.16
Phenol, 3,5-dimethyl	1.65
Phenol, 2-(1-methylethyl)-	0.38

p-Cumenol	0.74	
Phenol, 3-ethyl-5-methyl	3.27	
Phenol, 3-phenoxy	1.16	
	12.38	
Acid		
Hexadecenoic acid, Z-11-	2.96	
Nonanoic acid	1.12	
9,12-Octadecadienoic acid (Z,Z)-	2.82	
Erucic acid	0.89	
9,12-Octadecadienoic acid (Z,Z)-E	1.83	
n-Hexadecanoic acid	3.76	
	13.38	
Ether		
Oxirane, tetradecyl	0.53	
Benzene, (1,2-dimethylpropyl)-	1.82	
Benzene, (1,2-dimethylpropyl)-	0.79	
Octadecane, 1-(ethenyloxy)-	0.92	
Benzene, 1,1'-(oxydiethylidene)bis	1.09	
Naphthalene, 1,4-dimethyl	0.34	
		5.49
Ester		
9,12-Octadecadienoic acid, methyl ester, (E,E)-	3.28	
9-Octadecenoic acid, methyl ester, (E)-	0.93	
Hexadecanoic acid, methyl ester	0.2	
Palmitic acid vinyl ester	0.37	
Linoleic acid ethyl ester	1.92	
Phenol, 2,3-dimethyl	1.45	
	8.15	
Amide		
Hexadecanamide	1.47	
Tetradecanamide	1.95	
9-Octadecenamide, (Z)-	0.56	
	3.98	
Amine		
N-Benzyl-2-phenethylamine	0.98	
Nitrile		
Octadecanenitrile	0.72	
Heptadecanenitrile	1.35	
	2.07	

Table A6. GC-MS analysis of thermal pyrolytic oil of CK

Compounds	Relative area (%)
Phenols	
Phenol	1.07
Phenol, 2-methyl	1.02
Phenol, 2-ethyl	0.68
2-Methoxy-5-methylphenol	1.89
Phenol, 2-propyl	2.5
Phenol, 3-ethyl-5-methyl	0.5
Phenol, 2-ethyl-5-methyl	0.82
p-Cumenol	0.29
Phenol, 2-methoxy-4-(1-propenyl)-, (Z)-	1.13
Phenol, 2,6-dimethoxy-4-(2-propenyl)-	0.68
	10.58
Hydrocarbons	
Benzene, 1,3-dimethyl	0.42
Ethylbenzene	1.12
o-Xylene	1.11
3-Heptene, 2,6-dimethyl	0.37
Tridecane, 3-methyl	0.41
1,3,5,7-Cyclooctatetraene	1.78
Cyclohexene, 3,5-dimethyl	0.63
Benzene, propyl	0.8
Heptadecane, 2-methyl	0.93
Mesitylene	0.62
Benzene, (2-nitropropen-1-yl)-	0.58
11-Tetradecen-1-ol, (E)-	1.12
6-Dodecene, (E)-	0.23
2-Tridecanone	1.36
Heptadecane, 2-methyl	0.98
2-Cyclopenten-1-one, 3,4,5-trimethyl	0.76
9-Hexadecen-1-ol, (Z)-	0.89
9-Tetradecen-1-ol, (E)-	0.59
Benzene, pentyl	1.3
2-Methylindene	0.26
3-Dodecene, (Z)-	1.63
2-Dodecanone	1.65
2-Undecanone	0.68
Octadecane, 1-(ethenyloxy)-	1.52
Heptadecane, 2-methyl	1.1
Naphthalene	1.41
5,7-Dodecadiene, (E,Z)-	1.15
Benzene, hexyl	1.19
Hexatriacontane	0.71
Dotriacontane	1.7

Naphthalene, 1-methyl	0.61
1-Pentadecyne	0.52
7-Tetradecene	0.98
Nonadecane	0.25
Cyclopentene, 1-pentyl	0.85
6-Dodecene, (E)-	0.86
Heptacosane	1.03
17-Pentatriacontene	0.64
9-Tetradecen-1-ol, (E)-	0.92
5-Dodecyne	0.11
1-Hexadecyne	0.41
4-Nonene, 5-butyl	0.85
Naphthalene, 2,3,6-trimethyl	0.24
Heptadecane, 2-methyl	1.1
1,11-Dodecadiene	1.06
1,19-Eicosadiene	0.95
1,7-Dimethyl-4-(1-methylethyl)cyclodecane	1
Dodecane, 2,6,10-trimethyl	0.65
	42.03
Aldehyde	
2-Furancarboxaldehyde, 5-methyl	**1.04**
Ethers	
Benzofuran	0.32
Benzofuran, 2-methyl	0.66
Naphthalene, 1,7-dimethyl	1.2
Naphthalene, 1,4-dimethyl	1.61
Naphthalene, 1,3-dimethyl	1.18
	4.97
Esters	
1,2-Benzenedicarboxylic acid, butyl cyclohexyl ester	2.17
9,12-Octadecadienoic acid, methyl ester, (E,E)-	0.26
13-Octadecenoic acid, methyl ester	1.47
7-Hexadecenoic acid, methyl ester, (Z)-	2.19
9,12-Octadecadienoic acid, methyl ester, (E,E)-	1.26
	7.35
Ketons	
2-Cyclopenten-1-one, 2,3-dimethyl	0.62
2-Pentadecanone, 6,10,14-trimethyl	1.88
	2.5
Alcohols	
1,2-Ethanediol, 1,2-diphenyl	0.19
1-Cyclohexene-1-carboxaldehyde, 4-(1-methylethenyl)-	1.25
1-Octanol, 2,7-dimethyl	0.86
1,22-Docosanediol	0.18
	2.48
Acids	

n-Hexadecanoic acid	7.31
Oleic acid	5.5
Pentadecanoic acid	0.26
	13.07
Others	
3-Furanmethanol	3.37
Mequinol	4.17
Creosol	1.82
E-11-Tetradecen-1-ol trifluoroacetate	3.27
2-Furancarboxaldehyde, 5-methyl	1.61
	14.77

Table A7. GC-MS analysis of thermal oil of MH

Compounds	Relative area (%)
Phenols	
2-Methoxy phenol	0.72
Phenol, 2,4-dichloro-6-nitro-	1.63
2,4-Dichloro-6-nitrophenol	0.87
Phenol, 2-methoxy	0.92
Phenol, 2-ethyl	0.33
Phenol, 3,4-dimethyl	0.62
Phenol, 3,5-dimethyl	4.45
Phenol, 3,4-dimethyl	1.20
Phenol, 4-ethyl	4.38
Phenol, 2,4,6-trimethyl	0.62
2-Methoxy-5-methylphenol	0.37
Resorcinol	1.19
Phenol, 3,4,5-trimethyl-, methylcarbamate	0.85
Phenol, 2-ethyl-5-methyl	1.38
1,2-Benzenediol, 4-methyl	1.03
Hydrocarbons	
Hentriacontane	1.68
Benzene, (2-bromo-1-methylethyl)-	1.02
1H,1H,2H-Perfluoro-1-decene	1.93
Hentriacontane	1.28
Oxacyclohexadecan-2-one	2.36
5-Undecene	2.46
n-Undecane	1.83
Cyclooctene	1.63
1-Dodecene	2.20
2-Cyclopenten-1-one, 3,4,5-trimethyl	1.76
n-Tetradecan	2.34
Pentadecane	2.15

Hexadecane	2.41
Ethers	
Benzofuran	0.30
Benzene, 1-methoxy-4-methyl	1.61
Benzene, 1-ethyl-4-methoxy	2.67
Acids	
Fumaric acid	1.66
Ptrin-6-carboxylic acid	1.09
Acetic acid	0.98
Oleic acid	0.24
n-Hexadecanoic acid	2.85
13-Octadecenoic acid, methyl ester	2.12
Esters	
Nitric acid, ethyl ester	5.35
Phosphonic acid methyl-, bis(Trimethylsilyl) ester	0.53
N-(4-trifluoromethylbenzoyl)-, dodecyl ester	0.63
Acetic acid butoxyethanol ester	0.53
4-chlorobutyric acid, octadecyl ester	0.67
Fumaric acid, decyl 2,3,5-trichlorophenyl ester	0.78
1,2-Benzenedicarboxylic acid, 4-nitro-,dimethyl ester	2.14
Aldehyde	
3-Pyridinecarboxaldehyde	0.96
hydroxyacetaldehyde	0.53
glyceraldehyde	0.29
Nitrogen containing groups	
1-Amino-2-ethylhexane	0.82
Pyridine, 3-(trifluoromethyl)-	0.83
N-methyldodecanamide	2.05
Hexadecanamide	0.26
1,4-Benzenediamine, N-(1-methylethyl)-N 0-phenyl	1.49

Octadecanamide	0.92
Ketons	
2-Cyclopenten-1-one, 2-methyl	1.21
2-Cyclopenten-1-one, 2,3-dimethyl	1.84
Ethanedione, diphenyl	1.70
Others	
Pyrimidine, 4,6-dichloro-5-nitro-	0.97
Acetamide, N-(4-bromophenyl)-2, 2-dichloro-	1.52
Benzamide, N-(2-iodo-4-methylphenyl)-3- fluoro	1.50
Benzamide, N,N-didecyl-3-methoxy	1.62
Benzamide, N,N-diundecyl-2-fluoro-	1.65
Benzamide, N,N-diundecyl-3-methyl-	1.02

Table A8. GC-MS analysis of thermal pyroltic oil of Neem seeds

Compounds name	Relative area (%)
Aromatic Hydrocarbons	
o-Xylene	0.56
Benzene, 1-ethyl-2-methyl	0.56
Benzene, 2-propenyl	0.90
Benzene, 1-propynyl	1.20
Cycloprop[a]indene, 1,1a,6,6a-tetrahydro	0.77
1,4-Dihydronaphthalene	1.6
Naphthalene	1.9
Benzene, (2-methylpentyl)-	0.94
Naphthalene, 2-methyl	1.90
1H-Indene, 1-ethylidene	0.96
4-Ethylbiphenyl	3.02
Benzene, 1,1'-propylidenebis	1.19
Naphthalene, 1,6,7-trimethyl	0.57
Tridecene, (Z)	
Benzene, (1-methyldecyl)-	1.02
Anthracene	0.56
Acids	
4-Pentenoic acid	1.25
Erucic acid	0.60
n-Hexadecanoic acid	3.85
13-Octadecenoic acid, methyl ester	1.12
Hydrocarbons	
1,3,5,7-Cyclooctatetraene	0.34
3-Heptene, 2,6-dimethyl	2.20
1H-Indene, octahydro-, trans	0.65
Benzene, pentyl	1.5
Azulene	0.20
5,7-Dodecadiene, (E,Z)-	0.54

6-Dodecene, (E)-	0.80
7-Tetradecene	1.45
Hexatriacontane	1.27
Cyclodecene, (Z)-	1.25
Cyclohexene,3-propyl	1.89
3-Dodecene, (Z)-	1.89
Dotriacontane	0.34
1-Octadecyne	0.62
Tetratetracontane	1.09
Ketons	
2-Cyclopenten-1-one, 2-methyl	1.31
2-Cyclopenten-1-one, 2,3-dimethyl	0.74
Ethanedione, diphenyl	0.20
2-Cyclopenten-1-one, 3-ethyl-2-hydroxy	0.73
Phenols	
Phenol	6.11
Phenol, 2-methyl	1.3
Phenol, 2-methoxy	0.92
Phenol, 2-ethyl	0.33
Phenol, 3,4-dimethyl	0.62
Phenol, 3,5-dimethyl	4.45
Phenol, 3,4-dimethyl	1.20
Phenol, 4-ethyl	4.38
Phenol, 2,4,6-trimethyl	0.62
2-Methoxy-5-methylphenol	0.37
Resorcinol	1.19
Phenol, 3,4,5-trimethyl-, methylcarbamate	0.85
Phenol, 2-ethyl-5-methyl	1.38
1,2-Benzenediol, 4-methyl	1.03
1,2-Benzenediol, 4-methyl	0.63
Phenol, 3,4,5-trimethyl-, methylcarbamate	0.86

Phenol, 2,6-dimethoxy	3.08
Phenol, 2-methoxy-6-(2-propenyl)-	2.02
Phenol, 2,6-dimethoxy-4-(2-propenyl)-	0.41
Phenol, 2,6-dimethoxy-4-(2-propenyl)-	1.09
Nitrogen groups	
Benzonitrile	1.4
Pyrazine, 2,6-diethyl	0.92
Octadecanenitrile	1.78
Ethers	
Benzofuran	0.30
Benzene, 1-methoxy-4-methyl	1.61
Benzene, 1-ethyl-4-methoxy	2.67
Naphthalene, 1,7-dimethyl	2.19
Esters	
9-Octadecenoic acid, methyl ester, (E)-	3.53
13-Octadecenoic acid, methyl ester	1.11
Tridecanoic acid, 12-methyl-, methyl ester	1.52
Alcohol	
Benzyl alcohol	2.85
meso-Hydrobenzoin	0.20
9-Octadecen-1-ol, (Z)-	1.65
3-Furanmethanol	1.42
Amide group	
9-Octadecenamide, (Z)-	1.26
Amines	
Silane, trimethyl(4-methyl-3-penten-1-ynyl)-	3.36
Others	
Benzenemethanol, 3,5-dimethyl	1.8

Table A9. GC-MS analysis of thermal pyrolytic oil of SS

Compounds	Relative area (%)
Phenols	
Phenol,2,6 dimethoxy-4-(2-propenyl)	1.20
Phenol	1.54
Phenol, 2-Methyl-	0.78
Phenol, 4-Methyl-	0.95
Phenol, 2-Ethyl-	0.65
Phenol, 3-(1-Methylethyl)-	0.78
Phenol, 2-methoxy	0.92
Phenol, 3,4-dimethyl	1.62
Resorcinol	1.19
Phenol, 2-methoxy-6-(2-propenyl)-	2.02
Esters	
Methyl 12,15-Octadecadienoate	1.42
I-Propyl 9-Octadecenoate	1.02
9-Octadecenoic acid, methyl ester, (E)-	1.73
Ethers	
1,4-Dimethoxybenzene	0.89
Toluene, 3,4,5-trimethoxy-	0.63
Pyrogallol 1,3-dimethyl ether	2.40
Naphthalene, 1,7-dimethyl	2.19
Hydrocarbons	
1-Octadecene	1.63
Heneicosane	1.89
1-Nonadecene	1.26
Nonadecane	1.63
Benzene, 1-Ethyl-3-Methyl-	0.56
1R,2C,3T,4T-Tetramethyl-cyclohexane	0.89
1-Hexen-3-Yne, 2,5,5-Trimethyl-	0.85
Cyclododecene	1.69

Hentriacontane	0.49
1-Hentriacontane	3.10
Bicyclo[4.1.0]Heptane, 7-Pentyl-	0.72
Hexadecane	1.86
8-Heptadecene	6.35
Acids	
Carbonic acid	0.57
Chloroacetic Acid	1.89
n-Hexadecanoic acid	3.85
Octadecenoic acid	3.89
Ketons	
2-Pentacosanone	1.02
2-Cyclopenten-1-one, 2,3-dimethyl	0.75
4-Piperidinone, 2,2,6,6-tetramethyl	4.88
2-Dodecanone	2.2
2-Pentadecanone, 6,10,14-trimethyl	4.85
Nitrogen containing groups	
9-Octadecenamide, (Z)-	1.09
N-Methyldodecanamide	1.09
Hexadecanenitrile	3.20
Oleanitrile	8.12
Octadecanenitrile	3.43
Hexadecanamide	1.86
Others	
Dodecane, 1-Fluoro-	0.59
Trans-2-Methyl-4-N-Pentylthiane, S,S-Dioxide	3.20
2,20-Bifuran	0.710
Methyl 3,4-Di-O-Methyl-.Beta.-L-Arabinopyranoside	4.02

Table A10. GC-MS analysis of thermal pyrolytic oil of SK

Compounds name	Relative area (%)
Hydrocarbons	
Benzene, propyl	1.75
2-Tridecanone	0.75
Naphthalene	1.11
5,7-Dodecadiene, (Z,Z)-	0.32
7-Tetradecene	1.93
6-Dodecene, (E)-	0.68
1H-Indene, 1-ethylidene	0.23
Benzocycloheptatriene	0.86
6-Dodecene, (E)-	3.75
Hexatriacontane	1.25
3-Tetradecene, (E)-	0.89
Dotriacontane	6.25
8-Hexadecyne	0.98
5-Tetradecene, (E)-	2.69
Nonadecane	0.62
Benzene, (1-methylnonyl)-	1.27
Benzene, (1-butyloctyl)-	0.69
Benzene, (1-propylnonyl)-	0.78
9-Tricosene, (Z)-	4.82
1,19-Eicosadiene	1.55
17-Pentatriacontene	0.52
Tetratetracontane	3.2
Benzene, (1-methyldecyl)-	0.62
Benzene, (1,2-dimethylpropyl)-	1.12
7-Tetradecyne	0.25
Benzene, (1-methylundecyl)-	0.63
Hexacosane	0.89
Benzene, (1,2-dimethylpropyl)-	1.2
	41.6
Phenols	
Phenol, 2-methyl	1.2
Benzene, n-butyl	1.04
p-Cresol	2.16
Phenol, 3,5-dimethyl	0.65
Benzene, pentyl	0.26
Phenol	1.68
Phenol, 3-phenoxy	1.5
	8.49
Ethers	
Oxirane, tetradecyl	0.53
Benzene, (1,2-dimethylpropyl)-	1.82
Benzene, (1,2-dimethylpropyl)-	0.79

Octadecane, 1-(ethenyloxy)-	0.92
Benzene, 1,1'-(oxydiethylidene)bis	1.09
Naphthalene, 1,4-dimethyl	0.34
Esters	5.49
2(5H)-Furanone	1.3
9,12-Octadecadienoic acid, methyl ester, (E,E)-	0.63
9-Octadecenoic acid, methyl ester, (E)-	3.93
	5.86
Aldehyde	
2-Furancarboxaldehyde	0.36
Alcohol	
1-Octyn-3-ol, 4-ethyl	0.35
2-Furanmethanol	1.26
	1.61
Hexadecanamide	3.47
Tetradecanamide	2.95
	6.42
Amide	
Acetic acid	2.26
Hexadecenoic acid, Z-11-	1.96
Nonanoic acid	1.12
9,12-Octadecadienoic acid (Z,Z)-	0.82
Erucic acid	0.89
9,12-Octadecadienoic acid (Z,Z)-E	1.25
n-Hexadecanoic acid	3.76
	12.06
Ketons	
2-Cyclopenten-1-one, 2,3-dimethyl	0.75
Cyclohexanone, 2-ethyl	1.84
	2.59
Nitrile group	
Heptadecanenitrile	**7.35**
Others	
Hexadecane, 1-chloro	0.36
E-11-Tetradecen-1-ol trifluoroacetate	1.2
exo-2-Bromonorbornane	0.2
4-Piperidinone, 2,2,6,6-tetramethyl	0.81
Indole	1.2
Indole, 3-methyl	3.33
	7.1

Table A11. GC-MS analysis of catalytic pyrolytic oil at SK+ZSM-5(8:1)

Compounds name	Relative area (%)
Hydrocarbons	
Indane	1.2
5,7-Dodecadiene, (E,Z)-	1.27
6-Dodecene, (E)-	3.03
Naphthalene	3.87
5,7-Dodecadiene, (E,Z)-	1.3
7-Tetradecene	1.22
Naphthalene, 1-methyl	2.83
1H-Indene, 1-ethylidene	0.58
Benzene, heptyl	0.52
6-Dodecene, (E)-	5.15
Hexatriacontane	0.58
Naphthalene, 1-ethyl	0.78
Naphthalene, 2,3-dimethyl	1.2
8-Hexadecyne	2.32
6-Tridecene, (Z)-	2.21
Dotriacontane	3.94
1-Hexadecyne	1.5
Dodecane, 2,6,10-trimethyl	0.72
Benzene, (1-methylnonyl)-	0.89
Benzene, (1-propylnonyl)-	1.01
1,7-Dimethyl-4-(1-methylethyl)cyclodecane	2.08
3-Dodecene, (Z)-	0.68
Tetratetracontane	2.89
Benzene, (1-methyldecyl)-	0.12
Benzene, (2-iodoethyl)-	0.32
8-Hexadecyne	0.86
Benzene, (1-methylundecyl)-	0.62
Heptacosane	0.45
Benzene, (1,2-dimethylpropyl)-	0.69
	44.83
Phenols	
p-Cresol	1.31
Benzene, n-butyl	1.04
p-Cresol	2.16
	4.51
Esters	
Oxacycloheptadec-8-en-2-one, (8Z)-	0.69
9-Octadecenoic acid (Z)-, 2,3-dihydroxypropyl ester	0.94
	1.63
Alcohol	
1,2-Ethanediol, 1,2-diphenyl	1.32
3-Hexen-1-ol, (E)-	1.2

	2.52
Tetradecanamide	2.93
9-Octadecenamide, (Z)-	1.46
	4.39
Amide	
Oxirane, tetradecyl	**1.43**
Acid	
Acetic acid	1.06
Hexanoic acid	1.89
Octanoic acid	0.49
n-Decanoic acid	0.73
9,12-Octadecadienoic acid (Z,Z)-	0.65
Erucic acid	1.55
n-Hexadecanoic acid	2.35
	8.72
Aldehyde	
2-Furancarboxaldehyde	5.36
4-Hydroxy-benzaldehyde	1.68
	7.04
Nitrile group	
Hexadecanenitrile	3.15
Octadecanenitrile	0.95
	4.1
Others	
4-Piperidinone, 2,2,6,6-tetramethyl	3.71
2-Furanmethanol	2.26
Indole	1.5
Indole, 3-methyl	1.65
Tryptamine	0.36
9,12-Octadecadienoyl chloride, (Z,Z)-	0.95
E-11-Tetradecen-1-ol trifluoroacetate	1.49
Levoglucosan	6.58
	18.5

Table A12. GC-MS analysis of neem thermal pyrolytic oil

Compounds Name	Relative area (%)
Aromatic Hydrocarbons	**17.65**
o-Xylene	0.56
Benzene, 1-ethyl-2-methyl	0.56
Benzene, 2-propenyl	0.9
Benzene, 1-propynyl	1.2
Cycloprop[a]indene, 1,1a,6,6a-tetrahydro	0.77
1,4-Dihydronaphthalene	1.6
Naphthalene	1.9
Benzene, (2-methylpentyl)-	0.94
Naphthalene, 2-methyl	1.9
1H-Indene, 1-ethylidene	0.96
4-Ethylbiphenyl	3.02
Benzene, 1,1'-propylidenebis	1.19
Naphthalene, 1,6,7-trimethyl	0.57
Tridecane, (Z)	
Benzene, (1-methyldecyl)-	1.02
Anthracene	0.56
Acids	**6.82**
4-Pentenoic acid	1.25
Erucic acid	0.6
n-Hexadecanoic acid	3.85
13-Octadecenoic acid, methyl ester	1.12
Hydrocarbons	**16.03**
1,3,5,7-Cyclooctatetraene	0.34
3-Heptene, 2,6-dimethyl	2.2
1H-Indene, octahydro-, trans	0.65
Benzene, pentyl	1.5
Azulene	0.2
5,7-Dodecadiene, (E,Z)-	0.54
6-Dodecene, (E)-	0.8
7-Tetradecene	1.45
Hexatriacontane	1.27
Cyclodecene, (Z)-	1.25
Cyclohexene,3-propyl	1.89
3-Dodecene, (Z)-	1.89
Dotriacontane	0.34
1-Octadecyne	0.62
Tetratetracontane	1.09
Ketones	**2.98**
2-Cyclopenten-1-one, 2-methyl	1.31
2-Cyclopenten-1-one, 2,3-dimethyl	0.74
Ethanedione, diphenyl	0.2
2-Cyclopenten-1-one, 3-ethyl-2-hydroxy	0.73

Phenols	**32.84**
Phenol	6.11
Phenol, 2-methyl	1.3
Phenol, 2-methoxy	0.92
Phenol, 2-ethyl	0.33
Phenol, 3,4-dimethyl	0.62
Phenol, 3,5-dimethyl	4.45
Phenol, 3,4-dimethyl	1.2
Phenol, 4-ethyl	4.38
Phenol, 2,4,6-trimethyl	0.62
2-Methoxy-5-methylphenol	0.37
Resorcinol	1.19
Phenol, 3,4,5-trimethyl-, methylcarbamate	0.85
Phenol, 2-ethyl-5-methyl	1.38
1,2-Benzenediol, 4-methyl	1.03
1,2-Benzenediol, 4-methyl	0.63
Phenol, 3,4,5-trimethyl-, methylcarbamate	0.86
Phenol, 2,6-dimethoxy	3.08
Phenol, 2-methoxy-6-(2-propenyl)-	2.02
Phenol, 2,6-dimethoxy-4-(2-propenyl)-	0.41
Phenol, 2,6-dimethoxy-4-(2-propenyl)-	1.09
Nitrogen containing groups	4.1
Benzonitrile	1.4
Pyrazine, 2,6-diethyl	0.92
Octadecanenitrile	1.78
Ethers	**6.77**
Benzofuran	0.3
Benzene, 1-methoxy-4-methyl	1.61
Benzene, 1-ethyl-4-methoxy	2.67
Naphthalene, 1,7-dimethyl	2.19
Esters	**5.69**
9-Octadecenoic acid, methyl ester, (E)-	1.53
9-Octadecenoic acid, methyl ester, (E)-	1.53
13-Octadecenoic acid, methyl ester	1.11
Tridecanoic acid, 12-methyl-, methyl ester	1.52
Alcohol	**6.12**
Benzyl alcohol	2.85
meso-Hydrobenzoin	0.2
9-Octadecen-1-ol, (Z)-	1.65
3-Furanmethanol	1.42
Amide group	**1.26**
9-Octadecenamide, (Z)-	1.26
Amines	**3.36**
Silane, trimethyl(4-methyl-3-penten-1-ynyl)-	3.36
Chlorine containing	**1.8**
Benzenemethanol, 3,5-dimethyl	1.8

Table A13. GC-MS analysis of NM+WNG (3:1) thermal pyrolytic oil

Compounds name	Relative area (%)
Aromatic Hydrocarbons	**37.74**
Benzene, 1,3-dimethyl	3.09
o-Xylene	2.94
Benzene, (1-methylethyl)-	0.2
Benzene, propyl	1.42
Benzene, 1-ethyl-3-methyl	1.89
Benzene, (1-methylethyl)-	1.04
Benzene, 2-propenyl	1.54
Indane	0.35
Benzene, 1-propynyl	5.51
Benzene, 1-methyl-3-propyl	0.41
Naphthalene, 1,2-dihydro	3.63
2-Methylindene	2.25
6-Methyl-1,2,3,4-tetrahydroquinoline	0.66
Naphthalene	3.22
1H-Indene, 1,1-dimethyl	1.63
Benzene, 1-cyclopenten-1-yl	0.7
Naphthalene, 1-methyl	1.77
Naphthalene, 2-methyl	0.59
Benzene, heptyl	0.23
Hexatriacontane	0.87
4-Ethylbiphenyl	2.69
Fluorene	0.91
Phenanthrene	0.2
Acids	**1.78**
13-Octadecenoic acid, methyl ester	0.86
9-Octadecenoic acid (Z)-, 2,3-dihydroxypropyl ester	0.92
Hydrocarbons	**11.1**
1,3,5-Cyclooctatriene	2.45
2,8-Decadiyne	0.88
6-Dodecene, (E)-	0.59
7-Tetradecene	0.95
Hexatriacontane	0.87
6-Dodecene, (E)-	0.68
1,7-Dimethyl-4-(1-methylethyl)cyclodecane	1.29
6-Dodecene, (E)-	2.1
Tetratetracontane	1.2
Ketones	**2.86**
2-Cyclopenten-1-one, 2,3-dimethyl	0.5
2-Cyclopenten-1-one, 3,4,5-trimethyl	2
2-Propanone, 1,1-diphenyl	0.36
Phenols	**15.54**
Phenol	3.57

Phenol, 2-ethyl	0.35
Phenol, 2,3-dimethyl	3.44
Phenol, 3-ethyl-5-methyl	0.93
Phenol, 2,6-dimethoxy	4.08
Phenol, 2-methoxy-4-(1-propenyl)-	1.2
Phenol, 2,6-dimethoxy-4-(2-propenyl)-	0.71
Phenol, 2,6-dimethoxy-4-(2-propenyl)-	1.26
Nitrogen containing groups	**15.77**
Pyridine, 2,5-dimethyl	1.2
Benzonitrile	2.03
Benzonitrile, 4-methyl	1.3
1H-Indole, 2,3-dihydro	3.91
Quinoline, 5,6,7,8-tetrahydro	1.56
Quinoline	1.85
Indole, 3-methyl	0.77
2-Naphthalenecarbonitrile	1.2
1-Naphthaleneacetonitrile	1.2
9H-Carbazole, 9-methyl	0.2
Pentadecanenitrile	0.55
Ethers	**2.15**
Cyclopentene, 3,3'-oxybis	0.52
Naphthalene, 1,7-dimethyl	1.63
Esters	**2.18**
Hexadecanoic acid, methyl ester	0.96
9,12-Tetradecadien-1-ol, acetate, (Z,E)-	1.22
Alcohol	**6.02**
3-Furanmethanol	0.58
1,2-Ethanediol, 1,2-diphenyl	3.79
n-Tridecan-1-ol	1.65
Amide group	**3.12**
Tetradecanamide	0.71
9-Octadecenamide, (Z)-	2.41
Chlorine containing	**0.63**
Benzenemethanol, 3,5-dimethyl	0.63

Table A14. GC-MS analysis of NM+WNG(3:1)+CaO(5:1) catalytic pyrolytic oil

Compounds name	Relative area (%)
Aromatic Hydrocarbons	**31.71**
Benzene, 1,3-dimethyl	2.96
o-Xylene	2.39
p-Xylene	2.43
Benzene, propyl	1.35
Indane	0.48
Benzene, 1-ethenyl-2-methyl	1.53
Benzene, 1-propynyl	4.38
Benzene, 1-methyl-3-propyl	2.31
Naphthalene, 1,2-dihydro	3.24
6-Methyl-1,2,3,4-tetrahydroquinoline	0.5
Naphthalene	2.3
1-Phenyl-1-pentyne	0.92
Naphthalene, 2-methyl	1.58
1H-Indene, 1-ethylidene	1.07
Naphthalene, 2-ethyl	1.52
Benzene, (1-ethyldecyl)-	0.55
Benzene, (1-methyldecyl)-	1.07
Benzene, (1,2-dimethylpropyl)-	1.13
Acids	**5.21**
9,11-Octadecadienoic acid, methyl ester, (E,E)-	3.15
13-Octadecenoic acid, methyl ester	2.06
Hydrocarbons	**8.16**
Cyclohexane, 1,4-bis(methylene)-	0.32
3-Heptene, 2,6-dimethyl	0.72
Cyclopentene, 3-propyl	0.56
Heptadecane, 2-methyl	1.14
7-Tetradecene	1.25
Hexatriacontane	1.3
6-Dodecene, (E)-	1.1
Nonadecane	0.73
Heptacosane	1.04
Ketones	**5.52**
2-Cyclopenten-1-one, 2,3-dimethyl	1.03
2-Cyclopenten-1-one, 3,4,5-trimethyl	1.41
2-Heptadecanone	3.08
Phenols	**5.1**
Phenol, 2-methyl	1.26
Phenol, 2,5-dimethyl	2.3
Phenol, 3,4-dimethoxy	1.11
Phenol, 2-methoxy-6-(2-propenyl)-	0.43
Aldehyde	**3.26**
1-Cyclohexene-1-carboxaldehyde, 4-(1-methylethyl)-	3.26

Nitrogen containing groups	**12.25**
Pyridine, 2,3-dimethyl	1.36
Benzonitrile	1.86
Benzonitrile, 4-methyl	1.18
1H-Indole, 2,3-dihydro	0.82
Quinoline, 1,2,3,4-tetrahydro	1.57
1H-Indole-3-ethanamine, N-methy-	1.39
1H-Indole, 2-aminomethyl	0.89
Indole	1.94
Indole, 3-methyl	1.24
Ethers	**2.87**
2,4-Dimethylfuran	1.65
Benzene, 1-ethyl-4-methyl	0.53
Naphthalene, 1,7-dimethyl	0.69
Esters	**2.22**
9,12-Tetradecadien-1-ol, acetate, (Z,E)-	2.22
Alcohol	**2.78**
3-Furanmethanol	1.1
Bicyclo [3.1.1]heptan-3-one, 2,6,6-trimethyl-, (1.alpha.,2.beta.,5.alpha.)-	1.19
1-Hexadecanol	0.49
Amide group	**1.38**
9-Octadecenamide, (Z)	1.38

Table A15. GC-MS analysis of NM+WNG (3:1) + Al_2O_3(5:1) catalytic pyrolytic oil

Compounds name	Relative area (%)
Aromatic Hydrocarbons	**42.98**
Benzene, 1,3-dimethyl	1.01
o-Xylene	1.97
p-Xylene	1.98
Benzene, (1-methylethyl)-	0.65
Benzene, propyl	1.35
Benzene, 1-ethyl-3-methyl	1.29
Mesitylene	2.61
Benzene, 1-ethenyl-2-methyl	1.8
Benzene, 1-propynyl	6.04
Benzene, 1-methyl-4-(1-methylethenyl)-	1.2
2-Methylindene	4.62
Benzene, (cyclopropylidenemethyl)-	2.65
1,4-Dihydronaphthalene	0.98
Cycloprop[a]indene, 1,1a,6,6a-tetrahydro	0.26
Naphthalene	3.12
1H-Indene, 1,1-dimethyl	1.65
Naphthalene, 1-methyl	1.78
Naphthalene, 2-methyl	2.14
1,2,3-Trimethylindene	0.71
Naphthalene, 2-ethyl	0.65
Naphthalene, 1,3-dimethyl	0.45
Acenaphthene	1.51
Diphenylmethane	1.36
5H-Indeno[1,2-b]pyridine	1.2
Acids	**2.84**
13-Octadecenoic acid, methyl ester	1.12
9-Octadecenoic acid (Z)-, 2,3-dihydroxypropyl ester	1.72
Hydrocarbons	**9.48**
Cyclohexane, 1,4-bis(methylene)-	1.96
6-Dodecene, (E)-	2.1
7-Tetradecene	1.2
Hexatriacontane	0.74
3-Dodecene, (Z)-	0.96
1,7-Dimethyl-4-(1-methylethyl)cyclodecane	0.69
1,7-Dimethyl-4-(1-methylethyl)cyclodecane	0.89
Dotriacontane	0.94
Ketones	**0.59**
2-Cyclopenten-1-one, 2,3-dimethyl	0.59
Phenols	**11.58**
Phenol	3.31
Phenol, 2,3-dimethyl	4.19
Phenol, 3-(1-methylethyl)-	0.82

Phenol, 2-methoxy-6-(2-propenyl)-	0.43
Phenol, 2,6-dimethoxy	1.63
Phenol, 2-methoxy-6-(2-propenyl)-	1.2
Aldehyde	**2.26**
1-Cyclohexene-1-carboxaldehyde, 4-(1-methylethyl)-	2.26
Nitrogen containing groups	**13.42**
Pyridine, 2,5-dimethyl	1.23
Benzonitrile	1.23
Benzonitrile, 4-methyl	0.51
Benzyl nitrile	0.87
1H-Indole, 2,3-dihydro	3.6
2,6-Dimethylbenzonitrile	1.01
6-Methyl-1,2,3,4-tetrahydroquinoline	0.61
Indole, 3-methyl	1.08
Isoquinoline	0.69
1H-Indole, 2-aminomethyl	0.32
1H-Indole, 1,3-dimethyl	0.58
9H-Carbazole, 9-methyl-	0.78
Heptadecanenitrile	0.91
Ethers	**3.57**
Benzene, 1-ethyl-4-methyl	1.44
Oxirane, 2-methyl-2-phenyl	1.04
Benzene, (1,2-dimethylpropyl)-	1.09
Esters	**0.63**
13-Octadecenoic acid, methyl ester	0.11
Tridecanoic acid, 12-methyl-, methyl ester	0.52
Alcohol	**6.23**
1,2-Ethanediol, 1,2-diphenyl	1.38
1,2-Ethanediol, 1,2-diphenyl	3.96
Fluorene-9-methanol	0.89
Amide group	**0.98**
9-Octadecenamide, (Z)-	0.98
Amine	**0.48**
Silane, trimethylphenyl	0.48
Others	**0.35**
1H-Imidazole-4-methanol	0.35

Research Outputs

Manuscripts Published in Peer-reviewed Journals

- R. K. Mishra, K. Mohanty, Pyrolysis kinetics and thermal behaviour of waste sawdust biomass using thermogravimetric analysis**, Bioresource Technology,** 251**, 2018,** 63-74.
- R. K. Mishra, K. Mohanty, Pyrolysis characteristics and kinetic parameters assessment of three waste biomass, **Journal of Renewable and Sustainable Energy**, 10, **2018**, 013102-18.
- R. K. Mishra, K. Mohanty, Thermocatalytic conversion of non-edible Neem seeds towards clean fuel and chemicals, **Journal of Analytical and Applied Pyrolysis,** 134, **2018**, 83-92.
- R. K. Mishra, K. Mohanty, Characterization of non-edible lignocellulosic biomass in terms of their candidacy towards alternative renewable fuels. **Biomass Conversion and Biorefinery,** 4, **2018**, 1-14.
- R. K. Mishra, K. Mohanty, Thermal and catalytic pyrolysis of pine sawdust (*Pinus ponderosa*) and Gulmohar seed (*Delonix regia*) towards production of fuel and chemicals, **Materials Science for Energy Technologies** 2.2 **(2019):** 139-149.
- R. K. Mishra, K. Mohanty, Pyrolysis of three waste biomass: Effect of biomass bed thickness and distance between successive beds on pyrolytic products yield and properties, **Renewable Energy** 141 **(2019)**: 549-558.
- R. K. Mishra, J. S. Iyer, and K. Mohanty, Conversion of waste biomass and waste nitrile gloves into renewable fuel, **Waste Management** 89 **(2019):** 397-407.

Manuscripts Communicated to Peer-reviewed Journals

- R. K. Mishra, K. Mohanty, Kinetic behaviour and pyrolysis of Madhuca longifolia seeds: Production of renewable fuel and its characterization" **Biomass Conversion and Biorefinery** (Revision submitted).
- R. K. Mishra, K. Mohanty, Pyrolysis kinetics and synergetic effect in co-pyrolysis of Samanea saman seeds and plastic waste using thermogravimetric analyzer" **Bioresource Technology** (Revision submitted).
- R. K. Mishra, K. Mohanty, Pyrolysis kinetic behavior and Py-GC-MS analysis of waste dahlia flowers into renewable fuel and value-added chemicals.

- R. K. Mishra, K. Mohanty, Pyrolysis of *cascabela thevetia* seeds over ZSM-5 catalysts: Fuel properties and compositional analysis.

Book Chapters

- R. K. Mishra, K. Mohanty, Mahua and Neem seeds as sustainable renewable resources towards producing clean fuel and chemicals, **Sustainable Energy Technology & Policies – A Transformational Journey, Volume 2** (Editors: De, S., Bandyopadhyay, S., Assadi, M., Mukherjee, D.A.), **2018**, Springer.
- R.K. Mishra, K. Mohanty, An overview of techno-economic analysis of thermochemical conversion of lignocellulosic biomass and life cycle assessment, **Recent Advancements in Biofuels and Bioenergy Utilization** (Editors: P.K. Sarangi, S. Nanda, P. Mohanty), **2018**, Springer Nature, Singapore.

Conference Presentations

International

- R. K. Mishra, K. Mohanty, Utilization of non-edible *Azadirachta indica* seeds: Possible route for production of clean fuel and chemicals. Oral presentation in **Bioprocess India 2017,** Guwahati, India.
- R. K. Mishra, K. Mohanty, Thermal and catalytic pyrolysis of *Madhuca Indica* seeds: A possible route for production of clean fuel and chemicals. Oral presentation in **Sustainable Energy and Environmental Challenges (SEEC-2018),** Indian Institute of Science, Bangalore, India.
- R. K. Mishra, K. Mohanty, Kinetic analysis and thermocatalytic pyrolysis of *Madhuca longifolia* seeds towards production of fuel and chemicals. Oral presentation in **Indo-Japan Bilateral Symposium on Future Perspective of Bioresource Utilization in North-East India 2017**, Guwahati, India.
- R. K. Mishra, K. Mohanty, Pyrolysis characteristics and kinetic parameters investigation of non-edible oil containing seeds by Thermogravimetric analysis. Oral presentation in **Recycle 2018,** Guwahati, India.
- R. K. Mishra, K. Mohanty, Thermal pyrolysis and kinetic parameter assessment of waste biomass using TGA and semi batch reactor. Oral presentation in **Recycle 2018,** Guwahati, India.

- R. K. Mishra, K. Mohanty, Thermocatalytic co-pyrolysis of *Azadirachta indica* seeds and Waste nitrile gloves: A sustainable way to reduce waste plastic by converting into renewable fuel. Poster presentation in 2nd International Conference on **Bioresource Technology for Bioenergy, Bioproducts and Environmental Sustainability (Biorestec2018),** Barcelona, Sitges, Spain.

National

- R. K. Mishra, K. Mohanty, Characterization of lignocellulosic biomass towards production of fuel and chemicals. Oral presentation in **CHEMCON 2015,** Guwahati, India.
- R. K. Mishra, K. Mohanty, Thermal and catalytic pyrolysis of Areca nut husk biomass towards production of fuel and chemicals. Oral presentation in **National Conference on Non-Conventional energy: Harvesting Technology and Its Challenge (NCEHTC-2017),** Guwahati.
- R. K. Mishra, K. Mohanty, Feasibility study and thermal pyrolysis of *Shorea robusta* and *Madhuca indica* seeds: A sustainable source for fuel and chemical production. (Poster presentation), in Symposium on Advances in **Biology of Algae and Cyanobacteria (ABAC-2018),** Banaras Hindu University (BHU), Varanasi, India.

Workshops/Training/Award

- Got selected in IGCS Winter School on "*Liquid Biofuels 2016*", 22 February – 5 March **2016** at **IIT Madras, Chennai, India.**
- Got selected in IGCS Summer School on "*Biomass and Coal– Two Carbon Fuels of Different Ages: German and Indian Perspectives*", 09-18 July, **2016** at **Technical University, Berlin, Germany.**
- Won **Third Prize** for Poster Presentation at **Research Conclave 2016** held at Indian Institute of Technology Guwahati, Guwahati, India.
- Received "**Young Scientist International Travel Award**" from SERB (Department of Science and Technology, Government of India for attending **BIORECTEC2018** organised by Elsevier during September 16-19, 2018 at **Sitges, Spain**.